# Production of activated carbon from date palm pits and its use in industrial wastewater treatment

## Thesis

UNRESTRICTED

# "PRODUCTION OF ACTIVATED CARBON FROM DATE PALM PITS AND ITS USE IN INDUSTRIAL WASTEWATER TREATMENT"


By

**Mohammed Hussain Essa, BSc., MSc.**


A Dissertation Presented to the

**Department of Design, Development, Environment & Materials**

**Faculty of Mathematics, Computing & Technology**

**The Open University**

In Partial Fulfillment of the Requirements for the Degree of

**Doctor of Philosophy in Environmental Engineering**

Date: October, 2008


Submission date: 19 Feb. 2008
Date of award: 27 Oct. 2008

*Dedicated to my parents, my wife and children*

# ACKNOWLEDGEMENTS

I would like to express profound thanks and appreciation to my internal advisor, Dr. Suresh T. Nesaratnam, and to my external advisor, Dr. Muhammad A. Al-Zahrani, for their invaluable guidance, support, advice and endless patience and help during the course of this work. I thank them for being a valuable source of ideas and motivation as well. I would like to express my gratitude for the many helpful comments and suggestions I have received over the last few years regarding the expository and critical aspects of my thesis, and especially for those comments which bear directly on my various arguments for the central thesis statement. Most importantly, I would like to thank my supervisors for their nearly five years of supervision, and especially for their commitment to guiding me through my doctoral research, as well as for the time they have spent reading the various drafts of this thesis. Their critical commentaries on my work have played a major role in both the content and presentation of my discussion and arguments. I am deeply grateful to the Civil Engineering Department of King Fahd University of Petroleum & Minerals, for providing me with a warm atmosphere and continuous support, and for making available all the laboratory facilities that I needed.

I am also grateful to the Research Committee at KFUPM for providing the financial support through Grant No. SABIC 2003/09 for the completion of this research study.

Acknowledgement is also due to Dr. Ahmed Aidid of King Saud University for his help in the characterization of the produced activated carbon.

I owe my family an expression of gratitude for their patience and understanding during my research work.

# Table of Contents

**Appendix B : Data for Activated Carbons Produced Using an Activation Time of 2 hours**

**Appendix C : Data for Activated Carbons Produced Using an Activation Time of 3 hours**

# List of Abbreviations

AC = Activated carbon

BET = Brunauer-Emmett-Teller

EBCT = Empty Bed Contact Time

GAC = Granular activated carbon

MTBE = Methyl Tertiary Butyl Ether

PAC = Powdered activated carbon

R = Impregnation ratio

$S_{BET}$ = Specific surface area using BET model

SE Fit = Standard error of fit

TCE = Trichloroethylene

$V_p$ = Pore volume

# List of Tables

# List of Figures

# List of Plates

The Open University

EX12

# RESEARCH SCHOOL

## Library Authorisation Form

Please return this form to the Research School with the two bound copies of your thesis to be deposited with the University Library. All candidates should complete parts one and two of the form. Part three only applies to PhD candidates.

**Part One: Candidates Details**

Name: MOHAMMED HUSSEIN ESSA PI: U9942912

Degree: DOCTOR OF PHILOSOPHY IN ENV. ENG.

Thesis title: PRODUCTION OF ACTIVATED CARBON FROM DATE PALM PITS & ITS USE IN INDUSTRIAL WASTEWATER TREATMENT

**Part Two: Open University Library Authorisation**

I confirm that I am willing for my thesis to be made available to readers by The Open University Library, and that it may be photocopied, subject to the discretion of the Librarian.

Signed: ..... Date: 15-11-08

**Part Three: British Library Authorisation** [PhD candidates only]

If you want a copy of your PhD thesis to be available on loan to the British Library Thesis Service as and when it is requested, you must sign a British Library Doctoral Thesis Agreement Form. Please return it to the Research School with this form. The British Library will publicise the details of your thesis and may request a copy on loan from the University Library. Information on the presentation of the thesis is given in the Agreement Form.

Please note the British Library have requested that theses should be printed on one side only to enable them to produce a clear microfilm. The Open University Library sends a soft bound copy of theses to the British Library.

The University has agreed that your participation in the British Library Thesis Service should be voluntary. Please tick either (a) or (b) to indicate your intentions.

(a) ☑ I am willing for The Open University to loan the British Library a copy of my thesis. A signed Agreement Form is attached

(b) ☐ I do not wish The Open University to loan the British Library a copy of my thesis.

Signed: ..... Date: 15-11-08

# ABSTRACT

The present study investigates, for the first time, the production of granular activated carbon (GAC) from date palm pits, a waste material. Reported data indicates that the yearly production of dates in the Kingdom of Saudi Arabia (KSA) is more than 800 ktonnes of which a significant portion is de-stoned prior to sale. Hence the use of date palm pits for the production of GAC would confer two benefits, i.e., reduction in waste disposal costs and concerns and production of a very useful material from this waste, i.e., GAC, which at the present is imported in the KSA for several industrial applications.

Considering these facts, date palm pits from a local source were used for the production of GAC. Several GAC production variables were investigated in detail, to study their effect on the BET specific surface area ($SSA_{BET}$), porosity, and the pore size distribution of the produced material. Variables studied included sample pre-drying, time of carbonization, time of activation, strength of the activating agent (i.e., phosphoric acid), acid impregnation ratio, pH, and temperature. Nitrogen adsorption isotherm data was used for the determination of respective $SSA_{BET}$, and porosity values.

The optimum conditions that produced the best activated carbon were, $H_3PO_4$ concentration equal to 70%, acid to pits ratio of 1.6:1, and carbonization temperature of 500°C. Additionally, a maximum yield of 24% was noted for the best GAC sample which showed the following characteristics 590 kg $m^{-3}$ bulk density, 0.5% ash content, 1100 mg $g^{-1}$ iodine number, and 1319 $m^2$ $g^{-1}$ $SSA_{BET}$. Furthermore, this GAC sample showed substantial capability to adsorb phenol and 2-Methylphenol (o-cresol) from the aqueous phase. The respective adsorption data fitted well to the

Freundlich adsorption isotherm. Several continuous column studies (using operational variables including flowrate, initial pollutant concentration, pH, temperature and dissolved oxygen) were also conducted to find the suitability of the produced optimum GAC sample for the removal of phenol and 2-Methylphenol from the aqueous phase. For example, the adsorption of both phenol and 2-Methylphenol was influenced both by the flowrate and the initial pollutant concentration. Also, the breakthrough time decreased when the flowrate and the initial concentration values were increased, probably due to insufficient pollutant residence time. The respective optimum activated carbon was also successfully used for the reduction of total organic carbon from an industrial wastewater sample.

Furthermore, to minimize waste disposal cost and concerns related to the exhausted GAC, an attempt was also made to regenerate the used GAC sample from the present work using chemical and electrochemical desorption methodologies. The electrochemical desorption method, which so far has been scantly investigated in the literature, was noted to successfully regenerate the used GAC sample, using a current density value of 50 mA $cm^{-2}$.

Factorial experimental design and optimization of parameters for the production of GAC from date pits, using Response Surface Methodology (RSM), was also completed. The respective results were acid to pits ratio of 1.5:1, carbonization temperature of 430°C, and $H_3PO_4$ concentration of 55%.

In summary, a high efficiency GAC sample was successfully produced from an otherwise waste material i.e., the palm date pits. The produced GAC was also noted to be very efficient for the removal of organic pollutants from the aqueous phase.

It is suggested that the use of activated carbon produced from date pits would be economical, since date pits are a waste product and available in large quantity in the

Kingdom of Saudi Arabia, and phosphoric acid is manufactured from local resources in the Kingdom.

# Chapter 1:

# INTRODUCTION

## 1.1 Background

Adsorption is one of the most effective processes of advanced wastewater treatment to reduce trace hazardous organic and inorganic compounds left in effluents after conventional treatment. It is also used to remove toxic inorganic and organic compounds from contaminated groundwater. In water treatment, the most widely used method is adsorption by the use of activated carbon. The relative advantages of adsorption over other conventional advanced treatment methods such as chemical treatment are: (1) it can remove both organic as well as inorganic constituents even at very low concentrations, (2) it is relatively easy and safe to use, (3) both batch and continuous processes can be used, (4) there is no sludge formation, and (5) the adsorbent can be regenerated and used again. Moreover, the process is economical because it requires low capital cost and there are abundant low-cost materials available which can be used as adsorbents, after suitable preparation.

Activated carbon is perhaps one of the most widely used adsorbents and is produced from a wide variety of carbon-rich raw materials, including wood, coal, peat, coconut shells, nut shells, bones and fruit stones. New materials such as molasses and palm oil trunks are currently under investigation as raw materials for activated carbon. Almost any organic matter with a large percentage of carbon could theoretically be activated to enhance its adsorptive characteristics. In practice, however, the best candidates for activated carbon contain a minimum amount of organic material, have a long storage life, are robust enough to maintain their properties under usage

conditions, are obtained at a low cost, and are capable of producing a high-quality activated product when processed. The continuously increasing list of environmental concerns and the interest in utilization of various wastes have awakened the interest in development of new processes for production of carbon adsorbents using agricultural wastes. As the production of an activated carbon must satisfy economical viability with high performance, cheap precursor materials readily available and convertible to an activated carbon using the minimum of resources could become very attractive raw materials. In recent years, there has been an increasing awareness of limited water resources. This recognition has led to the concept of water reuse rather than disposal. Acceptance of the concept of reuse has been accelerated by the development of new wastewater treatment processes that can economically yield clean, high quality water. One such process involves the adsorption of wastewater contaminants by activated carbon. The raw material from which a given activated carbon is produced often has a significant effect on its porosity distribution and surface area. As a result, activated carbons (ACs) produced from different raw materials may have very different adsorbent qualities. Surface features, such as porosity, surface chemistry, density, and mechanical stability govern the application of activated carbon as adsorbents. Nutshells, including coconut shells and pecan shells, produce activated carbons with high micropore (pores which are less than 2 nm in equivalent pore diameter) volumes. In the United States, about 55% of activated carbons are produced in powder form, and about 40% in granular form; the remainder is manufactured as pellets (Bansal *et al.*, 1988). One of the most widespread uses of activated carbons for liquid-phase adsorption is in water treatment. Many synthetic organic chemicals, such as pesticides, herbicides, detergents, polycyclic aromatic hydrocarbons, phenolic compounds, trihalomethanes

and other pollutants, have been identified in water supplies, and these have to be removed to ensure safety. The use of granular activated carbon for the treatment of municipal and industrial wastewaters has developed rapidly in the last few years. Moving beds, downflow fixed beds and upflow expanded beds have all been used in industrial wastewater applications. In most wastewater applications, the cost of virgin carbon usually precludes its use on a throwaway basis. Although there are many studies in the literature relating to the preparation and characterization of activated carbon from agricultural wastes as mentioned before, there is no information on the preparation of activated carbon using palm date pits as the precursor with phosphoric acid as the chemical activating agent.

Considering this, the main goal of the present work is to investigate the production of granular activated carbon (GAC) from the palm date pits and test the optimum GAC sample for the treatment of both synthetic and industrial wastewater. The GAC surface properties that play a very critical role during the removal of target pollutants from the aqueous phase, would also be optimized using several production phase variables such as the impregnation ratio (or acid to pits ratio, w/w).

## 1.2 Dissertation Organization

This research work is divided into six chapters. This first chapter deals briefly with the various raw materials used for the production of activated carbons. The second chapter reviews the state-of-the-art of activated carbon production from agricultural by-products and its use in various fields. Special consideration is given to the production process and various precursors as raw materials. The third chapter highlights the materials and methods used in this study. The fourth and fifth chapters

are devoted to a discussion of the generated data in analytical and statistical terms, respectively. Finally, the sixth chapter summarizes the results of the research work and also includes recommendations for future work.

# Chapter 2:

## STATE-OF-THE-ART REVIEW

Many industrial wastewaters contain organics which are difficult, or impossible, to remove by conventional biological treatment processes (Crauford and Cline, 1990). Phenols as a class of organics are similar in structure to the more common herbicides and insecticides in that they are resistant to biodegradation. Their presence in water supplies is noticed as a bad taste and odour (Mostafa *et al.*, 1989). In the presence of chlorine in drinking water, phenols form chlorophenol, which has a medicinal taste, which is quite pronounced and objectionable. Phenolics constitute the 11th of the 126 chemicals which have been designated as priority pollutants by the United States Environmental Protection Agency (Caturla *et al.*, 1998). There are many methods such as oxidation, precipitation, ion exchange and solvent extraction to remove phenolic materials from aqueous solution. However, in water treatment the most widely used method worldwide is adsorption onto the surface of activated carbon (Halhouli *et al.*, 1995). Activated carbons remove many of the impurities occurring in water and wastewater.

Textile dyeing industry wastewater is one of the major environmental pollutants of our time. It is difficult to treat dye effluent because hot and strongly coloured dyeing wastewater contains a large amount of suspended solids, with a high chemical oxygen demand (COD) concentration and greatly fluctuating pH. Colour is the most obvious indicator of water pollution. The discharge of coloured wastewater is not only damaging to the aesthetic nature of receiving streams, but also it may be toxic to aquatic life. In addition, colour interferes with the transmission of sunlight into a

stream and therefore reduces photosynthetic action. Recently a number of non-conventional adsorbents have been used for colour removal from wastewater by several investigators. These include agricultural solid wastes such as biogas residual slurry (Namasivayam and Yamuna, 1995), coconut husk (Low and Lee, 1999), orange peel (Namasivayam *et al.*, 1996), bagasse and paddy straw (Deo and Ali, 1993), and industrial solid wastes such as Fe(III)/Cr(III) hydroxide (Namasivayam *et al.*, 1996), red mud (Namasivayam and Arasi, 1997), and fly ash (Gupta *et al.*, 1998). In Saudi Arabia, pretreatment is required before discharging coloured water to general treatment facilities. The removal of dyes from effluents in an economic fashion remains an important problem. Considerable work has been carried out on the removal of colour from textile dying industry wastewater through adsorption (Namasivayam and Kadirvelu, 1994, Namasivayam and Yamuna, 1994, and Namasivayam and Kanchana, 1993). Adsorption seems to offer the best prospects over all other treatment techniques. The advantages and disadvantages of some methods of dye removal from wastewaters are summarized in Table 2.1.

Activated carbon is considered to be the most popular adsorbent and has been used with great success, but it is expensive. The high cost of activated carbon has stimulated interest in examining the feasibility of using cheaper raw materials. Substitute materials tested include straw, automobile tyres, fly ash, coal reject, sewage sludge, bagasse, fertilizer waste and sawdust (Streat *et al.*, 1995, Lu *et al.*, 1995, Lu, 1996, Srivastava *et al.*, 1995, Gupta *et al.*, 1998, and Vinod *et al.*, 2000). Because of the high cost and variable performance of carbon regeneration, single use materials are desirable (Ding *et al.*, 1987).

**Table 2.1: Advantages and disadvantages of the methods used for dye removal from industrial effluents (Robinson *et al.*, 2001)**

| Methods | Advantage(s) | Disadvantage(s) |
|---|---|---|
| Ozonation | No change in effluent volume | Short half life (1200 sec) |
| Photochemical | No sludge generation | Formation of byproducts |
| Electrochemical | Non-hazardous end products | High cost of electricity |
| Activated carbon | Highly effective for dyes | Very expensive |
| Peat | Good adsorbent | Surface area is low |
| Silica gel | Effective for basic dyes | Side reactions in effluents |
| Membrane filtration | Removes all dyes | Concentrated sludge production |
| Ion exchange | No adsorbent loss | Not effective for all dyes |

Carbon adsorbents are complex products which are difficult to classify on the basis of their behaviour, surface characteristics, properties or utility. However, they are usually categorized according to their particle shape and size. As mentioned earlier, about 55% of activated carbons are produced in powder form, and about 40% in granular form; the remainder is manufactured as pellets. About 80% of the total production (powder, granular and pellets) is used in liquid-phase applications, with the remaining 20% in gaseous-phase applications (Bansal *et al.*, 1988). The suitability of an activated carbon for a particular application depends on the ratio in which pores of different sizes are present. While granular forms are more desirable for continuous or cycling processes, powdered carbons find greater use in once-through processes.

## 2.1 Raw Materials for the Production of Activated Carbons

The principal adsorptive and physical properties of manufactured activated carbons depend on the type and properties of the raw material used. Any cheap substance with a high carbon and low inorganic content can be used as a starting material for the production of activated carbon. Important considerations when choosing a commercial carbon precursor include cost, availability, quality, workability, and, particularly in the case of coals, peat and lignite, the mineral matter and sulfur contents.

A wide range of carbons exists for possible use as adsorbents. A large number of activated carbons have been prepared from different raw materials, such as coconut shells, rice husks, nut shells, peat moss, and peat. Each has its own applications and limitations. Commercially-available activated carbon is expensive. The selection of raw materials is based mainly on criteria such as low inorganic matter, ease of

activation, availability and low cost, and low degradation upon storage (Rodriguez-Reinoso, 1997).

Table 2.2 shows the properties of some raw materials and the characteristics of activated carbon prepared from them.

Table 2.3 shows the chemical composition of some agricultural wastes. From the Table, it is evident that apricot tree waste is low in ash content and high in carbon content, and this makes it a very good candidate for activated carbon production.

Table 2.4 presents some carbonization and activation conditions for the production of the activated carbon from agricultural residues. The temperatures used for these wastes vary from 127 °C to 1000 °C. Chemical activation was the most widely used treatment process for agricultural wastes.

## 2.2 Production of Activated Carbons

Activated carbon is produced by exposing selected carbonaceous materials to a series of treatment processes referred to as dehydration, carbonization and activation. As a result of carbonization, volatiles are eliminated, hydrogen is lost, and a fixed carbon mass with a rudimentary porosity is formed. This pore structure is developed further during activation. Carbon activation procedures can be broadly divided into two main types: physical and chemical. Physical activation is a heterogeneous, solid-gas reaction, involving the gasification of the more reactive portions of the carbon skeleton of the carbonized precursor by oxidation with water vapour or carbon dioxide in the 850-1000 °C temperature range. In the chemical activation process, carbonization and activation are carried out in a single step by thermal decomposition of the starting material with reagents such as phosphoric acid, zinc

**Table 2.2: Properties of materials used in the production of activated carbon (Streat *et al.*, 1995)**

| Raw material | Carbon (mass %) | Volatiles (mass %) | Density (kg $m^{-3}$) | Ash (mass %) | Texture of the carbon |
|---|---|---|---|---|---|
| Soft wood | 40-45 | 55-60 | 400-500 | 0.3-1.1 | Soft, large pore volume |
| Hard wood | 40-42 | 55-60 | 550-800 | 0.3-1.2 | Soft, large pore volume |
| Lignin | 35-40 | 58-60 | 300-400 | - | Soft, large pore volume |
| Nutshells | 40-45 | 55-60 | 1400 | - | Hard, large micropore volume |
| Lignite | 55-70 | 25-40 | 1000-1350 | 5-6 | Hard, small pore volume |
| Soft coal | 65-80 | 20-30 | 1250-1500 | 2-12 | Medium pore volume |
| Hard coal | 85-95 | 5-15 | 1500-1800 | 2-15 | Hard, large pore volume |

**Table 2.3: Agricultural residues availability, proximate and ultimate analysis (Skoulou and Zabaniotou, 2005)**

| Agricultural Wastes | Moisture %ww | Ash %ww | Volatiles %ww | C %ww | H %ww | O %ww | N %ww | S %ww |
|---|---|---|---|---|---|---|---|---|
| Cotton stalks | 6 | 13.3 | n.a | 41.23 | 5.03 | 34 | 2.63 | 0 |
| Corn stalks | 0 | 6.4 | n.a | 45.53 | 6.15 | 41.11 | 0.78 | 0.13 |
| Soft wheat straw | 15 | 13.7 | 69.8 | n.a | n.a | n.a | n.a | n.a |
| Corn cobs | 7.1 | 5.34 | n.a | 46.3 | 5.6 | 42.19 | 0.57 | 0 |
| Sugar beet leaves | 75 | 4.8 | n.a | 44.5 | 5.9 | 42.8 | 1.84 | 0.13 |
| Rice straw | 25 | 13.4 | 69.3 | 41.8 | 4.63 | 36.6 | 0.7 | 0.08 |
| Oat straw | 15 | 4.9 | n.a | 46 | 5.91 | 43.5 | 1.13 | 0.015 |
| Sunflower straw | 40 | 3 | n.a | 52.9 | 6.58 | 35.9 | 1.38 | 0.15 |
| Cherry tree prunings | 40 | 1 | 84.2 | n.a | n.a | n.a | n.a | n.a |
| Apricot tree prunings | 40 | 0.2 | 80.4 | 51.4 | 6.29 | 41.2 | 0.8 | 0.1 |

**Table 2.4: Carbonization and activation conditions of agricultural residues, for the production of activated carbon**

| Reference | Raw material | Particle size | Carbonization conditions (°C/h) | Activation conditions (°C/h) | Treatment Processes | Additional information |
|---|---|---|---|---|---|---|
| Ahmedroup and Do, 1997 | Macadamia nutshell | 212–300 μm | 300/1 h | 500/1 h | Chemical ($ZnCl_2$) | Chemical activation with both $ZnCl_2$ and KOH |
| Lanzetta and DiBlasi, 1998 | Wheat | 100 μm | 127–375 °C/1 h | | | |
| Ahmedna *et al.*, 2000 | Sugarcane bagasse | 10–20 mesh and 12–40 mesh | 750 °C/1 h | 900/4 and 20 | $CO_2/N_2$ | |
| Ahmedna *et al.*, 2000 | Rice-straw | 10–20 mesh and 12–40 mesh | 750/1 h | 900/4 and 20 | $CO_2/N_2$ | |
| Marcilla *et al.*, 2000 | Almond shells | 1.5–2 mm | 400/1 h | 850/1 h | Physical | Different samples (either with $CO_2$ or $N_2$) |
| Minkova *et al.*, 2001 | Olive (steam)/($N_2$) | | | 750/2 (10 °C) | Steam/$CO_2$ | One-step pyrolysis/activation |
| Minkova *et al.*, 2001 | Straw (steam)/($N_2$) | | | 750/2 (10 °C) | Steam/$CO_2$ | One-step pyrolysis/activation |
| Minkova *et al.*, 2001 | Bagasse (steam)/($N_2$) | | | 750/2 (10 °C) | Steam/$CO_2$ | One-step pyrolysis/activation |
| Savova *et al.*, 2001 | Cherry stones/product | 0.2–1 mm | 800/1 h (15 °C/min) | 800/1 h | Steam | One-step pyrolysis/activation |
| Savova *et al.*, 2001 | Nutshells/product | 0.2–1 mm | 800/1 h (15 °C/min) | 800/1 h | Steam | One-step pyrolysis/activation |
| El-Hendawy *et al.*, 2001 | Corn cob | 0.5–2 mm | 500/2 hrs | 850/1 h | Steam | Physical activation/two-steps |

**Table 2.4: (continued)**

| Reference | Raw material | Particle size | Carbonization conditions (°C/h) | Activation conditions (°C/h) | Treatment Processes | Additional information |
|---|---|---|---|---|---|---|
| Girgis *et al.*, 2002 | Peanut hulls | n.a. | 500/2 hrs | 700–900 °C/ 1 h | Physical | Two-step process |
| Oh and Park, 2002 | Rice-straw | ca.3 cm | 700–1000/1 h (10 °C/min) | 900/2 hrs | KOH | Two-stage method |
| Aygun *et al.*, 2003 | Apricot stones | 1–1.25 mm | | 800/18 hrs | Chemical ($ZnCl_2$) | |
| Aygun *et al.*, 2003 | Almond shells | 1–1.25 mm | | 750/10 hrs | Chemical ($ZnCl_2$) | |
| Cetin *et al.*, 2004 | Eycalyptus | 1–2 mm | 950 °C (20 °C/s) | | | Suite of rectors (a wire mesh reactor, a tubular reactor and a drop tube furnace) |
| Ahmedna *et al.*, 2004 | Pecan shells | n.a. | | | Chemical ($H_3PO_4$) | |
| Putun *et al.*, 2005 | Cotton stalk | 0.25–1.8 mm (1.2) | 400 °C/1 h | | | Increase of residence time resulted in formation of activated carbon |
| Sudaryanto *et al.*, 2006 | Cassava peel | n.a. | n.a. | 750/2 hrs | Chemical (KOH) | For 3 h and 650 °C $S_{BET}$ = 1183 $m^2 g^{-1}$, impregnation ratio 1:1 |

chloride or potassium hydroxide. These activating agents act as both dehydrating agents and oxidants. The yield of the process is relatively large and it may exceed that of physical activation by up to 30% by mass. Other advantages of chemical activation are: (a) simplicity (no need of previous carbonization of raw material), (b) lower temperatures of activation and (c) good development of the pore structures (Rodriguez-Reinoso, 1997). Following activation, a final sizing operation takes place using sieve analysis.

## 2.3 Activated Carbon Production Using Agricultural By-products

As mentioned previously, several researchers have investigated the viability of producing activated carbon by using agricultural wastes, such as wheat straw, corncobs, soybean hulls, and cottonseed hulls. Gergova *et al.* (1992) investigated the processes of formation of the porous structure and the changes taking place on the surface of carbon adsorbents made from agricultural by-products during their preparation by water-vapour pyrolysis. They determined some of the sorption parameters of the adsorbents, such as specific surface area, assessed by argon thermal desorption, heat of wetting using hexane, and thermal effects of argon adsorption at 25 °C. Their experimental data proved that adsorbent properties depended on the nature of the raw material, the final temperature of the treatment process, and the duration of treatment at the final temperature.

Jagtoyen *et al.* (1992) conducted a study on the chemical activation of a bituminous coal. They found that there were clear differences in porosity development after thermal treatment in the range 350-650 °C, and after heat treatment in the same temperature range following reaction with phosphoric acid.

This process was accompanied by development of a mainly microporous structure which reached a maximum BET (Brunauer-Emmett-Teller) surface area of 750 $m^2 g^{-1}$. They concluded in their study that pore structure development could be tailored to some extent by varying both phosphoric acid strength and final heat treatment temperature.

Mirasol *et al.* (1993) investigated preparations of activated carbons from eucalyptus kraft lignin. They studied carbonization at different temperatures, and prepared activated carbons from carbon dioxide partial gasification of chars obtained at 550 and 800 °C. They found that activation increases both total and narrow microporosity and developed a substantial mesoporosity (equivalent pore diameter between 2 and 50 nm). BET surface areas in the vicinity of 1300 $m^2 g^{-1}$ were achieved.

Ahmadpour *et al.* (1996) prepared activated carbons from bituminous coal by chemical activation with zinc chloride. They studied the effect of process variables such as carbonization time, temperature, method of mixing, and impregnation ratio (acid to date pits ratio) in the chemical activation process. They found that out of these process variables, the impregnation ratio was the most important in the chemical activation of coal.

Warhurst *et al.* (1996) worked on the production of activated carbon for water treatment in Malawi using the waste seeds of *Moringa oleifera*. They showed that the crushed seeds of this tree could be used as a coagulant in water treatment. The same seeds could be converted into activated carbon by carbonization at 485 °C under $N_2$ for 30 minutes, followed by activation in steam at 850 °C for 5 minutes.

Philip and Girgis (1996) studied the feasibility of chemically activating apricot stone shells. They used different concentrations of phosphoric acid (20-50 wt %) for the chemical activation, followed by carbonization at 300-500 °C. A series of wide range

microporous activated carbons were obtained, with $SSA_{BET}$ of 640 to 1600 $m^2 g^{-1}$. It was found that increasing the acid concentration at 300 and 400 °C increased the surface area and pore volume, whereas at 460 °C a small decrease in both surface area and pore volume appeared at higher $H_3PO_4$ concentrations.

Johns *et al.* (1997) characterized and evaluated granular activated carbon (GAC), made from low value agricultural by-products, as effective removers of organics and metals from water. The by-products included rice straw, soybean hull, sugarcane bagasse, peanut shell, and harder materials such as pecan and walnut shells as shown in Table 2.5.

The softer materials were combined with molasses as a binder, to produce briquettes and pellets. All precursors were carbonized at 750 °C in $N_2$ for 1 h using a Grieve model bench furnace. The resulting chars were then crushed and sieved to produce granules of 10-20 mesh. The pellets or granulated chars were activated with carbon dioxide or steam. Steam was produced by the injection of water, using a peristaltic pump set at 0.4 $cm^3 min^{-1}$, into the bench furnace for 12 hours duration. Many of the GACs produced had acceptable physical GAC attributes, such as durability, for commercial usage. GACs made from pecan and walnut shells adsorbed higher levels of benzene, toluene, methanol, and acetonitrile from an aqueous mixture than certain commercial GACs.

Sai *et al.* (1997) succeeded in producing an activated carbon from coconut shell char using steam or carbon dioxide as the reacting gas in a 100-mm diameter fluidized bed reactor. The effect of process parameters such as reaction time, fluidizing velocity, particle size, static bed height, temperature of activation, fluidizing medium, and solid raw material on activation, were studied, and it was found that the

**Table 2.5: Granular activated carbons from agricultural by-products (Johns *et al.*, 1997)**

| Type of By-product | Char Yield (%)* | Activation Temp. (°C) | Duration (Hours) | Activant | Burn-off (%)** | Surface Area ( $m^2 g^{-1}$) |
|---|---|---|---|---|---|---|
| Peanut Shell Pellets | 30 | 850 | 10 | $CO_2$ | 17.3 | 127 |
| Peanut Shell Pellets | 30 | 800 | 12 | Steam | 25.0 | 478 |
| Rice Straw Pellets | 35 | 850 | 10 | $CO_2$ | 27.2 | 127 |
| Rice Straw Pellets | 35 | 800 | 12 | Steam | 11.7 | 400 |
| Sugarcane Bagasse Pellets | 35 | 850 | 10 | $CO_2$ | 20.3 | 490 |
| Sugarcane Pellets | 35 | 800 | 12 | Steam | 15.1 | 365 |
| Soybean Hull Pellets | 25 | 850 | 5 | $CO_2$ | 27.2 | 38 |
| Soybean Hull Pellets | 25 | 800 | 12 | Steam | 57.0 | 380 |
| Walnut Shell | 26 | 850 | 15 | $CO_2$ | 20.7 | 456 |
| Walnut Shell | 26 | 800 | 12 | Steam | 16.7 | 602 |
| Pecan Shell | 27 | 800 | 15 | $CO_2$ | 34.0 | 547 |
| Pecan Shell | 26 | 800 | 12 | Steam | 32.0 | 721 |

*Char yield is the ratio as a percentage between weight after carbonization and weight before carbonization.

**Burn-off is the % of volatiles after carbonization.

increase in all these process parameters resulted in better activation. It was observed that the maximum surface areas were obtained for the following conditions: 0.24 m $s^{-1}$ fluidization velocity, 1.55 m particle size, 100 mm static bed height, temperature of 850 °C, and steam as fluidization medium. Finally, it was concluded from the experimental investigations that the fluidized bed reactor could be more effectively employed for the production of activated carbon from coconut shell char compared to the conventional process.

Pitch-based activated carbons with high specific surface area were produced by Qiao *et al.* (1997) through a direct chemical activation route in which oxidized and stabilized pitch derived from ethylene tar oil was reacted with potassium hydroxide (KOH) under various activation conditions. It was found that activated carbons with surface area between 2600 and 3600 $m^2$ $g^{-1}$ could be obtained under suitable activation conditions. Compared with a commercially-available activated carbon, it was concluded that the specimens had larger adsorptive capacity for benzene due to their higher surface area. The surface area, pore volume, and average pore diameter of the resulting carbons increased with the carbonization temperature to a maximum at 500 °C and then began to decrease. The equilibrium and dynamic characteristics of the activated carbons produced were then compared in terms of the following micropore properties: surface area, volume, and half-width of the pore. Carbons activated by KOH resulted in a more microporous structure, while those activated by zinc chloride were more mesoporous (pores between 2 and 50 nm). High surface area samples were further studied in terms of their methane adsorption uptake and it was found that macadamia nutshell-derived activated carbons had a higher adsorption capacity per unit mass than those derived from coal.

Teng and Yeh (1998) also prepared activated carbons by chemical activation of two

Australian bituminous coals by zinc chloride impregnation, followed by carbonization in nitrogen. The carbonization temperature ranged from 400 to 700 °C. The experimental results revealed that an acid-washing process following the carbonization with $ZnCl_2$ was necessary for preparing high-porosity carbons. Table 2.6 summarizes the effect of carbonization temperature on the surface properties of the carbons from $ZnCl_2$ activation. It was found that the surface area, pore volume, and average pore diameter of the resulting carbons increased with the carbonization temperature to a maximum at 500 °C and then began to decrease with further temperature rise.

Ahmadpour *et al.* (1998) produced activated carbons by using chemical activation of coal and macadamia nutshell precursors with KOH and $ZnCl_2$. Table 2.7 shows the physical characteristics of the activated carbons produced.

Pecan shell chars were activated by Johns *et al.* (1999) using either steam, carbon dioxide ($CO_2$), or phosphoric acid ($H_3PO_4$) to produce granular activated carbon. The GACs were characterized for selected physical, chemical and adsorption properties. The Brunauer-Emmett-Teller (BET) surface areas of the pecan carbons were equal to or greater than those of a selection of commercial GACs, as shown in Table 2.8. Carbon dioxide activation favoured microporosity (<2 nm equivalent diameter), while the other activations increased both mesoporosity (between 2 and 50 nm) and microporosity (<2 nm).

Porous carbons with a very high porosity were prepared from an Australian bituminous coal with potassium hydroxide (KOH) activation by Teng and Hsu (1999). The preparation process consisted of KOH impregnation followed by carbonization in nitrogen at 500-1000 °C for 0-3 hours. The surface area and pore volume of the resulting carbons were found to increase with the carbonization

**Table 2.6: Effect of carbonization temperature on the surface properties of two types of activated carbon produced by zinc chloride activation of two Australian bituminous coals (Teng & Yeh, 1998)**

| Carbonization temperature (°C) | Surface area ($m^2 g^{-1}$) | Pore volume ($cm^3 g^{-1}$) | Average pore diameter (nm) |
|---|---|---|---|
| **(Type I)** | | | |
| 400 | 501 | 0. 28 | 2.2 |
| 500 | 1300 | 0. 83 | 2.5 |
| 600 | 895 | 0. 55 | 2.4 |
| 700 | 858 | 0. 49 | 2.3 |
| **(Type II)** | | | |
| 400 | 775 | 0.00041 | 2.1 |
| 500 | 1080 | 0.00065 | 2.4 |
| 600 | 994 | 0.00058 | 2.3 |
| 700 | 874 | 0.00050 | 2.3 |

**Table 2.7: Physical characteristics of activated carbons produced by chemical activation of coal and macadamia nutshell (Ahmadpour *et al.*, 1998)**

| Sample | Activant | Temperature (°C) | Activation time (sec) | Surface area ( $m^2 g^{-1}$) |
|---|---|---|---|---|
| Coal | KOH | 700 | 7200 | 850 |
| Coal | $ZnCl_2$ | 500 | 3600 | 1062 |
| Nutshell | KOH | 700 | 3600 | 1075 |
| Nutshell | $ZnCl_2$ | 500 | 3600 | 1718 |

**Table 2.8: Surface areas of commercial activated carbons and pecan shell carbons activated by steam, carbon dioxide and phosphoric acid (Johns *et al.*, 1999)**

| **Pecan Shell Carbons** | |
|---|---|
| **Activation Type** | **Surface Area ($m^2 g^{-1}$)** |
| Steam | 1149 |
| Carbon Dioxide ($CO_2$) | 877 |
| Phosphoric Acid ($H_3PO_4$) | 1561 |
| **Commercial Activated Carbons** | |
| **Commercial Activated Carbon Type** | **Surface Area ( $m^2 g^{-1}$)** |
| Filtrasorb 400 | 944 |
| GRC-20 | 928 |
| RO 3515 | 791 |
| Hydrodarco GCW | 874 |
| Hydrodarco 4000 | 575 |

temperature to a maximum at 800 °C, and then began to decrease. It has been suggested that carbon gasification by the released $CO_2$ and the oxygen in potassium-containing compounds plays an important role in determining the pore structure. The porosity development was affected by the chemical ratio of KOH to coal. The optimum chemical ratio for preparing a high-porosity carbon varies with carbonization conditions. A process consisting of impregnation at a chemical ratio of 4.25 followed by carbonization at 800 °C for 1 h, was recommended for producing a high surface area (>3000 $m^2$ $g^{-1}$) carbon.

Cox e*t al.* (1999) produced carbon adsorbent from flax shive by treatment with sulfuric acid. Several factors were considered in the preparation: reaction time, temperature, and the amount and concentration of sulfuric acid. Based on the temperature considered, two types of carbon were produced, C160 and C200. The first type (C160) was made with a mixture of flax shive and sulfuric acid heated to 160 °C for 15-20 minutes, whereas the second type (C200) was made with the mixture heated to a temperature of 200 °C for the same duration. The two types of carbon were tested for the removal of cadmium (II) and mercury (II) from aqueous solution. It was concluded that the carbon prepared at 160 °C, which is C160, was suitable for the removal of mercury (II) from aqueous solution.

Lua and Guo (1999) studied the chars carbonized from extracted oil palm fibers for the production of activated carbons. The effects of carbonization temperature and duration on density, porosity, yield, micropore surface areas, total pore volume, and pore size distributions of chars were investigated. The optimum temperature and time for the carbonization were found to be 850 °C and 3.5 hours, respectively. The experimental results showed that it was feasible to produce chars with high surface areas (520.6 $m^2$ $g^{-1}$) from extracted oil palm fibers. Then, the produced chars were

subjected to steam or carbon dioxide activation to prepare the activated carbon to be used as gas adsorbent for air pollution control.

Tam and Antal (1999) adopted a three-step process for the production of high quality activated carbons from macadamia nutshell and coconut shell charcoals. In this process, the charcoal was (i) heated to a high temperature of 900 °C for 15 minutes in an inert environment (carbonized), (ii) oxidized in air following a stepwise heating programme from low (177 °C) to high (387 °C) temperatures (oxygenated), and (iii) heated again in an inert environment to a high temperature of 827 °C (activated). Activated carbons with surface areas greater than 1000 $m^2$ $g^{-1}$ were produced.

Dai and Antal (1999) produced an activated carbon from macadamia nutshell charcoal by heating it in an inert environment to temperatures above 727 °C for 25 minutes (carbonized), reacted with oxygen at temperatures between 252 and 313 °C for a period varying from 4.5 minutes to 260 minutes (oxygenated), and heated again in an inert environment to temperatures above 727 °C for 15 minutes (activated). Activated carbons with surface areas ranging between 101 and 138 $m^2$ $g^{-1}$ were produced. These low values of surface area could be attributed to the fact that the material is very hard and dense and thus there is a strong possibility that the precursor material could have an effect on the adsorptive properties of the adsorbent. The processing conditions employing low oxidation temperatures and short processing times, and applying cheap activation agents ($O_2$), were found to be attractive compared to the conventional activation methods.

Evans *et al.* (1999) carried out production of activated carbon from sucrose in an inert environment with an excess of potassium hydroxide. The material was subjected to a regulated temperature-time profile to elevated temperatures

(400-900 °C) and subsequently cooled. The product was then exposed to an atmosphere of methanol vapour. This technique of exposing the material to methanol vapour was aimed at increasing the microporosity in the carbon. High yields of good microporous activated carbon were made at activation temperatures as low as 540 °C.

An activated carbon from oil-palm shells was produced by Guo and Lua (2000). This type of carbon was produced by impregnating the oil-palm shells with potassium hydroxide (KOH). The carbon was prepared by crushing and sieving the oil-palm shells to different sizes. After impregnating with 10% KOH at room temperature for 24 hours, the shells were filtered, washed with hot water and dried. Thereafter, the sample was carbonized in a vertical tube furnace under a flow of nitrogen. The furnace temperature was increased from room temperature to 600°C at the rate of 10 °C $min^{-1}$. This temperature was maintained for 2 hours. The resulting char was activated with carbon dioxide at 800 °C for 1 hour to produce the final product. The surface area of the activated carbon produced was found to be 1408 $m^2$ $g^{-1}$. The produced carbon was then used to study the adsorption of sulfur dioxide ($SO_2$). The experimental results showed that $SO_2$ could be adsorbed effectively by KOH-impregnated oil-palm shell activated carbons, whose adsorptive capacities were comparable to those of some commercial activated carbons.

Daud *et al.* (2000) conducted a series of experiments to study the effects of carbonization temperature on pore development in palm shell activated carbon. They undertook activation of char at 500, 800 and 900 °C. For all carbonization temperatures investigated, both micropore and macropore volumes showed maximum values at intermediate carbon burn-off. They found that only a small amount of mesopore developed in the initial stage of activation.

Hayashi *et al.* (2000) prepared activated carbon from lignin by chemical activation with phosphoric acid. They investigated the influence of carbonization and chemical agents on the pore structure. They found that maximum surface areas were obtained at the carbonization temperature of 600 °C in phosphoric acid activation, and that the surface areas were as large as those of commercial activated carbon (1000 $m^2$ $g^{-1}$).

Salame and Bandosz (2000) compared the surface features of two carbons of wood origin. One sample was manufactured using phosphoric acid activation and the other using potassium hydroxide activation. The carbon obtained using KOH activation was found to be homogeneously microporous with a high surface area of around 2300 $m^2$ $g^{-1}$. On the other hand, the carbon produced using phosphoric acid was found to contain high volume of mesopores and its surface area was significantly lower, being 1280 $m^2$ $g^{-1}$.

Mameri *et al.* (2000) developed a process for producing high quality activated carbon from Algerian olive mill waste. The solid olive mill residue was carbonized at 800 °C and physically activated with $CO_2$, air or steam. An optimum activation temperature of about 850 °C was determined for all the activation agents used. Steam appeared to be the most efficient activator (compared to air and $CO_2$) with an optimal activation time of about 2 hours. The specific surface areas produced exceeded 1500 $m^2$ $g^{-1}$. Then, experiments were conducted on the adsorption of phenol onto the activated carbon prepared. It was found that the activated carbon effectively adsorbed phenol with the adsorption capacity being 11.24 mg of phenol per gram of activated carbon.

Puziy *et al.* (2001) prepared synthetic activated carbon by phosphoric acid activation of a styrene-divinylbenzene copolymer at various temperatures in the range 400-1000 °C. The resulting carbons were characterized by elemental analysis, cation-

exchange capacity measurements, infrared spectroscopy, potentiometric titration with calculation of proton affinity spectra, and copper adsorption from solution. They found that the synthetic carbons possessed acidic character and cation exchange properties similar to those of oxidized carbons. They also found that carbons activated with phosphoric acid may be regarded as prospective cation-exchangers for the removal of heavy metals, such as copper, from water solutions.

Ariyadejwanich *et al. (2002)* produced and characterized activated carbons made from waste tyres. They carbonized rubber separated from waste tyres at 500 °C in the presence of nitrogen. As a result, mesoporous activated carbons with mesopore volumes and BET surface area up to 1.09 $cm^3 g^{-1}$ and 737 $m^2 g^{-1}$, respectively, were obtained. They found that the activated carbon from waste tyres was a suitable adsorbent for use in wastewater treatment, especially for the adsorption of high molecular weight compounds.

## 2.4 Applications and Uses of Agricultural based Activated Carbons

Adsorption on activated carbon (AC) has been an effective process for the purification of industrial and hazardous wastewaters, for advanced treatment of secondary effluents, and for the removal of organic pollutants from drinking water. Industrial wastes often contain organic pollutants that can be either toxic or resistant to common microorganisms, which means that the effluent cannot be adequately treated by biological action (Vidic *et al.*, 1990).

Urano *et al.* (1991) studied adsorption of chlorinated organic compounds on activated carbon from water. They investigated the feasibility of using granular activated carbon for the removal of seven principal chlorinated organic compounds. They found that the magnitude of adsorption of the chlorinated organic compounds

was in the order: tetrachloroethylene> trichloroethylene> dichloroethylene> dichloethane> carbon tetra-chloride> trichloroethane> chloroform. The respective activated carbon samples showed most affinity for tetrachloroethylene and trichloroethylene which are carcinogenic and the main pollutants in groundwater (Urano et al., 1991).

High-quality activated carbon was prepared from the waste husks of *Moringa oleifera* by Pollard *et al.* (1995). Steam activated husks exhibited a well-developed micropore volume of 0.57 $cm^3$ $g^{-1}$ and a corresponding apparent surface area 734 $m^2$ $g^{-1}$, as determined by BET $N_2$ adsorption hysteresis. In an assessment of aqueous phase adsorptive performance, *Moringa* carbon was found to be comparable to commercial powdered activated carbons (PACs) used in water treatment, and exhibited a Langmuir monolayer coverage constant ($Q^0$) of 1.89 mmol $g^{-1}$ for phenol adsorption from the aqueous phase.

Perez-Candela *et al.* (1995) conducted an experiment on the removal of Chromium (VI) by activated carbon. They carried out Cr (VI)-adsorption experiments to analyze the influence of pH, initial chromium concentration and carbon-solution contact time on the efficiency of Cr (VI) retention by the activated carbon. They found that the amount of chromium retained increased with increasing pH and initial chromium concentration. They came to the conclusion that the extent of adsorption and reduction processes depended on the porous texture and preparation procedure of the activated carbons.

Walker and Weatherly (1997) used Filtrasorb 400 granular activated carbon from Calgon Inc. to treat industrial wastewater from a nylon-carpet printing plant in a fixed bed treatment unit. They observed that the breakthrough curves from the fixed bed column were shallow, even at low flow rates, which indicated a large mass

transfer zone and inefficient use of adsorbent. They found that a decrease in adsorbent particle size and a decrease in linear flow rate produced better bed performance.

Gharaibeh *et al.* (1998) compared the carbonized solid residue of olive mill products (called J-carbon) with Sigma activated carbon (powder) and Chemviron activated carbon (0.6-0.7 mm) in the removal of $NH_3$, TOC (as non-specific organics), and six specific leading organic pollutants (benzothiazole, 1,2-dihydro-2,2,4-trimethyl-equinoline, N-dimorpholinyl ketone, methylsulphyl benzothiazole, methyl-2-benzothiazole sulphone and tetrachloroethene), from an industrial effluent. All the three different carbon sources had almost similar behaviour in removing the above pollutants. The removal efficiencies (percent removal) are shown in Table 2.9.

Dastgheib and Rockstraw (2001) used activated carbon from pecan shell for the removal of copper from aqueous solution. They came to the conclusion that the adsorptive capacity of pecan shell-based carbon was significantly higher than that of commercial carbons in the removal of copper from aqueous solution.

Ikuo *et al.* (2001) used activated carbon made from natural raw materials for removal of chloroform from drinking water. Chloroform adsorption was found to be enhanced by an increase in the specific surface area of the microporous carbon, but suppressed by enlargement of micropore size. This suppression was due to a decrease in the interaction, governed by the London dispersion force which is the weakest intermolecular force, between the chloroform molecules and the pore walls of the microporous carbon. These forces are the attractive forces that cause nonpolar substances to condense to liquids and to freeze into solids when the temperature is lowered sufficiently. Carbon with iodine adsorption capacity of around 760 mg $g^{-1}$ demonstrated the greatest chloroform adsorption, regardless of the raw material used.

**Table 2.9: Removal of $NH_3$ and six organic pollutants by different activated carbons** (Gharaibeh *et al.*, 1998)

| Pollutants | Sigma carbon (%) | Chemviron carbon (%) | J-carbon (%) |
|---|---|---|---|
| Benzothiazole | 100 | 100 | 100 |
| 1,2-dihydro-2,2,4-trimethylequinoline | 100 | 100 | 70 |
| N-dimorpholinyl ketone | 100 | 100 | 58 |
| Methyl-sulphyl benzothiazole | 100 | 100 | 100 |
| Methyl-2-benzothiazole sulphone | 100 | 100 | 100 |
| Tetrachloroethene | 50 | 31 | 70 |
| TOC | 94 | 40 | |
| $NH_3$ | 82 | 87 | |

The effectiveness of orange peel in adsorbing acid violet 17 from aqueous solutions has been studied by Sivaraj *et al.* (2001). They studied the removal as a function of agitation time, adsorbent dosage, initial dye concentration, and pH. They found that the adsorption process conformed to both the Langmuir and Freundlich isotherms. The equilibrium time was found to be 80 minutes for 10, 20, 30 and 40 mg $l^{-1}$ dye concentrations. They also found a maximum removal of 87% at pH 2.0 for an adsorbent dose of 600 mg per 50 ml of 10 mg $l^{-1}$ dye concentration.

The adsorption of basic dyes from aqueous solution onto granular activated carbon and natural zeolite has been studied by Meshko *et al.* (2001). They used an agitated batch adsorber and looked into the influence of agitation, initial dye concentration and adsorbent mass. They found that the dependence of solid diffusion coefficient on initial concentration and mass adsorbent was very high.

Patricia *et al.* (2002) developed activated carbon selection criteria that assure the effective removal of trace organic contaminants from aqueous solution and based the selection criteria on physical and chemical adsorbent characteristics. They used three granular activated carbons and two common drinking water contaminants (Methyl-Tertiary-Butyl-Ether, MTBE, and Tetrachloroethane, TCE) served as adsorbate probes. They found that TCE was adsorbed primarily in micropores in the 0.7-1.0 nm width range while MTBE was adsorbed primarily in micropores in the 0.8-1.1 nm width range. They found that effective adsorbents exhibit a large volume of micropores with widths that are about 1.3 to 1.8 times larger than the effective diameter of the target adsorbate. They also found that hydrophobic adsorbents more effectively removed TCE and MTBE from aqueous solution than did hydrophilic adsorbents.

Adsorption of nitrophenol onto activated carbon has been studied by Chern and Chien (2002). They experimentally determined by batch tests the adsorption isotherms of nitrophenol. They used a series of column tests to determine the breakthrough curves with varying bed depths (3-6 cm) and water flow rates (21.6-86.4 $cm^3$ $h^{-1}$). The effects of solution temperature and pH on the adsorption isotherms were also studied.

Cyr *et al.* (2002) studied the removal of organic mercury (Thimerosal) from pharmaceutical wastewater using Calgon F-400 granular activated carbon. They conducted a pilot scale study by using two GAC columns in series, each of 30 minutes empty bed contact times (EBCT). Simultaneous removal of copper, turbidity, phenol, and colour from the wastewater was also studied.

Guava seeds have been used for the production of activated carbon by Rahman and Saad (2003). The adsorption capacity of the activated carbon produced was demonstrated by the isotherms of tetramethylthionine chloride (methylene blue) from aqueous solution. They found that pyrolysis alone yielded a poor adsorbing carbon due to the blockage of pores by decomposition products of lignocellulosic materials. They concluded that optimum adsorption capacity was achieved when the samples were subjected to Zinc Chloride activation followed by pyrolysis at 700 °C.

Al-Zahrani *et al.* (2005) conducted an investigation of industrial pollutant removal using produced activated carbon amended with sand. They studied the best combination of carbon-sand percentage and the optimum column depth for achieving maximal removal of pollutants. They found that the removal of pollutants was significantly affected by bed depth and the percentage of the produced activated carbon amended with sand.

Activated carbons are used in industries as diverse as food processing, pharmaceuticals, chemical, petroleum, mining, nuclear, automobile and vacuum manufacturing, because of their adsorptive properties due to the high available area which is presented in their extensive internal pore structure. Such high porosity is a function of both the precursor as well as the scheme of activation (Dabrowski *et al.*, 2005).

The chemical nature of activated carbons significantly influences their adsorptive, electrochemical, catalytic, and other properties. Generally speaking, activated carbons with acidic surface chemical properties are favourable for adsorption of basic gases such as ammonia, while activated carbons with basic surface chemical properties are suitable for adsorption of acidic gases such as sulphur dioxide (Aslan and Turkman, 2005).

It is evident from the above discussion that high efficiency activated carbon can both be produced from several agricultural waste materials and successfully used for the treatment of wastewater. The respective findings have been summarized in Table 2.10.

## 2.5 Effects of Functional Groups and pH Value of Solution

The chemical nature of the surface of an activated carbon is the most important factor - apart from its porous structure - that determines its adsorption properties. In the adsorption of liquids on solids, the role of surface functionalities increases significantly relative to the pore size distribution or surface area. The predominant impact of oxidation and the consequent reduction of activated carbon surface area on phenol and 2-Methylphenol adsorption were first pointed out by Coughlin and Ezra

(1968). According to their results, the groups on the oxidized carbon were mainly carboxyl and hydroxyl ones, and a very small quantity of carbonyl groups. It was concluded that the carboxyl and hydroxyl groups inhibited the adsorption of phenol and 2-Methylphenol, and increased the affinity of the carbon towards water, and, therefore, the solvent molecules could effectively block some micropores.

**Table 2.10: Uses of activated carbons produced by agricultural residues**

| Reference | Uses | Raw material |
|---|---|---|
| Ahmedroup & Do, 1997 | Adsorption of methylene blue (liquid purification) | Peanut hulls, rice straw |
| Manju *et al.*, 1998 | Removal of arsenic | Wheat bran |
| Marcilla *et al.*, 2000 | Treatment of industrial gases and indoor air (air pollution control) | Almond shells |
| Gullon & Font, 2001 | Adsorption of atrazine | Pitch-based carbons |
| Malik, 2003 | Adsorption of acid dyes | Rice husk, orange peel |
| Kadirvelu *et al.*, 2003 | Removal of lead ions | Palm kernel fibre |
| Daifullah *et al.*, 2003 | Wastewater treatment | Rice husks |
| El-Sheikh *et al.*, 2004 | Groundwater treatment | Jordanian olive stones |
| Ahmedna *et al.*, 2004 | Removal of trace metals | Nutshell |
| Aslan and Turkman, 2005 | Removal of nitrate and pesticides | Wheat straw |
| Dabrowski *et al.*, 2005 | Removal of phenols and phenolic compounds | Wood, fruit stone, peat and lignite |

Hsieh and Teng (2000) studied the liquid-phase adsorption of phenol onto activated carbons prepared with different activation levels. Activated carbons of different porosities were prepared by carbonizing Australian bituminous coal to different extents of burn-off. Both the surface area and pore volume were shown to increase with the extent of carbon burn-off. It was shown that the function of mesopores was simply to provide an easy access for phenol molecules to micropores, and the amount of phenol adsorbed by the mesopores was, in fact, negligible.

## 2.6 Regeneration Methods of Exhausted Activated Carbons

Martin and Ng (1985) carried out, at the University of Birmingham, U.K., chemical regeneration of exhausted activated carbon. A wide range of regenerants, inorganic and organic, was evaluated in the treatment of carbon samples exhausted with 2-naphthol, 2-methoxyphenol, 2-chlorophenol, 2-Methylphenol and 2-nitrophenol, in order to compare the effects of the introduction of a second benzene ring. They found that there was a marked correlation between decreasing molecular weight of adsorbate and decreasing value of regeneration efficiency: the smaller the adsorbate, the further it could penetrate into the micropores of the carbon, thereby resisting displacement by the regenerant. Furthermore, they observed that the smaller the organic regenerant, the further it could penetrate into the micropores of the carbon and displace the adsorbate.

Ferro-Garcia *et al.* (1993) studied the regeneration of activated carbons exhausted with chlorophenols. They carried out chemical regeneration with solvents such as acetone, methanol, ethanol, and benzene. The best regenerant solvent was found to be ethanol. They found that the regeneration rate was dependent on both the porosity of the carbon and the chlorophenol isomer. Thermal regeneration was also used. The

spent activated carbons were heated up to 800 and 950 °C in an inert flow of nitrogen. In both regeneration methods, degradation reactions took place, giving light products such as water, carbon monoxide, carbon dioxide and hydrogen.

Moreno-Castilla *et al.* (1995a and b) studied the thermal desorption process of phenol from an exhausted activated carbon. They found that during heat treatment, part of the phenol exited from the activated carbon and was deposited at the outlet of the reactor and the remaining part underwent degradation to light gases and to a residue that remained on the surface of the carbon.

Ryoo *et al.* (1999) developed a countercurrent oxygen reaction for regeneration of exhausted activated carbon. They found that the regeneration technique was affected strongly by gradual loss and physical changes of activated carbon, energy consumption, and effective removal of adsorbed materials.

## 2.7 Different Uses of Date Pits

Date palm (*Phoenix dactylifera*) is a principal fruit that is grown in many regions of the world, resulting in a surplus production of dates. Date seeds (pits) constitute approximately 10-20% of the fruit (Al-Mana & Mahmoud, 1994). In the United States, date pits have been a problem to the date industry as a waste stream. Pulverized ground date pits are being used on a small scale, on dirt roads as a type of road base gravel. However, finding a way to make a profit out of the pits would benefit date farmers substantially. Occasionally, in the Middle East, date pits are used to feed animals such as horses.

## 2.8 Palm Dates in Saudi Arabia

Before oil became Saudi Arabia's primary industry, date farming was an important part of the national economy. During the early 1970s, date cultivation in the Kingdom became stagnant due to a lack of labour, poor technology and disappointing harvests. With the encouragement and assistance of the Saudi Government, the date industry was revived by the early 1980s. Today, the Kingdom is the world's second largest producer of dates, supplying 17.6 percent of the world market, with an annual production of 648 kilotonnes. The date farms of Saudi Arabia contain 14 million palm trees (www.saudiembassy.net). They grow primarily in the world's largest oasis, Al-Hasa, in the Eastern Province. There are about 400 varieties of dates in the Kingdom. The most popular in the Eastern Province are the *khalas*, *ruzeiz*, *kheneizy*, and *bukeira*. Pits from *khalas* were used in this study since it is one of the varieties that is most abundant in the market here in the Eastern Province of Saudi Arabia. The aim of the study is to explore the use of the pits for activated carbon (AC) production, in order to reduce the costs of importing activated carbon (Table 2.11) into the Kingdom of Saudi Arabia. Between 1995 and 2006, the Kingdom imported a total of 19731 tonnes of activated carbon, costing approximately $ 26.876 million. The Chamber of Commerce did not provide the quantity of imported activated carbon from 2003 to 2005.

The date production and estimated date pits generation in the Kingdom between 1996 and 2000 were 3,361,366 and 605,046 tonnes, respectively (Table 2.12), considering that the pits constitute approximately 18% by weight of the whole date. The high cost of imported activated carbon has stimulated interest in examining the feasibility of producing activated carbon locally, using available raw materials.

**Table 2.11: Activated carbon imported into the Kingdom in the period 1995-2006 (Chamber of Commerce, Eastern Province, KSA, 2007)**

| Serial # | Year | Quantity (tonnes) | Value (1000) US $ |
|---|---|---|---|
| 1 | 1995 | 414 | 835.1 |
| 2 | 1996 | 316 | 771 |
| 3 | 1997 | 880 | 2674 |
| 4 | 1998 | 2188 | 1787 |
| 5 | 1999 | 860 | 13928 |
| 6 | 2000 | 621 | 1412 |
| 7 | 2001 | 554 | 765 |
| 8 | 2002 | 674 | 960 |
| 9 | 2006 | 13224 | 3744 |

**Table 2.12: Date production data for several regions within the Kingdom of Saudi Arabia (Ministry of Agriculture, KSA, 2002)**

| YEAR | 2000* | | 1999 | | 1998 | | 1997 | | 1996 | |
|---|---|---|---|---|---|---|---|---|---|---|
| Regions | Dates | Pits | Dates | Pits | Dates | Pits | Dates | Pits | Dates | Pits |
| EASTERN | 95823 | 17248 | 93124 | 16762 | 97989 | 17638 | 98179 | 17672 | 91955 | 16552 |
| RIYADH | 185680 | 33422 | 162484 | 29247 | 171942 | 30949 | 172342 | 31022 | 171894 | 30941 |
| QASEEM | 112355 | 20224 | 108768 | 19578 | 78960 | 14213 | 79860 | 14375 | 69894 | 12581 |
| HAIL | 60545 | 10898 | 61491 | 11068 | 53569 | 9642 | 53269 | 9588 | 53859 | 9695 |
| TABOUK | 24345 | 4382 | 25650 | 4617 | 23414 | 4214 | 22214 | 3998 | 16132 | 2904 |
| MEDINAH | 82345 | 14822 | 82363 | 14825 | 58507 | 10532 | 58957 | 10612 | 58263 | 10487 |
| MAKKAH | 55342 | 9962 | 65833 | 11850 | 47086 | 8475 | 48086 | 8655 | 48635 | 8754 |
| ASEER | 75325 | 13559 | 79521 | 14314 | 80205 | 14437 | 79005 | 14221 | 68179 | 12272 |
| AL-BAHA | 2315 | 417 | 3315 | 597 | 980 | 176 | 905 | 163 | 1560 | 281 |
| JIZAN | 125 | 23 | 130 | 23.4 | 431 | 77 | 411 | 74 | 582 | 105 |
| NAJRAN | 12355 | 2224 | 13030 | 2345 | 9865 | 1776 | 10665 | 1920 | 10773 | 1939 |
| AL-JOUF | 28233 | 5082 | 16490 | 2968 | 25105 | 4519 | 25303 | 4554 | 25144 | 4526 |
| N.FRONTIER | 56 | 10 | 67 | 12 | 56 | 10 | 43 | 7.74 | 38 | 6.84 |
| **TOTAL** | **734844** | **132272** | **712266** | **128208** | **648109** | **116660** | **649239** | **116863** | **616908** | **111043** |

*Production in tonnes

## 2.9 Objectives of the Research

The primary objective of this research work, entitled "Production of activated carbon from palm date pits and its use in industrial wastewater treatment", was to evaluate the feasibility of the production of chemically-activated carbons with well-developed porosity from date pits and to find the optimum conditions for doing so. The proposed research, among other benefits, will contribute to measures for abating the environmental degradation caused by the indiscriminate dumping of palm date pits. It was decided to use phosphoric acid for activation of the carbon, as this is a resource that is available locally in Saudi Arabia. The Kingdom has an estimated 4.5 million tonnes of natural phosphate.

This research study is an extension of a project entitled "Industrial Pollutants Removal Using Produced Activated Carbon Amended Sand", funded by Saudi Basic Industries Corporation (SABIC) under Grant No. SABIC 2003/09.

Specific objectives can be summarized as follows:

- To produce activated carbon from palm date pits using three different stages of treatment (dehydration, carbonization, and activation).
- To determine the effectiveness of the activated carbons by conducting isotherm experiments for phenol and 2-Methylphenol adsorption.
- To run column studies for the determination of breakthrough curves for phenol and 2-Methylphenol.
- To find out the effect of environmental and operational variables such as pH and temperature on adsorption equilibrium.
- To carry out statistical analysis of the data.

- To conduct a preliminary investigation of the possibility of regenerating phenol-exhausted carbon.

# Chapter 3:

# MATERIALS & METHODS

The experimental part consisted of three major sections, namely, preparation of activated carbon, characterization of activated carbon, and adsorption measurements.

## 3.1 Activated Carbons

Date palm pits from the *khalas* variety of dates was used as the starting material in this research. Washed-clean whole date pits were dried in an air oven at 120 °C for 24 hours, which proved effective to facilitate subsequent crushing and grinding by using a Pulverisette 19 universal cutting mill, manufactured by Fritsch. The chemical composition of the oven-dried date pits is given in Table 3.1.

## 3.2 Activated Carbon Preparation

The date pits were first dried in an oven (manufactured by Fischer, model 750F) at 120 °C for 86400 seconds, ground, and sieved. Fractions of average size 0.002 m were used. Phosphoric acid was dissolved in water and added to date pits. The amount of solution was adjusted to obtain the desired ratio of phosphoric acid (dry basis) to dry pits. Excess water was then evaporated by drying in an oven at 120 °C overnight. The impregnated pits were packed into 0.025 m ID, 0.30 m long stainless steel tubes manufactured in the Department of Civil Engineering at the King Fahd University of Petroleum & Minerals (KFUPM). The tubes were nearly filled with the dry impregnated mixture then sealed, leaving a head-space of 0.5 mm at both ends of the tube. The tubes had two 0.001 m ports for release of any vapour produced.

**Table 3.1: Chemical composition of the oven-dried date pits**

| Compound | % |
|---|---|
| Moisture | 5–10 |
| Protein (N × 6.25) | 5–7 |
| Oil | 7–10 |
| Ash | 1–2 |
| Crude fibre | 10–20 |
| Carbohydrates | 55–65 |

The desired number of tubes containing samples impregnated with various ratios of phosphoric acid to date pits (R), namely 0.5:1, 0.8:1, 1.0:1.0, 1.2:1.0, 1.4:1.0, 1.6:1.0, 1.8:1.0, 2.0:1.0, 2.2:1.0, and 2.4:1.0, were placed inside a muffle furnace (manufactured by Lenton, model AWF12/42) and heated to the desired temperature (300, 400, 500, 600, or 700 °C). At a given temperature, one sample of each ratio was withdrawn at predetermined time intervals, namely after 1, 2 and 3 hours. The time to withdraw the samples from the furnace was calculated from the moment the furnace reached the desired temperature. The activated carbon obtained was removed from the cylinders. It was then thoroughly washed with 500 ml of 0.10 N HCl, and then rewashed thoroughly with distilled water and soaked in distilled water for 86400 seconds at room temperature. The solution was decanted and the activated carbon was dried at 120 °C for about 86400 seconds, and then weighed and stored for characterization. It was expected that this procedure was enough to remove any residual phosphoric acid and any soluble phosphate salts in the activated product because of the high solubility of phosphoric acid in water. This procedure has been used by several researchers in the past (Wu *et al.*, 1997, Jagtoyen and Derbyshire, 1998). Finally, the samples were dried at 120 °C for two hours, cooled and stored in closed containers. A total of 150 samples were thus produced. The stages of the production of activated carbon are shown in Figures 3.1 and 3.2, while the equipment used are shown in Plates 3.1, 3.2, 3.3, and 3.4.

## 3.3 Characterization of the Produced Activated Carbon

The produced carbon (PC) was characterized using standard procedures (American Public Health Association *et al.*, 1998). The specific surface area (SSA), pore

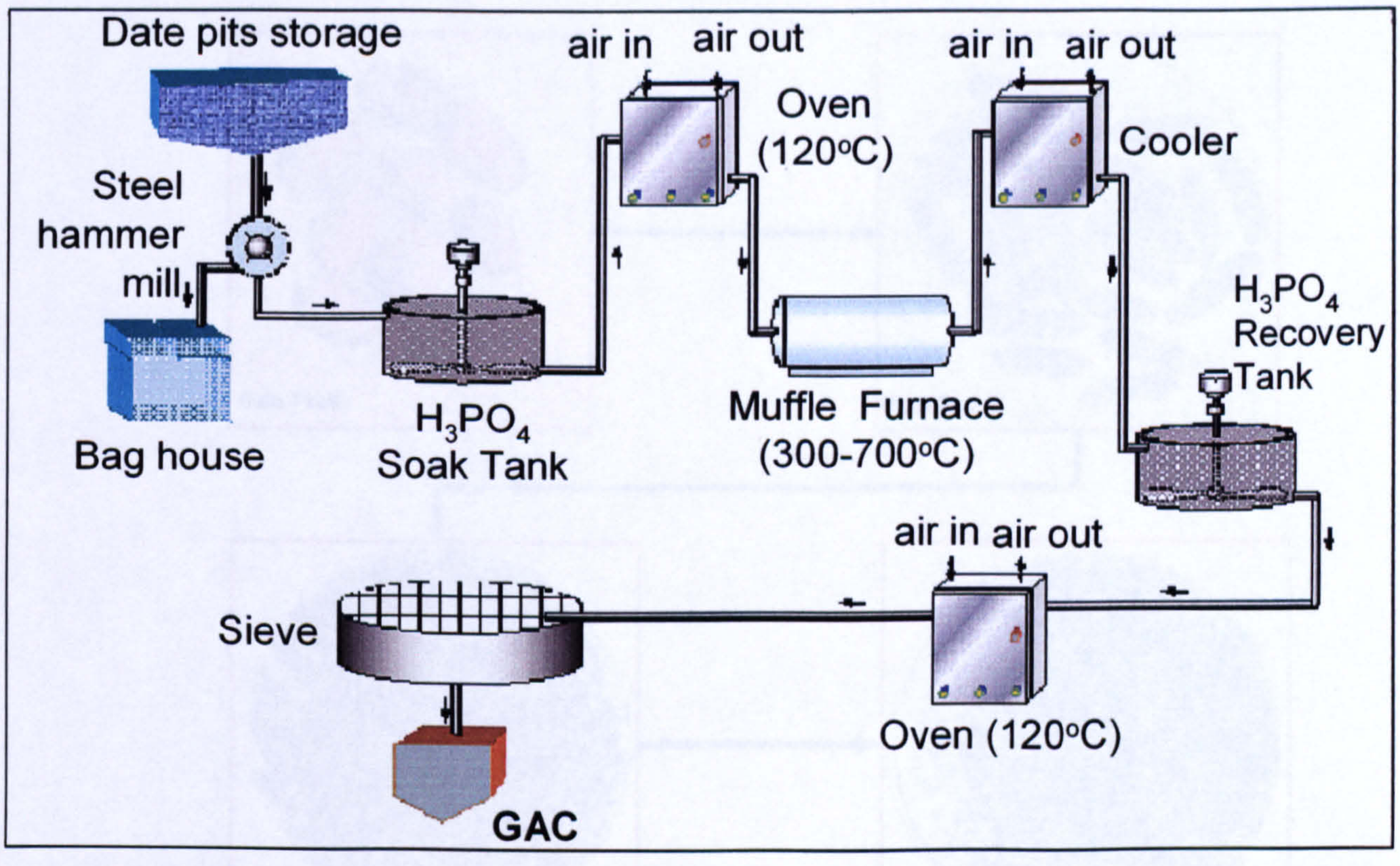


**Figure 3.1: Process flow diagram for the production of phosphoric acid-activated carbon from date pits**

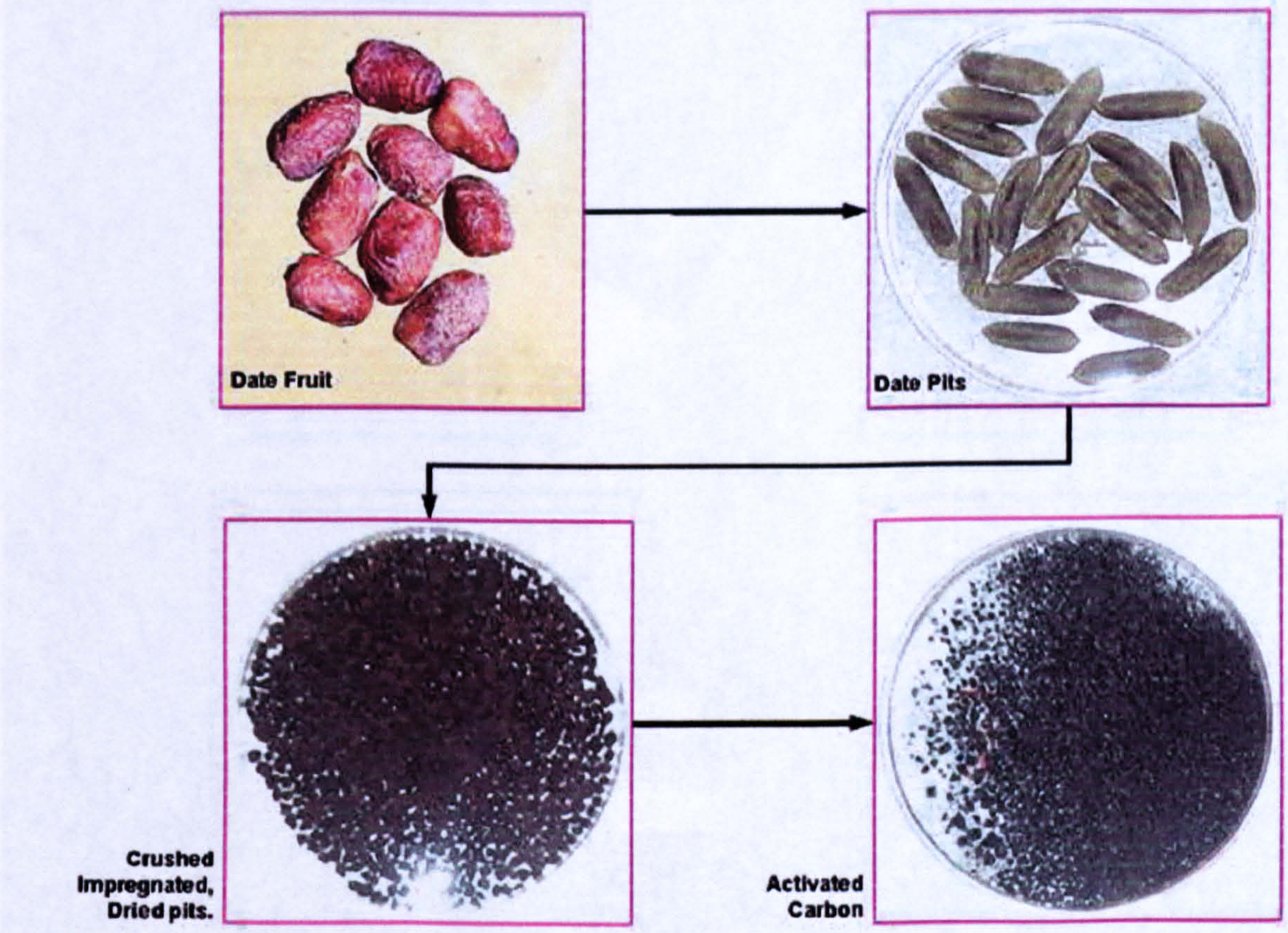


**Figure 3.2: Illustration of activated carbon production from date pits**


**Plate 3.1: Universal cutting mill, Pulverisette 19**


**Plate 3.2: Impregnated date pits in the oven overnight**

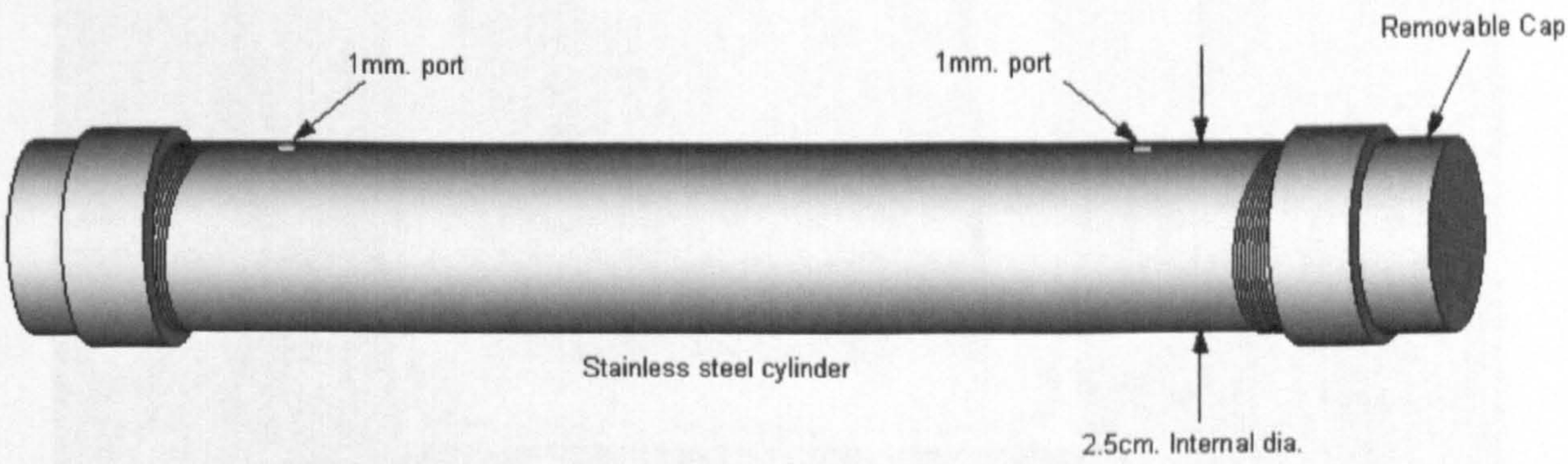


**Plate 3.3: The stainless steel cylinder used in the experiments**

**Plate 3.4: Carbonization of date pits in the muffle furnace**

volume, and iodine number (to assess the carbon's ability to remove low molecular weight compounds) were among the properties determined. The BET surface area, $S_{BET}$, was obtained using $N_2$ adsorption isotherms measured at -195.6 °C using an ASAP 2010 adsorption apparatus (accelerated surface area and porosimetry system, manufactured by Micromeritics Instrument Corporation) at the Research Institute, King Fahd University of Petroleum and Minerals. Total pore volume was measured with a Quantachrome NOVA 2200 series volumetric gas adsorption instrument (manufactured by Quantachrome Instruments Co.) at the Research Center, King Saud University.

The carbon sample was first out-gassed under vacuum at 250 °C for 7200 seconds. The SSA was estimated from the BET equation in a range of $P/P_o$ = 0.05-0.30, where P and $P_o$ are the equilibrium and the saturation vapour pressure of adsorbates at the temperature of adsorption. The total pore volume was determined from the amount of liquid $N_2$ held at $P/P_o$ = 0.98, and the mean pore radius from the empirical relation $R = 2\ V_p / S_{BET}$, where $V_p$ is the pore volume.

Gas sorption (both adsorption and desorption) at the clean surface of dry solid powders is the most popular method for determining the surface area of these powders as well as the pore size distribution of porous materials. The principle is that the material is heated and degassed by vacuum force or inert gas purging to remove adsorbed foreign molecules. Controlled doses of an inert gas (nitrogen in our case) are introduced and the gas is adsorbed, or alternatively, withdrawn and desorbed. The sample material (0.46 g) is placed in a vacuum chamber at a constant and very low temperature, usually at the temperature of liquid nitrogen (-195.6 °C), and subjected to a wide range of pressures, to generate adsorption and desorption isotherms. The amounts of gas molecules adsorbed or desorbed are determined by the pressure

variations due to the adsorption or desorption of the gas molecules by the material (the adsorbent). Knowing the area occupied by one adsorbate molecule, $\sigma$ ($\sigma = 0.162$ $nm^2$ for nitrogen), and using an adsorption model, the total surface area of the material can be determined. The most well known and widely used model is based on the BET equation for multilayer adsorption (Equation 3.1):

$$\frac{P}{n(P_o - P)} = \frac{1}{cn_m} + \frac{c-1}{cn_m}\frac{P}{P_o} \qquad (3.1)$$

In Equation (3.1), P, $P_o$, c, n, $n_m$ are the adsorption pressure, the saturation vapour pressure, a constant, the amount adsorbed (moles per gram of adsorbent) at the relative pressure $P/P_o$, and the monolayer capacity (moles of molecules needed to make a monolayer coverage on the surface of one gram of adsorbent), respectively. Through the slope and intercept of a plot of $P/[n(P_o–P)]$ against $(P/P_o)$, $n_m$ can be resolved. The specific surface area, S, can then be derived:

$$S = N_A n_m \sigma. \qquad (3.2)$$

In Equation (3.2), $N_A$ is Avogadro's number. The specific surface area that can be determined by gas sorption ranges from 0.01 to over 2000 $m^2 kg^{-1}$.

Bulk density was determined using ASTM standard D 2854. This was done by measuring the volume of activated carbon packed by free fall from a vibrating feeder into an appropriately-sized graduated cylinder and determining the mass of the known volume. The ratio between the mass of activated carbon and carbon volume gave the bulk density. The volume of activated carbon used was 0.1 $m^3$.

The percentage ash was determined following ASTM standard D 2866. An accurately weighed sample of dried activated carbon was placed in a controlled-temperature muffle furnace at 650 °C until constant weight had been achieved. This

was found to be true after 10 hours of drying. The crucible was cooled to ambient temperature in a desiccator and reweighed. The weight of the ashed carbon was expressed as a percentage of the weight of the original sample.

The pH of a water extract of activated carbon was measured following ASTM standard D 3838. An activated carbon sample was boiled in distilled water using a reflex condenser to recycle water vapour. The particles of carbon were filtered out and the filtrate cooled to ambient temperature and the pH determined using electrometric measurement.

The iodine number was determined using ASTM standard D 4607. A mass of 0.1 kg of activated carbon was ground up and put into a solution of iodine in water. After mixing, a certain amount of the iodine was adsorbed. By finding out how much iodine was left in the solution, it was possible to determine how much iodine had been adsorbed by the amount of activated carbon used.

The produced carbon was then compared with a commercial carbon (CC) Filtrasorb-400.

Table 3.2 shows several properties for the GAC produced from the date palm pits (PC) and also for a commercial GAC sample, i.e., Filtrasorb 400 (CC). The values indicated for the commercial carbon (CC) were taken from company literature. A quick comparison between the two GAC samples indicates that the PC has better surface properties (that are important for pollution control applications) and also much less ash content. It should be noted that the pH, bulk density, % weight loss, and % ash values for PC were determined using standard ASTM methods.

## 3.4 Apparatus Used in the Experiments

### *3.4.1 Universal Cutting Mill*

This cutting mill, Pulverisette 19", shown in Plate 3.1, was used in size reduction of the dried date pits. The mill allows a maximum feed size of 0.90×0.79 m with a maximum capacity of 0.0166 kg $s^{-1}$. The final fineness lies in the range 2.5-6 mm. The mill is suitable for sizing of hard material.

**Table 3.2: Properties of the produced activated carbon (PC) and commercial activated carbon (CC)**

| Sample | pH | Bulk Density, kg $m^{-3}$ | %Weight Loss | % Ash | Pore Volume, $cm^3 g^{-1}$ | Pore Radius, nm | Iodine # | $S_{BET}$ ($m^2 g^{-1}$) |
|---|---|---|---|---|---|---|---|---|
| PC | 6.7 | 590 | 36 | 0.50 | 0.785 | 1.19 | 110 | 1319 |
| CC | 6.2 | 440 | – | < 9 | 0.6 | 1.27 | 105 | 944 |

### *3.4.2 Shakers*

A G10 rotary shaker (New Brunswick Scientific, New Jersey, USA) was used in all experiments. The shaker can be used in environments from 4 °C -65 °C, allowing for cold room use as well as incubated applications. The shaker comprises the shaker base and the shaker platform. The shaker holds up to 48 bottles at a time. The shaker platform has a circular spring allowing it to hold bottles. The speed of the shaker can be varied from 10-200 rpm.

### *3.4.3 Mixers*

Four closed mixers used for mixing the test solution and keeping carbon in suspension were manufactured in the research workshop of the King Fahd University of Petroleum and Minerals (KFUPM). They were made from plexiglass with a capacity of 4 litres. The produced activated carbon particles were trapped in a basket around the wall of the mixer and the liquid was agitated by impellers at a speed of about 180 rpm. The mixer temperature was controlled by water circulating from a temperature controlled water bath in a surrounding water jacket. Figure 3.3 shows a schematic of the mixer setup.

### *3.4.4 pH Meter*

For pH measurements, a benchtop pH meter Model 550A (manufactured by Thermo Orion) was used. Auto-calibration is the feature of this meter that automatically recognizes as many as five Thermo Orion buffers: pH 1.68, 4.01, 7.00, 10.01, and 12.46, within a range of ± 0.5 pH units. Results greater than ± 0.5 pH unit from the correct value will trigger the meter to indicate that auto calibration is not being used. At this point, a manual calibration can be performed, or the calibration can be ended and repeated with fresh buffers. During calibration, one has to wait for a stable pH

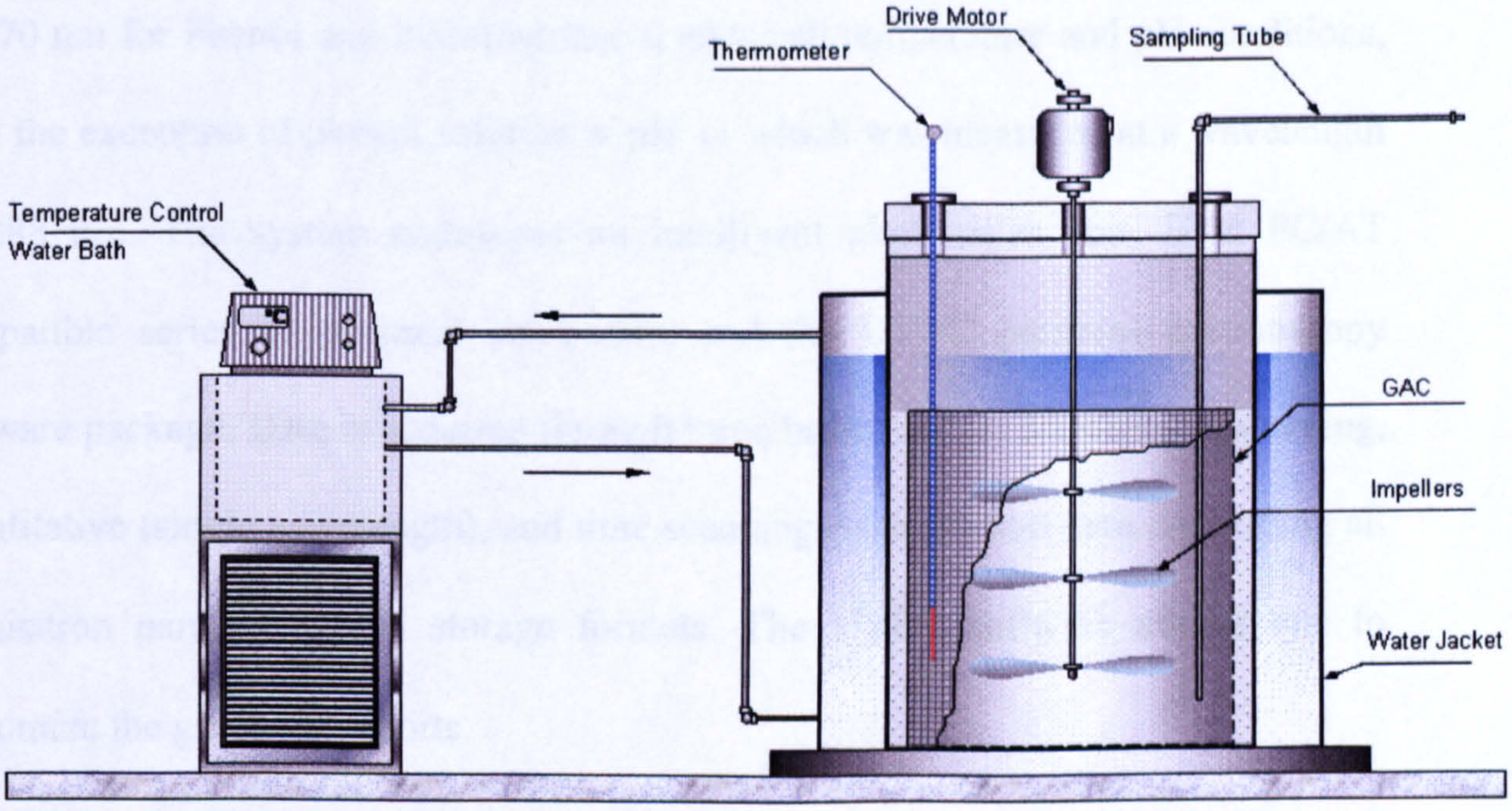


**Figure 3.3: Schematic diagram of the kinetics experimental setup**

reading. Once the electrode is stable, the meter automatically recognizes and displays the temperature-corrected value for that buffer.

### *3.4.5 UV Spectrophotometry*

A Shimadzu UV Spectrophotometer, Model UV-1601PC was used at a wavelength of 270 nm for Phenol and 2-Methylphenol under all temperature and pH conditions, with the exception of phenol solution at pH 11 which was measured at a wavelength of 288 nm. The system comprises an intelligent photometer unit, IBM PC/AT compatible series of personal computers, and the UVPC personal spectroscopy software package. Data is acquired through three basic modes: wavelength scanning, quantitative (single wavelength), and time scanning, with the software controlling all acquisition parameters and storage formats. The UVPC software allows one to customize the graphical reports.

### *3.4.6 Total Organic Carbon Analyzer*

A high-temperature TOC analyzer (DC-190), manufactured by Dohmann, was used for the measurement of total organic carbon (TOC) and total inorganic carbon (TIC) contents. The DC-190 system features a vertical quartz combustion tube packed with supported platinum catalyst which receives a continuous flow of oxygen at 200 cc $min^{-1}$. The furnace is normally maintained at 680 °C. Organic-containing samples are automatically introduced into the combustion tube via an air-actuated injection port. Through catalytic oxidation, the sample is completely oxidized to $CO_2$ and $H_2O$. The gas flow sweeps the $CO_2$-containing steam out of the combustion tube, through a condenser, and into a gas/liquid separator (inorganic carbon (IC) reactor) to trap most of the $H_2O$. Final $H_2O$ removal is accomplished by a dehumidifier. The dried $CO_2$ containing gas is then passed through a halogen scrubber and to a $CO_2$ specific non-

dispersive infrared detector (NDIR) for peak quantification. IC samples are automatically introduced in the IC reactor, which contains acidic solution at room temperature, via an air-operated injection port. In this acidic environment, all forms of inorganic carbon are purged out of the solution as $CO_2$ by the continuous flow of gas. The gas then continues on through the dehumidifier where it is dried and then passed through the NDIR detector for quantification.

### *3.4.7 Adsorbates*

Single solute stock solutions (1000 mg $l^{-1}$ each) of phenol and 2-Methylphenol of analytical grade (ANALAR) were prepared and subsequently buffered with $KH_2PO_4$ to maintain neutral pH. For each compound, two sets of 160-ml bottles containing identical amounts of 0.20 kg activated carbon were prepared and filled with $0.001m^3$ of adsorbate solution.

### *3.4.8 Effect of Dissolved Oxygen (DO)*

As oxygen is said to affect the adsorptive capacity of activated carbon, this aspect was investigated. After preparing the two adsorbates, for each activated carbon of interest, one set was purged with nitrogen until a zero level of dissolved oxygen (DO) was attained (Anoxic), and the bottles were quickly closed with a rubber stopper. Oxygen was purged in the other set until saturation was achieved as evidenced by a DO concentration around 30 mg $l^{-1}$ (Oxic). For the DO measurements, a DO Meter Model 862A (manufactured by Thermo Orion) was used. Before performing measurements, the oxygen probe had to be calibrated. This model has four types of calibration. The meter may be calibrated via air calibration (using water-saturated air as the calibration standard), water calibration (using air-saturated water as the calibration standard), or Winkler calibration (using the Winkler titration

as the basis for the calibration). The meter may also be calibrated by performing a Probe Zero calibration. If the expected sample DO range is at the lower end of the dissolved oxygen scale, it is recommended to perform a zeroing of the probe. If the probe exhibits any residual current, this calibration will compensate for it.

Each set of sample bottles included two bottles without activated carbon to serve as blanks to check for sorbate volatilization, and adsorption of sorbate onto the walls of the bottles. All the bottles were placed in a rotary shaker for a period of 14 days. At the end of the equilibrium period, samples were withdrawn from each bottle, filtered through 0.45 μm Millipore filter paper, and analyzed for residual sorbate concentration by using a spectrophotometer at a wavelength of 270 nm for both adsorbates.

### *3.4.9 Effect of Temperature*

In the case of temperature effect, the procedure of section 3.4.7 for phenol and 2-Methylphenol was repeated at temperatures of 10, 25, and 45 °C. The experiments were run using temperature-controlled shakers (Figure 3.3).

### *3.4.10 Source of Wastewater*

Industrial wastewater samples (5 litres) were collected in brown glass collection bottles with Teflon-lined caps directly from the outlet of the Jubail Petrochemical Plant (a phenolic-based industry) located at Jubail in the Eastern Province of the Kingdom of Saudi Arabia, during operation of the plant. Its physicochemical characteristics are listed in Table 3.3.

The samples were immediately brought to the laboratory to be placed in a deep freezer at a temperature of −6 °C. Before analysis, the sample was filtered with Whatmann filter paper No. 44. Analyses of parameters given in Table 3.3 were

conducted following the procedures outlined in Standard Methods for the Examination of Water and Wastewater, 20th edition.

Method 4500-H (pH Value) in Standard Methods for the Examination of Water and Wastewater, 20th Edition was used for the determination of the pH of the wastewater sample. A benchtop pH meter Model 550 A was used. The meter was first calibrated with three buffer standard solutions. The pH values for three replicates of the wastewater sample were then measured and the average value calculated. Method 5220 in Standard Methods for the Examination of Water and Wastewater, 20th Edition was used for the determination of Chemical Oxygen Demand. Three replicates of the same wastewater sample were refluxed in a strongly acidic solution with a known excess of potassium dichromate. After digestion, the remaining unreduced potassium dichromate in each replicate was titrated with ferrous ammonium sulphate to determine the amount of potassium dichromate consumed, and the oxidizable organic matter was then calculated in terms of oxygen equivalent.

Method 4500-Cl in Standard Methods for the Examination of Water and Wastewater, 20th Edition was used for determination of Chloride in the wastewater sample. Three replicates of the same sample were titrated with mercuric nitrate and the readings were averaged.

For the determination of Sulphate and Phenol, a Shimadzu UV Spectrophotometer was used at wavelengths of 420 and 269 nm, respectively. Solutions were diluted as required so that their absorbance remained within the linear calibration range. Absorbance readings were converted into concentration values by using the prepared calibration curves.

Method 2540 in Standard Methods for the Examination of Water and Wastewater, 20th Edition was used for the determination of Total Dissolved Solids. A well-mixed

sample was filtered through a standard glass fiber filter, and the filtrate was evaporated to dryness in a weighed dish and dried to a constant weight at 180 °C. The increase in dish weight represented the total dissolved solids.

Method 2510 in Standard Methods for the Examination of Water and Wastewater 20th Edition was used for the determination of Electrical Conductivity. Electrical conductivity is a function of the quantity and specific types of cations and anions in the water sample.

**Table 3.3: Physico-chemical characteristics of industrial wastewater obtained from Jubail, Saudi Arabia**

| Parameter | Value |
|---|---|
| pH | 7.2 |
| Electrical Conductivity ($\mu S\ cm^{-1}$) | 280 |
| Sulphate ($mg\ l^{-1}$) | 60 |
| Chloride ($mg\ l^{-1}$) | 53 |
| Total Dissolved Solids ($mg\ l^{-1}$) | 230 |
| Chemical Oxygen Demand ($mg\ l^{-1}$) | 480 |
| Phenol ($mg\ l^{-1}$) | 120 |

## 3.5 Adsorption Experiments

Before conducting adsorption measurements, activated carbon samples were washed with double distilled water and dried at 120 °C in an oven for at least 7200 seconds. The adsorption of tetramethylthionine chloride from aqueous solution was used to assess the quality of the AC obtained. For this purpose, 250 g of each the AC samples was added to 50 ml of tetramethylthionine chloride solution (350 mg $l^{-1}$) in a 200 ml conical flask and allowed to equilibrate at room temperature (23 °C) for an hour under continuous shaking. The carbon was then filtered and the concentration of tetramethylthionine chloride in the filtrate was determined using a spectrophotometer.

Adsorption of phenol was used to assess the quality of the produced carbon as compared to commercial carbons. Adsorption isotherms were constructed by making adsorption measurements at room temperature. For this purpose the desired amount of AC (previously washed with double distilled water then dried at 120 °C in an oven for at least 2 hours and kept in a closed container) was added to 25 ml of 500 ppm phenol solution in tightly closed conical flasks. The samples were shaken for two hours. This time was sufficient to establish equilibrium between the carbon and the solution. The carbon was filtered out and the residual concentration of phenol was determined using a UV-V spectrophotometer. Absorbance at 269 nm was used for quantification of phenol.

### *3.5.1 Batch Experiments*

To determine adsorption of phenol and tetramethylthionine chloride in admixture, 100 ml each of phenol and tetramethylthionine chloride (100 and 50 mg $l^{-1}$, respectively) were taken in 250 ml bottles and known amount of carbons was added.

The solution was equilibrated for 24 hours at 23 °C in a rotary shaker (New Brunswick Scientific, New Jersey, USA) at 90 rpm. Each set of bottles included two bottles without activated carbon to serve as blanks to check for sorbate volatilization, biodegradation, and adsorption of sorbate onto the walls of the bottles. After the equilibration period, the carbons were filtered and the filtrate analysed for tetramethylthionine chloride and phenol residual by using a UV-spectrophotometer (Shimadzu) at wavelengths of 664 and 269 nm, respectively.

### *3.5.2 Isotherm Tests*

Single-solute stock solutions of phenol and tetramethylthionine chloride (1000 and 100 mg $l^{-1}$, respectively) were prepared. For each compound, two sets of 160-ml bottles containing identical amounts of carbons were prepared and subsequently filled with 100 ml of adsorbate solution. All bottles were placed on a rotary shaker for a period of 14 days. At the end of the equilibration period, samples were withdrawn from each bottle, filtered through 0.45 um Millipore filter paper, and analyzed for sorbate residual concentrations using a UV-spectrophotometer at wavelengths of 269 and 664 nm for phenol and tetramethylthionine chloride, respectively.

### *3.5.3 Column Studies*

Phenol and 2-Methylphenol breakthrough curves were obtained using 60-cm long, 2.54-cm internal diameter plexiglass columns packed with the carbons. Prior to use, the columns were flushed with sweet water to check for leaks. Leaks discovered were sealed using epoxy until the columns were found to be leak-free. The plexiglass columns were covered with black plastic so as to cut out all light entering the columns. This was done to minimize photochemical reactions in the carbon columns

once the adsorbates were fed into it. The influent concentrations of adsorbates were maintained at 100 mg $l^{-1}$ for phenol and 2-Methylphenol for all the column experiments. The small ratio between the diameter and the length of the column prevented short-circuiting. The activated carbon columns were operated in a downflow mode at a flow rate of 60 ml $min^{-1}$, thus pumping 86.4 litres of feed solution through each column each day.

The same experiment was repeated but in upflow mode. Drawings of the experimental setup for both column tests are shown in Figures 3.4 and 3.5. In the process of loading the columns, the carbons to be used were first thoroughly wetted. This was done to remove air trapped in the carbon pores, as this would prevent the feed solution from contacting the pores. Once the carbon was soaked, the fines were removed. If fines are not removed, they can cause an excessive pressure drop across the carbon column and shorten the service life of the column.

## 3.6 Desorption Studies

Due to its large specific surface area and adequate pore size distribution, activated carbon (AC) has been widely employed in water and wastewater treatment. But AC is relatively expensive and readily saturated, thus it would not only be uneconomic but also bring about environmental pollution if the exhausted AC is not effectively regenerated for reuse. Therefore AC regeneration methods are urgently required for wide application of AC in treatment processes. There are many well-established techniques for the regeneration of AC including chemical regeneration, thermal regeneration, and electrochemical regeneration. Thermal regeneration is the most extensively used method in industry, but this process is time-consuming and has a high energy demand.

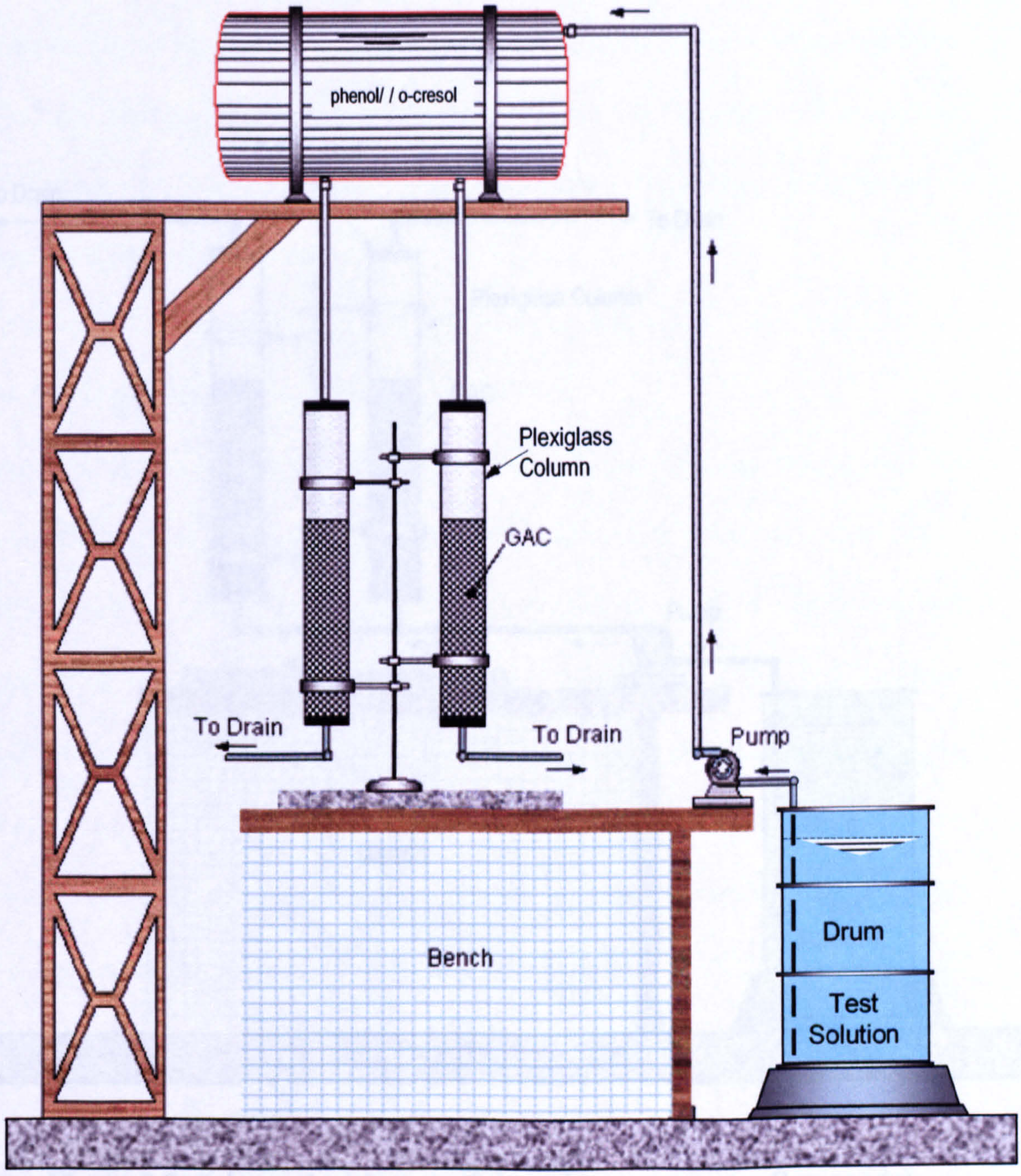


**Figure 3.4: Schematic diagram of the columns setup (downflow mode)**

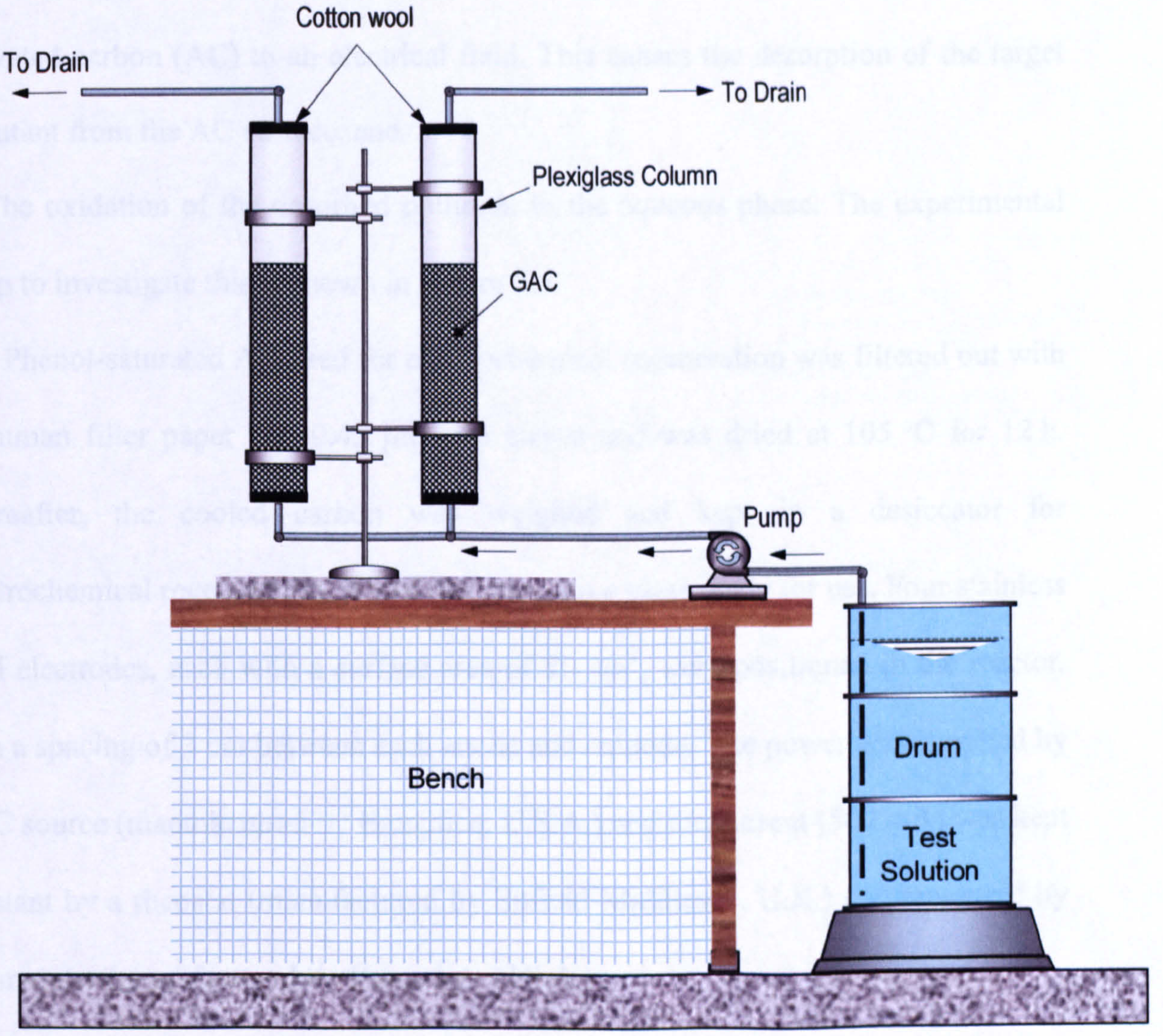


**Figure 3.5: Schematic diagram of the columns setup (upflow mode)**

Recently, AC regeneration by electrochemical oxidation has been reported as a promising option since a highly effective regeneration is possible with this method. The regeneration of exhausted activated carbon using an electrodesorption method as described by Zhang (2002) consists of two steps, i.e., 1) Exposure of exhausted activated carbon (AC) to an electrical field. This causes the desorption of the target pollutant from the AC surface, and

2) The oxidation of the desorbed pollutant in the aqueous phase. The experimental setup to investigate this is shown in Figure 3.6.

The Phenol-saturated AC used for electrochemical regeneration was filtered out with Whatman filter paper and 0.45 μm size sieves and was dried at 105 °C for 12 h. Thereafter, the cooled carbon was weighed and kept in a desiccator for electrochemical regeneration. It was then put into a glass ready for use. Four stainless steel electrodes, each with a surface area of 50 $cm^2$, were positioned in the reactor, with a spacing of 3 cm between each anode and cathode. The power was supplied by a DC source (manufactured by Hampden, U.S.A.) and the current (500 mA) was kept constant by a rheostat (manufactured by Enfield-Middlesex, U.K.) and measured by an ammeter (manufactured by Hampden, U.S.A.).

## 3.7 Experiment Flow Diagram

The experiment flow diagram is shown in Figure 3.7. The figure shows how the different production parameters are linked to each other. As it is shown, there are five carbonization temperatures, five percentages of $H_3PO_4$, ten impregnation ratios and three different holding times (10 × 5 × 5 × 3). The results of these experiments are shown in Appendices A, B and C.

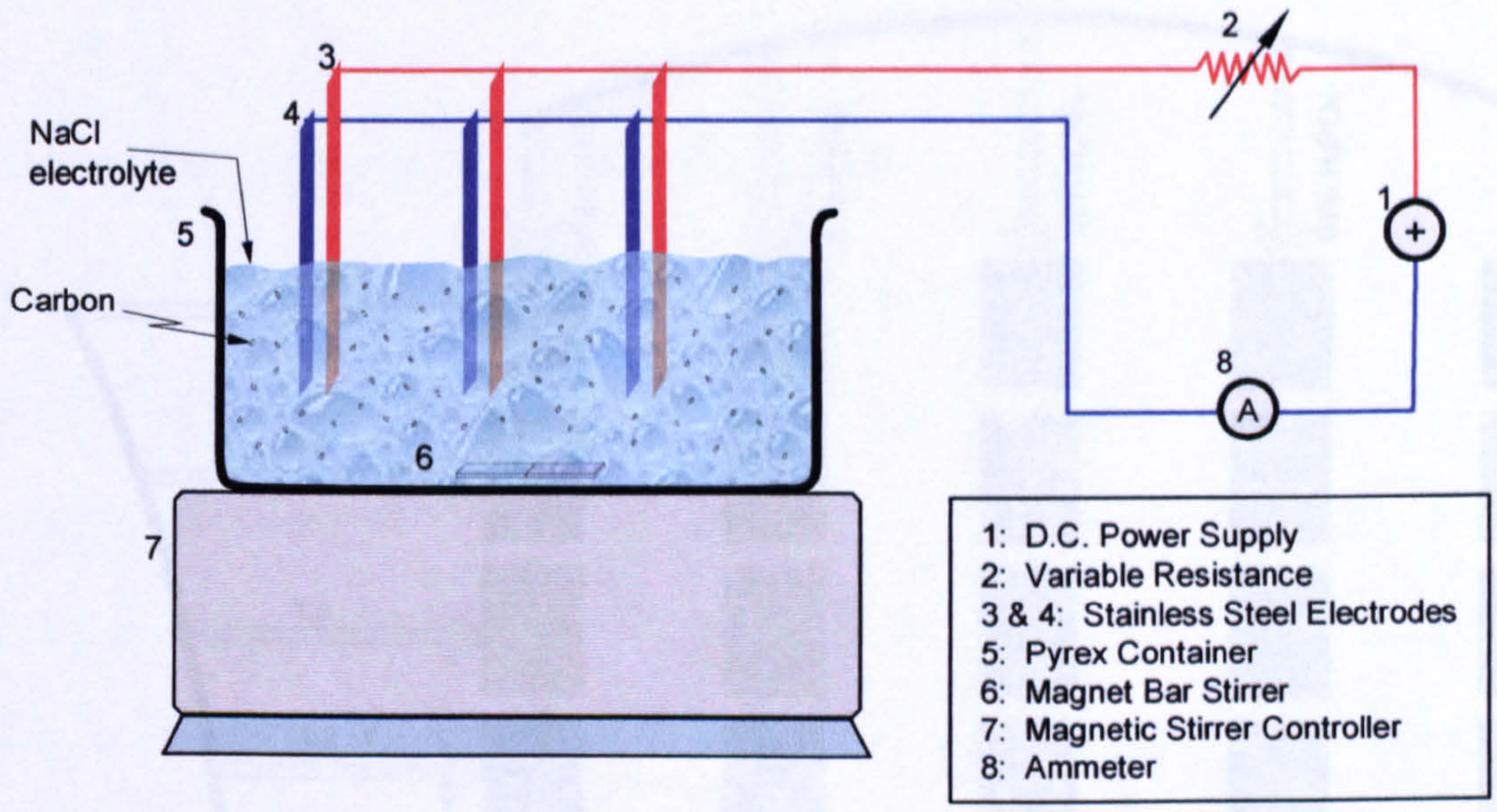


**Figure 3.6: Experimental setup for electrochemical regeneration**

1: D.C. Power Supply; 2: Variable Resistance; 3 & 4: Stainless Steel Electrodes; 5: Pyrex Container; 6: Magnetic Bar Stirrer; 7: Magnetic Stirrer Controller; 8: Ammeter

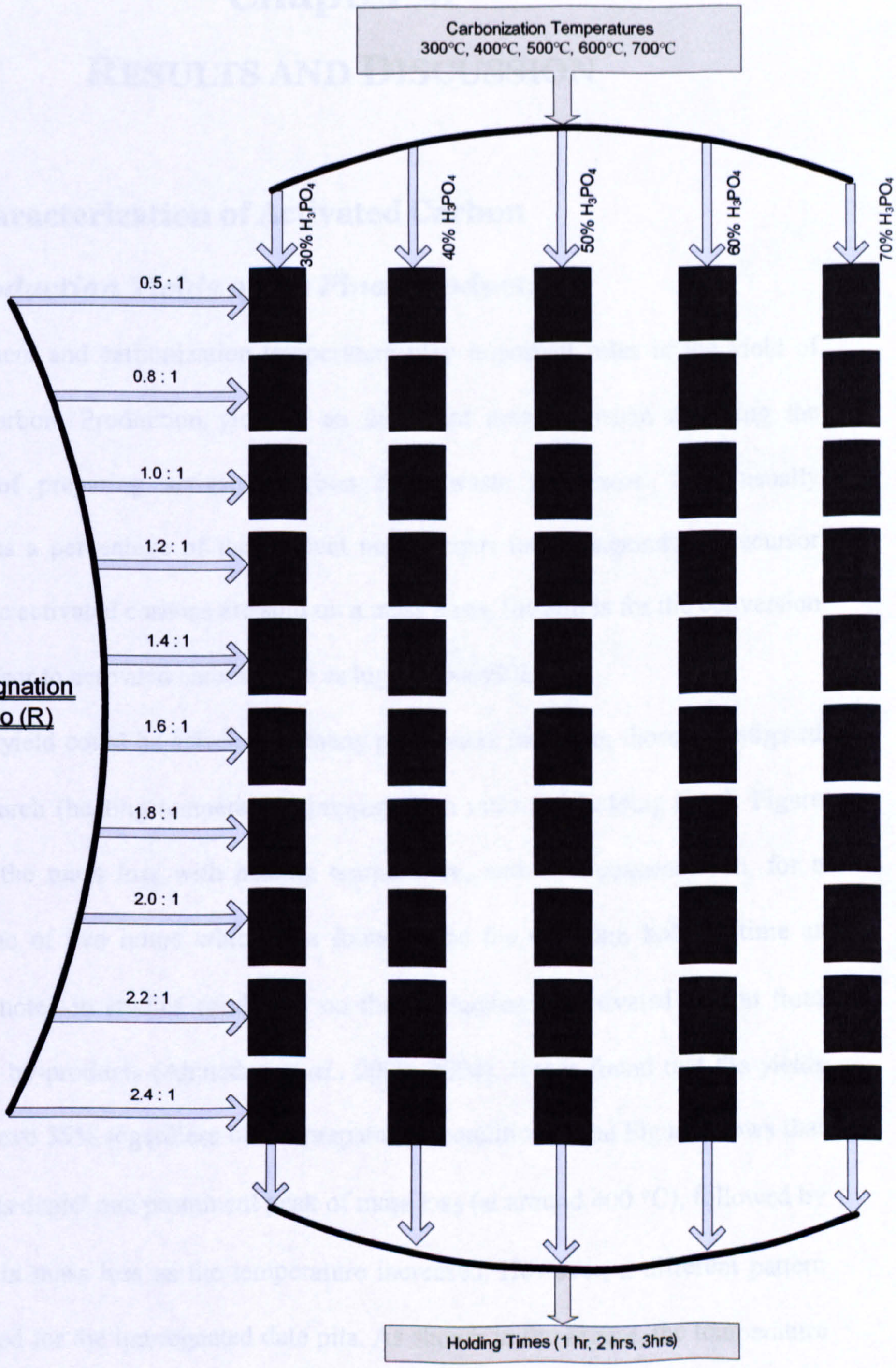


**Figure 3.7: Conceptual design of experimental setup**

# Chapter 4:

# RESULTS AND DISCUSSION

## 4.1 Characterization of Activated Carbon

### *4.1.1 Production Yields of the Final Products*

Acid treatment and carbonization temperature play important roles in the yield of activated carbon. Production yield is an important measure when assessing the feasibility of preparing activated carbon from waste precursors. It is usually calculated as a percentage of the product mass versus its corresponding precursor mass. As the activated carbons are sold on a mass basis, the aim is for the conversion from precursor to activated carbon to be as high as possible.

Production yield could be affected by many parameters including those investigated in this research (heating temperature, impregnation ratio and holding time). Figure 4.1 shows the mass loss with heating temperature, and acid concentration, for a holding time of two hours which was found to be the optimum holding time as previously noted in studies conducted on the production of activated carbon from agricultural by-products (Ahmedna *et al.*, 2000, 2004). It was found that the yields were all above 35% regardless of the preparation conditions. The Figure shows that raw date pits depict one prominent peak of mass loss (at around 400 °C), followed by a decrease in mass loss as the temperature increased. However, a different pattern was observed for the impregnated date pits. As shown in the Figure, the temperature did not significantly affect the mass of the date pits. Since phosphoric acid has a considerable influence on the structure of the date pits, the concentration of the impregnant and the conditions under which impregnation is effected must play a very

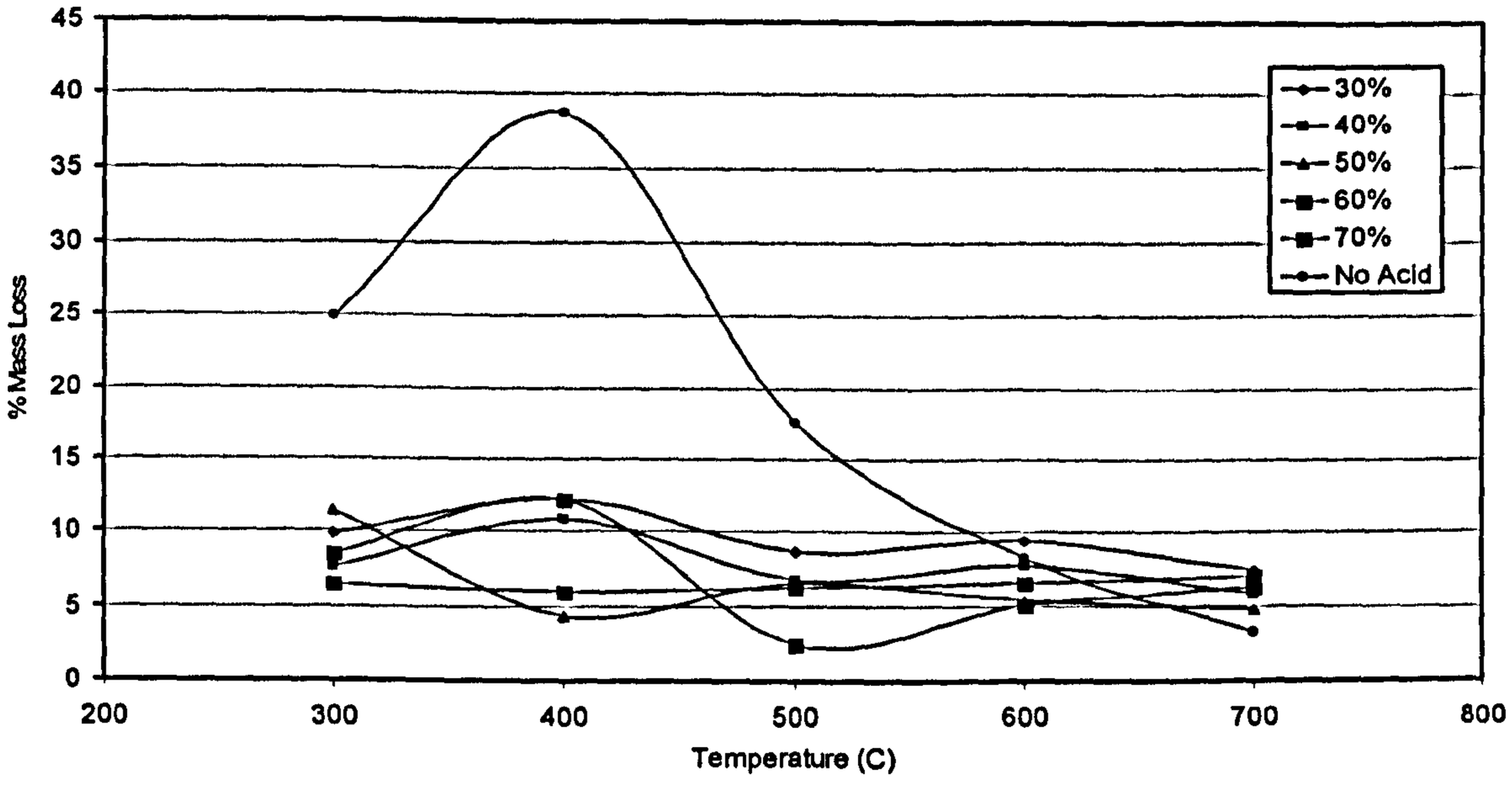


**Figure 4.1: Mass loss of raw date pits and acid-impregnated date pits at different temperatures, for a holding time of 2 hours**

important role in the overall process. The orthophosphoric acid impregnating the material plays a double role: (i) it hydrolyses the lignocellulosic matter and aids the subsequent extraction of some components, thus weakening the material, which swells and (ii) the acid occupies a volume which inhibits the contraction of the material during heat treatment, by forming phosphate and polyphosphate bridges that connect and crosslink biopolymer fragments, thus leaving a porosity in the material when it is extracted by washing after carbonization (Jagtoyen *et al.*, 1992). During pyrolysis later, decomposition of the mass occurs with subsequent mass loss.

The activated carbons produced at an activation temperature of 500 °C generally had larger specific surface areas. Tables 4.1, 4.2 and 4.3 summarize the porosity characteristics of the activated carbons at different carbonization times for 500 °C. Inspection of the data shows that the carbon with the largest specific surface area was attained at 500 °C, with 70% $H_3PO_4$ and a carbonization time of 2 hrs, with a $S_{BET}$ reaching 1319 $m^2\ g^{-1}$ and a corresponding total pore volume of 0.785 $cm^3\ g^{-1}$ (Table 4.2). It is worth mentioning that simple carbonization of raw pits did not produce good adsorbing carbons as shown in the graphs of methylene blue removal. This is a clear demonstration of the important effect of acid in the development of porosity.

In practical manufacture of activated carbon, a compromise would be made between the production yield and the adsorptive properties of the product. For carbons obtained at 700 °C, an increased impregnation ratio seems to generate good porosity (Table B.30, Appendix B). From the data given in the Appendix, it is evident that additional acid is not beneficial as it does not lead to further improvement in porosity and probably forms an insulating layer (or skin) covering the particles, thus reducing the activation process. As the precursors in the present study (date pits) are all wastes

**Table 4.1: Texture characteristics of activated carbons obtained at 500 °C ($R = 1.6$, $t = 1$ hour)**

| Parameter | Texture Characteristics | | | | | |
|---|---|---|---|---|---|---|
| % $H_3PO_4$ | 0% | 30% | 40% | 50% | 60% | 70% |
| $S_{BET}$ ($m^2/g$) | 36 | 276.4 | 808.4 | 954.6 | 928.3 | 1007.8 |
| Total Pore Volume, $V_p$ ($cm^3\ g^{-1}$) | 0.11 | 0.48 | 0.38 | 0.33 | 0.48 | 0.67 |
| Average Pore Radius, nm | 0.006 | 1.24 | 0.94 | 0.69 | 1.03 | 1.23 |

**Table 4.2: Texture characteristics of activated carbons obtained at 500 °C ($R = 1.6$, $t = 2$ hours)**

| Parameter | Texture Characteristics | | | | | |
|---|---|---|---|---|---|---|
| % $H_3PO_4$ | 0% | 30% | 40% | 50% | 60% | 70% |
| $S_{BET}$ ($m^2/g$) | 84 | 898.6 | 937.5 | 1314 | 1022 | 1319 |
| Total Pore Volume, $V_p$ ($cm^3\ g^{-1}$) | 0.16 | 0.492 | 0.498 | 0.572 | 0.536 | 0.785 |
| Average Pore Radius, nm | 0.0038 | 1.095 | 1.062 | 0.871 | 1.049 | 1.19 |

**Table 4.3: Texture characteristics of activated carbons obtained at 500 °C ($R = 1.6$, $t = 3$ hours)**

| Parameter | Texture Characteristics | | | | | |
|---|---|---|---|---|---|---|
| % $H_3PO_4$ | 0% | 30% | 40% | 50% | 60% | 70% |
| $S_{BET}$ ($m^2/g$) | 25 | 814.5 | 876.6 | 1008.3 | 967.6 | 1287.3 |
| Total Pore Volume, $V_p$ ($cm^3\ g^{-1}$) | 0.08 | 0.55 | 0.62 | 0.19 | 0.36 | 0.61 |
| Average Pore Radius, nm | 0.0064 | 1.35 | 1.41 | 0.38 | 0.74 | 0.95 |

which actually involve no or little cost, sacrifice of production yield could be made for better adsorptive properties of the products. As far as economics is concerned, the produced granular activated carbon from date palm pits would be of great monetary benefit to the KSA considering the following :

1) It will result in a reduction in waste disposal costs and concerns, and 2) it would lead to the production of a very useful material from a waste, replacing activated carbon which at the present is imported into the KSA at a very high cost for several industrial applications. A rough estimate based on the present date production data for the KSA (approx. 800 ktonnes/year) and considering the average pit weight in a single date fruit (approx. 18% w/w) and the net granular activated carbon (GAC) yield (approx. 24% w/w), suggests that enough raw waste material is available for the present local GAC needs.

### *4.1.2 Effect of Temperature on Pore Structure of the Carbon*

Figure 4.2 shows the variation of specific surface area with heating temperature and acid concentration for a carbonization time of two hours. As seen in the Figure, the highest surface area was obtained at 500 °C with 70% acid concentration.

The effect of carbonization temperature in the pore development is very significant as seen in Figure 4.2. Increasing the carbonization temperature from 400 °C to 500 °C increases the evolution of volatile matter from the precursor, leading to an increase in pore development and thus surface area. Raising the temperature from 500 °C to 700 °C leads to a decrease in surface area as shown in Figure 4.2. This indicates that pore widening takes place as a result of higher temperature.

### *4.1.3 Effect of Chemical Ratio*

The impregnation ratio has been found to be one of the important parameters in the preparation of activated carbon using chemical activation (Ahmadpour *et al.*, 1998). A carbonization time of 2 hours and a temperature of 500 °C (chosen based on earlier findings) were used to study the effect of impregnation ratio on the pore characteristics of the activated carbons. The data obtained are shown in Figure 4.3, which indicates that the BET surface area and pore volume increase with impregnation ratio till an impregnation ratio of 1.6:1 is reached. The pores were created due to the evolution of gaseous carbonization products and catalytic oxidation of the carbon surface by phosphorus metallic salts. The catalytic oxidation causes the widening of some micropores to mesopores. At high ratios of

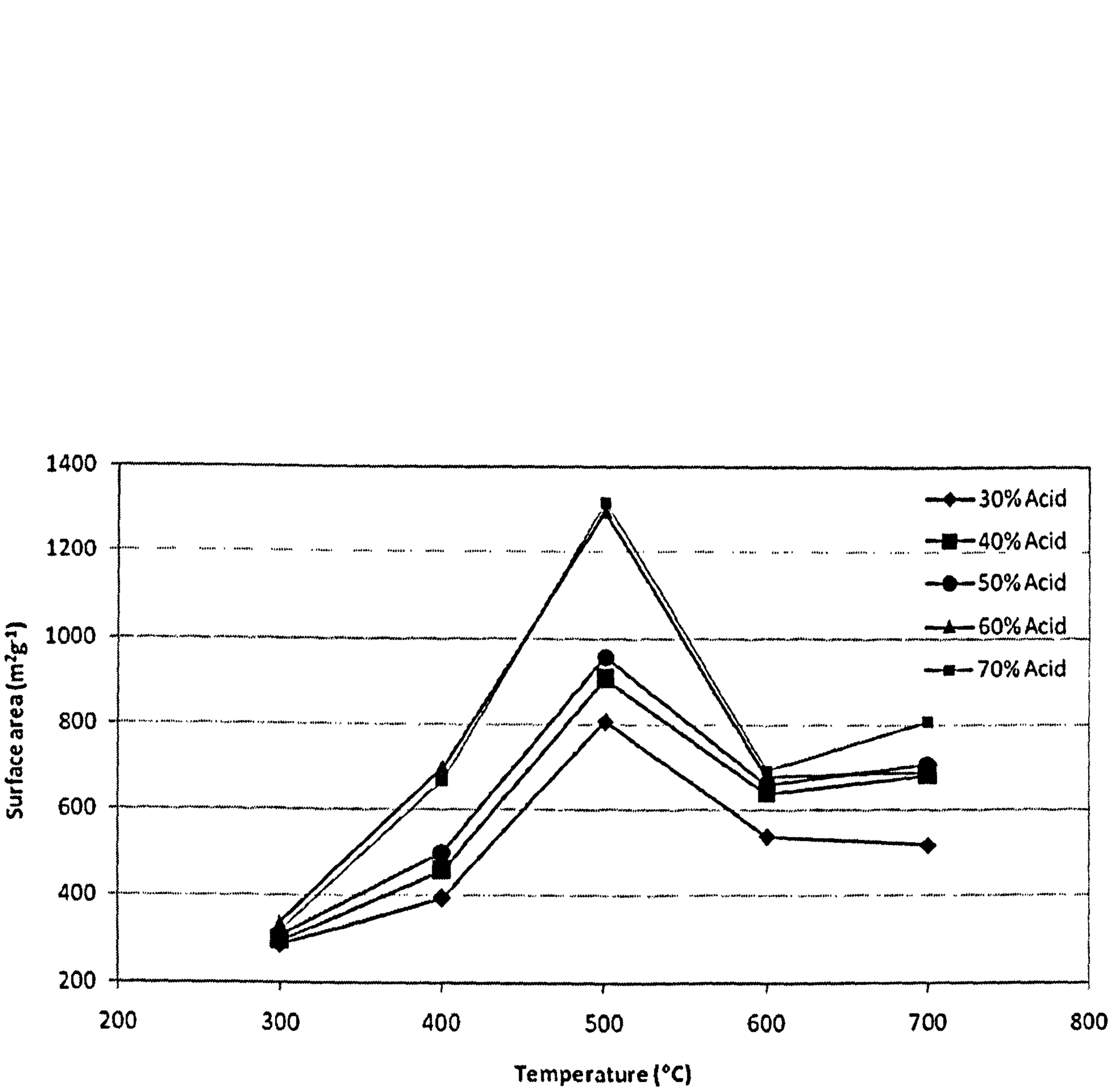


**Figure 4.2: Specific surface area variation as a function of temperature and $H_3PO_4$ concentration, for a carbonization time of 2 hours**

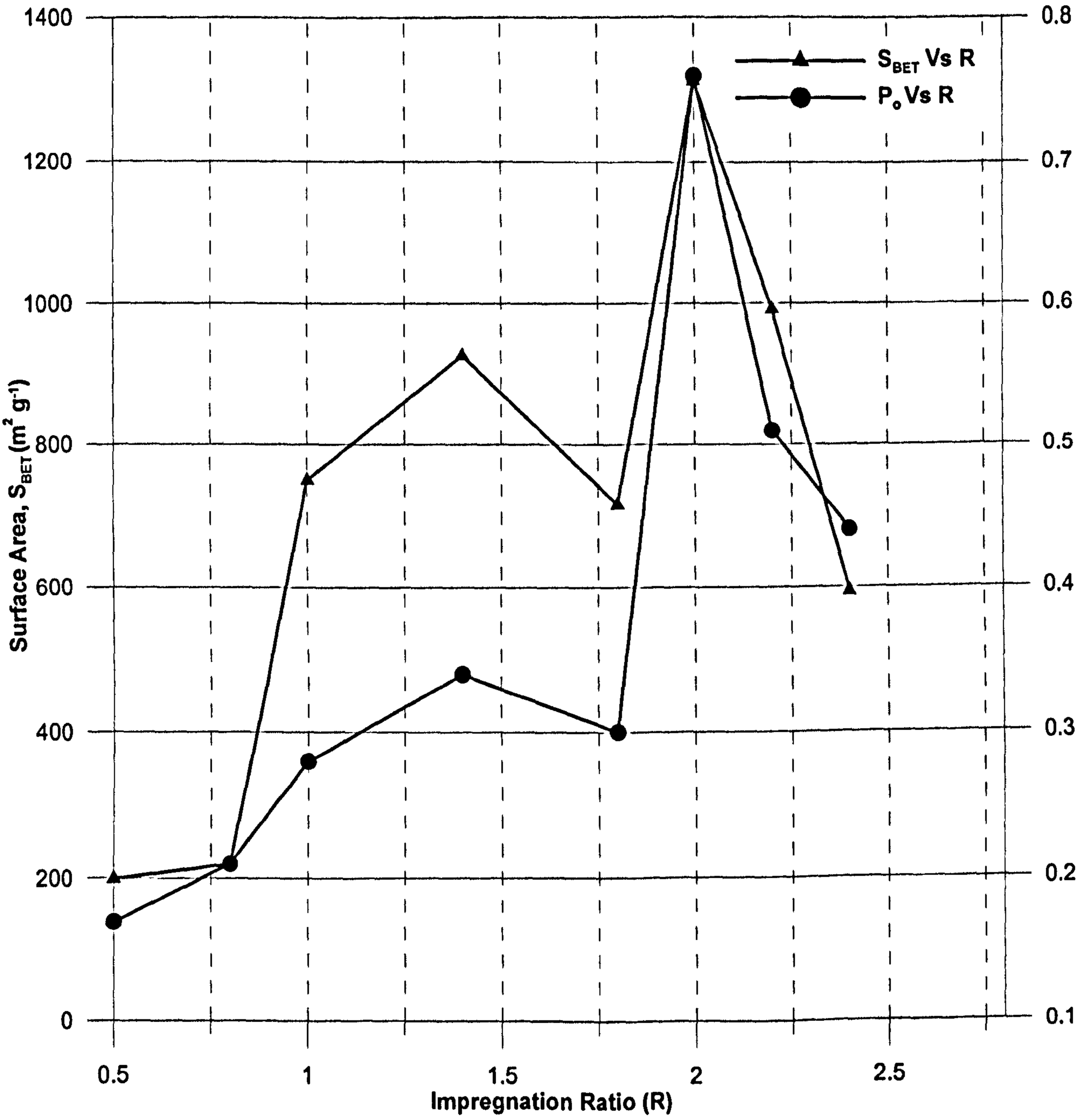


**Figure 4.3: Surface area and pore volume of activated carbon at different acid impregnation ratios (carbonization temperature 500 °C)**

phosphoric acid to date pits, the microporosity development is mostly due to the intercalation (the reversible inclusion of a molecule between two other molecules) of phosphorous in the carbon structure.

At low impregnation ratios (i.e. 0.5-1.0:1), the pore structure of activated carbon produced consists mainly of micropores (Sudaryanto *et al.*, 2006). However, with the increase of impregnation ratio, the creation and widening of micropores to mesopores increases.

### *4.1.4 Effect of Carbonization Time on the Pore Characteristics*

As mentioned before in section 4.1.1, the carbonization time had no significant effect on the yield of activated carbon. Table 4.4 summarizes the effect of carbonization time on the pore characteristics of chemically-activated carbons under conditions of carbonization temperature 500 °C and impregnation ratio 1.6:1 (mass of acid to mass of date pits). The results clearly indicate that carbonization time does have a major effect on the pore characteristics of the produced activated carbon.

### *4.1.5 Effects of Operating Conditions on the BET Surface Area and Yield*

Figure 4.4 is a three-dimensional plot of the BET surface area at 400 °C for different acid Impregnation Ratios, for a constant time period of activation of 2 hours and different acid concentrations, while Figure 4.5 shows the results for the same parameters at 500 °C. These plots were generated using a design (response surface methodology) suitable for the construction of second-order polynomial models. Since the activation process is overall an endothermic process (Raygobal *et al.*, 2006), we would expect the rate of reaction to increase with increasing temperature.

**Table 4.4: Effect of carbonization time on the pore characteristics of chemically activated carbons under conditions of: carbonization temperature 500 °C, acid impregnation ratio 1.6:1**

| Carbonization time (h) | Produced Carbon Characteristics | | |
|---|---|---|---|
| | BET ($m^2 g^{-1}$) | $V_T$ ($cm^3 g^{-1}$) | Average pore radius nm |
| 1.0 | 754 | 0.519 | 1.37 |
| 2.0 | 1319 | 0.79 | 1.19 |
| 3.0 | 1083 | 0.520 | 0.960 |

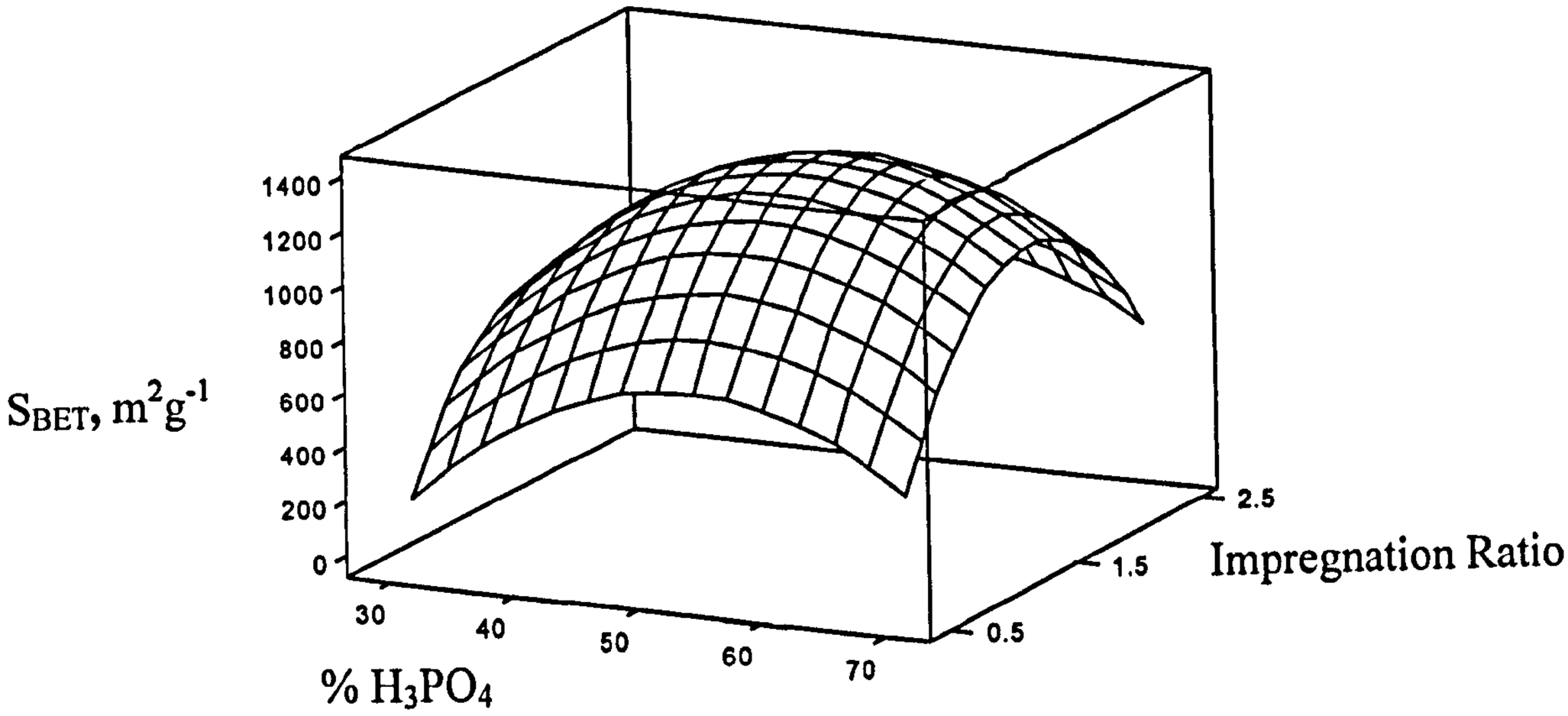


**Figure 4.4: Three-dimensional response surface plot of BET surface area at 400 °C (for $t = 2$ h)**

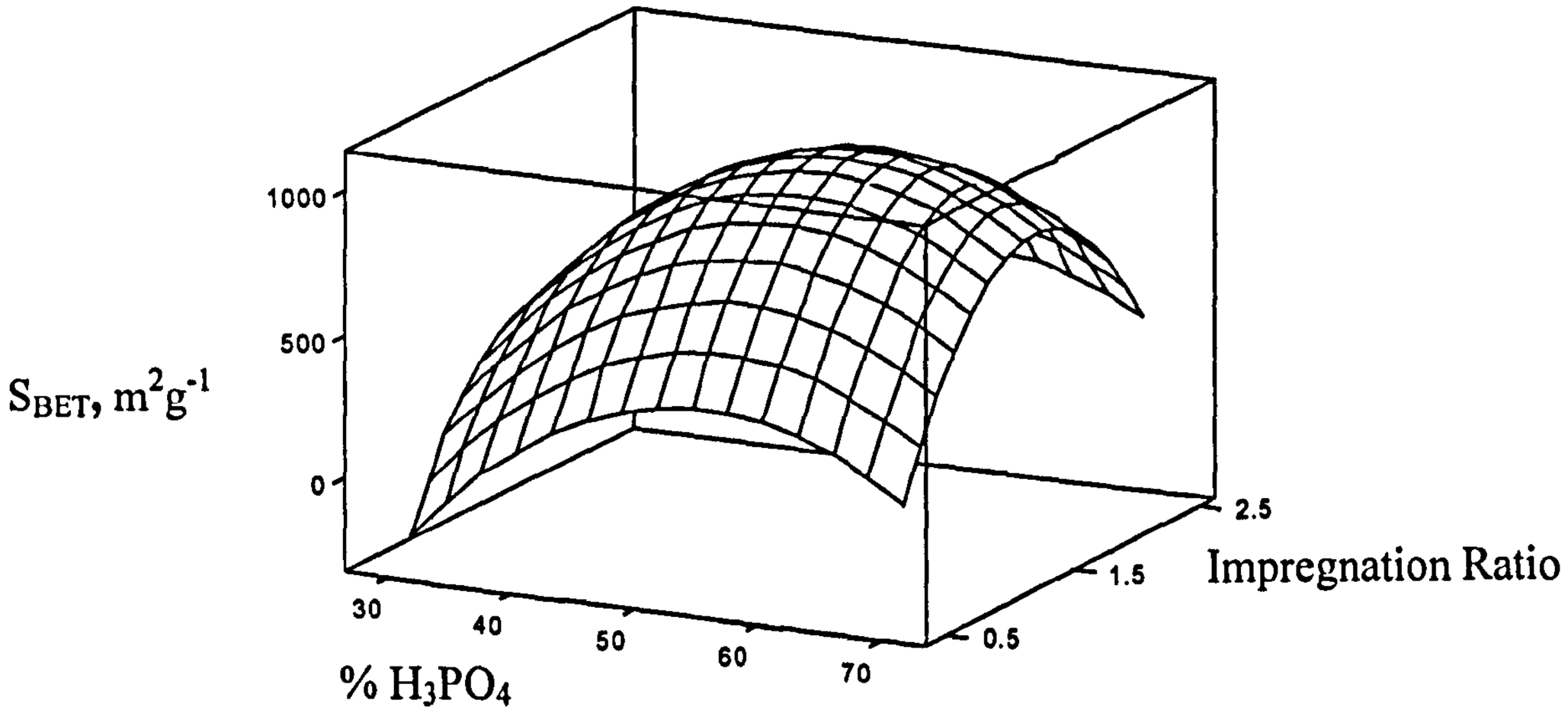


**Figure 4.5: Three-dimensional response surface plot of BET surface area at 500 °C (for $t$ = 2 h)**

However, Figures 4.4 and 4.5 show that when the temperature goes beyond a certain limit, the surface area decreases. Possible reasons might be due to the following (Daud *et al.*, 2000):

(a) If activation is pursued beyond a certain level, the walls of the pores become so thin that they collapse and cause a reduction in the available surface area.

(b) By increasing the temperature, the ash content increases or in other words, the ash content increases in direct proportion to the degree of activation. The ash offers a resistance to the diffusion of the activating agent. This ash that acts as catalyst at lower temperatures, may sinter and block pores and reduce the surface area. In addition, the presence of ash can reduce the surface area available.

(c) The thermal annealing at high temperatures leads to pore collapse, decreasing the surface area of activated carbon.

## 4.2 Removal of Tetramethylthionine Chloride (Methylene Blue)

Many industries use dyes to colour their products. Wastewater effluents from such industries contain residues of dyes. The presence of very low concentrations of dyes in effluent is highly visible and undesirable. Typically, natural dye disposal would not be subject to any stringent environmental regulations because it does not contain toxic substances, but there is a special disposal requirement in Saudi Arabia. It is against regulations to discharge anything to a sewer system that will alter the colour of the contents of that system. Thus, dyes cannot be dumped down a drain, but must be combined with an absorbent material and disposed of as a solid. Furthermore, if any of the contents of the natural dyes exhibit certain characteristics, such as toxicity,

that qualify those contents as a hazardous waste, the substance must be disposed of according to hazardous waste regulations. The disposal of toxic dyes without sufficient treatment affects aquatic life. Dyes can pose a problem if they are carcinogenic or toxic. Therefore, it is necessary to decrease the concentration of dyes to the lowest possible limit. Tetramethylthionine chloride has been widely reported in the activated carbon literature as a model pollutant for several reasons: 1) it is a visible pollutant that can be easily traced during the course of a bench study, 2) and as an indicator of mesoporosity it is chosen as a test dye because it is one of the most widely recognized probe molecules for assessing the removal capacity of a specific carbon for moderate size pollutant molecules (Bestani *et al.*, 2004, Hameed *et al.*, 2007, Rahman and Saad, 2003, Ahmad *et al.*, 2007, Nagarathinam and Mariappam, 2001).

### *4.2.1 Adsorption of Tetramethylthionine chloride (Methylene Blue)*

The equilibrium removal of tetramethylthionine chloride using the activated carbon produced and the commercial carbons was mathematically expressed in terms of adsorption isotherms. The Freundlich adsorption isotherm was chosen for this study as the Langmuir isotherm is generally used for gas mixtures. The equation for the Freundlich isotherm is $\left(x/m = kC_e^{1/n}\right)$ where $(x/m)$ is the amount of tetramethylthionine chloride adsorbed per unit of carbon at equilibrium $C_e$. The experimental results obtained for each of the carbon samples at room temperature (22 ± 1°C) and optimum pH condition of 6.8, and contact time of approximately 50 minutes and dose of adsorbent were found to obey Freundlich adsorption isotherms as shown in Figure 4.6. From the Figure, it is clearly evident that both carbons have

the same adsorptive capacity at an equilibrium concentration of 12 mg $g^{-1}$. The figure also indicates that at lower concentrations of tetramethylthionine chloride, the commercial carbon has better adsorptive capacity. The isotherm constants **k** and **n** represent the adsorption capacity and intensity of adsorption, respectively. Both values of k and n, obtained by non-linear least square regression analysis, are reported in Table 4.5.

The data was found not to obey the Langmuir adsorption isotherm and this could be explained because this type of adsorption isotherm is commonly used for ideal gas mixtures.

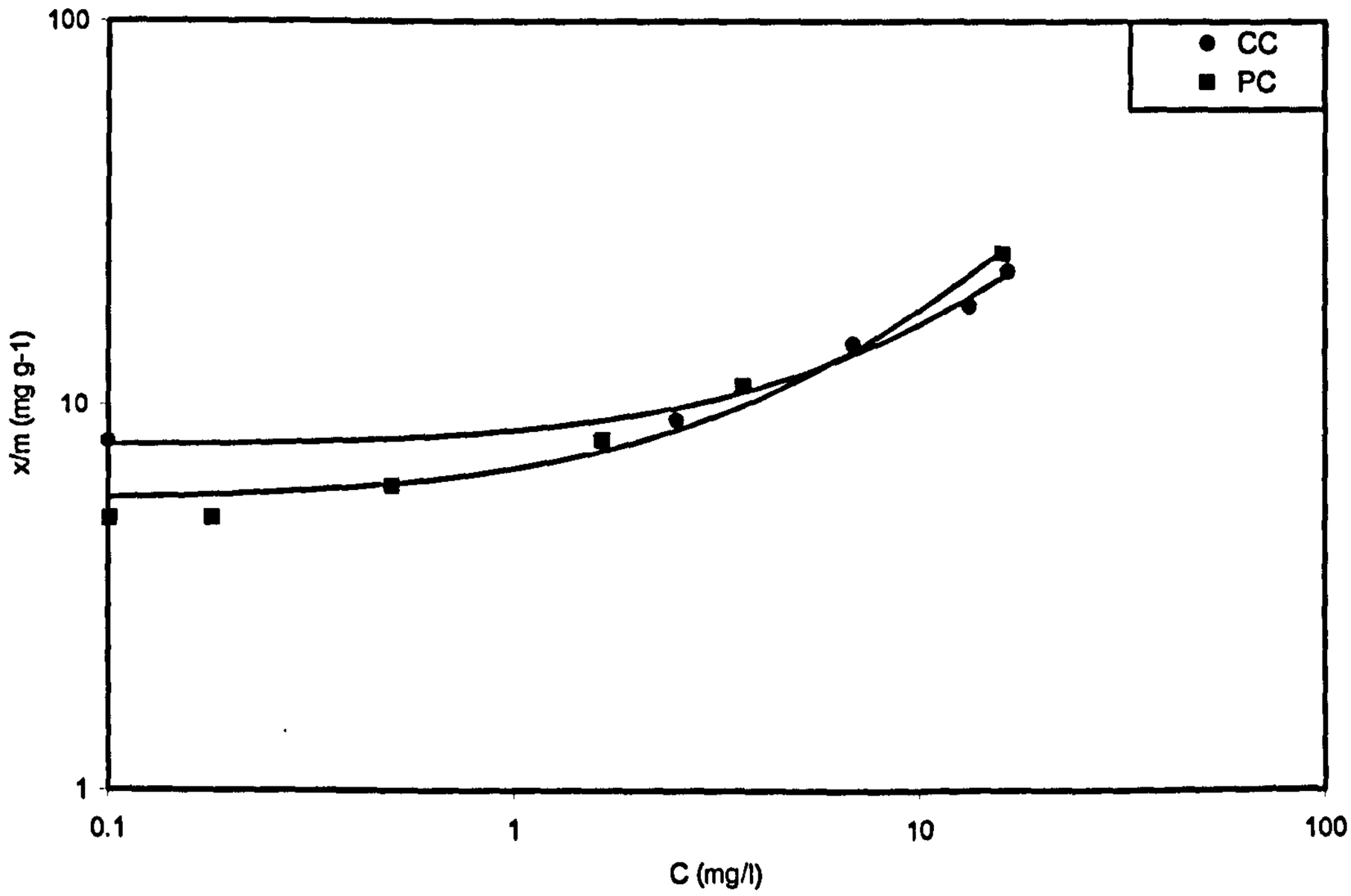


**Figure 4.6: Freundlich adsorption isotherm for tetramethylthionine chloride, for the commercial carbon (CC, Filtrasorb-400) and the produced carbon (PC)**

**Table 4.5: Tetramethylthionine chloride adsorption characteristics**

| Sample | Freundlich Parameters | | |
|---|---|---|---|
| | *K* | *1/n* | $R^2$ |
| Produced Carbon | 24 | 0.144 | 99.2 |
| Filtrasorb-400 | 18 | 0.223 | 97.4 |

The adsorption behaviours of the samples were studied by evaluating the removal efficiency (RE), of tetramethylthionine chloride, calculated as:

$$RE = (C_o - C)/C_o \times 100 \quad (4.1)$$

where $C_o$ is the initial aqueous concentration of tetramethylthionine chloride placed in a flask and $C$ is the concentration after adsorption. Figures 4.7-4.11 show the removal efficiency of the pyrolysed and raw AC samples with respect to shaking time. The overall adsorption pattern shows a fast initial removal rate, followed by a slower removal process, until equilibrium is reached. The equilibrium time reduced with a corresponding increase in the surface area of the samples (Figure 4.7). Low surface area carbons obtained at 300 °C also show good adsorption capacity. Here, the removal seems to be associated with an absorption process by the unsaturated free bonds and radicals of the partially-decomposed components irrespective of the available porosity (Meshko *et al.*, 2001). Samples prepared at 500 °C showed the acid to have a good effect on the date pits with regard to porosity development. This effect is enhanced with an increase in concentration of phosphoric acid. As mentioned earlier, the activated carbon with the largest specific surface area was attained at 500 °C with a $S_{BET}$ reaching 1319 $m^2/g$ and corresponding total pore volume of 0.785 $cm^3\ g^{-1}$. Again, simple carbonization of raw pits did not produce good adsorbing carbons, as seen in all the Figures for tetramethylthionine chloride removal. This is a clear demonstration of the important effect of acid in the development of porosity. The produced carbon with the optimum carbonization temperature (500 °C), optimum acid concentration (70%), with the optimum holding time (2 hours) and impregnation ratio (1.6) was chosen for subsequent studies in the removal of phenol and 2-methylphenol.

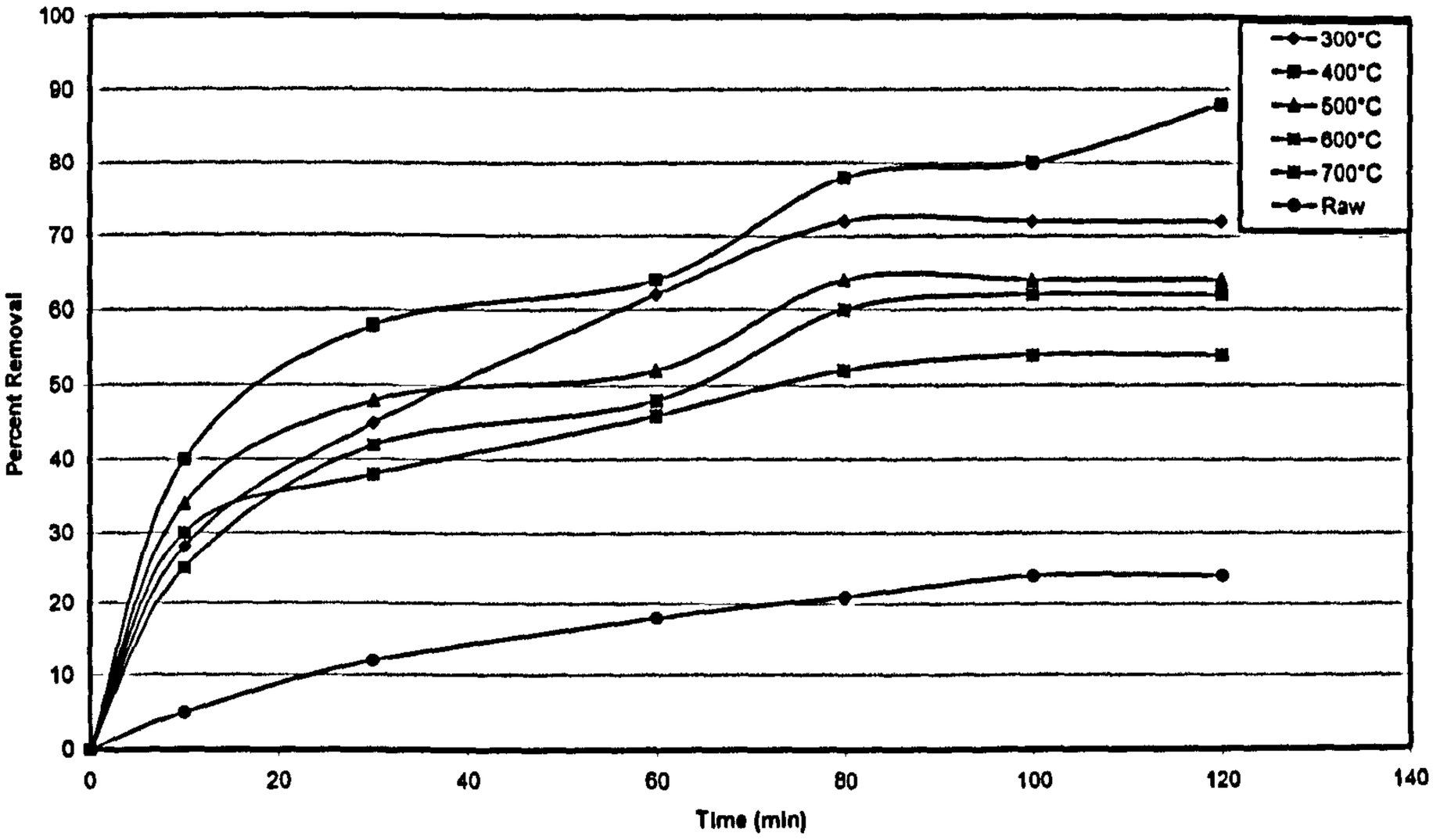


**Figure 4.7: Removal efficiency of tetramethylthionine chloride versus time (30% $H_3PO_4$)**

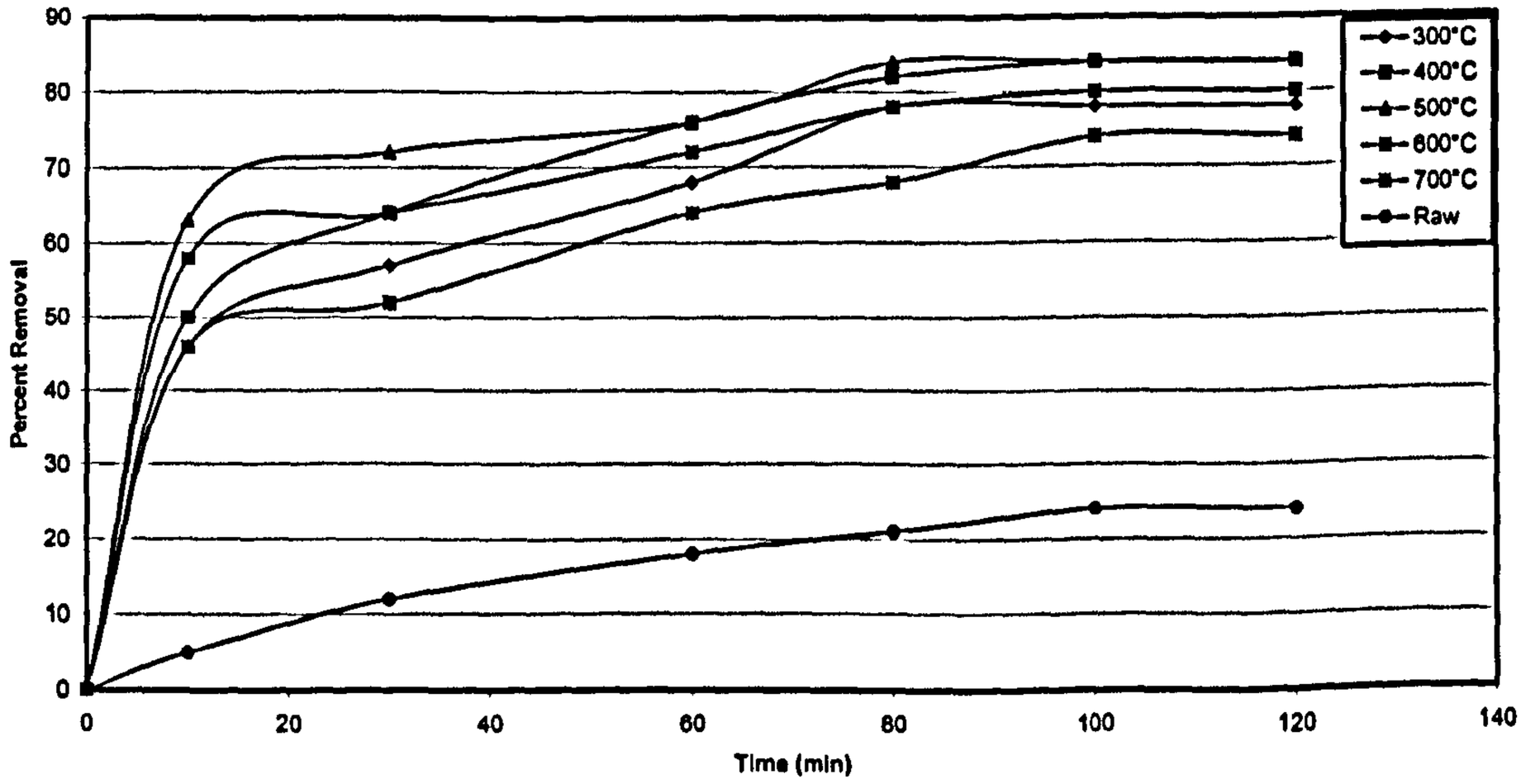


**Figure 4.8: Removal efficiency of tetramethylthionine chloride versus time (40% $H_3PO_4$)**

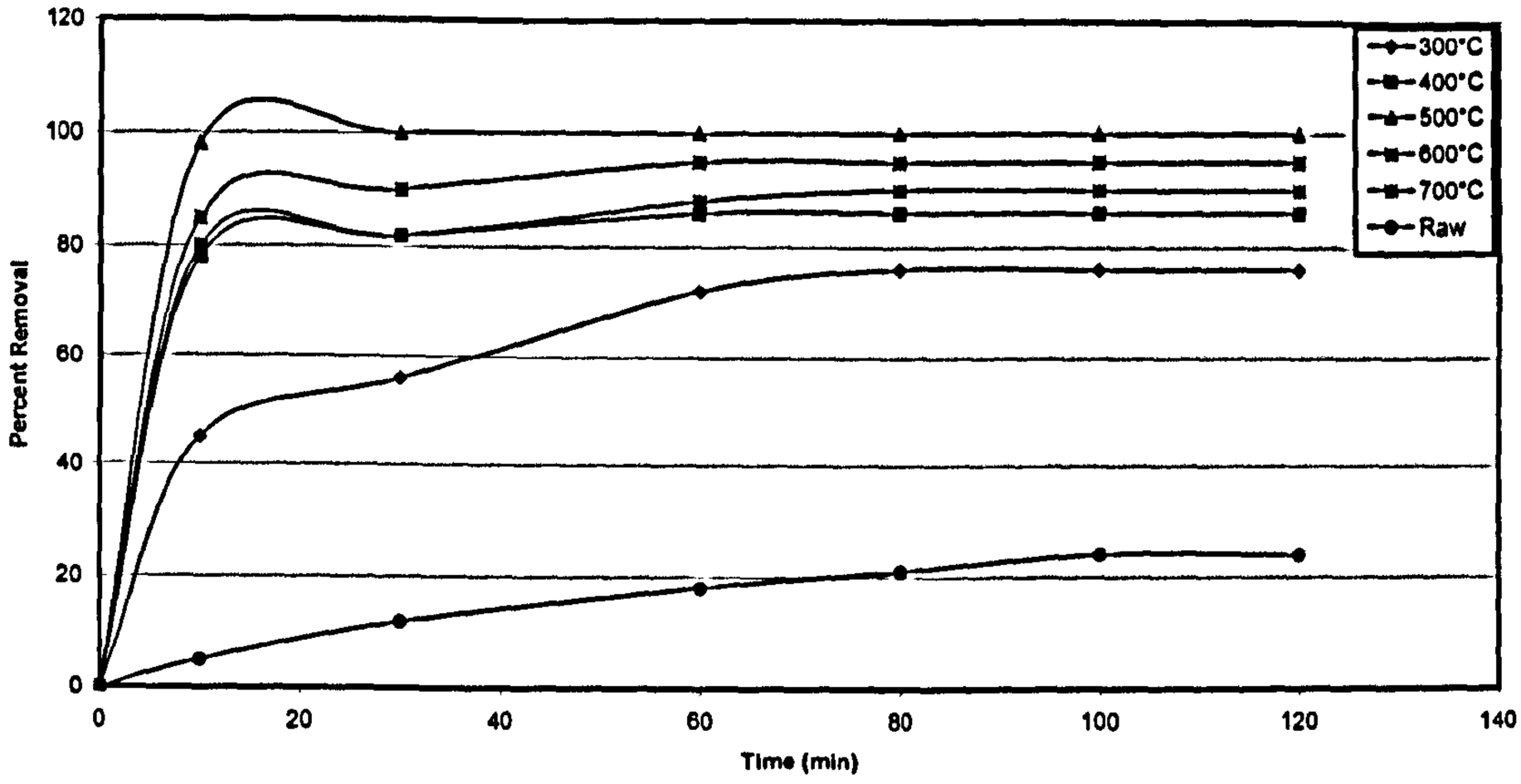


**Figure 4.9: Removal efficiency of tetramethylthionine chloride versus time (50% $H_3PO_4$)**

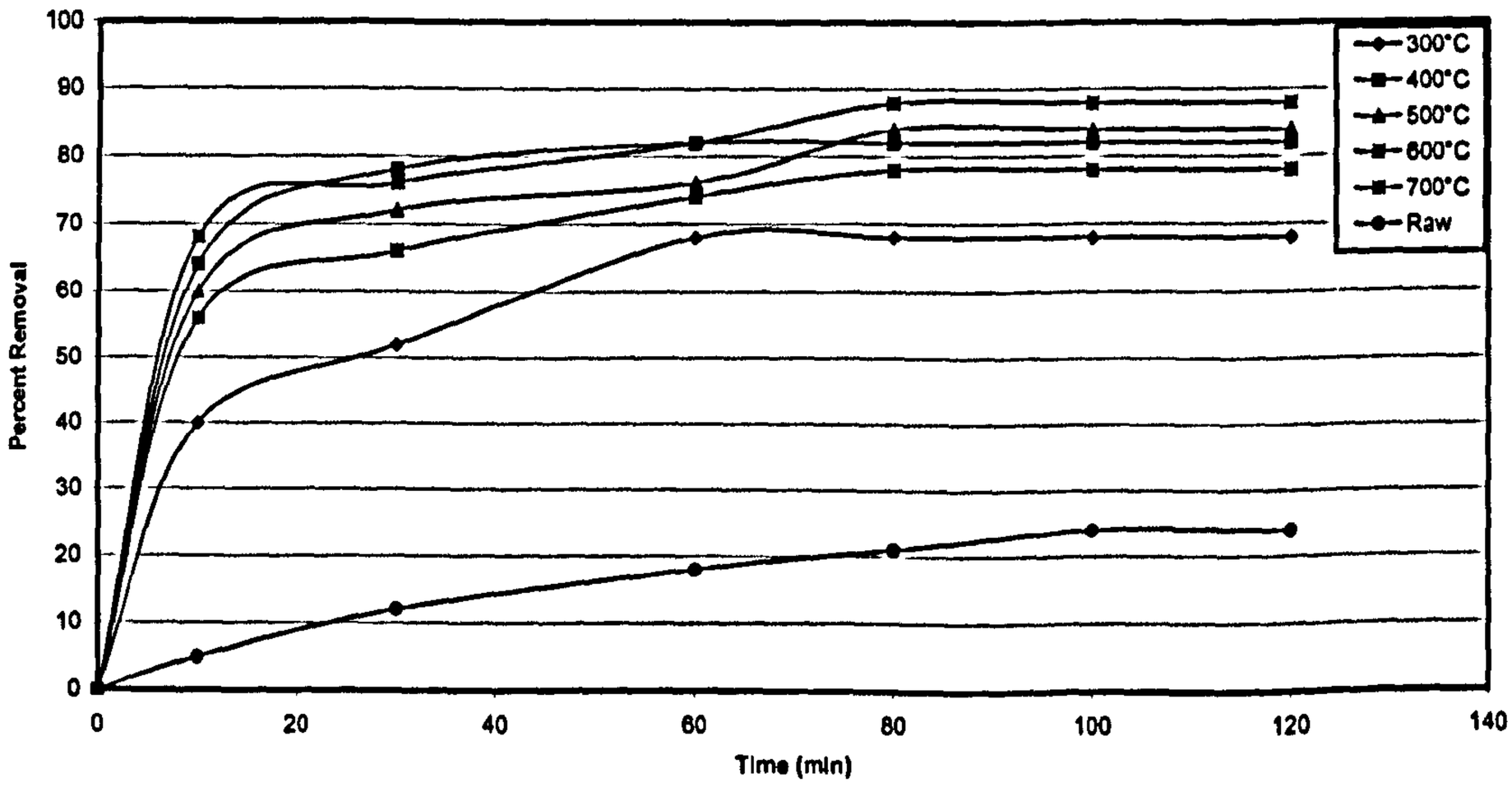


**Figure 4.10: Removal efficiency of tetramethylthionine chloride versus time (60% $H_3PO_4$)**

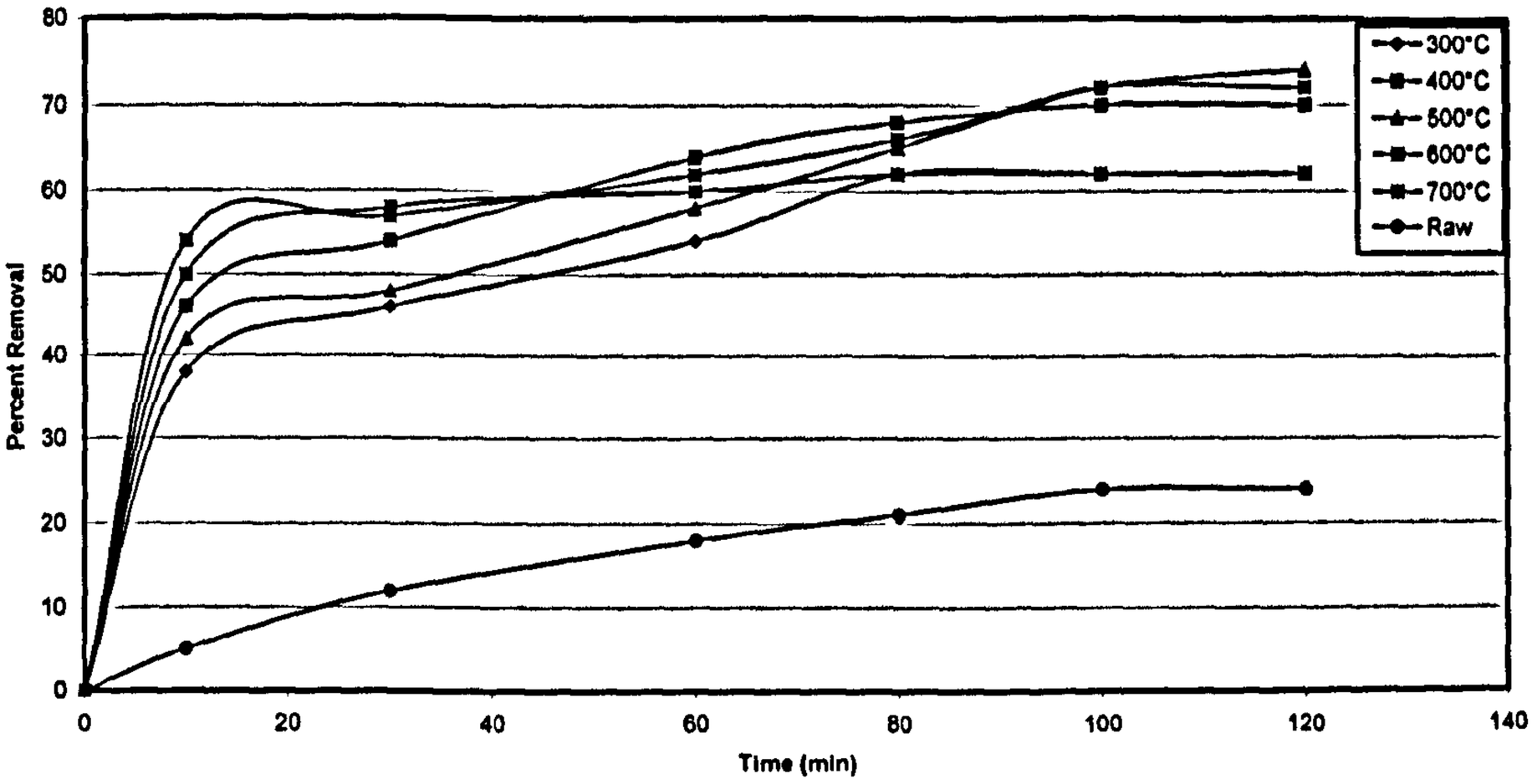


**Figure 4.11: Removal efficiency of tetramethylthionine chloride versus time (70% $H_3PO_4$)**

## 4.3 Removal of Phenol and 2-Methylphenol

Phenolic compounds are considered to be hazardous wastes, which are released into the aquatic environment by industries such as steel plants, petroleum refineries, petrochemical, phenolic resin, pharmaceutical, chemical, and dye industries, etc. The discharge of phenolic waste into waterways may adversely affect human health as well as that of flora and fauna. Ingestion of a small amount of phenol (TLV of 5 $ppm_v$) by human beings may cause nausea, vomiting, paralysis, coma, greenish or smoky-coloured urine, and even death from respiratory failure or cardiac arrest. Phenols also impart an undesirable taste to water, even at extremely low concentrations (the USEPA recommends a maximum allowable limit of 0.001 ppm). Fatal poisoning may also occur by absorption of phenol by the skin, if a large area of skin is exposed. It is therefore necessary to remove phenol completely from wastewater. The direct discharge limit of phenol in Saudi Arabia is 0.1 mg $l^{-1}$ (The Presidency of Meteorology and Environment (PME), Saudi Arabia, 2001). Basic information concerning phenol and its derivatives is summarized in Table 4.6.

### *4.3.1 Effect of Dissolved Oxygen*

The presence of molecular oxygen has a significant influence on the adsorptive capacity of activated carbon for several phenolic compounds. The amount of oxygen can be one of the key factors that explain differences in adsorption isotherms reported in literature for the same adsorbent-adsorbate pair. Oxygen induces polymerization reactions on the surface of activated carbon (Vidic *et al.*, 1993); thus, an anoxic procedure is recommended for obtaining data on true adsorption equilibrium. This procedure requires exclusion of oxygen from the experimental

**Table 4.6: Basic information concerning phenol and its derivatives (Vidic *et al.*, 1993)**

| Phenolic compound | Boiling point (°C) | pKa at 25 °C | Aqueous solubility at 25 °C (g $l^{-1}$) |
|---|---|---|---|
|  | 182 | 9.89 | 93 |
| 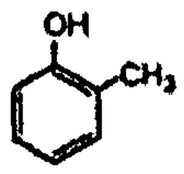 | 191 | 10.20 | 25 |
| 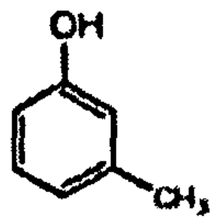 | 202 | 10.01 | 26 |
|  | 202 | 10.17 | 23 |
| 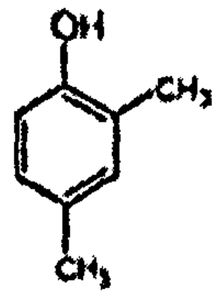 | 211 | 10.58 | Not available |
| 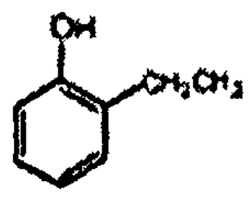 | 207 | 10.2 | Sparingly soluble |
| 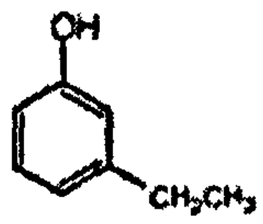 | 214 | 10.07 | Slightly soluble |
| 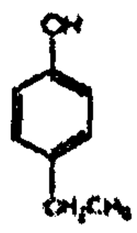 | 218 | 10.0 | Slightly soluble |
| 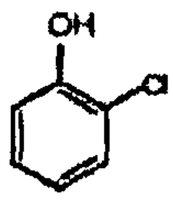 | 204 | 8.52 | 28 |
| 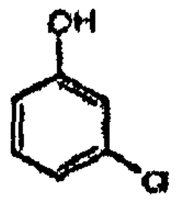 | 214 | 8.97 | 26 |

vessels. All experimental procedures described in literature can be denoted as *oxic* since they provide no control over the amount of oxygen. Adsorptive capacities obtained from these procedures are appreciably higher than the capacities determined by the anoxic procedure. Any amount of phenolic compound adsorbed above the amount predicted by the anoxic isotherm can be attributed to polymerization reactions. In this research work, the GAC adsorptive capacity for phenol and 2-Methylphenol attainable under oxic conditions was higher than that obtained in the absence of molecular oxygen (anoxic). Extraction of the carbon preloaded with phenol revealed that almost 100% of the originally adsorbed compound can be recovered from the surface of GAC by solvent extraction if the adsorption was carried out in the absence of molecular oxygen. Contrarily, only 20-35% of the adsorbed compound was recovered from GAC loaded under oxic conditions. Figure 4.12 shows the Freundlich curves for phenol and 2-Methylphenol for the cases of zero and saturation level of oxygen at pH 6.2 and room temperature of 23 °C. The Figure clearly depicts that the presence of dissolved oxygen in the environment greatly enhanced the uptake of Phenol and 2-Methylphenol by granular activated carbon. This significant oxygen-induced uptake is not attributable to biological degradation since no increase in the inorganic carbon content in the form of carbon dioxide was detected during the experiment.

### *4.3.2 Effect of pH*

The pH of the aqueous solution is an important controlling parameter in the adsorption process. This is partly due to the fact that protons are strong competing sorbates, and partly due to the fact that the solution pH influences the ionization of

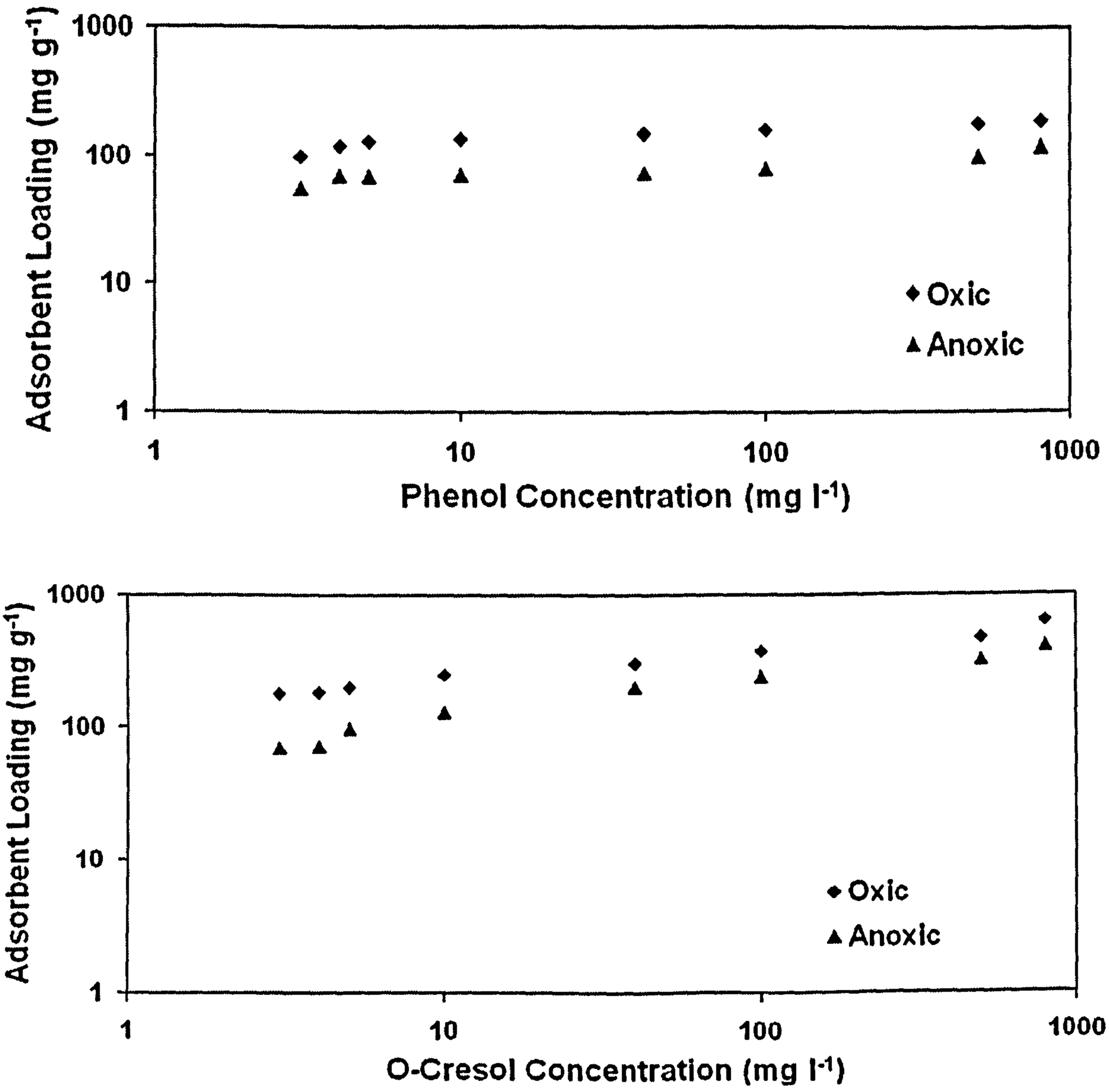


**Figure 4.12: Oxic and anoxic phenol and 2-Methylphenol (o-cresol) uptakes**

functional groups of the sorbate and the chemical speciation of ions in solution. Phenol has a limited solubility in water (8.3 g/100 ml) and it is slightly acidic. The phenol molecule has a weak tendency to lose the H+ ion from the hydroxyl group, resulting in the highly water-soluble phenoxide anion C6H5O− (or phenolate). Therefore, at any pH value, phenol would exist in two forms, i.e., undissociated phenol species and dissociated phenol species.

The pH of the aqueous solution of phenol affects its uptake on activated carbon and in general the uptake decreases at very low and very high pH values. At the lower pH values, the uptake of phenol is less due to the presence of $H^+$ ions suppressing the ionization of phenol and hence its uptake on the polar adsorbent. In the higher pH range, phenol forms salts which readily ionize, leaving a negative charge on the phenolic group. At the same time, the presence of $OH^-$ ions on the adsorbent prevents the uptake of phenolate ions (Singh *et al.*, 1994). Hence, in the present work, experiments were performed with the solution pH at 6.2. To determine the optimum pH for maximum contaminant removal, experiments were conducted with 100 ml phenol (100 mg $l^{-1}$) solutions, each containing 1.0 g carbon. The initial pH of the solution was varied from 2 to 14. The results, shown in Figure 4.13, indicate that phenol removal using both the Produced Activated Carbon & the Commercial Carbon reached a maximum in the pH range 4 to 10. The amount of phenol adsorbed decreased at both high and low pH values as mentioned in the literature. The pKa value for phenol is 9.89, so the adsorbing species above this pH is mostly anionic. Repulsion between the surface layer and the anionic phenolate results in reduced adsorption. Figure 4.13 also shows the phenol speciation results considering the following relationship:

$$\text{Phenol} \leftrightarrow \text{Phenolate} + H^+ \text{, pKa} = 9.82 \text{ at 22-25 °C)} \qquad (4.2)$$

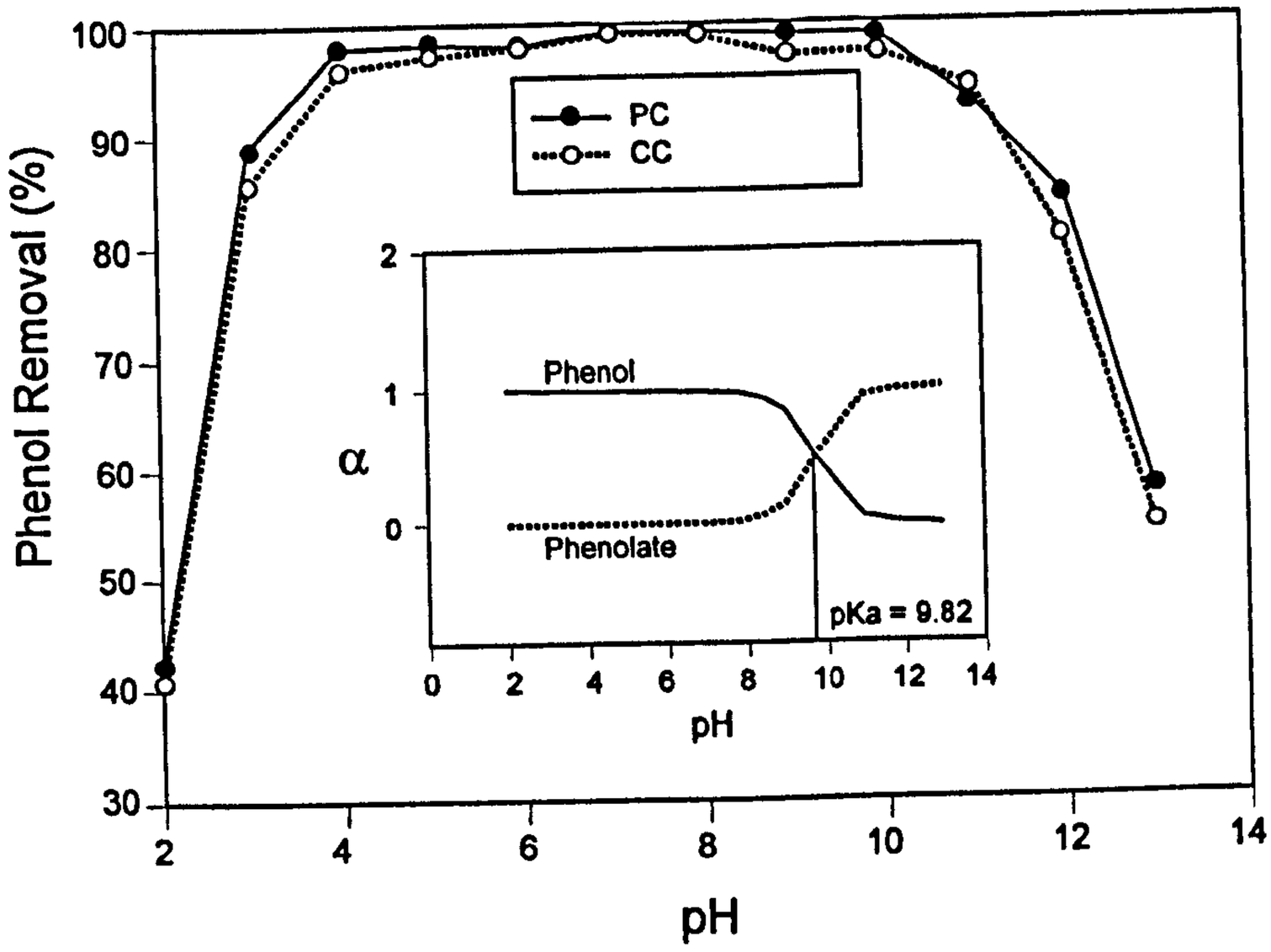


**Figure 4.13: Phenol removal by the produced carbon (PC) and commercial carbon (CC) as a function of pH**

$$\text{Total Phenol} = \text{Undissociated Phenol} + \text{Dissociated Phenol} \quad (4.3)$$

At pH = 3, both the functional groups on the carbon surface and the phenolic compounds are in the non-ionized forms, $pH < pK_a$. The surface groups are either neutral or positively-charged. This behaviour can be explained considering the nature of the adsorbent at different pH values in phenol adsorption. The surface of the activated carbon contains a large number of functional groups. The pH dependence of phenol adsorption can largely be related to the type and ionic state of these functional groups and also on phenol chemistry in solution. Adsorption of phenol up to pH 3.5 suggests that the positively-charged $C_6H_5OH_2^+$ ions (formed by $C_6H_5OH$ in acidic media) bind through electrostatic attraction to negatively-charged functional groups on the surface of activated carbon because at this pH more functional groups carrying negative charge would be exposed. But on raising the pH, as indicated in the Figure, the rate of removal is considerably reduced. At pH values above 3.5, the concentrations of $C_6H_5OH_2^+$ and $C_6H_5O^-$ both have to be considered. Experimental results conducted by Singh *et al.*, (1994) revealed that $C_6H_5O^-$ is relatively important at pH >3.5 and these negatively-charged ions are no longer attracted by the activated carbon, resulting in the reduction of phenol removal. Hence, it can be concluded that above pH 3.5, other mechanisms like physical adsorption on the surface of adsorbent, could have taken on an important role in the adsorption of phenol.

Vidic et al., (1998) showed that activated carbons exhibit significantly different behavior for the removal of phenolic compounds in the presence and absence of functional groups such as molecular oxygen. They evaluated some of the possible mechanisms of oxidative coupling of phenols that are promoted by the activated

carbon surface and which result in such a significant increase in capacity. In particular, acidic and basic surface functional groups and metals and metal oxide complexes that are commonly present on activated carbon surface were investigated for their role in catalyzing oxidative coupling of phenolic compounds under different conditions. The authors used bituminous coal-based carbon and a carbonaceous resin as model adsorbents in their study, while 2-methylphenol and 2-chlorophenol were used as model adsorbates. Metal content was altered either by prolonged acid washing of activated carbon or by addition of metal oxides to the carbonaceous resin. Oxygen-containing acidic and basic surface functional groups were modified by outgassing at different temperatures, or by exposure of out-gassed carbons to oxygenated water. Freundlich isotherm parameters and solvent extraction efficiencies for virgin and modified varieties of these adsorbents have shown that none of the parameters investigated in this study have a significant impact on the exhibited adsorptive and catalytic properties of activated carbon under oxic and anoxic conditions. It appears that oxygen-containing basic surface functional groups are primarily responsible for the catalytic properties of activated carbon towards oxidative coupling of phenolic compounds.

The phenol adsorption results in Figure 4.13 show an increasing phenol adsorption till approximately pH 6 that is followed by a plateau till pH 10. However above pH 10, the phenol adsorption decreases substantially. These results can be explained as follows. Table 4.7 and Figure 4.13 also provide the phenol speciation data; the respective data shows that up to pH 8 phenol remains the dominant species, however above pH 8 approximately phenol start to convert to phenoxide anion (phenolate species) with equal amounts existing at pH 9.82. However above pH 10 a significant

speciation change from phenol to phenoxide anion is noted, e.g., at pH 12 the phenol & phenoxide anion % concentrations in solution are 0.7% and 99.3%, respectively. Hence we suggest that that at low pH values (below 6) when most phenol is the dominant species adsorption results yield high values. Additionally at the intermediate pH values between 6 and 10, though phenol adsorption is high, however no increase is noted with an increase in pH. It is suggest that in this pH range, as phenol is adsorbed and removed from the aqueous phase, the remaining phenoxide anion converts back to phenol, thus yielding more phenol removal. However, at pH values greater than 10, when speciation will be highly favoured towards the phenoxide anion, a subsequent and significant drop in phenol removal also transpires, as the dissolution of the target species would be more favoured as compared to its adsorption.

**Table 4.7: Calculated phenol speciation results (pKa = 9.82, T = 22 °C)**

| pH | 2 | 4 | 6 | 8 | 10 | 12 | 14 |
|---|---|---|---|---|---|---|---|
| **Phenolate** | 0.000 | 0.001 | 0.002 | 0.015 | 0.602 | 0.993 | 0.999 |
| **Phenol** | 0.999 | 0.999 | 0.998 | 0.985 | 0.398 | 0.007 | 0.000 |

This eventually causes reduced phenol removal from the aqueous phase.

Figures 4.14a-c show the Freundlich phenol curves obtained at pH values of 3, 7, and 11, respectively, while Figures 4.15a-c show the Freundlich 2-Methylphenol curves obtained at pH values of 3, 7, and 11, respectively. For phenol, the increase in adsorbate removal of oxic versus anoxic at 1 mg $l^{-1}$ residual concentration were 12%, 129%, and 147%, at pH values of 3, 7, and 11, respectively. On the other hand, in the case of 2-Methylphenol, the percentage enhancement at 1 mg $l^{-1}$ residual concentration were 9%, 121%, and 38%, at pH values of 3, 7, and 11, respectively.

### *4.3.3 Effect of Temperature*

Temperature has a pronounced effect on the adsorption capacity of the adsorbents. Figures 4.16 and 4.17 show the plots of adsorbent loading versus equilibrium concentrations for phenol and 2-Methylphenol at temperatures of 10, 25 and 45 °C. The Figures show that with the increase in temperature, the adsorptivity of phenol increases. The Figures also show that at lower adsorbate concentrations, $q_e$ rises sharply and thereafter the increase is gradual with solute concentration in the solution. Since sorption is an exothermic process (Benefield *et al.*, 1982), it would be expected that an increase in temperature of the adsorbate-adsorbent system would result in decreased sorption capacity. However, if the adsorption process is controlled by the diffusion process (intraparticle transport-pore diffusion), the sorption capacity will show an increase with an increase in temperature. This is basically due to the fact that the diffusion process is an endothermic process (Weber, 1963). With an increase in temperature, the mobility of the phenolate ions increases and the retarding forces acting on the diffusing ions decrease, thereby increasing the sorptive capacity

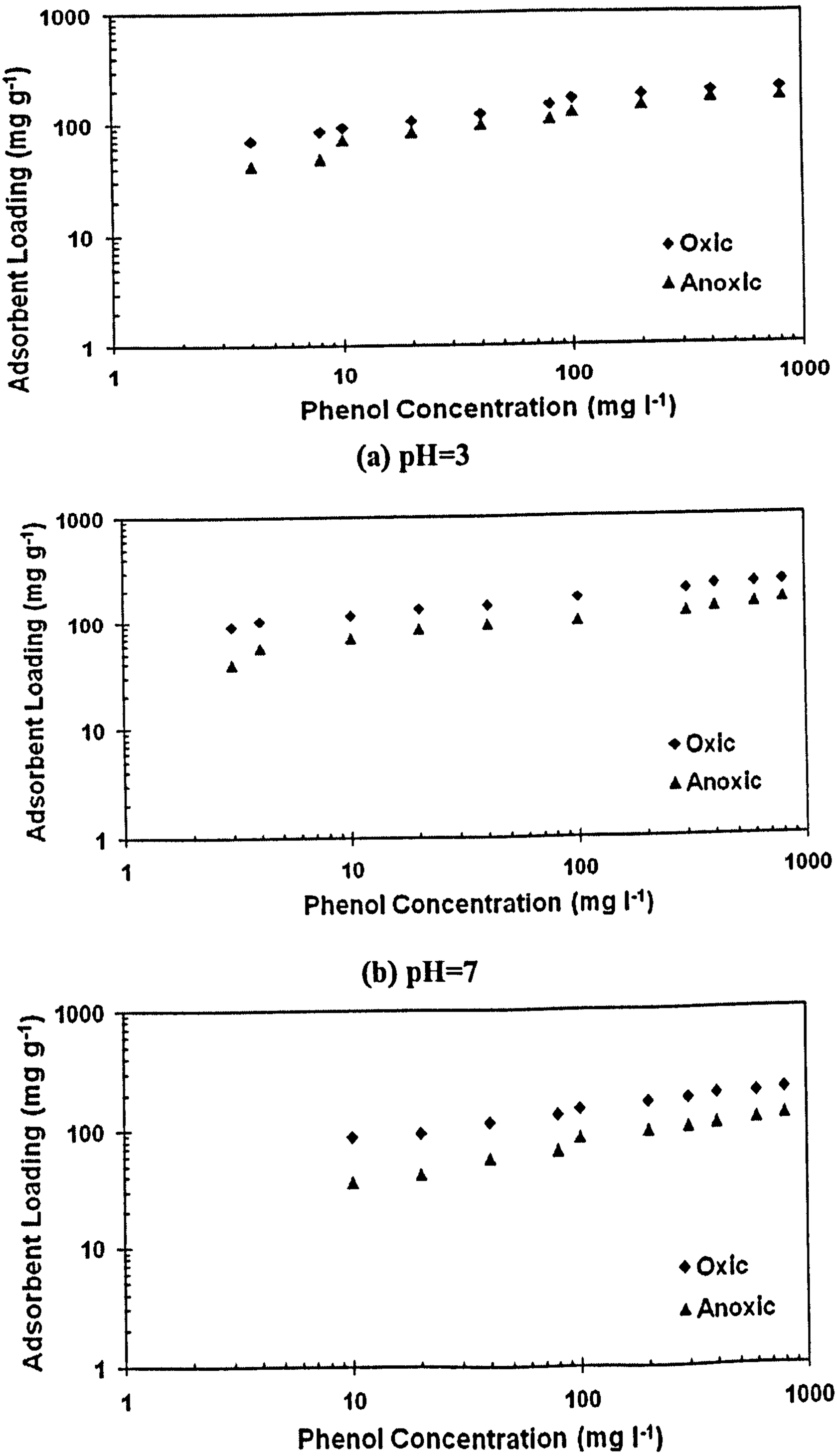


**(a) pH=3**




**(b) pH=7**




**(c) pH=11**

**Figure 4.14: Oxic and anoxic phenol uptakes at three different pH values**

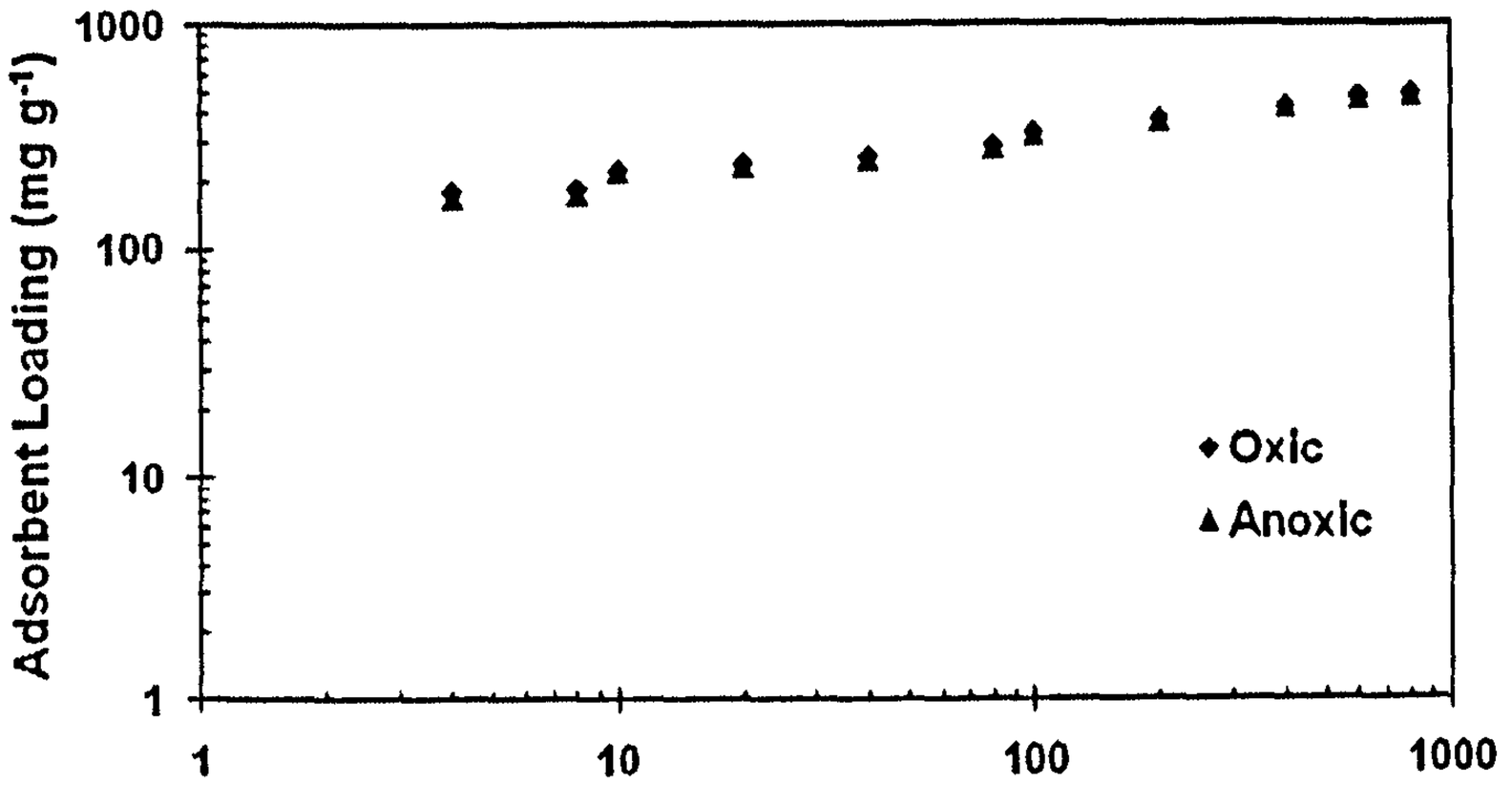


**(a) pH=3**

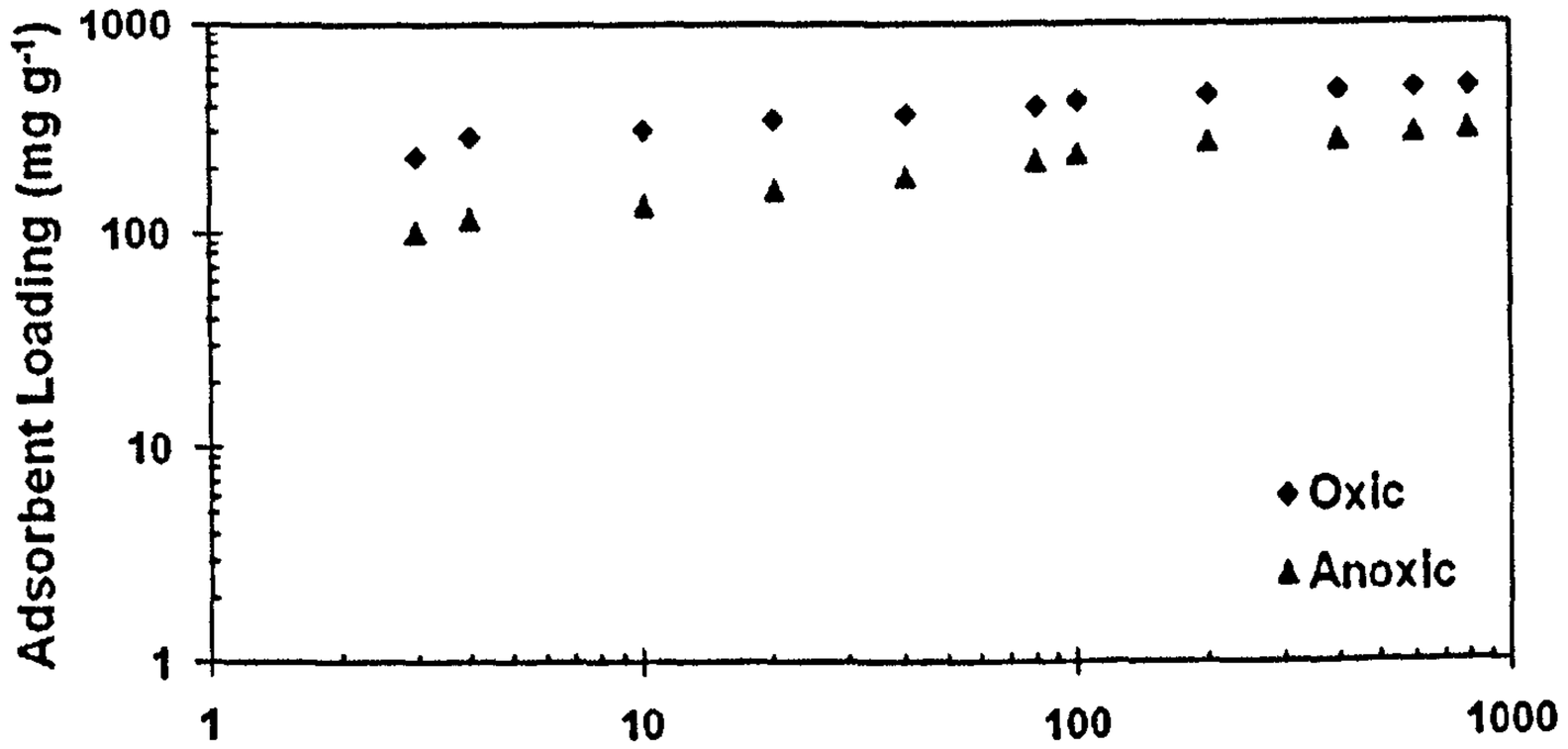


**(b) pH=7**

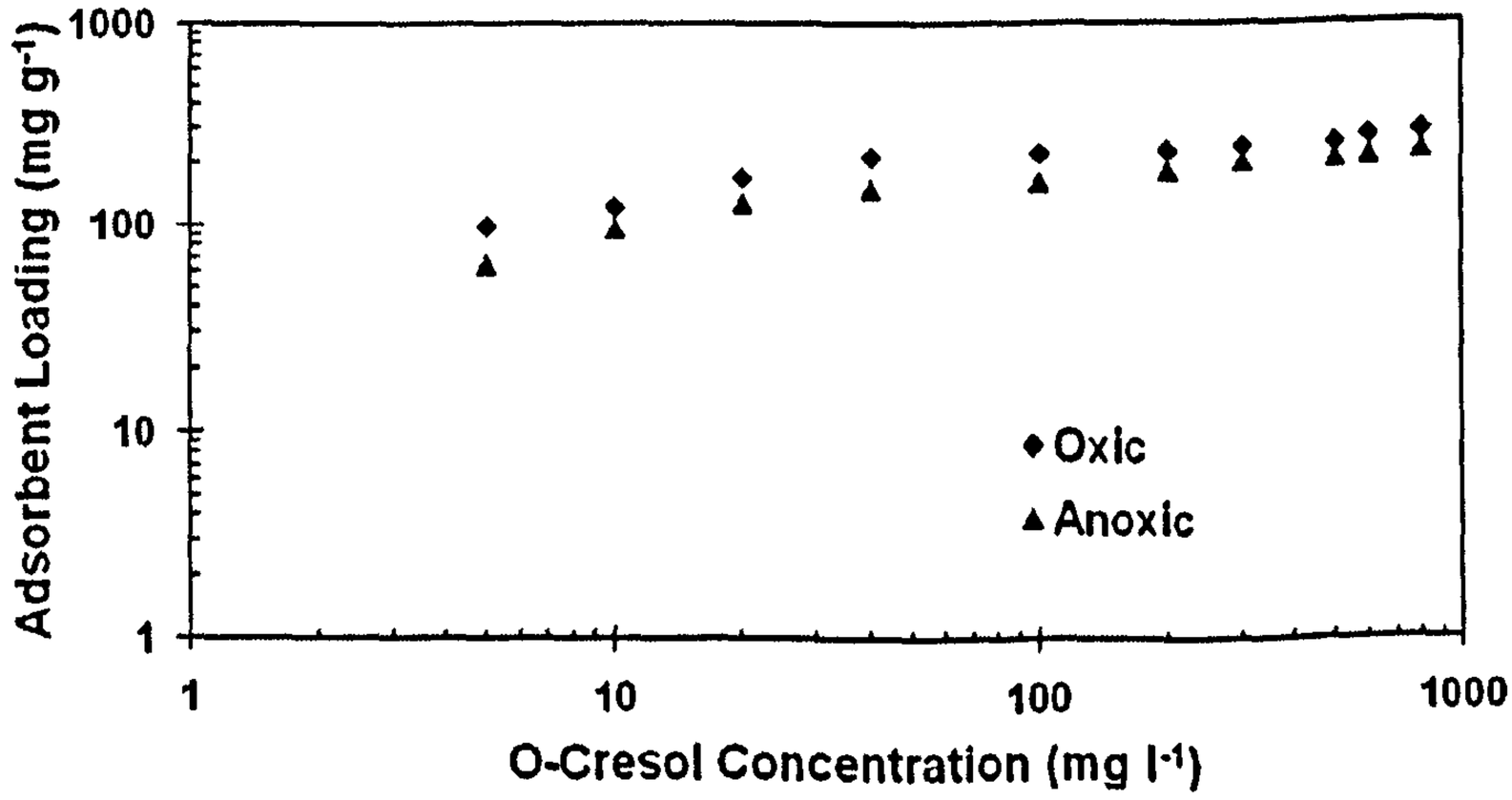


**(c) pH=11**

**Figure 4.15: Oxic and anoxic 2-Methylphenol (o-cresol) uptakes at three different pH values**

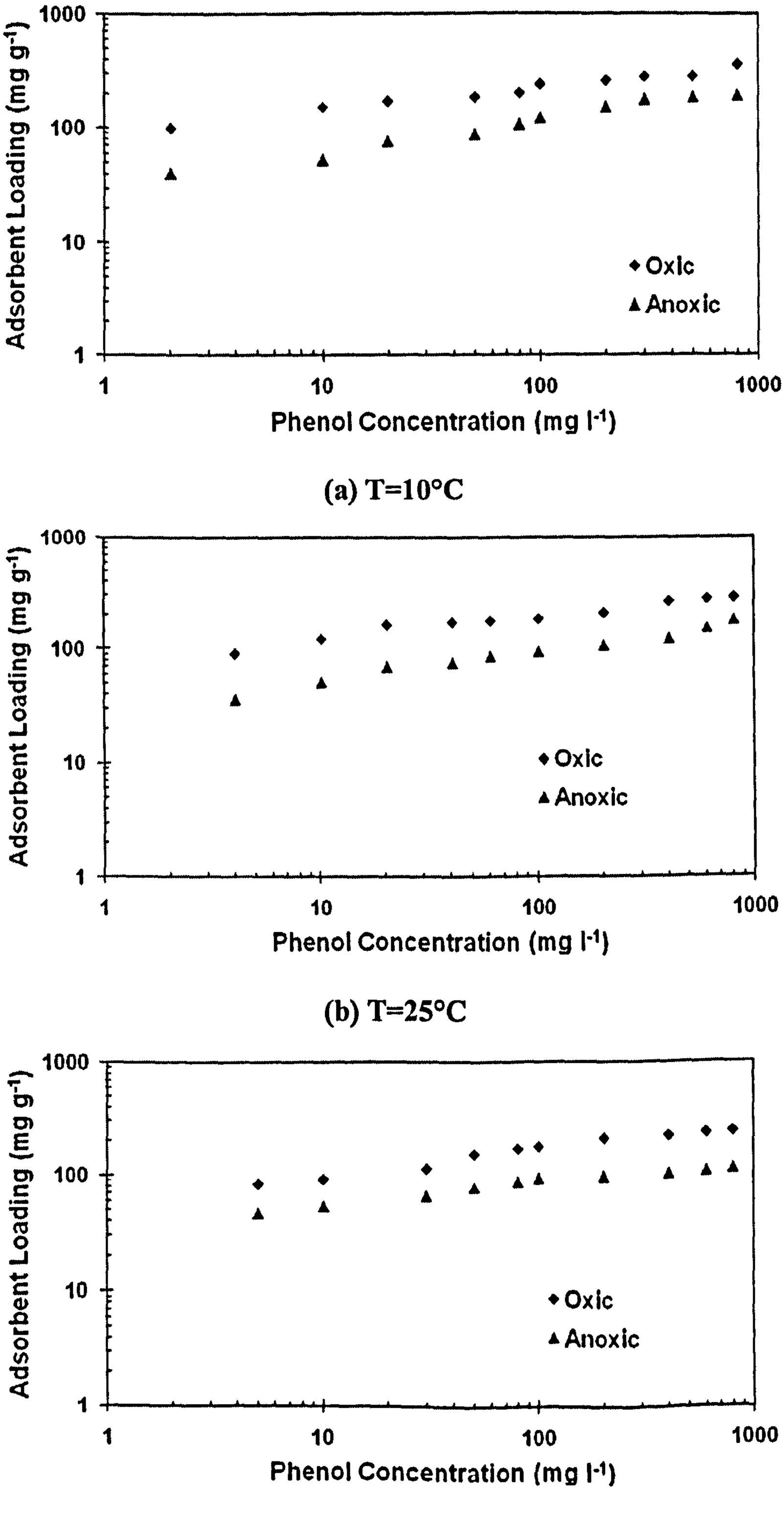


(a) T=10°C

(b) T=25°C

(c) T=45°C

**Figure 4.16: Oxic and anoxic phenol uptakes at three different temperature values**

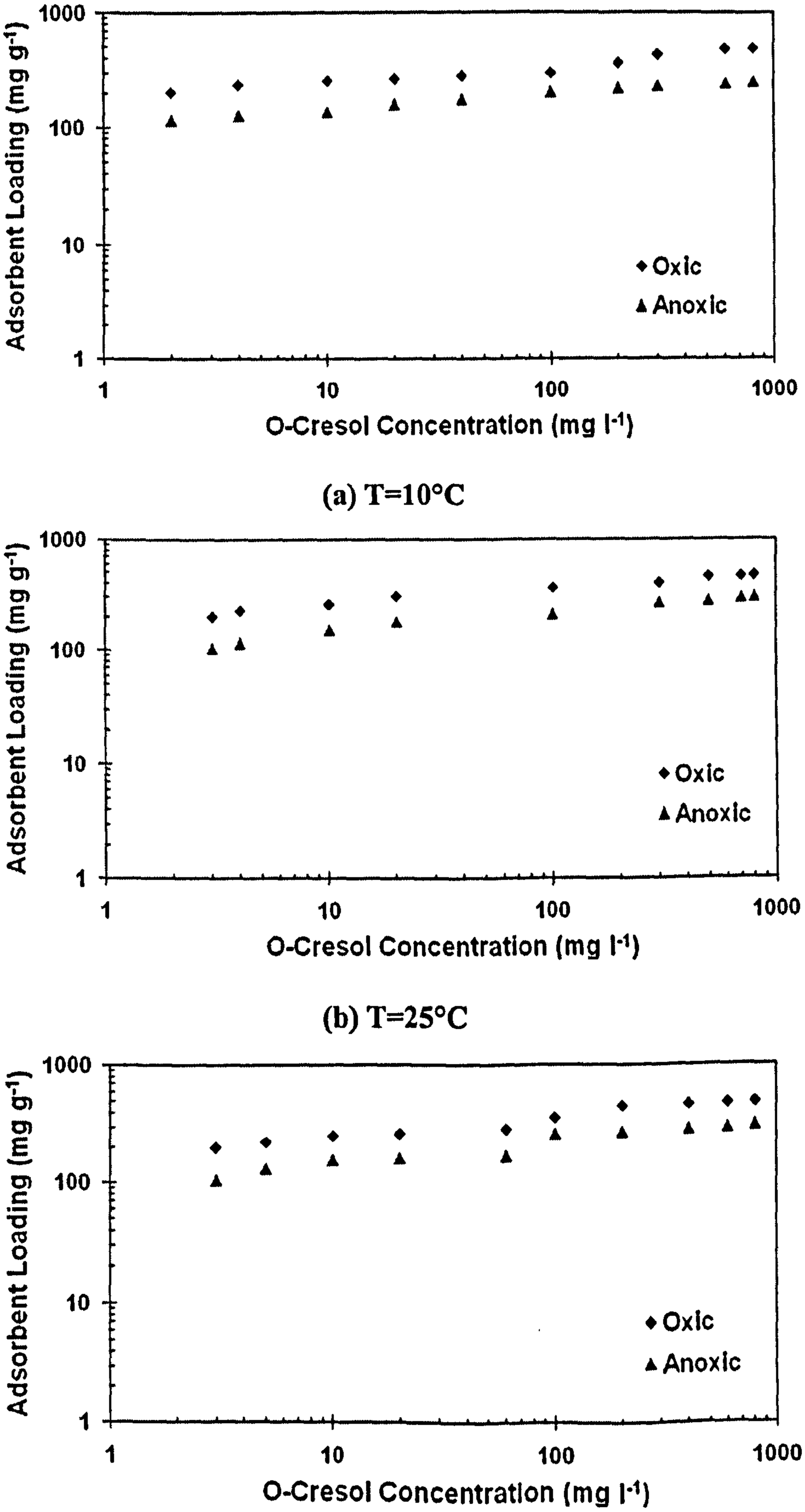


(a) T=10°C

(b) T=25°C

(c) T=45°C

**Figure 4.17: Oxic and anoxic 2-Methylphenol (o-cresol) uptakes at three different temperature values**

of adsorbent. As has been shown earlier, the diffusion of adsorbate into pores of the sorbent is not the only rate-controlling step, and the diffusion process could be ignored with adequate contact time. Therefore, the increase in sorption capacity with an increase in temperature may be attributed to chemisorption.

As in the case of pH variation, the aforementioned Figures show higher capacities for oxic conditions compared to the anoxic state for the three temperatures investigated.

The sorptive uptake was strongly dependent upon temperature. For phenol, the percentage enhancement in sorptive uptake at 1 mg $l^{-1}$ residual concentration was 94%, 88%, and 82%, at temperatures of 10 °C, 25 °C, and 45 °C, respectively, while for 2-Methylphenol, the percentage enhancement in uptake at 1 mg $l^{-1}$ residual concentration was 52%, 46%, and 88%, at temperatures of 10 °C, 25 °C, and 45 °C, respectively. In the case of phenol, the uptake increased with decreasing temperatures, while with 2-Methylphenol, the uptake was found to be relatively independent of temperature, thus suggesting that the positive and adverse impact of temperature on chemical reactions and physical adsorption, respectively, tended to balance.

### *4.3.4 Optimum Carbon Dosage*

Figure 4.18 depicts phenol removal as a function of carbon dosage at a solution pH of 6.8 obtained by dissolving 50 mg phenol in 1 litre of distilled water. Carbon dosage was varied from 1.0 mg to 1.0 g $l^{-1}$ and equilibrated for 24 hours. Carbon dosages of 0.8 g $l^{-1}$ of the produced carbon (PC) and 1.0 g $l^{-1}$ commercial carbon (CC) are required for 98% removal of phenol. The data clearly shows that the activated carbon made from date pits is more effective than the commercial activated

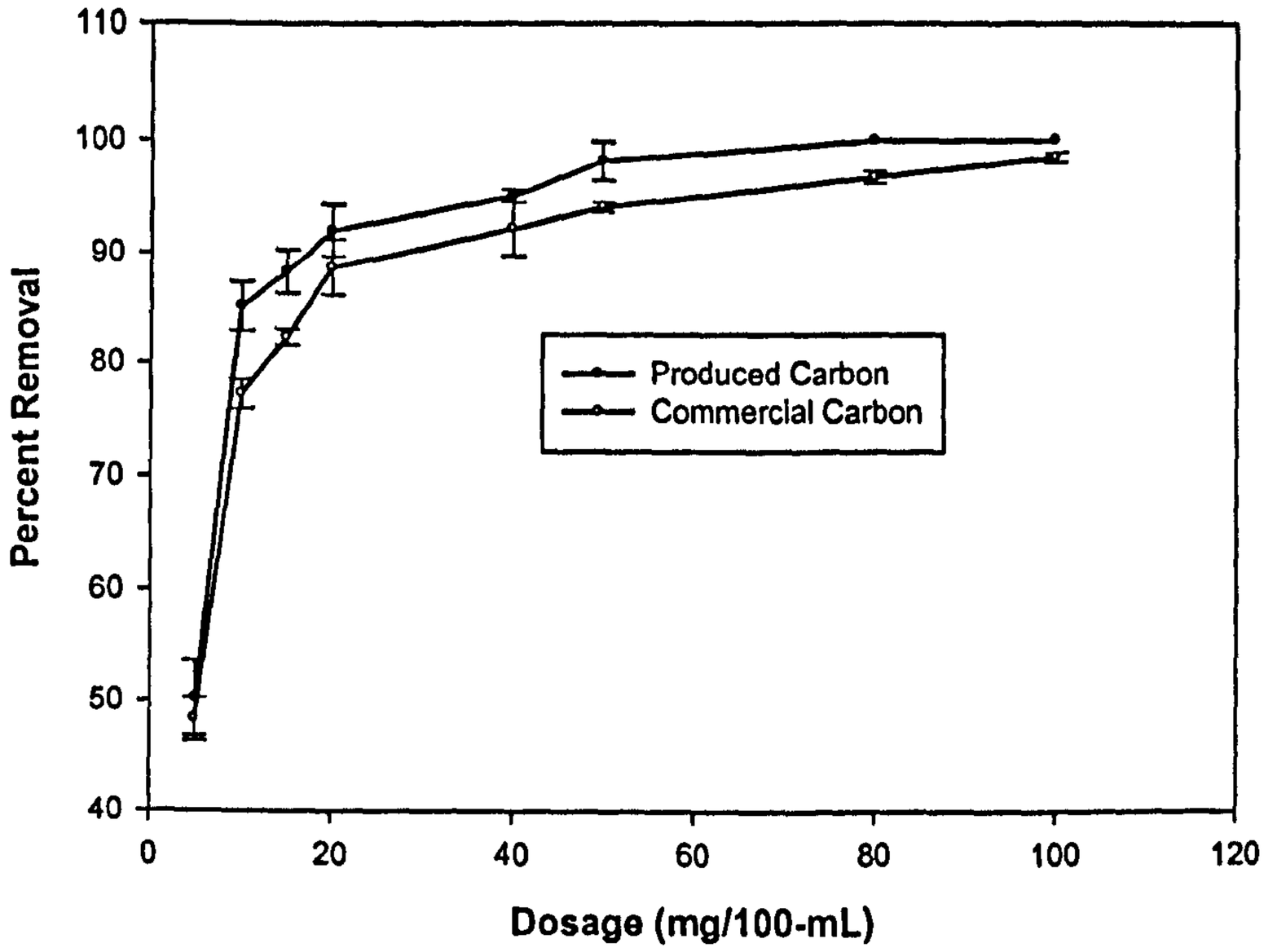


**Figure 4.18: Effect of carbon dosage on phenol removal by activated carbon produced from date pits, and commercial activated carbon**

carbon for the removal of phenol. The results also clearly indicate that the removal efficiency increases up to the optimum dosage beyond which increased dosage gives negligible increase in removal efficiency.

### *4.3.5 Effect of Contact Time*

The rate at which sorption takes place is very important when designing batch sorption experiments. Consequently, it is important to establish the time dependence of such systems under various process conditions. Available adsorption results (Vidic *et al.*, 1993) reveal that the uptake of adsorbate species is fast at the initial stages of the contact period, and thereafter it becomes slower near the equilibrium level. In between these two stages of the uptake, the rate of adsorption is found to be nearly constant. This is obvious from the fact that a large number of vacant surface sites are available for adsorption during the initial stage, and after a lapse of time, the remaining vacant surface sites are difficult to be occupied due to repulsive forces between the solute molecules in the solid and bulk phases.

To study the effect of contact time, 10 flasks with 100 ml phenol at 100 mg $l^{-1}$, at pH of 6.5 with 350 mg of the two types of activated carbon, were kept in a rotary shaker and equilibrated for periods ranging from 1-24 hours. The experimental adsorption rate curves for the activated carbons are shown in Figure 4.19. It is clearly seen from the Figure that the contact times required for 100% removal of phenol are 5 h for the locally-produced carbon and 10 h for the commercial carbon. This indicates that the locally-produced activated carbon would require less residence time for the complete removal of phenol compared to the commercial activated carbon. The Figure shows a smooth and continuous curve leading to saturation, suggesting a possible monolayer coverage of phenol on the surface of the carbon.

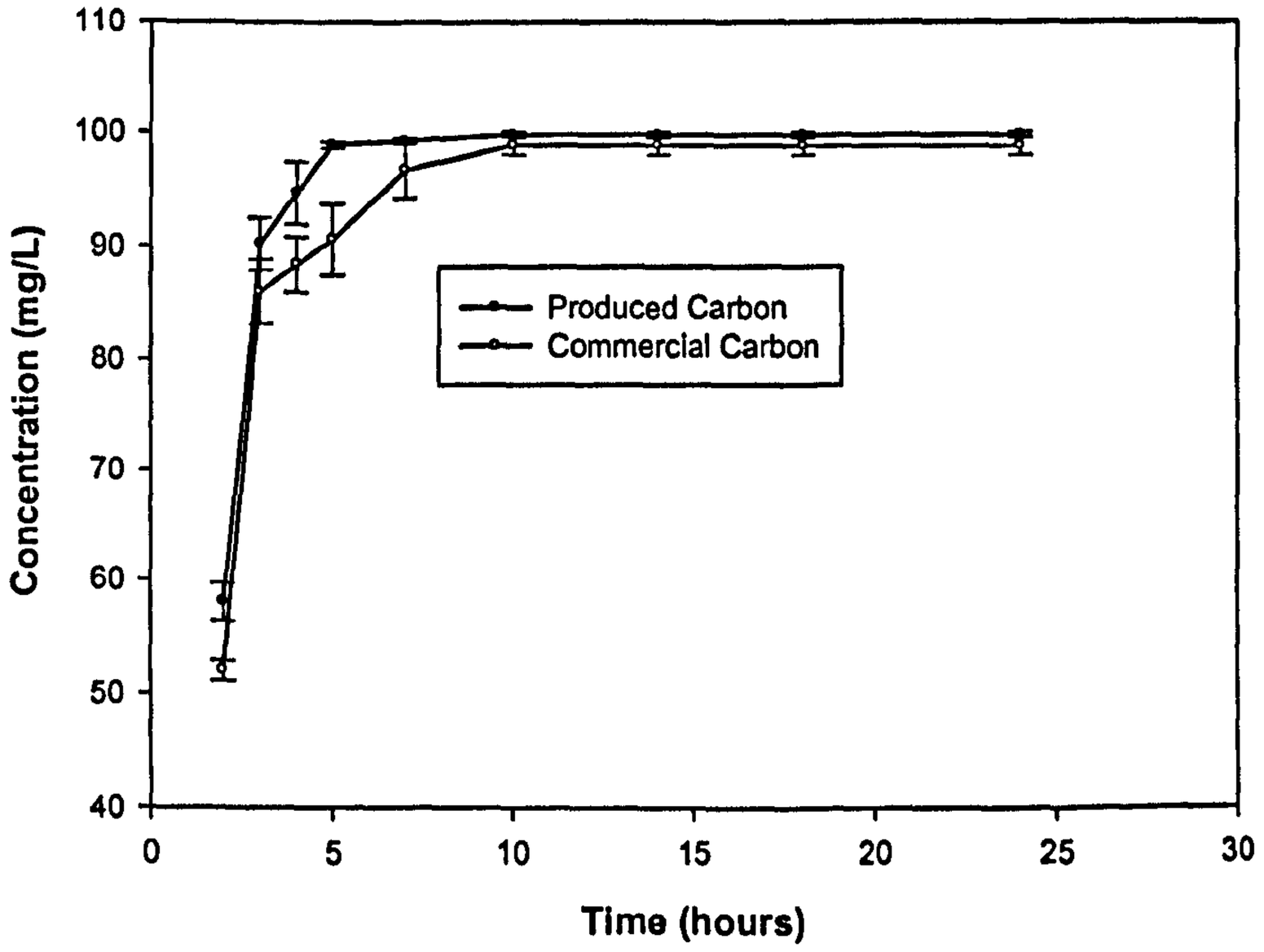


**Figure 4.19: Effect of contact time on the removal of phenol**

### *4.3.6 Desorption Studies*

Disposal of exhausted adsorbent is an environmental problem. In this study, an attempt was made to regenerate phenol/2-methylphenol-exhausted activated carbon for reuse, using chemical and electrochemical desorption studies.

#### *4.3.6.1 Chemical Desorption*

It is important to conduct desorption studies in order to understand the mechanism of desorption and at the same time recover the adsorbate and the adsorbent. One of the important issues in developing a new adsorbent is its regeneration capability. Different permutation and combinations of methods were used to desorb phenol and 2-methylphenol from the exhausted carbon using acids and bases of different strength. Sulphuric acid and sodium hydroxide were used for this purpose. Four different quantities (1, 5, 7 and 10 g) of exhausted carbon were separately put into 150 ml bottles filled with each of the above chemicals. To avoid any evaporation, no headspace was allowed in the bottles. The bottles were placed in a shaker for two weeks. The solutions in the bottles were then filtered through a 0.45 μm membrane filter and the residual phenol was measured using UV-vis spectrophotometer. Table 4.8 shows the results of desorption efficiency. This is the adsorption capacity achieved in the re-adsorption experiment divided by the virgin AC adsorption capacity multiplied by 100. From this, sodium hydroxide was found to be the better desorbing reagent. This could be due to the formation of a sodium salt of phenol which facilitated the desorption. The most effective concentration of sodium hydroxide to desorb phenol from the locally-produced activated carbon was found to be 1.0 N.

**Table 4.8: Results of desorption efficiency**

| Parameters | Sulphuric acid | | | Sodium hydroxide | | |
|---|---|---|---|---|---|---|
| | 0.05 N | 0.1 N | 1.0 N | 0.05 N | 0.1 N | 1.0 N |
| Regeneration efficiency % | 26 | 29 | 48 | 40 | 62 | 79.8 |
| Residual phenol conc. (mg $l^{-1}$) | 62.3 | 58.7 | 36.1 | 32.8 | 20.4 | 10.1 |

### *4.3.6.2 Electrochemical Desorption*

Prior to regeneration, a known mass of the Phenol -saturated AC was introduced into the electrochemical reactor. The supporting electrolyte of NaCl (1.5 *l*, concentration of 1-5.0 g $l^{-1}$), adjusted to a suitable pH value (pH = 6.8), was poured into the reactor. This pH value was selected because it is the optimum value obtained for maximum 2-methylphenol removal, as indicated in section 4.2.1 on page 85. The electrochemical regeneration of AC began when the direct-current power supply was turned on. Constant current density of 10 mA $cm^{-2}$ was maintained with only minor adjustments of the applied voltage. The distance between two electrodes was adjusted to 3 cm and a current intensity of 500 mA was applied. The residual concentrations of phenol at intervals of time were measured. The results are shown in Figure 4.20. From the Figure, it is evident that with increasing regeneration time, the phenol residual concentration decreases. Conventionally, the regeneration would last for 30-120 min. When the electrochemical regeneration ended, the AC in the reactor was filtered, and dried for 24 hours at 105 °C. After cooling and weighing, the AC was shifted into a column to determine its re-adsorption capacity. The regeneration process was evaluated by determining the percent regeneration efficiency (RE). This is the adsorption capacity achieved in the re-adsorption experiment divided by the virgin AC adsorption capacity multiplied by 100. The experimental data are presented in Table 4.9. From the Table, it can be seen that as the concentration of sodium chloride was increased from 1 to 5%, the effect of the electrolyte on regeneration efficiency was significant.

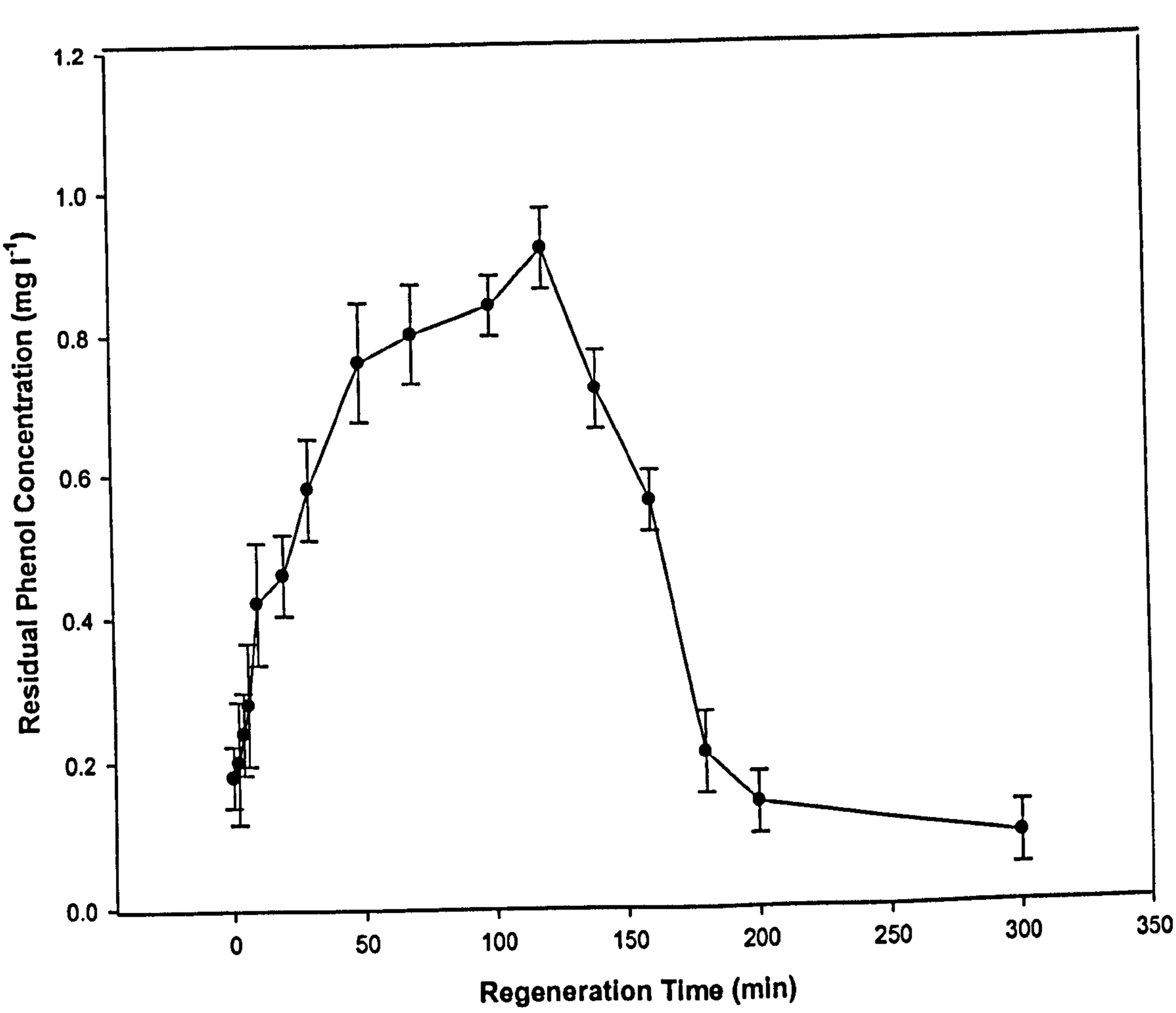


**Figure 4.20: Electrochemical regeneration of phenol exhausted carbon**

**Table 4.9: The effects of NaCl concentration on regeneration efficiency at a regeneration time of 1 hour**

| Parameters | Sodium chloride concentration | | | | |
|---|---|---|---|---|---|
| | 1% | 2% | 3% | 4% | 5% |
| Regeneration efficiency % | 66.2 | 72.4 | 78.6 | 81 | 86.4 |
| Residual phenol concentration (mg $l^{-1}$) | 29.9 | 23.4 | 18.9 | 11.4 | 10.6 |

### *4.3.7 Adsorption Isotherm*

The equilibrium removal of phenol was mathematically expressed in terms of adsorption isotherms. The Freundlich adsorption isotherm was applied for the adsorption of phenol by both the local (PC) and commercial carbons (CC). The experimental results obtained for the adsorption of phenol on both carbons at room temperature (22 ± 1 °C) and at optimum conditions of pH of 6.8, contact time of 2 hours and dose of 50 mg $l^{-1}$ of adsorbent were found to comply with the Freundlich adsorption isotherm (Equation 4.4) better than with the Langmuir isotherm commonly used for ideal gas mixtures.

For the Freundlich isotherm, $$\left(\frac{x}{m}\right) = kC_e^{1/n} \tag{4.4}$$

The logarithmic form of the equation is

$$\log\left(\frac{x}{m}\right) = \log(k) + \frac{1}{n}\log(C_e) \tag{4.5}$$

The Freundlich adsorption isotherm represents the relationship between the amount of phenol adsorbed per unit mass of the adsorbent ($x/m$) and the concentration of the phenol at equilibrium ($C_e$). The constants $k$ and $n$ represent the adsorption capacity and intensity of adsorption, respectively. The data obtained in this study were plotted using the fit for the Freundlich adsorption isotherm (Figure 4.21).

The plot of log ($x/m$) versus log $C_e$ for various initial concentrations of phenol was found to be nearly linear, indicating the appropriateness of the Freundlich isotherm model. For the locally-produced and the commercial carbons, the adsorption capacity ($k$) was found to be 15.5 and 9.94 mg $g^{-1}$, respectively, and the adsorption intensity ($n$) 1.32 and 3.57, respectively. The higher value of $k$ in the locally-produced carbon

indicates a higher affinity for phenol, and the values of $n$ between 1 and 10 indicate a favourable intensity of adsorption.

The Freundlich isotherm parameters for phenol are reported in Table 4.10.

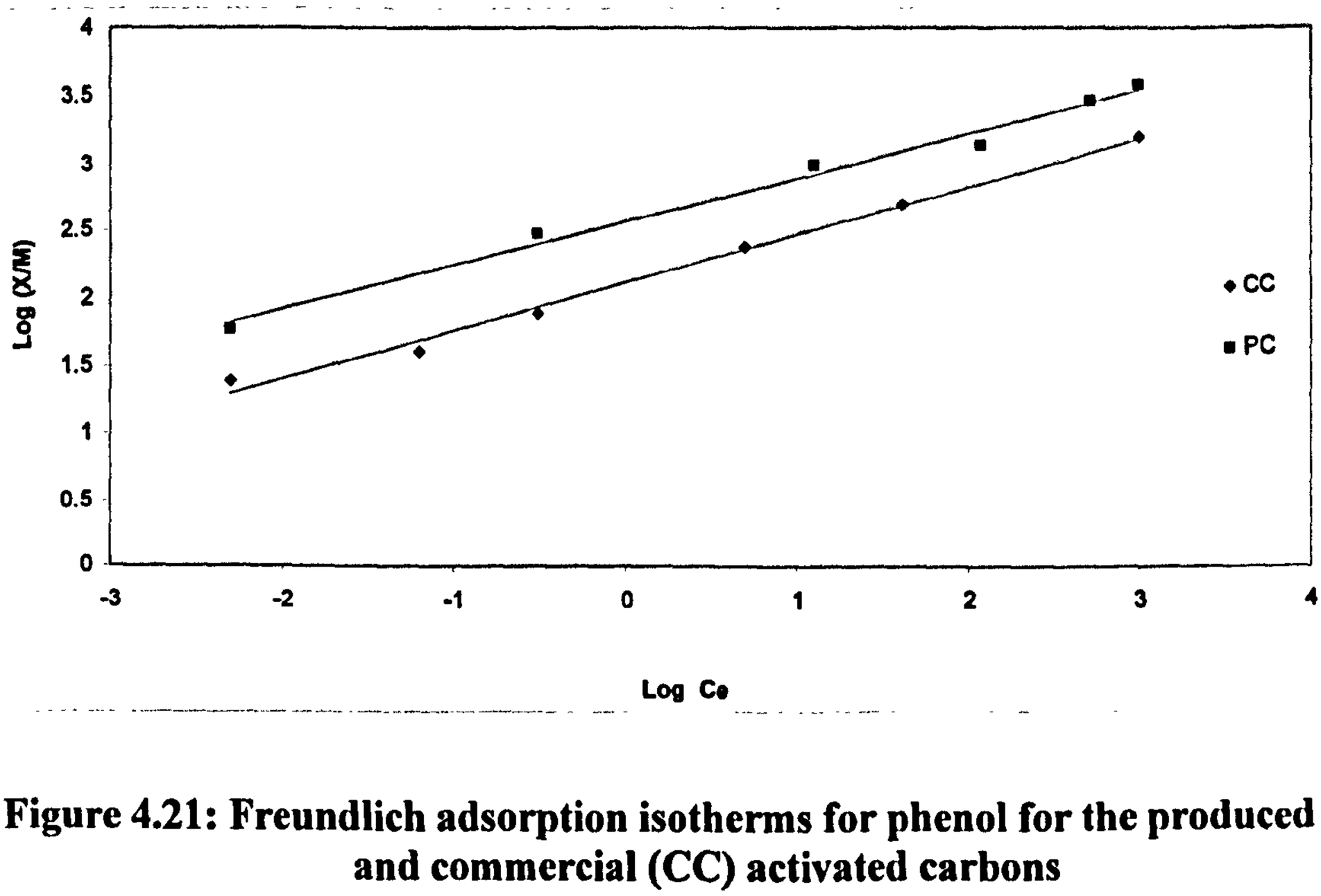


**Figure 4.21: Freundlich adsorption isotherms for phenol for the produced (PC) and commercial (CC) activated carbons**

**Table 4.10: Adsorption characteristics of phenol by the two carbons**

| Sample | Freundlich Parameters | | |
|---|---|---|---|
| | $k_f$ | $1/n$ | $R^2$ |
| Local Carbon | 15.50 | 0.76 | 99.0 |
| Filtrasorb-400 | 9.94 | 0.28 | 98.2 |

From Figure 4.21, it is clearly seen that the locally-produced activated carbon was more effective than the commercial specimen in the removal of phenol, since its isotherm lies above the isotherm for the commercial carbon over the entire range of concentrations investigated. Thus, for any equilibrium solute concentration, the amount of solute adsorbed per unit mass of carbon was greater for the locally-produced carbon than for the commercial specimen. Furthermore, the fact that both isotherms have steep slopes indicates that their adsorptive capacities increase at higher equilibrium solute concentrations over that at lower concentrations.

### *4.3.8 Adsorption Kinetics*

The kinetics of adsorption describe the solute uptake, which in turn govern the residence time required for the adsorption reaction. It is one of the important characteristics in defining the efficiency of adsorption. Hence, in the present study, the kinetics of phenol removal were determined to understand the behaviour of the adsorbent. The adsorption of phenol from an aqueous solution follows reversible first order kinetics, such as when a single species is considered on a heterogeneous surface. The heterogeneous equilibrium between the phenolic solution and the activated carbon may be expressed as,

$$A \underset{k_2}{\overset{k_1}{\rightleftharpoons}} B \tag{4.6}$$

where $A$ and $B$ are liquid and solid phase, respectively, $k_1$ is the forward reaction rate constant, and $k_2$ the backward reaction rate constant.

If '$a$' is the initial concentration of phenol and '$x$' the amount transferred from liquid phase to solid phase at any time $t$, then the rate of transfer of $x$ is given by

$$\frac{dx}{dt} = -\frac{d(a-x)}{dt} = k(a-x) \tag{4.7}$$

or

$$k = \frac{1}{t} \ln\left(\frac{a}{a-x}\right) \tag{4.8}$$

where $k$ is the overall reaction rate constant. Since $k_1$ and $k_2$ are the rate constants for the forward and reverse processes, respectively, the rate can be expressed as,

$$\frac{dx}{dt} = k_1(a-x) - k_2 x \tag{4.9}$$

If $X_e$ represents the concentration of phenol adsorbed at equilibrium, then at equilibrium,

$$k_1(a-X_e) - k_2 X_e = 0 \tag{4.10}$$

because under these conditions,

$$\frac{dx}{dt} = 0 \quad k_c = \frac{X_e}{a-X_e} = \frac{k_1}{k_2} \tag{4.11}$$

where $k_c$ is the equilibrium constant.

Substituting for '$a$'

$$\frac{dx}{dt} = (k_1+k_2)(X_e - x) \tag{4.12}$$

Integration of the equation leads to

$$k_1 + k_2 = \frac{1}{t} \ln\left(\frac{X_e}{X_e - x}\right) \tag{4.13}$$

The above equation can be written in the form of

$$\ln(1-U_t) = -(k_1+k_2)t = -kt \tag{4.14}$$

where $U_t = x/X_e$ and $(k_1 + k_2)$ is $k$, the overall rate constant.

Further,

$$k = k_1 + k_2 = k_1 + \frac{k_1}{k_e} = k_1\left[1 + \frac{1}{k_e}\right] \tag{4.15}$$

$U_t$ can be calculated using the expression

$$\frac{C_{A(0)} - C_{A(t)}}{C_{A(0)} - C_e} = \frac{x}{X_e} = U_t \tag{4.16}$$

where $C_{A(0)}$ is the initial concentration of phenol, $C_{A(t)}$ the concentration of phenol present at any time ($t$), and $C_e$ the concentration of phenol present at equilibrium condition. $U_t$ is called the fractional attainment of equilibrium of phenol and was calculated by considering phenol and 2-methylphenol adsorption by the activated carbon in a given time range 1-24 h. In the present study, concentrations of phenol and 2-methylphenol over the range 10-30 mg $l^{-1}$ were tested. Using the kinetic equations, the overall rate constant, and the forward and backward rate constants were calculated. For instance, by plotting $\ln(1-U_t)$ versus $t$ (Equation 4.14 and Figure 4.22), the overall rate constant '$k$' for a given concentration of phenol and 2-methylphenol was calculated by considering the slope of the line of best fit.

### *4.3.9 Test with Phenolic-based Petrochemical Industry Wastewater*

Although the adsorption of single components like phenol, 2-methylphenol and tetramethylthionine chloride from aqueous media onto activated carbon has been studied by many researchers, there are likely to be some differences in the adsorption behaviour when the activated carbon is used with genuine wastewater, which has a

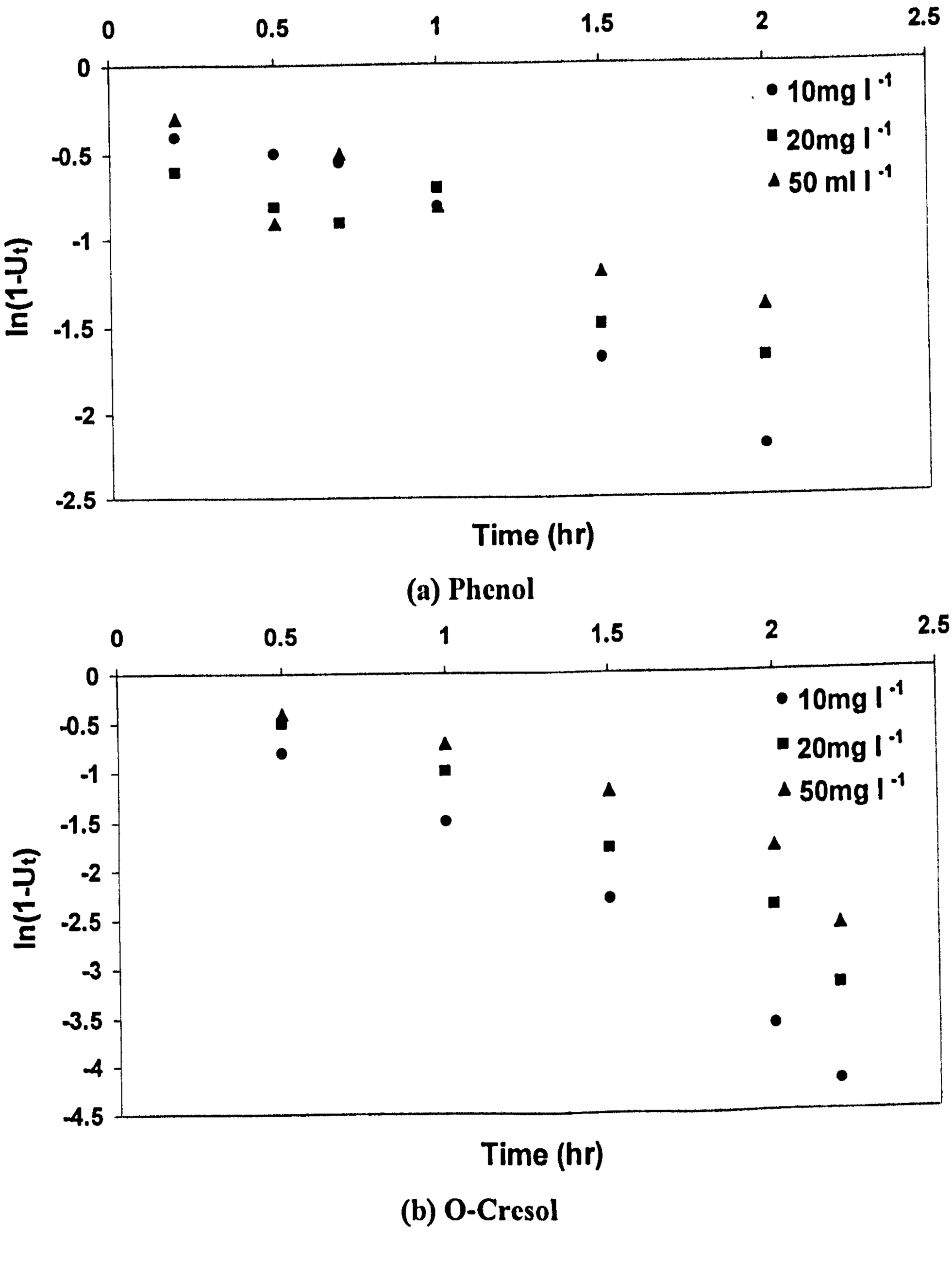


**Figure 4.22: Kinetic data for the adsorption of phenol and 2-methylphenol (o-cresol) by the PC**

mixture of components. The efficiency of the carbon in the removal of phenol in synthetic wastewater is likely to be higher than that of phenol in effluents from industry due to the presence of impurities present in the latter which may interfere with the adsorption process. Isotherm studies were performed on industrial wastewater samples collected from the Saudi Petrochemical Industry plant in Jubail to investigate this.

The process diagram of the industrial plant is shown in Figure 4.23. The wastewater was obtained from the petrochemical plant at a sampling point after the dissolved air flotation unit. The flow rate was 15 ml $min^{-1}$. The adsorption capacities for the local activated carbon and the commercial activated carbon were found to be 56 mg $g^{-1}$ for synthetic phenolic solution and 36 mg $g^{-1}$ for industrial phenolic wastewater (Figure 4.22). The efficiency of the produced carbons towards removal of phenol in synthetic wastewater was higher than that in industrial phenol effluents. The difference was probably due to the presence of other competing impurities present in the industrial wastewater which interfered with the adsorption process.

The equilibrium adsorption isotherms for the removal of Total Organic Carbon (TOC) from the wastewater sample are presented in Figure 4.24. The data show that there is significant enhancement in the uptake of the activated carbon for organic matter, in terms of TOC, when oxygen is present in the test environment. Biodegradation was discounted as a possible cause for this increase in uptake through monitoring of inorganic carbon, which showed no increase in $CO_2$ in the outlet of column. The impact of oxygen on the pollutant uptake was pronounced at all concentration levels. Thus, in practical operation of activated carbon adsorbers which are usually designed to meet stringent effluent criteria, the addition of oxygen

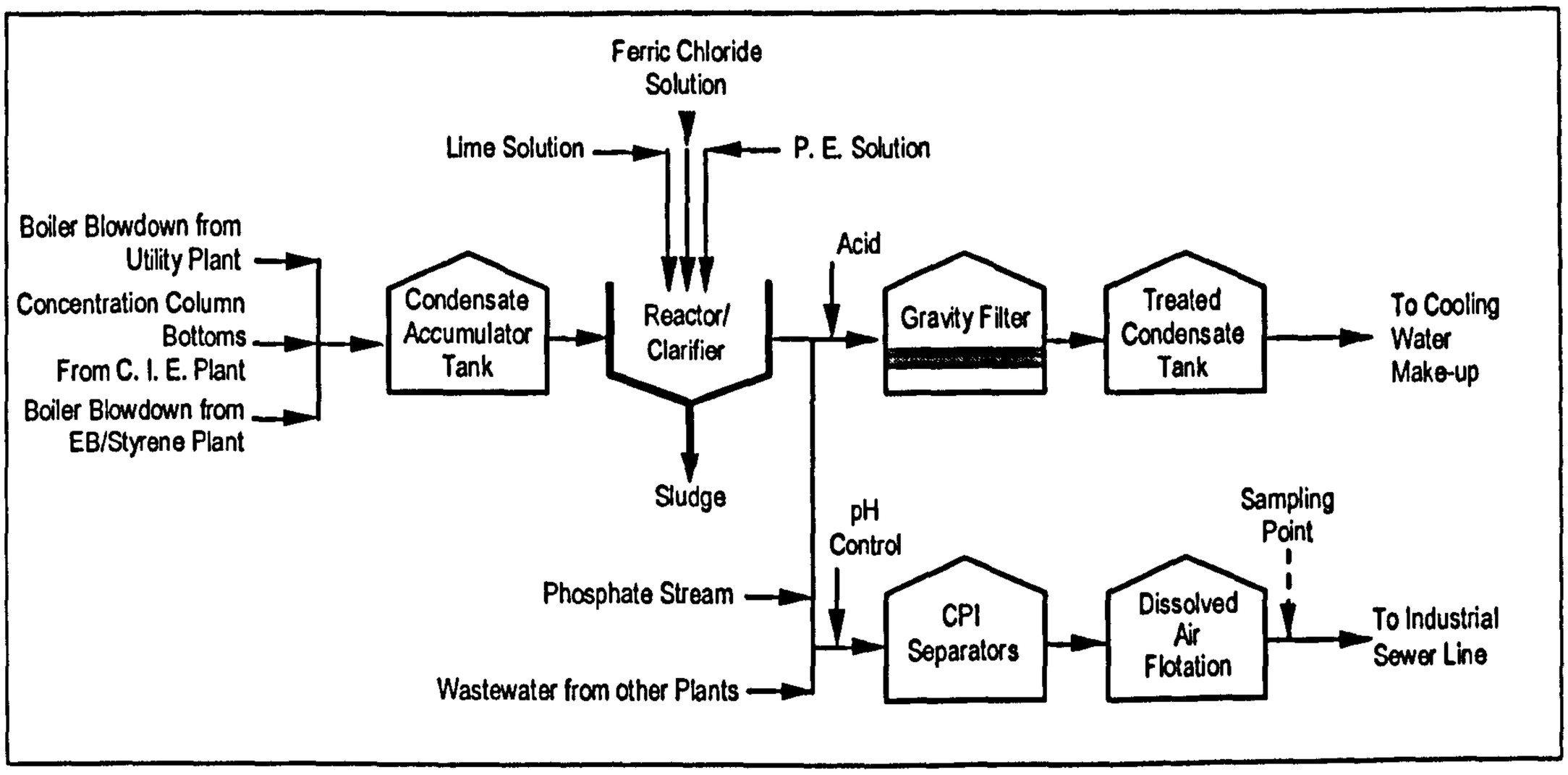


**Figure 4.23: Process diagram of the water treatment section of the Jubail Saudi Petrochemical Industry**

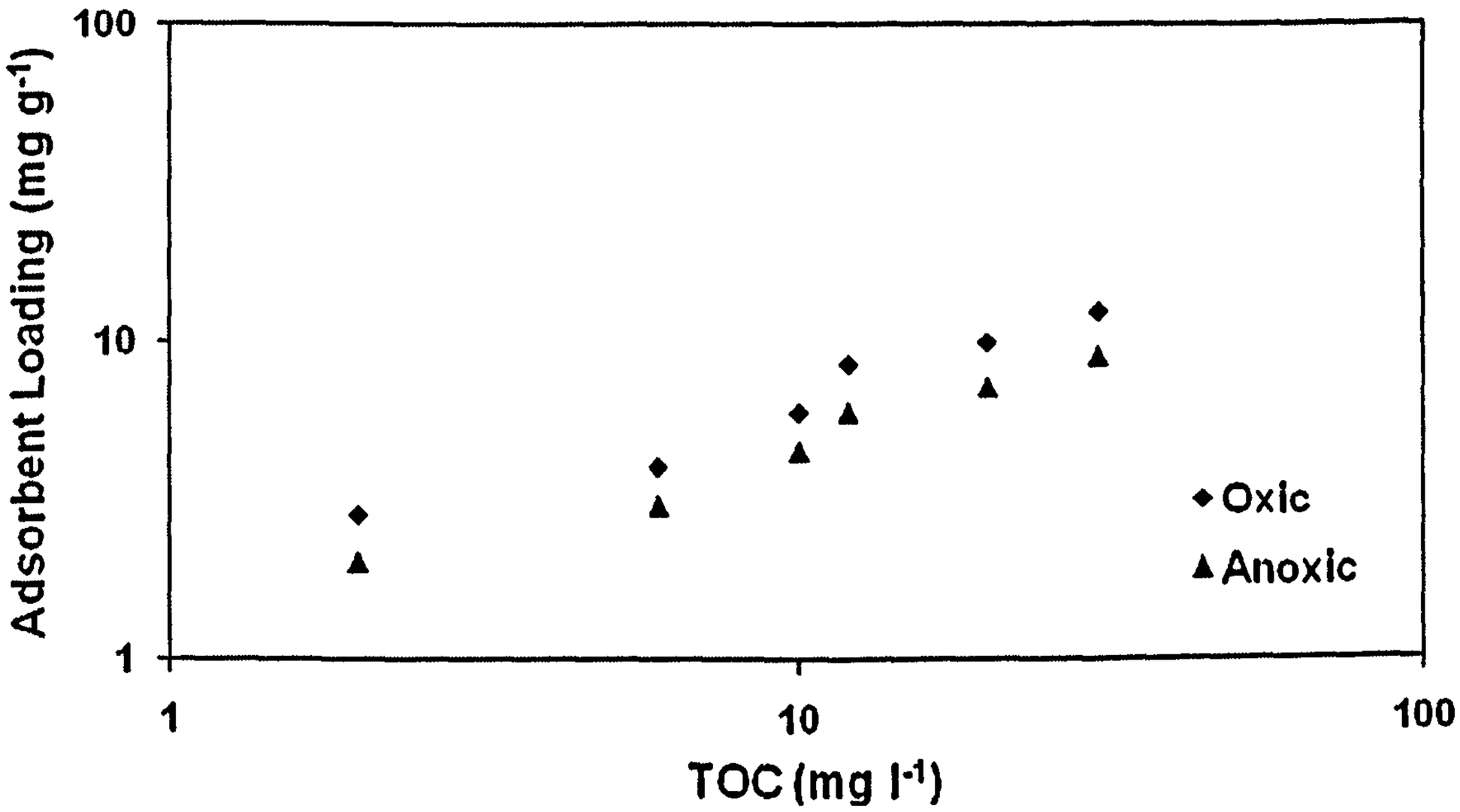


**Figure 4.24: Removal of TOC from industrial wastewater under oxic and anoxic conditions**

to the feed wastewater would result in a significant improvement in their performance.

### *4.3.10 Column Studies*

Column-type continuous flow operations appear to have a distinct advantage over batch type operations because the rate of adsorption depends on the concentration of solute in the solution being treated. For column operation the adsorbents are continuously in contact with a fresh solution. Consequently, the concentration in the solution in contact with a given layer of adsorbent in a column is relatively constant. For batch treatment, the concentration of solute in contact with a specific quantity of adsorbent steadily decreases as adsorption proceeds, thereby decreasing the effectiveness of the adsorbent for removing the solute. The breakthrough capacity, which is the amount adsorbed before the appearance of adsorbate in the effluent, and the total capacity, which is the amount adsorbed until the adsorbate concentration in the effluent is equal to the adsorbate concentration in the influent, are computed from breakthrough curves.

Breakthrough curves for upflow and downflow columns were determined for phenol and 2-methylphenol at room temperature and pH 6.5. The results of the column studies are shown in Figures 4.25 and 4.26. In these Figures, $C$ represents the concentration of adsorbate at any time and $C_o$ represents the initial adsorbate concentration. $C/C_o$ is the normalized solution phase concentration.

In Figure 4.25, it can be seen that after 50 minutes had elapsed, the carbon reached breakthrough in the case of phenol. Breakthrough for the column removing 2-methylphenol came 20 minutes later. In Figure 4.26, the breakthrough was observed after 30 minutes of operation for phenol and 80 minutes for 2-methylphenol. From

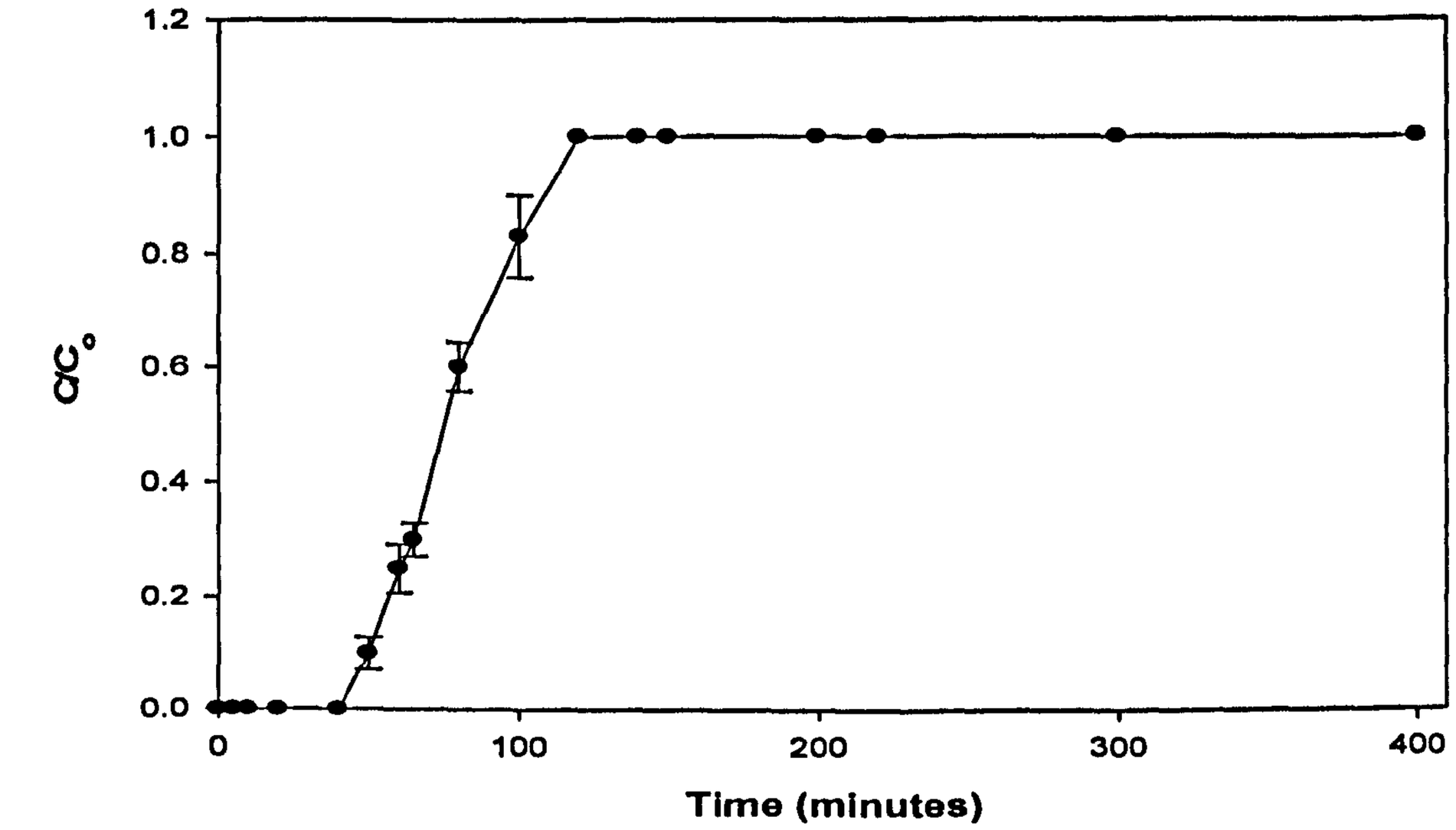


(a) Phenol

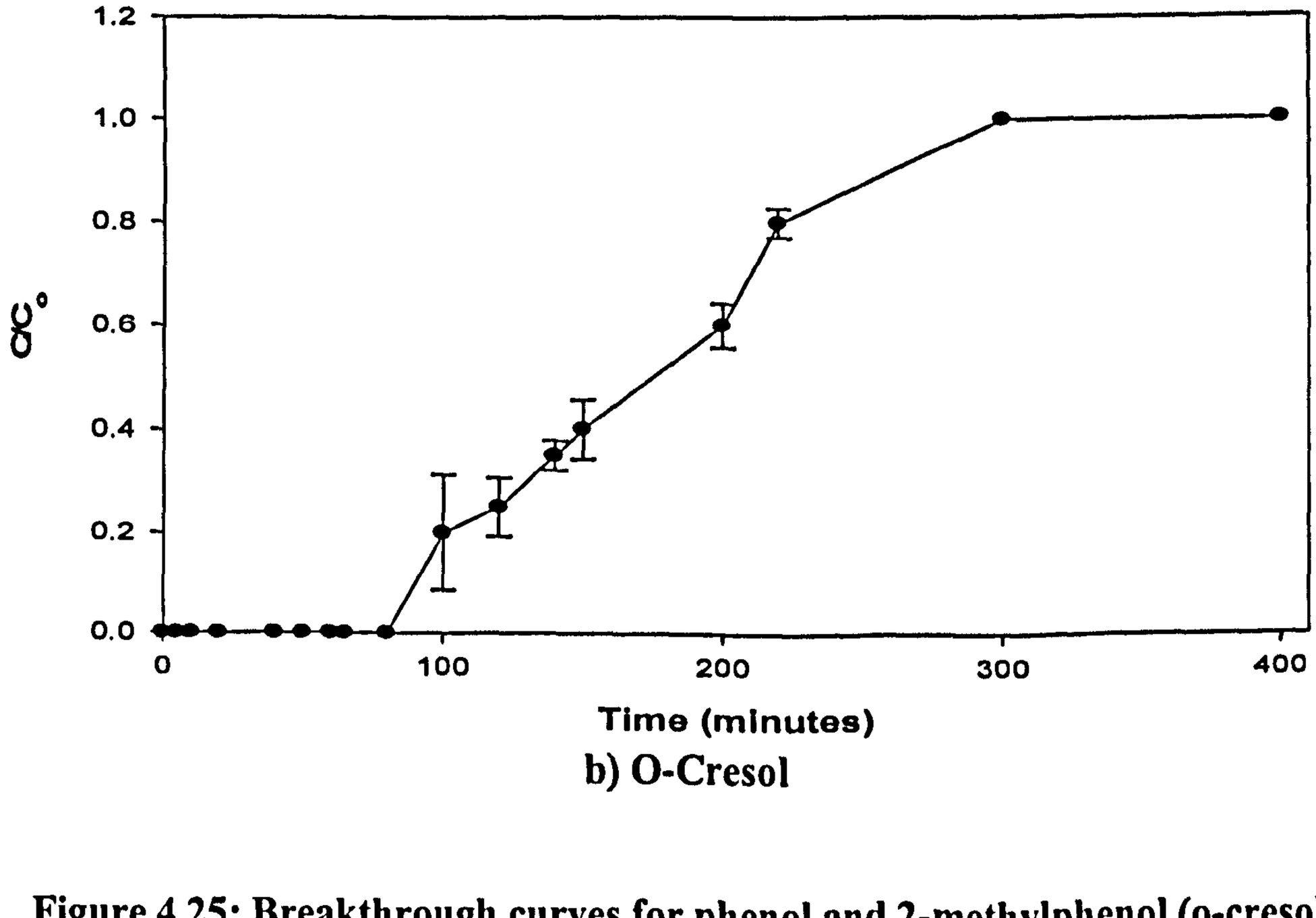


b) O-Cresol

**Figure 4.25: Breakthrough curves for phenol and 2-methylphenol (o-cresol) using the produced carbon (PC) in downflow mode**

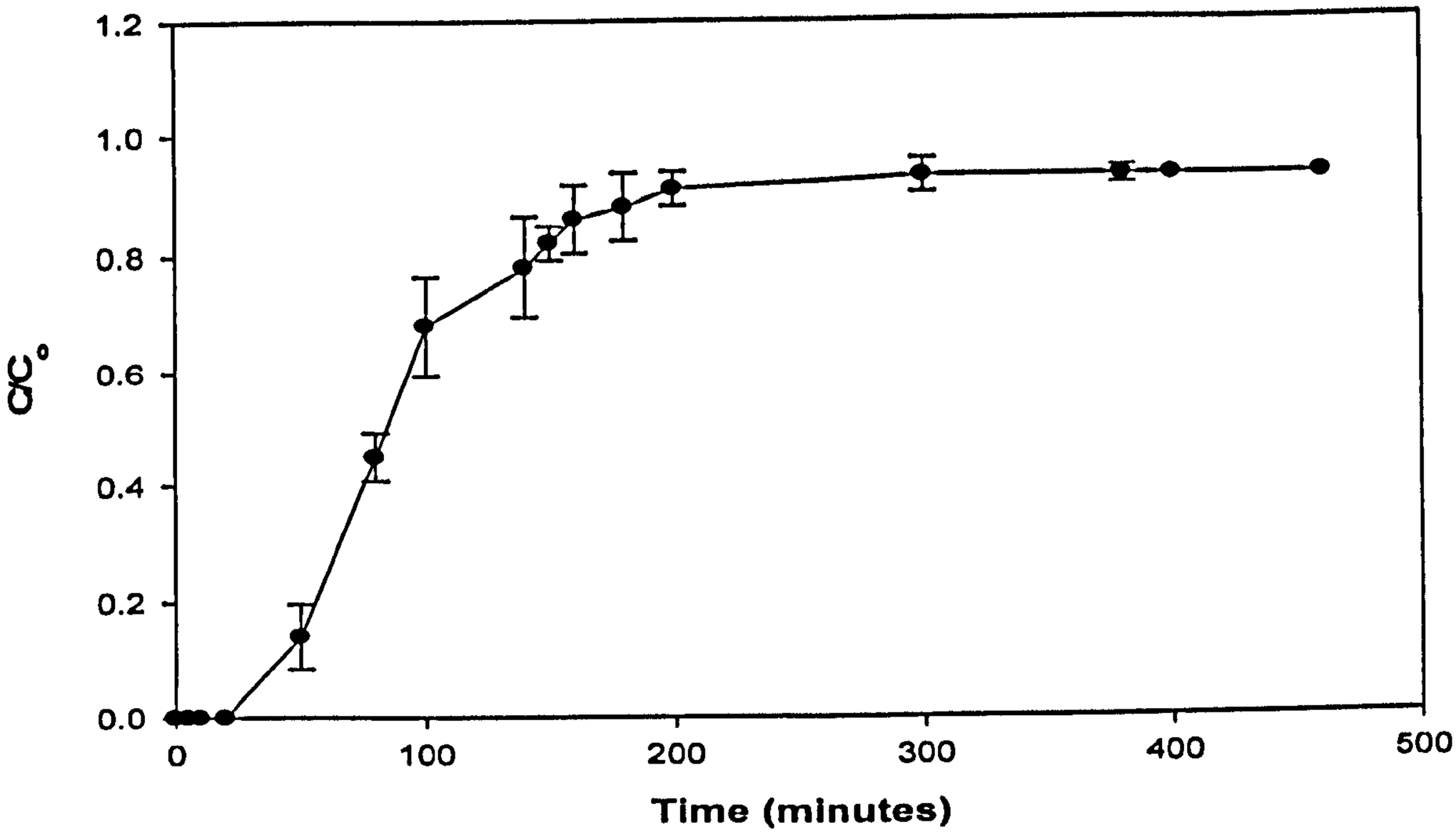


**(a) Phenol**

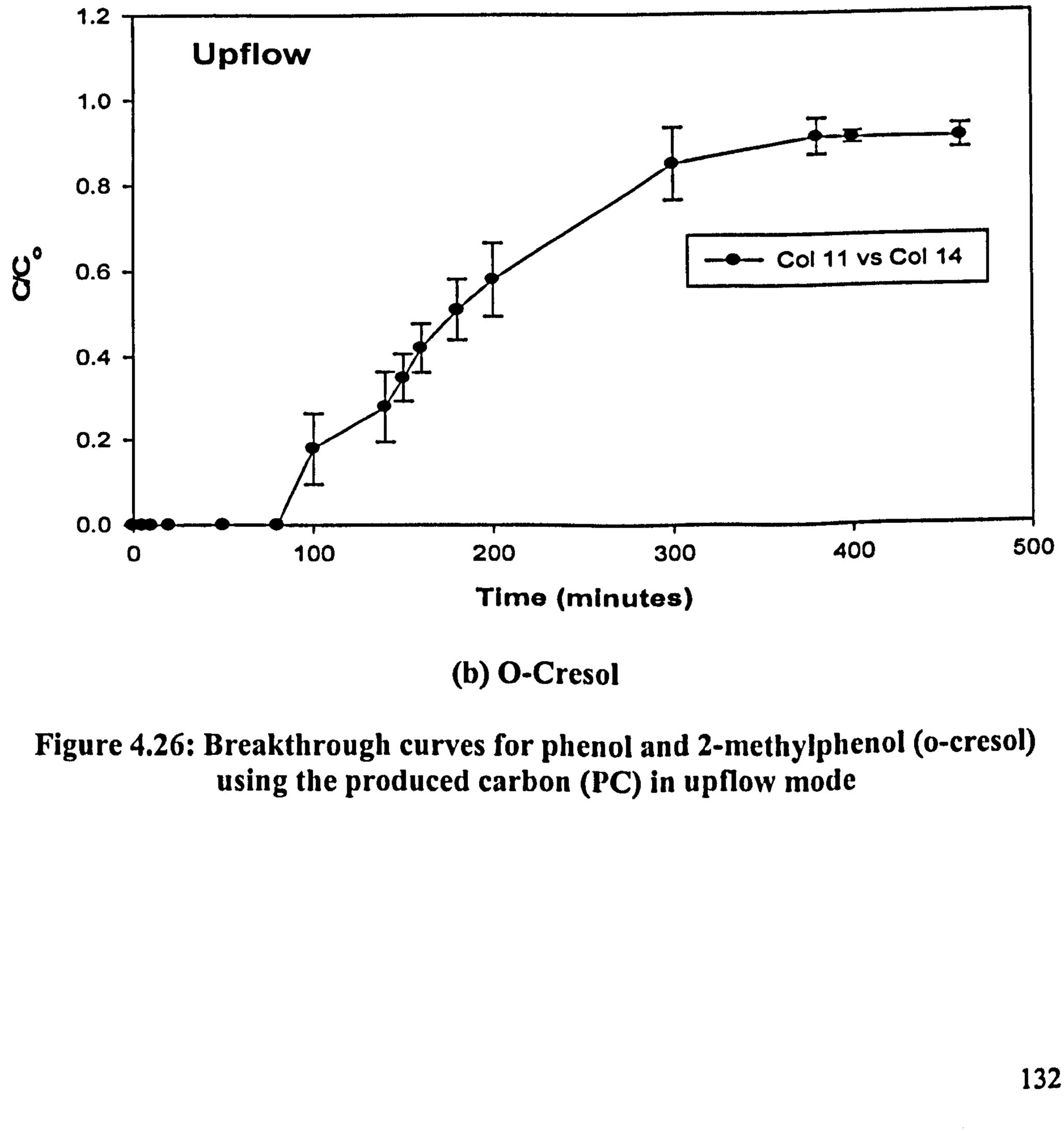


**(b) O-Cresol**

**Figure 4.26: Breakthrough curves for phenol and 2-methylphenol (o-cresol) using the produced carbon (PC) in upflow mode**

These two figures, it can be concluded that upflow and downflow modes for the columns studied had no significant difference. The effluent discharge criteria set by regulatory agencies usually governs the operation of granular activated carbon columns. These regulations specify limits based on the breakthrough in the adsorption columns. The breakthrough times in the present study were measured from the beginning of the experiment and give a very good indication of the additional capacity available in the locally-produced carbon for adsorption of 2-methylphenol, compared to phenol.

### *4.3.11 Effect of Flow Rate*

The effect of flow rate on the sorption of phenol by the locally-produced carbon was investigated using downflow mode. The breakthrough curves developed under three different flow rates (5, 15 and 30 ml $min^{-1}$) of phenol at 100 mg $l^{-1}$, and 2-methylphenol at 100 mg $l^{-1}$, at the same flow rates, are shown in Figure 4.27. As can be observed, initially, phenol and 2-methylphenol were rapidly adsorbed on the carbon and the effluent was almost free of solute. As the phenol and 2-methylphenol solutions continued to flow, the carbon was progressively saturated with phenol and 2-methylphenol and, therefore, the outlet concentration started to increase until the maximum point was reached, where no adsorption was taking place.

In industrial practice, system operation is interrupted when the pollutant concentration reaches a certain level, called the breakthrough concentration, above which it is not profitable to continue the operation. Although in the present study the experiments were continued until saturation of the bed, when calculating the characteristic parameters of the system, a breakthrough concentration of 1 mg $l^{-1}$ was

considered. As can be observed, the breakthrough point decreased when flow rate increased, and the service time of the carbon bed was then reduced.

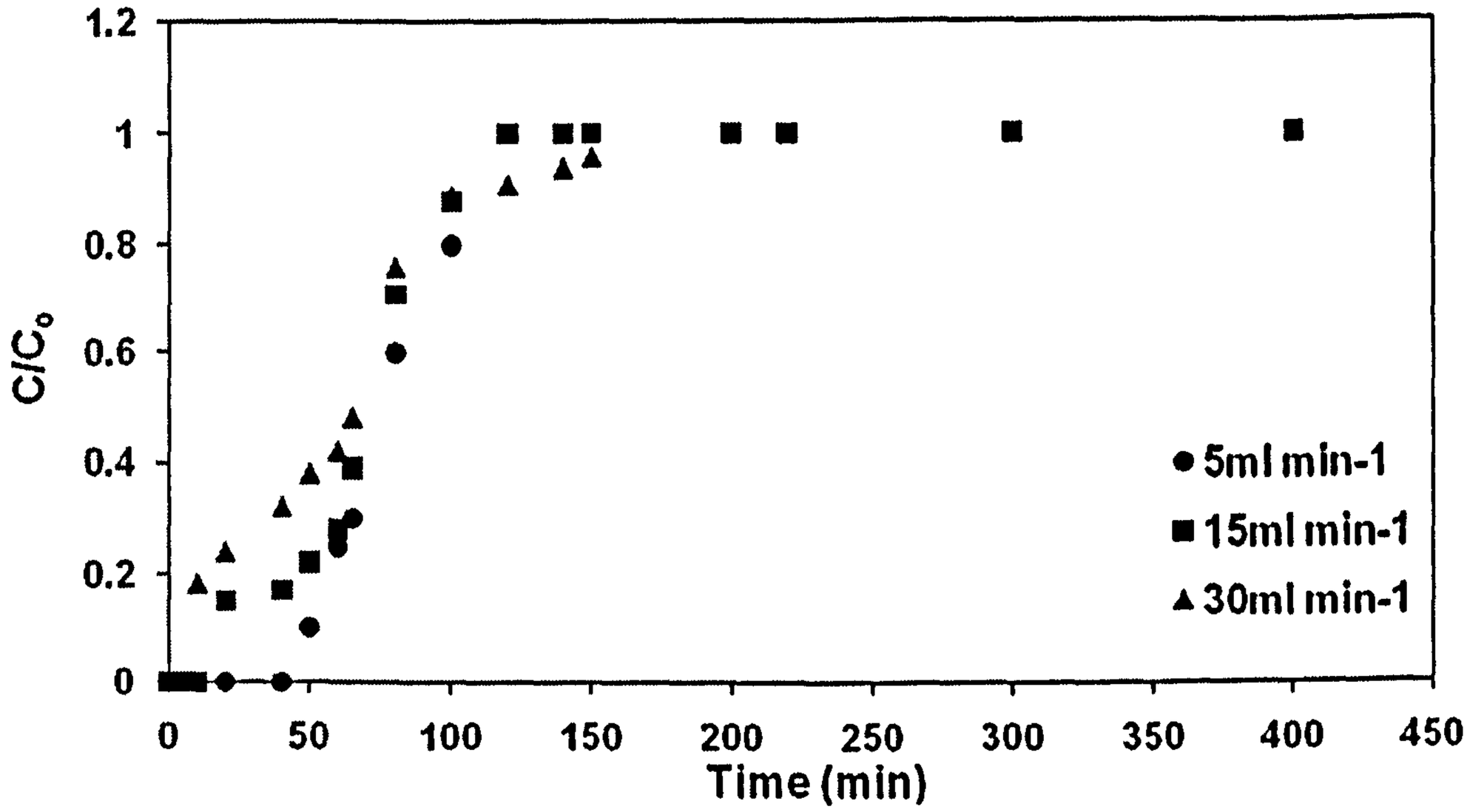


**(a) Phenol**

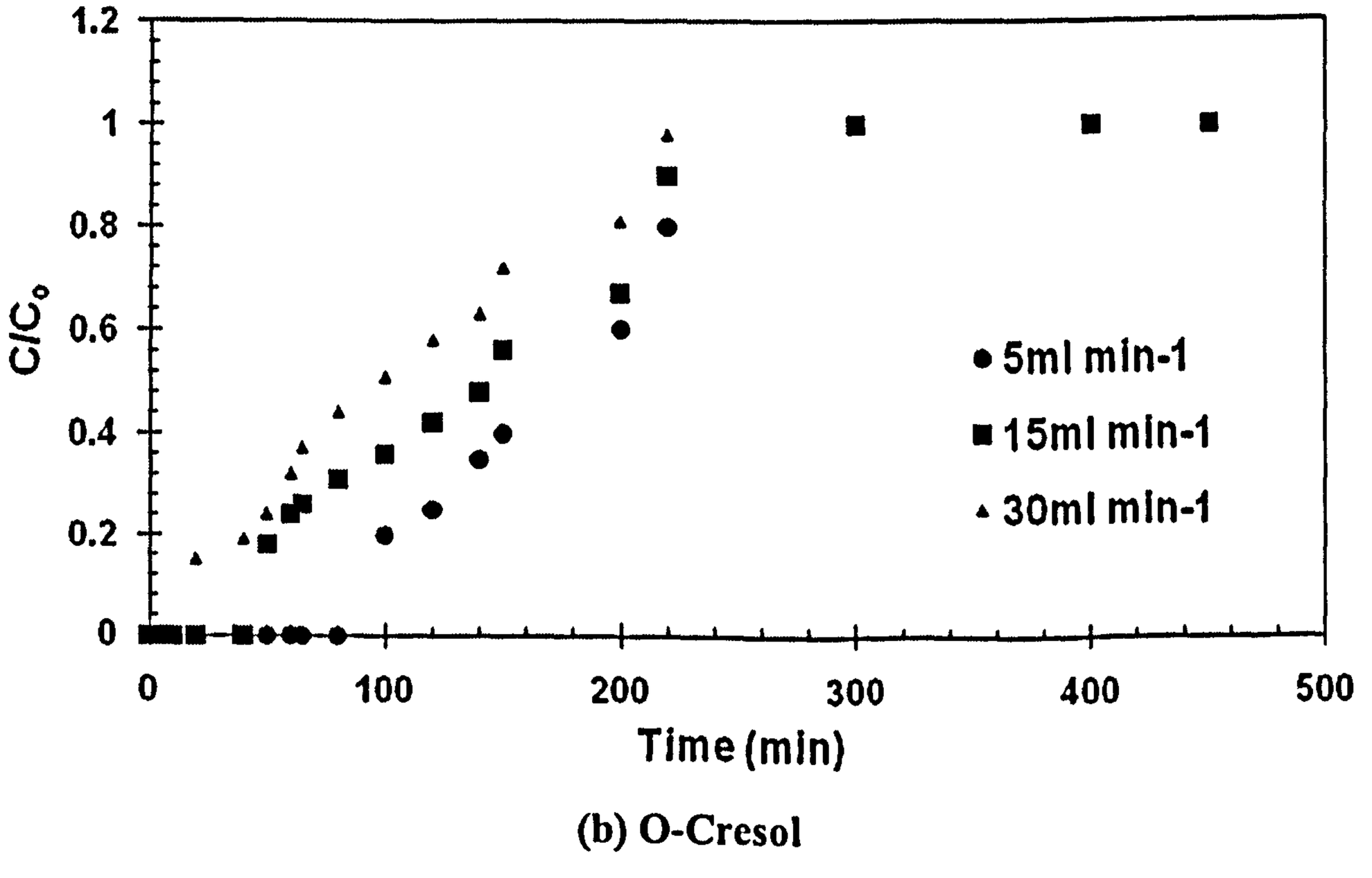


**(b) O-Cresol**

**Figure 4.27: Breakthrough curves for phenol and 2-methylphenol (o-cresol) at different flow rates**

In addition, decreasing the flow rate resulted not only in the breakthrough time increasing but also in the breakthrough curve broadening, which in turn resulted in an increase in the difference between the breakthrough time and the saturation time. The use of high flow rates reduces the contact time between the phenol and 2-methylphenol solutions and the carbon, thus allowing less tim2-methylphenol e for adsorption to occur. This leads to an earlier breakthrough of phenol and 2-methylphenol, as indicated in the Figures.

### *4.3.12 Effect of Initial Concentration*

The adsorption performance of the produced activated carbon was tested at various phenol and 2-methylphenol inlet concentrations. The sorption breakthrough curves obtained for both compounds, at inlet concentrations of 10, 20 and 50 mg $l^{-1}$ and at 5 ml $min^{-1}$ flow rate are given in Figure 4.28. As expected, a decreased inlet concentration gave a longer time before breakthrough, and the treated volume was the greatest at the lowest inlet concentration since the lower concentration gradient caused slower transport due to a decreased diffusion coefficient or decreased mass transfer coefficient. The breakpoint time decreased with increasing inlet concentration in both cases. Breakthrough ($C/C_0 = 0.05$) occurred after 10, 30 and 60 minutes at phenol inlet concentrations of 50, 20, and 10 mg $l^{-1}$, respectively. Breakthrough ($C/C_0 = 0.05$) occurred after 15, 60 and 180 minutes at 2-methylphenol inlet concentrations of 50, 20, and 10 mg $l^{-1}$, respectively. The driving force for adsorption is the concentration difference between the solute on the sorbent and the solute in the solution. A high concentration difference provides a high driving force for the adsorption process and this may explain why higher adsorption capacities

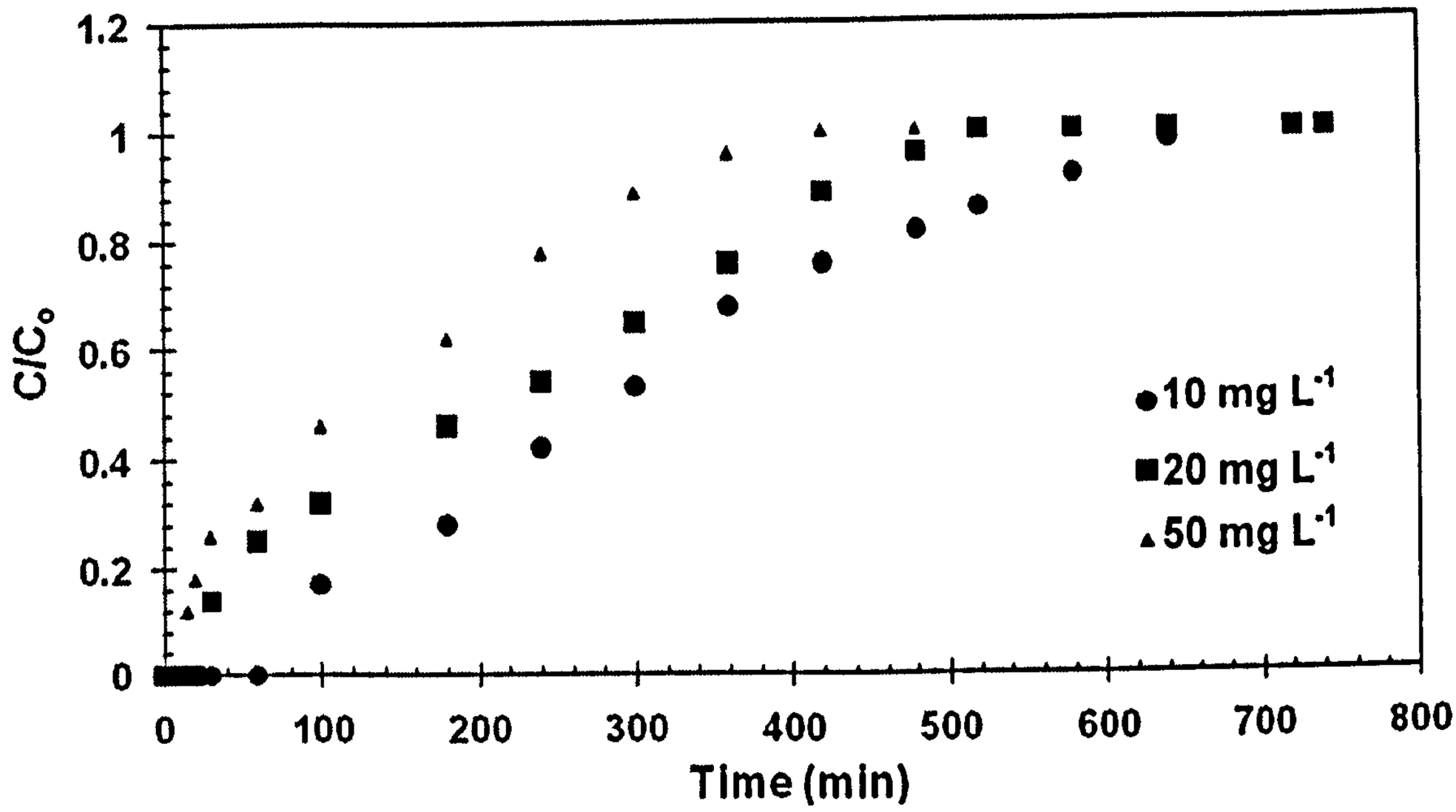


**(a) Phenol**

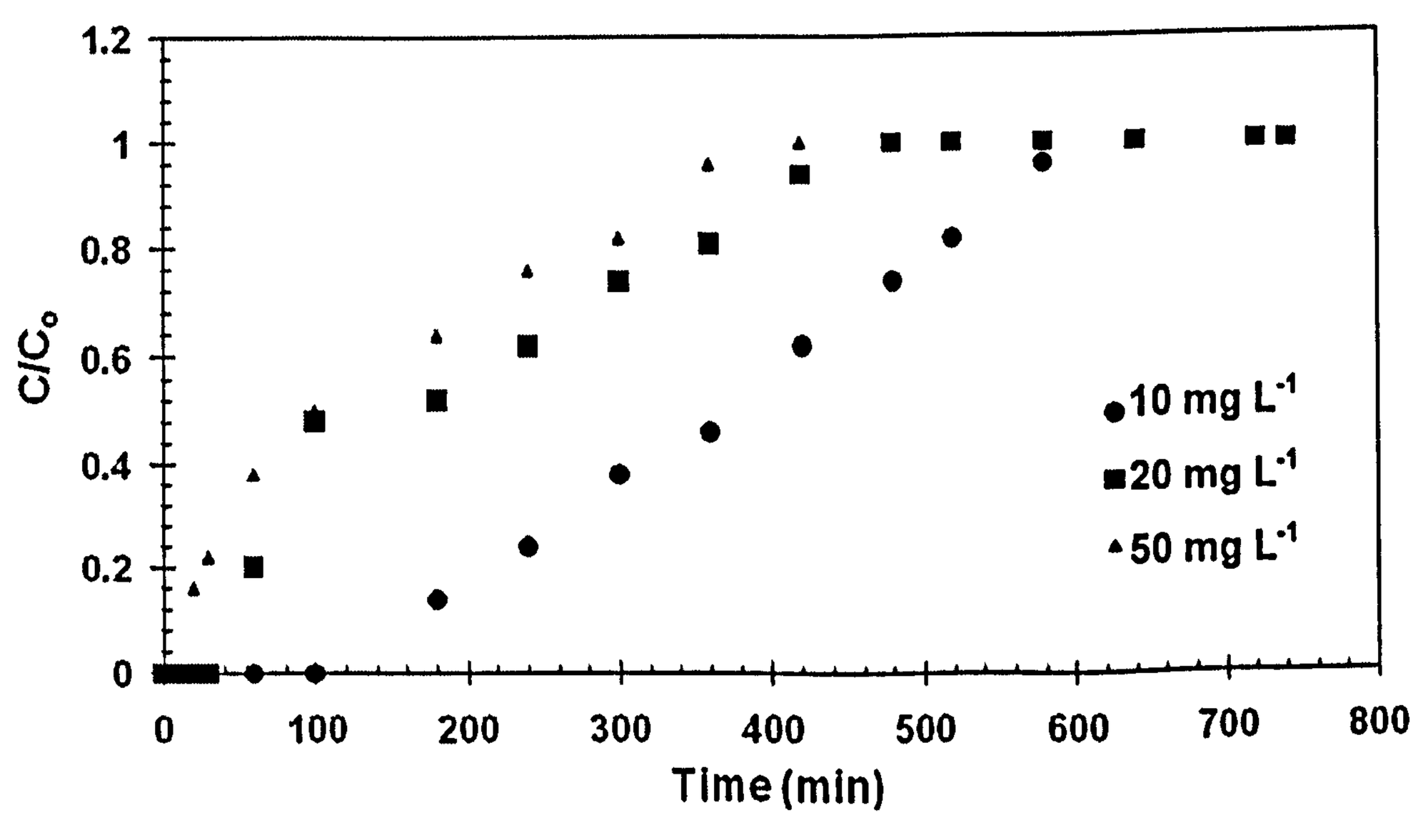


**(b) O-Cresol**

**Figure 4.28: Breakthrough curves for phenol and 2-methylphenol (o-cresol) at different inlet concentrations**

were achieved in the column fed with higher phenol and 2-methylphenol inlet concentrations.

### *4.3.13 Effect of Bed Depth*

Figure 4.29 shows breakthrough curves at four bed depths (10, 15, 25, and 40 cm) at the same influent concentrations of phenol and 2-methylphenol ($C_0$ = 10 mg $l^{-1}$) and flow rate ($v$ = 5 ml $min^{-1}$), respectively. As the bed height increased, the two contaminants had more time to contact with the produced carbon and this resulted in a decrease of breakpoint time. The slope of breakthrough curves decreased with increasing bed height, which resulted in broadened mass transfer zones. Sorbent bed height strongly affects the volume of solution treated or throughput volume because of its relationship to contact time. At lower contact times, the curves become steeper, showing faster exhaustion of the fixed bed. For the case of phenol and 2-methylphenol removals, the treated volume increased from 22 litres and 26 litres to 54 litres and 62 litres, respectively, as the bed height was increased from 10 to 40 cm.

### *4.3.14 Effect of Dissolved Oxygen on the Breakthrough Curves*

Column experiments show that in addition to the effect on the capacity and kinetics of activated carbon adsorbents, dissolved oxygen tremendously affects carbon performance. It does not only affect the shape of the breakthrough curves but also causes a delay in it, resulting in completely different curves. This finding is depicted in Figure 4.30 for phenol and 2-methylphenol under oxic and anoxic conditions. As shown in the Figures, in the anoxic experiments, the initial breakthrough started after 10 and 20 minutes for phenol and 2-methylphenol, respectively, while for the oxic experiments, the corresponding figures were 30 and 60 minutes. The 50%

breakthrough in the anoxic columns occurred after 105 and 130 minutes for phenol and 2-methylphenol, respectively, while for the oxic experiments, the corresponding figures were 180 and 240 minutes.

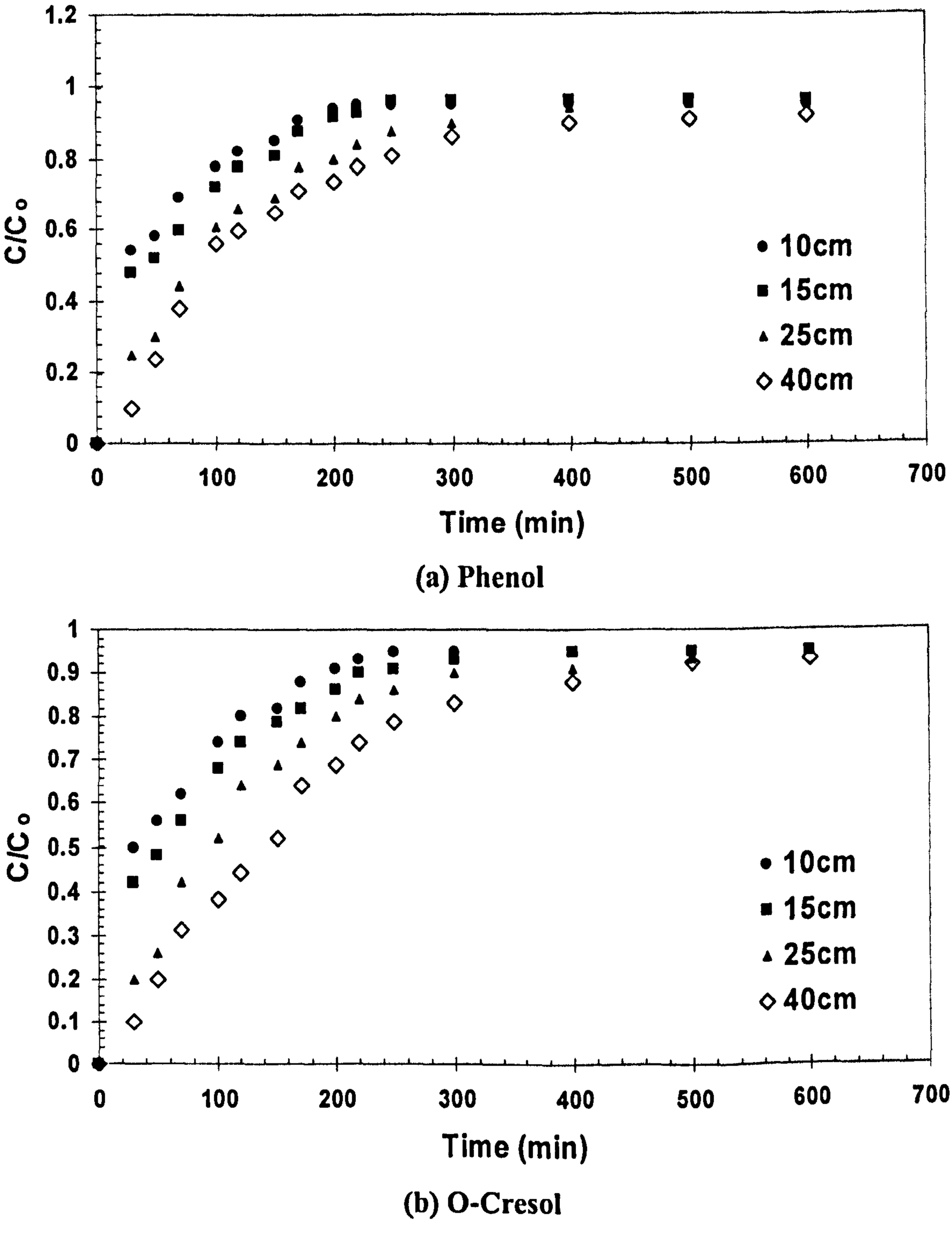


(a) Phenol




(b) O-Cresol

**Figure 4.29: Breakthrough curves for phenol and 2-methylphenol (o-cresol) at different bed depths**

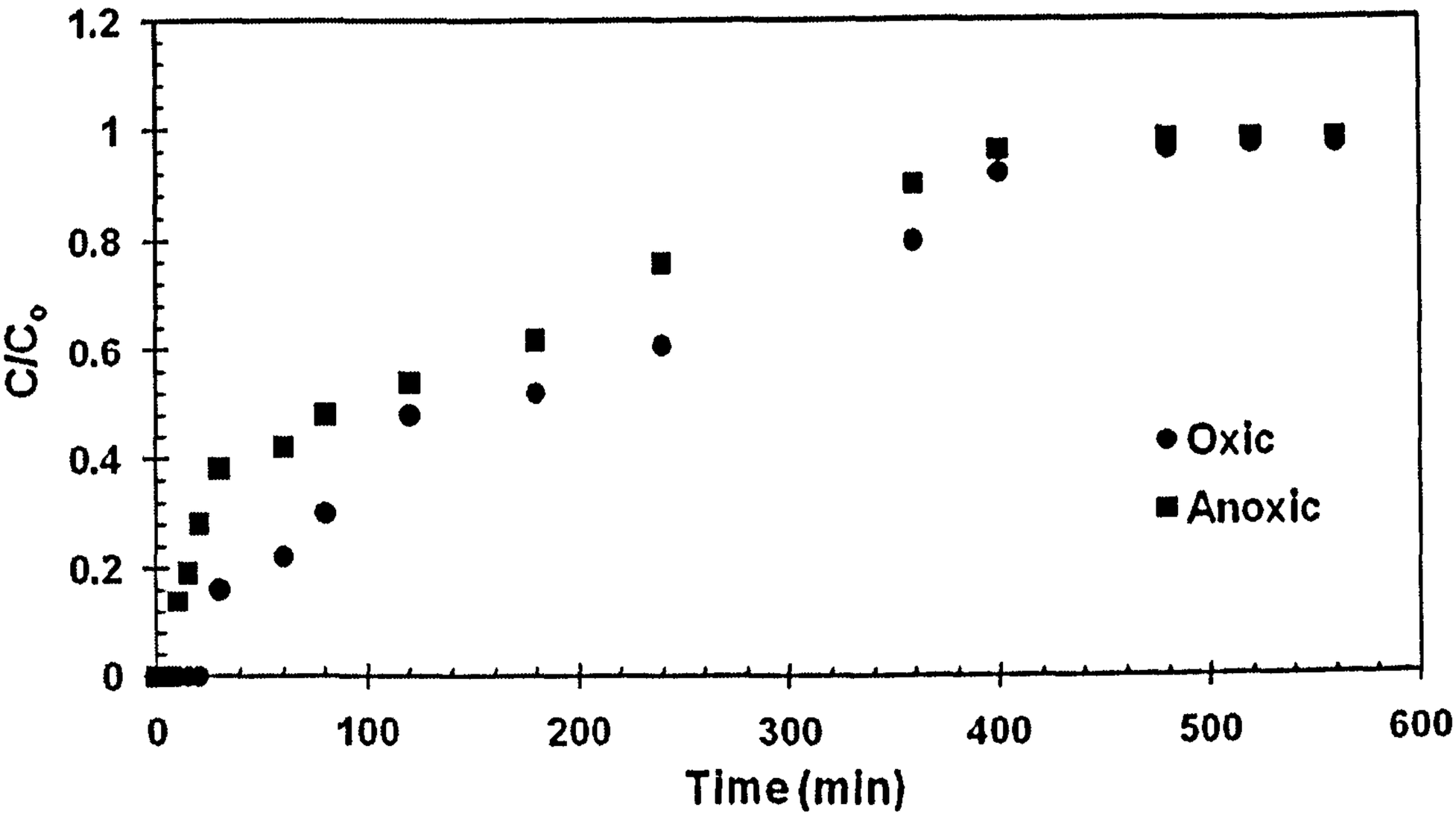


**(a) Phenol**

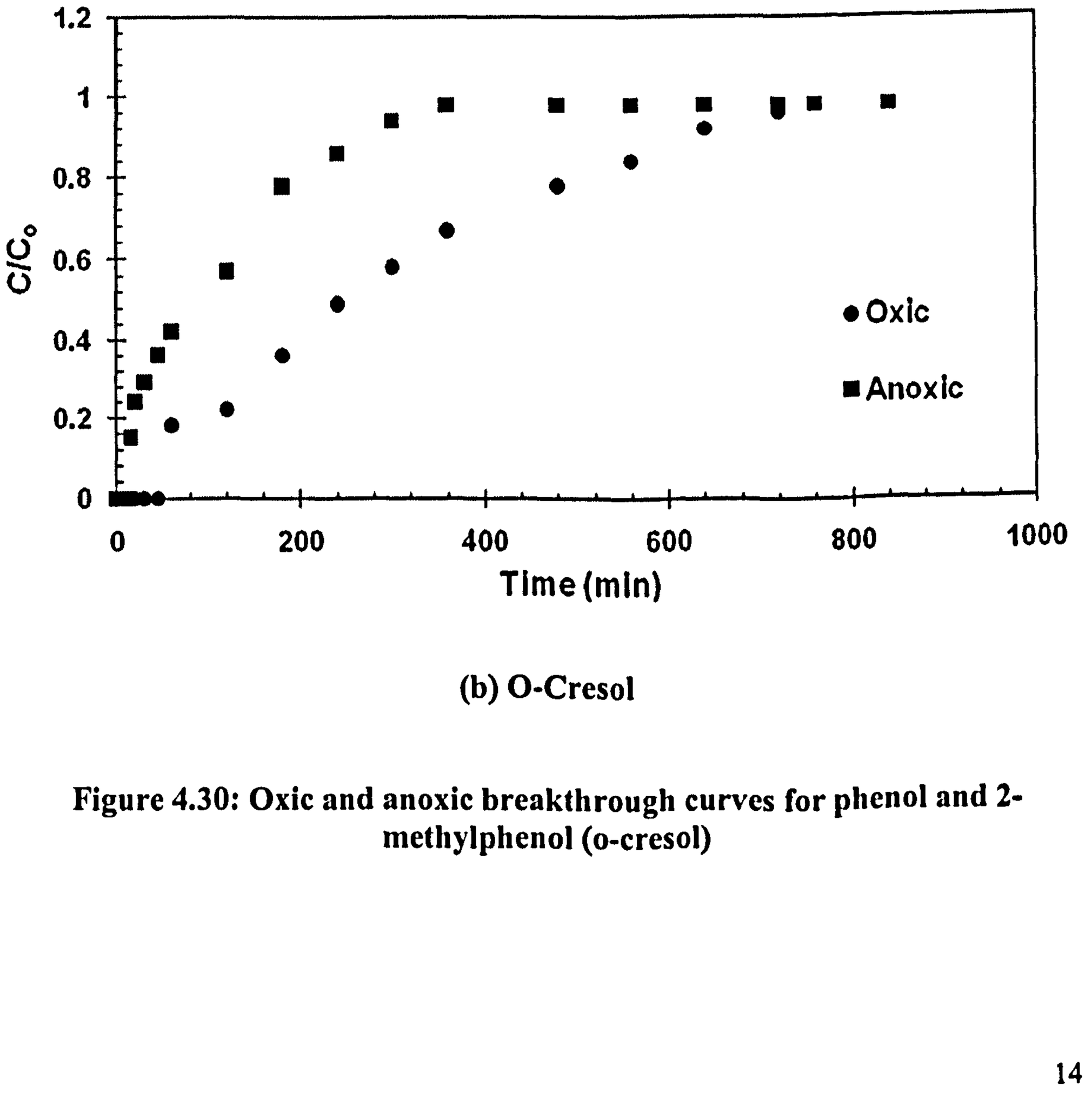


**(b) O-Cresol**

**Figure 4.30: Oxic and anoxic breakthrough curves for phenol and 2-methylphenol (o-cresol)**

Finally, column exhaustion characterized by 95% breakthrough capacities occurred in the anoxic column experiments after 400 and 360 minutes for phenol and 2-methylphenol, respectively, while for the oxic experiments, the corresponding figures were 480 and 720 minutes for phenol and 2-methylphenol, respectively. These times were measured from the beginning of the experiment and give a very good indication about the tremendous additional capacity available in the column in the case of oxic conditions compared to the anoxic conditions (Table 4.11). The above Figures show that the existence of dissolved oxygen in the adsorbate solution not only prolongs the time taken to reach breakthrough point or increase the capacity of the column, but also affects the shape of the breakthrough curve, resulting in a flatter curve. In the case of 2-methylphenol, the effect of dissolved oxygen is more pronounced.

**Table 4.11: Breakthrough values of phenol and 2-methylphenol for anoxic and oxic conditions**

| Anoxic | | | Oxic | |
|---|---|---|---|---|
| **Breakthrough** | **Phenol** | 2-methylphenol | **Phenol** | 2-methylphenol |
| Initial | 10 | 20 | 30 | 60 |
| 50% | 105 | 42 | 180 | 240 |
| 95% | 400 | 360 | 480 | 720 |

# Chapter 5:

# FACTORIAL DESIGN AND OPTIMIZATION OF PARAMETERS

## 5.1 Full-factorial for First-Order Model Design

Factorial design is a useful tool for characterizing multivariable processes. It gives the possibility of separating out the important factors from those that are not, and identifying any possible interactions between them. Factorial design is employed to reduce the total number of experiments in a study in order to achieve the best overall optimization of the system. Factorial designs allow the simultaneous study of the effects of several factors on the optimization of a particular process. Factorial design determines which factors have important effects on a response, as well as how the effect of one factor varies with the level of the other factors. Effects are differential quantities expressing how a response changes as the levels of one or more factors are changed. Also, factorial designs allow the measurement of the interaction between each group of factors. Interactions are the driving force in many optimizations. Without the use of factorial experiments, important interactions may remain undetected, and the overall optimization may not be attained. In this research work, a full-factorial design according to a first-order model assumption of linearity was conducted. Temperature, acid concentration, and impregnation ratio at ranges of 300-700, 30-50% and 0.5-2.4, respectively, were chosen as independent variables, and the surface area of the produced local activated carbon as the dependent output response variable. The adopted experimental design was a 5 × 5 × 10 three-factor, full-factorial study, with two-blocked replicates. Thus 250 experiments were employed

for the produced activated carbon for each replicate, making a total of 500 experiments.

## 5.2 Box-Behnken Design for Second-Order Model Design

A second factorial design employed in the study was a three-level three-factorial Box-Behnken experimental design with two replicates also. This design, a Response Surface Methodology (RSM), was used to evaluate the effects of the independent variables on the response, to characterize the response process, and to optimize the procedure for production of the best activated carbon. This was because the design was suitable for exploration of quadratic response surfaces and for construction of second order polynomial models; in addition, its optimization process required a small number of experimental runs. Moreover, the design caters for the curvature (i.e. non-linear nature of response surface) in the response function which cannot be achieved in the first-order design described above. The independent variables and their corresponding experimental ranges and levels are given in Table 5.1. For the three-level three-factorial Box-Behnken experimental design, a total of only 15 experimental runs as shown in Table 5.2, were needed.

This design also resolves the two-factor interaction effects of individual terms and allows a mid-level setting (0) for the combination of factors (Montgomery, 1991 and Singh *et al.*, 1994). The design consists of replicated center points and a set of points lying at the midpoints of each edge of the multidimensional cube that defines the region of interest. The behaviour of the mathematical response system was explained by the following general quadratic equation

$$y = \beta_0 + \sum_{i=1}^{k}\beta_i x_i + \sum_{i=1}^{k}\beta_i x_i^2 + \sum_{i=1}^{k-1}\sum_{j=2}^{k}\beta_{ij} x_i x_j + \varepsilon \qquad (5.1)$$

**Table 5.1: Independent variables and their levels for the Box-Behnken second-order model design**

| Independent variable | Range and level | | |
|---|---|---|---|
| | −1 | 0 | +1 |
| Temperature ($x_1$,°C) | 300 | 500 | 700 |
| Acid concentration ($x_2$, %) | 30 | 50 | 70 |
| Impregnation ratio ($x_3$, %) | 0.5 | 1.45 | 2.4 |

**Table 5.2: Box-Behnken second-order model design**

| Experiment (run) | Factor and factor level | | | $S_{BET}$ |
|---|---|---|---|---|
| | $x_1$ | $x_2$ | $x_3$ | $y$ |
| 1 | -1 | -1 | 0 | 286 |
| 2 | 1 | -1 | 0 | 358 |
| 3 | -1 | 1 | 0 | 545 |
| 4 | 1 | 1 | 0 | 823 |
| 5 | -1 | 0 | -1 | 223 |
| 6 | 1 | 0 | -1 | 376 |
| 7 | -1 | 0 | 1 | 178 |
| 8 | 1 | 0 | 1 | 450 |
| 9 | 0 | -1 | -1 | 176 |
| 10 | 0 | 1 | -1 | 349 |
| 11 | 0 | -1 | 1 | 200 |
| 12 | 0 | 1 | 1 | 594 |
| 13 | 0 | 0 | 0 | 1314 |
| 14 | 0 | 0 | 0 | 1314 |
| 15 | 0 | 0 | 0 | 1314 |

where for statistical calculations, the different variables ($X_i$) were coded as $x_i$ according to the following relationship:

$$x_i = \frac{(X_i - X_0)}{\sigma X} \tag{5.2}$$

where $X_i$ is the new value and $X_0$ is the original value.

Therefore, the design response surface in this study could be adequately represented by

$$y = b_0 + b_1x_1 + b_2x_2 + b_3x_3 + b_4x_1x_2 + b_5x_2x_3 + b_6x_1x_3 + b_7x_1^2 + b_8x_2^2 + b_9x_3^2 + E \tag{5.3}$$

where $y$ is the selected response, $b_0$–$b_9$ are the regression coefficients, $x_1$, $x_2$ and $x_3$ are the factors studied and $E$ is an error term. As the Box-Behnken experimental design is of an orthogonal design, the factor levels are evenly spaced and coded for low, medium and high settings, as −1, 0 and +1 (Montgomery, 1991) as shown in Table 5.1.

## 5.3 Statistical Analysis for the First-order Model

For estimation of significance of the model, its individual main effects, interactions and block effects, the analysis of variance (ANOVA) for full factorial design was applied. Using the 5% significance level, a model is considered significant if the *p*-value (significance probability value) is less than 0.05. Similarly, if the calculated $F$ from the ANOVA table is less than $F_0$ from the $F$-distribution table, then it could be concluded that the effect under consideration significantly affects the response. The statistical analysis was performed with the aid of the MINITAB statistical software package version 3.20 (PA, USA). The results summary of the analysis is displayed in Table 5.3 from which it can be concluded that all the main effects, i.e. temperature

**Table 5.3: ANOVA of the two-block 5×5×10 full-factorial design for the first-order model design**

| Source | DF | Seq SS | Adj SS | Adj MS | F | P |
|---|---|---|---|---|---|---|
| Blocks | 1 | 23052 | 23052 | 23052 | 0.45 | 0.504 |
| $x_1$ | 4 | 3312568 | 3312568 | 828142 | 16.16 | 0.000 |
| $x_2$ | 4 | 2853671 | 2853671 | 713418 | 13.92 | 0.000 |
| $x_3$ | 9 | 23534584 | 23534584 | 2614954 | 51.03 | 0.000 |
| $x_1*x_2$ | 16 | 268040 | 268040 | 16753 | 0.33 | 0.994 |
| $x_1*x_3$ | 36 | 4104766 | 4104766 | 114021 | 2.23 | 0.000 |
| $x_2*x_3$ | 36 | 1247416 | 1247416 | 34650 | 0.68 | 0.921 |
| $x_1*x_2*x_3$ | 144 | 1295765 | 1295765 | 8998 | 0.18 | 1.000 |
| Error | 249 | 12811335 | 12811335 | 51245 | | |
| Total | 499 | 49428145 | | | | |
| S = 264.6 | | R-Sq = 29.2% | | R-Sq (adj) = 28.4% | | |

($x_1$), % $H_3PO_4$ ($x_2$), and the impregnation ratio ($x_3$) have significant effects on the response ($y$) as all their $p$-values = 0.0000. The interaction $x_1*x_3$ (i.e. temperature and impregnation ratio) is the only interaction effect that affects the response ($y$), whereas the block effect and the interactions $x_1*x_2$ (temperature and acid concentration) and $x_2*x_3$ (acid concentration and impregnation ratio) and the highest level interaction $x_1*x_2*x_3$ (temperature, acid concentration and impregnation ratio) effects were found to be insignificant. This is based on the fact that the $p$-values for the former were all less than 0.05, whereas those of the latter were greater than 0.05. Similarly, the $F$-test in all cases confirmed the $p$-value test. Based on this, the conclusion can be reached that the response investigated has not much to do with a change in any combination of these independent variables ($x_1$ & $x_2$) and ($x_2$ & $x_3$) at fixed values of the third variable i.e. $x_3$ and $x_1$ respectively, for the range of values considered in this study.

The lack of fit of the linear first-order model was apparent, since the adjusted linear regression coefficient ($R^2$) was found to be only 0.284 (Table 5.3), meaning that the model could explain only about 28% of the variability in the response data. This undermines the reliability of the conclusions drawn from the first order statistical model. Because the first-order model's poor fitness could be attributed to the possible curvature in the interaction effects, a more elaborate and comprehensive statistical approach which takes curvature into cognizance is necessary. Consequently, the second-order model approach was adopted for the analysis and this is discussed in the following section.

## 5.4 Statistical Analysis for the Second-order Model

Again, the results of the experimental design were studied and interpreted by MINITAB statistical software package version 3.20 (PA, USA) to estimate the

response of the dependent variable. The software uses the least square regression method for the estimation of coefficients in the approximating polynomial function (Equation (5.3)) applying uncoded values of the factor levels obtained from Equation (5.2). Based on the result ($R^2 = 98.8\%$) displayed in Table 5.4, the model was felt to be appropriate. The equation of the response surface that takes into cognizance the curvature effects can be written as

$$y = -9136 + 33x_1 - 92x_2 + 1665x_3 + x_2^{\,2} - 654x_3^{\,2} + 3x_2 * x_3 \qquad (5.4)$$

In the same manner as undertaken for the first-order model, for estimation of the significance of the model, ANOVA was applied using the 5% significance level. It was apparent from the *p*-values presented in Table 5.4 that the cross-product contribution of the model was not significant, while all the linear and quadratic contributions of the model were highly significant in a positive and negative sense, respectively. Moreover, the linear effect contribution of the independent variables on the response was found to be in the order $x_3$ ($\beta_3 = 1665$) > $x_2$ ($\beta_2 = 92$) > $x_1$ ($\beta_1 = 33$) i.e. the effect of impregnation ratio was greatest, followed by the strength of the acid and then the temperature. The effect of the most influencing interaction term $x_2*x_3$ (strength of acid and impregnation ratio) ($\beta_5 = 3$) was at a much lower rate than the linear ones. Based on the its *p*-value (0.065), it could be concluded also that its effect on the studied response can be considered negligible. The insignificant effect of the interaction terms and significance of the linear and quadratic terms provided by the second-order model was corroborated from *p*-values of the condensed analysis of the model's ANOVA given in Table 5.5.

From the calculated Pearson adjusted correlation coefficients ($R^2$), it was found that 98.8% of the variability of experimental data could be explained by the model

**Table 5.4. ANOVA for coefficients for the second-order model for $S_{BET}$**

| Term | Coef | SE Coef | T | P |
|---|---|---|---|---|
| Constant | -9136 | 515.321 | -17.729 | 0.000 |
| $x_1$ | 33 | 2.075 | 15.703 | 0.000 |
| $x_2$ | -92 | 7.940 | 11.594 | 0.000 |
| $x_3$ | 1665 | 141.378 | 11.778 | 0.000 |
| $x_1^2$ | -0 | 0.002 | -17.096 | 0.000 |
| $x_2^2$ | 1 | 0.061 | -16.153 | 0.000 |
| $x_3^2$ | -645 | 27.027 | -24.198 | 0.000 |
| $x_1*x_2$ | 0 | 0.012 | 2.198 | 0.079 |
| $x_1*x_3$ | 0 | 0.247 | 1.269 | 0.260 |
| $x_2*x_3$ | 3 | 1.233 | 2.358 | 0.065 |
| S = 46.87 | R-Sq = 99.6% | | R-Sq (adj) = 98.8% | |

**Table 5.5: ANOVA for different effects for the $S_{BET}$**

| Source | DF | Seq SS | Adj SS | Adj MS | F | P |
|---|---|---|---|---|---|---|
| Regression | 9 | 2507353 | 2507353 | 278595 | 126.82 | 0.000 |
| Linear | 3 | 294514 | 855958 | 285319 | 129.88 | 0.000 |
| Square | 3 | 2186480 | 2186480 | 728827 | 331.76 | 0.000 |
| Interaction | 3 | 26359 | 26360 | 8787 | 4.00 | 0.085 |
| Residual Error | 5 | 10984 | 10984 | 2197 | | |
| Lack-of-Fit | 3 | 10984 | 10984 | 3661 | * | * |
| Pure Error | 2 | 0 | 0 | 0 | | |
| Total | 14 | 2518337 | | | | |

polynomial function given in $y$ in Equation (5.4). This implies that the second-order model which takes into account curvature in the response, is thus capable of representing the data of the $S_{BET}$ surface area of the produced local-activated carbon, obtained from the experimental work. The comparison between the experimental and predicted $S_{BET}$ is displayed in Table 5.6.

## 5.5 Three-dimensional (3D) Response Surface Plots for Second-order Model

Three-dimensional (3D) plots for the measured responses and their corresponding contour maps were formed, based on the response function obtained in the second-order model equation (5.4) above to further assess and visualize the change of the response surface with changes in the independent variables in more detailed perspective. Also, the relationship between the dependent and independent variables could be further understood and optimization performed.

The response plots are displayed in Figures 5.1-5.9. Since the model has more than two factors, by considering each of the factor levels, one factor was held constant for each diagram, therefore, a total of nine response surfaces with their corresponding contour diagrams was produced – three for each level (-1, 0, 1). Each plot represents the effect of two variables at their studied range with the other one maintained at its zero level. The shapes of contour plots indicate the nature and extent of the interactions. Prominent interactions are shown by the elliptical nature of the contour plots, while less prominent or negligible interactions are shown by the circular nature of the contour plots.

Figures 5.1, 5.2 and 5.3 are the response surface plots with their corresponding contour maps showing the effect of % $H_3PO_4$, and the impregnation ratio response at

**Table 5.6: Comparison between predicted and experimental values for the test formulations**

| Observation | $S_{BET}$, $m^2/g$ | Fit | SE Fit* | Residual | St Resid |
|---|---|---|---|---|---|
| 1 | 286.000 | 296.250 | 40.591 | -10.250 | -0.44 |
| 2 | 358.000 | 387.000 | 40.591 | -29.000 | -1.24 |
| 3 | 545.000 | 516.000 | 40.591 | 29.000 | 1.24 |
| 4 | 823.000 | 812.750 | 40.591 | 10.250 | 0.44 |
| 5 | 223.000 | 202.375 | 40.591 | 20.625 | 0.88 |
| 6 | 376.000 | 336.625 | 40.591 | 39.375 | 1.68 |
| 7 | 178.000 | 217.375 | 40.591 | -39.375 | -1.68 |
| 8 | 450.000 | 470.625 | 40.591 | -20.625 | -0.88 |
| 9 | 176.000 | 186.375 | 40.591 | -10.375 | -0.44 |
| 10 | 349.000 | 398.625 | 40.591 | -49.625 | -2.12R |
| 11 | 200.000 | 150.375 | 40.591 | 49.625 | 2.12R |
| 12 | 594.000 | 583.625 | 40.591 | 10.375 | 0.44 |
| 13 | 1314.000 | 1314.000 | 27.061 | 0.000 | 0.00 |
| 14 | 1314.000 | 1314.000 | 27.061 | 0.000 | 0.00 |
| 15 | 1314.000 | 1314.000 | 27.061 | 0.000 | 0.00 |

*Standard error of fit

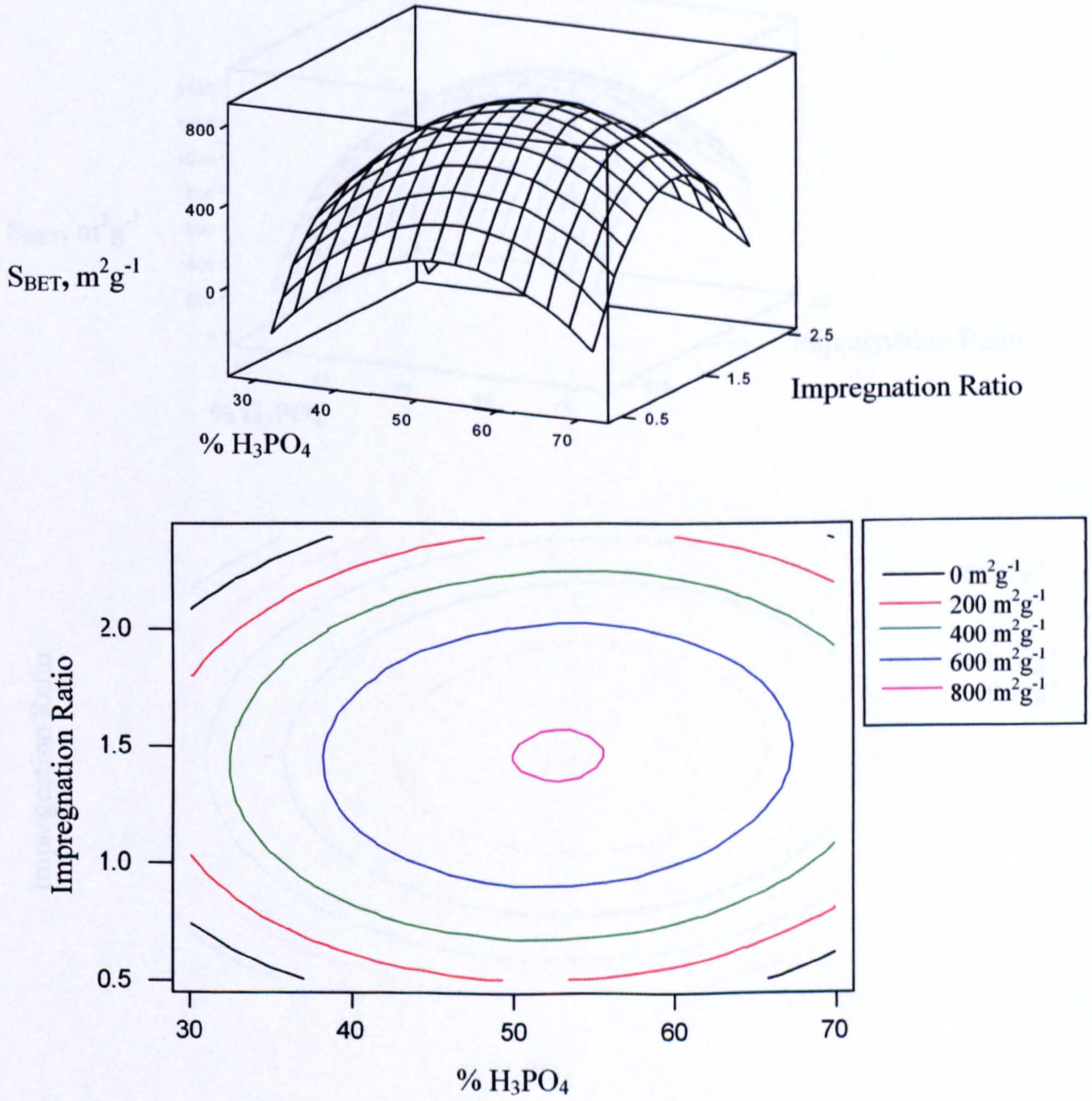


**Figure 5.1: Surface and contour response plots for the BET surface area for the locally-produced activated carbon (temperature = 300 °C)**

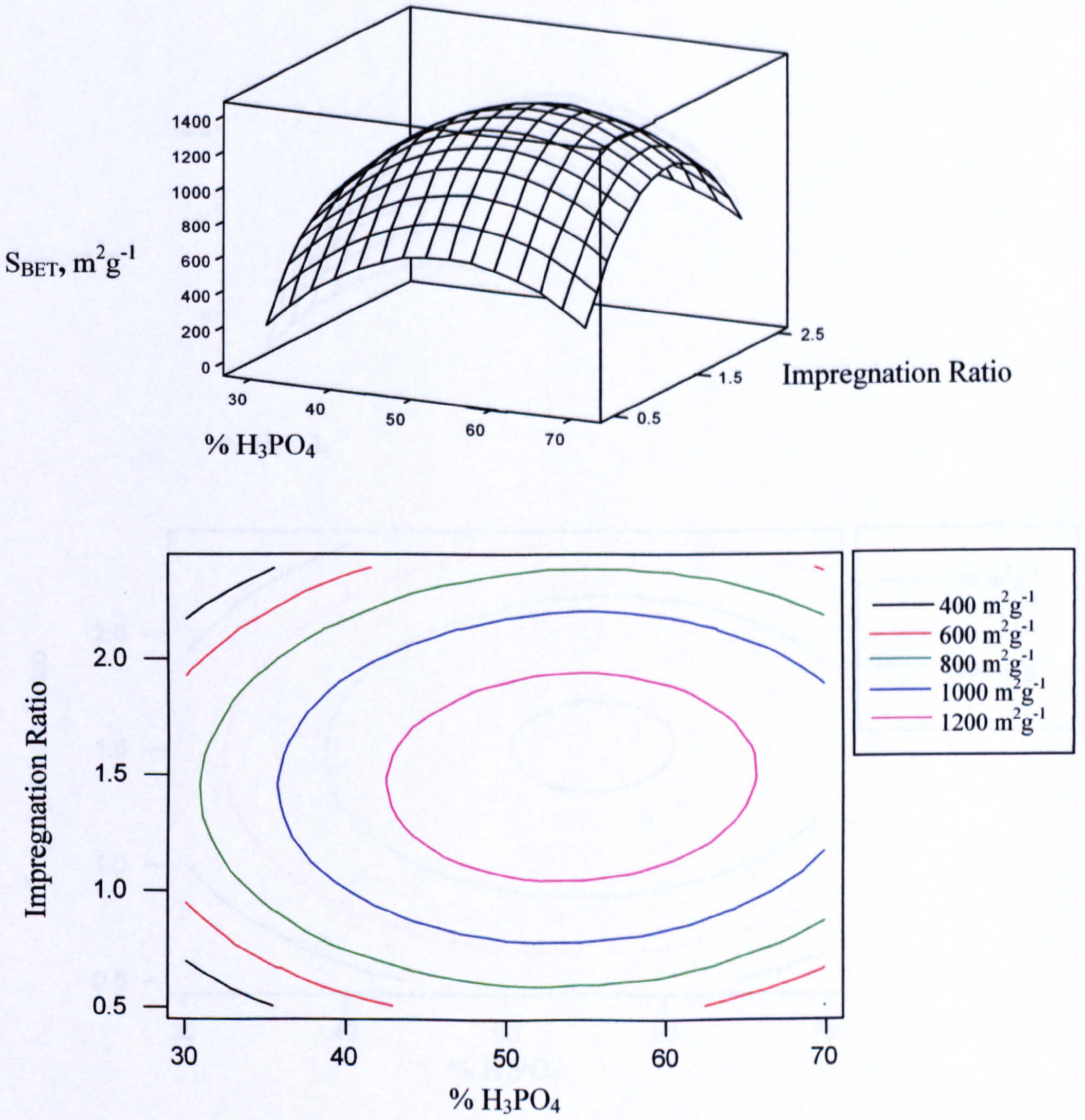


**Figure 5.2: Surface and contour response plots for the BET surface area for the locally-produced activated carbon (temperature = 500 °C)**

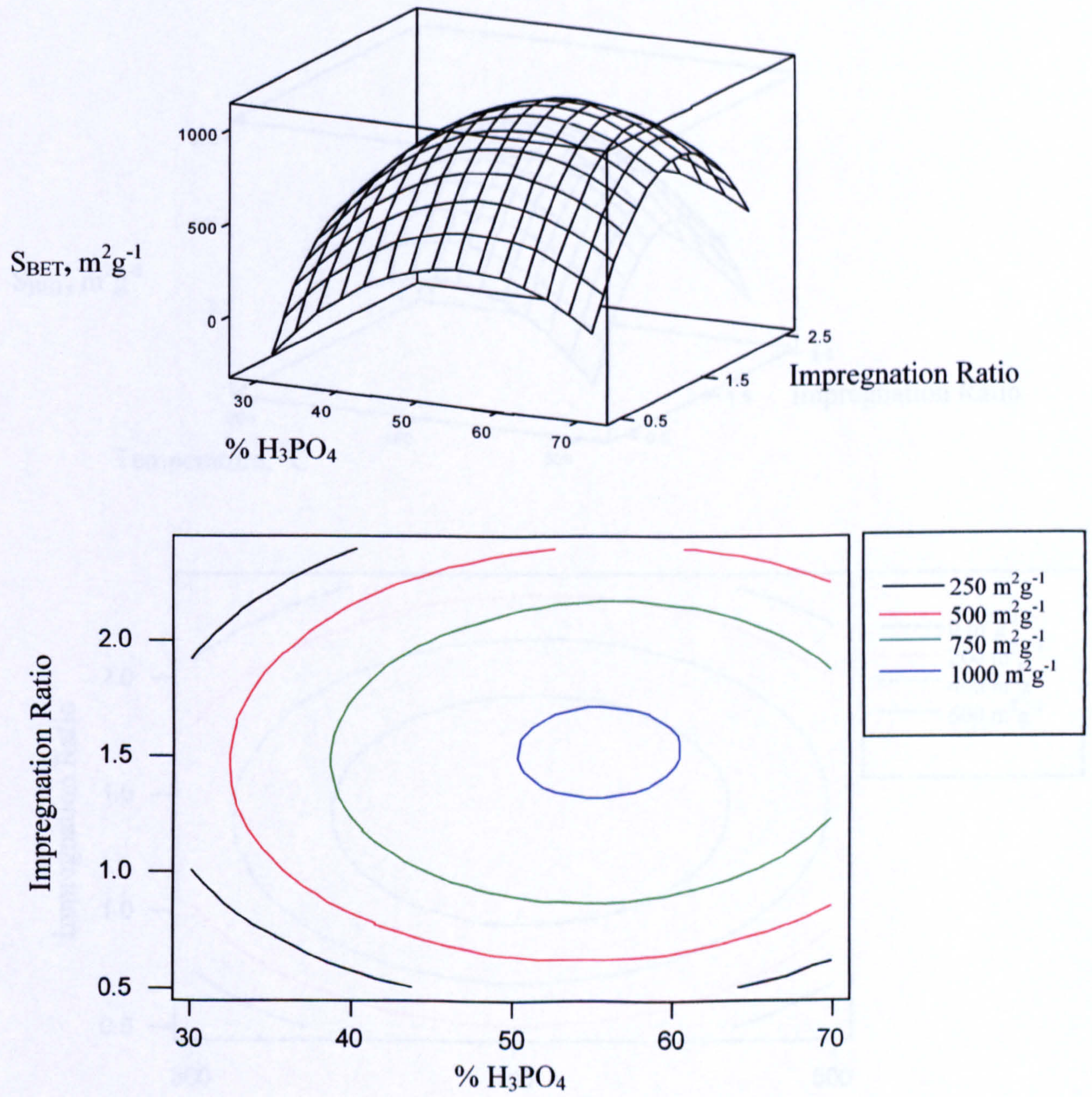


**Figure 5.3: Surface and contour response plots for the BET surface area for the locally-produced activated carbon (temperature = 700 °C)**

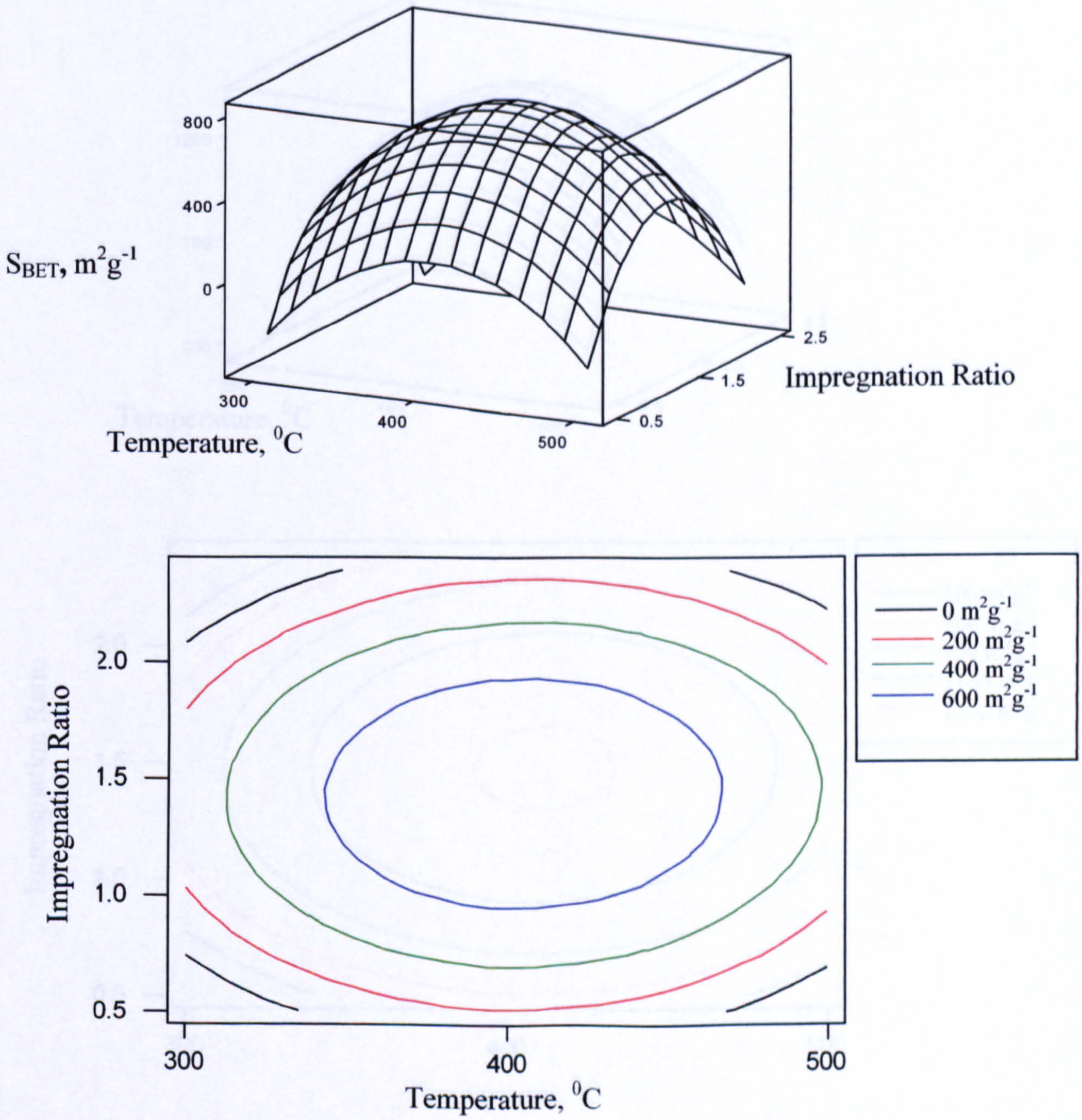


**Figure 5.4: Surface and contour response plots for the BET surface area for the locally-produced activated carbon (% $H_3PO_4$ = 30)**

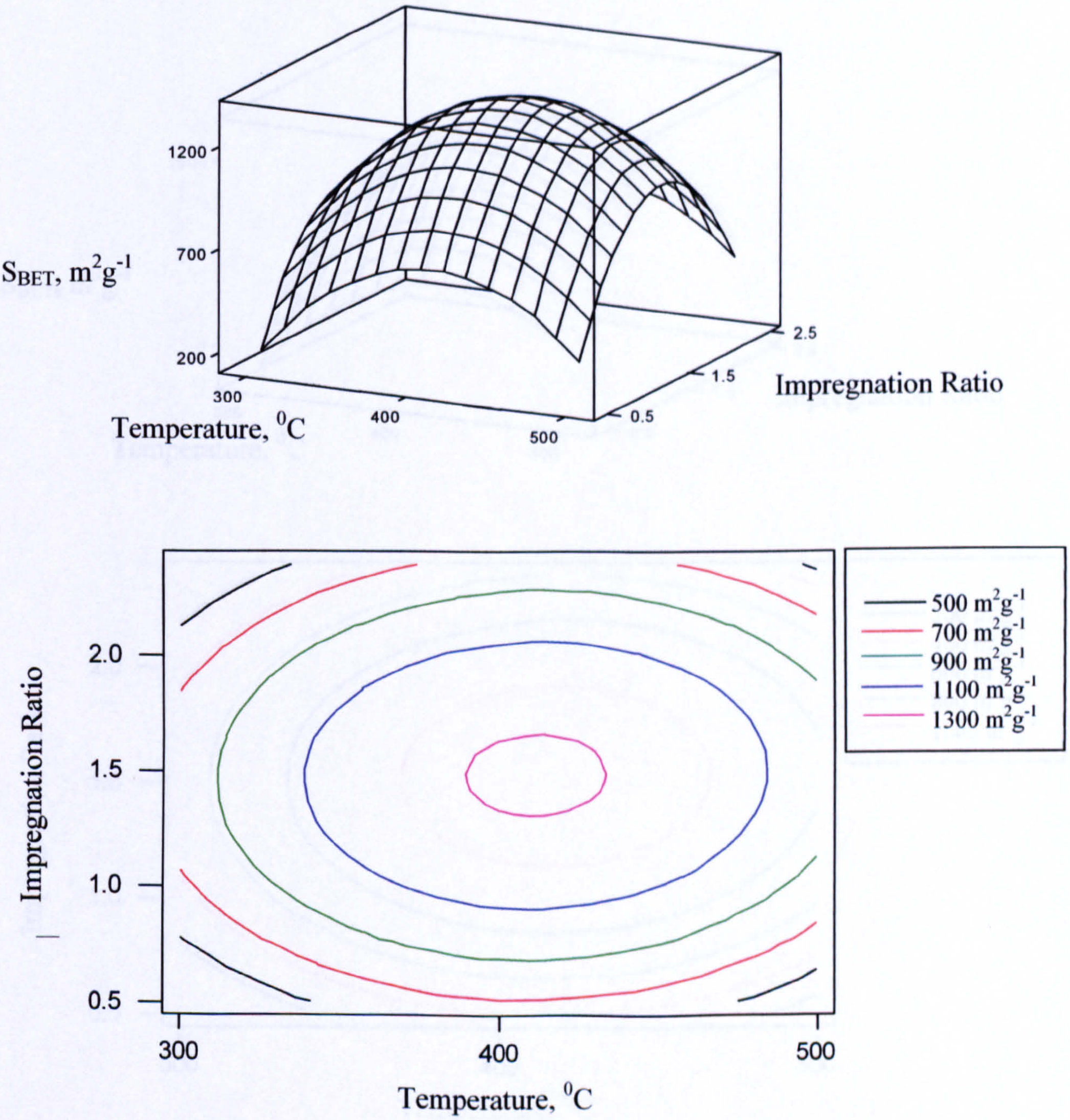


**Figure 5.5: Surface and contour response plots for the BET surface area for the locally-produced activated carbon (% $H_3PO_4$ = 50)**

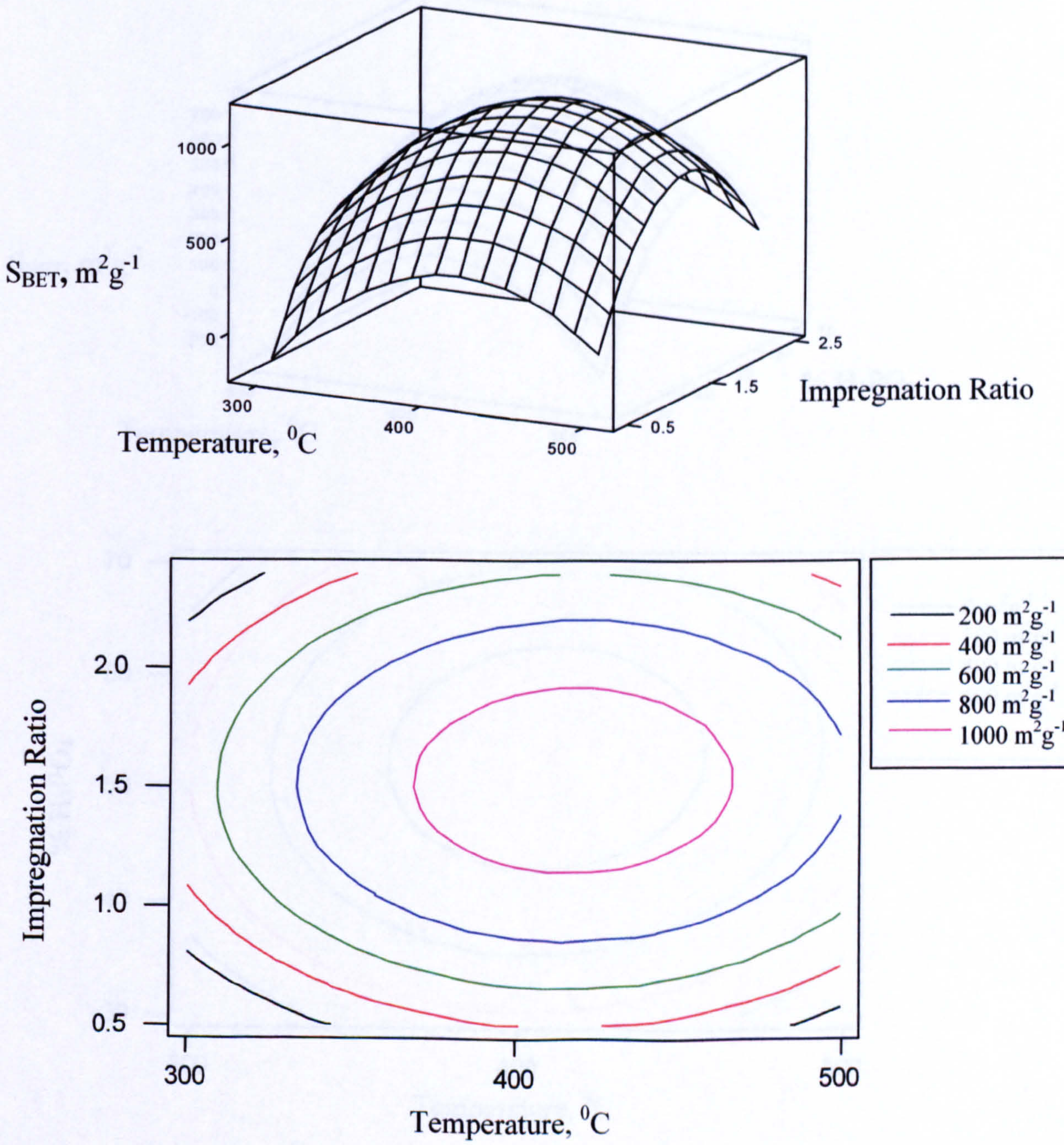


**Figure 5.6: Surface and contour response plots for the BET surface area for the locally-produced activated carbon (% $H_3PO_4$ = 70)**

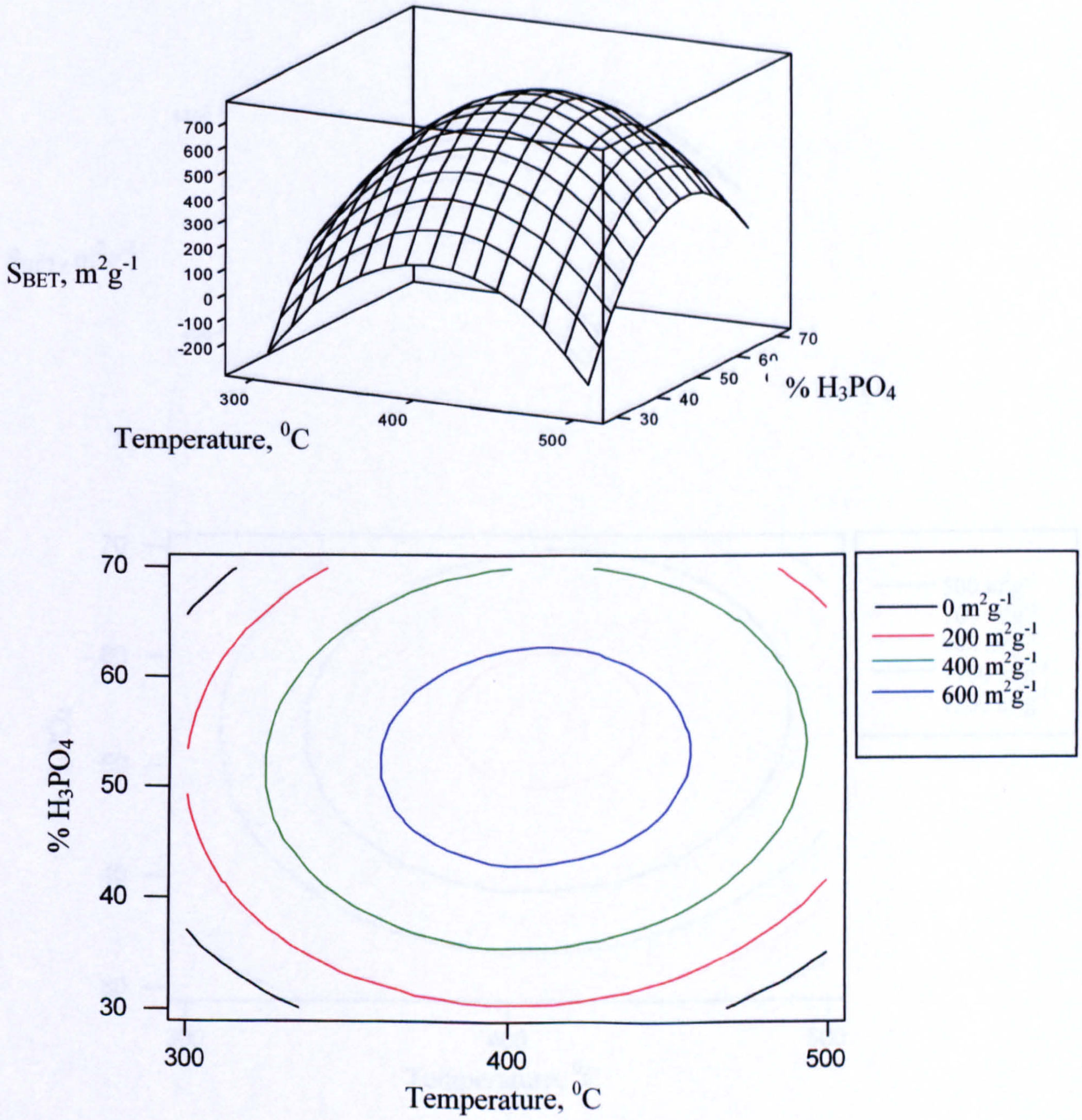


**Figure 5.7: Surface and contour response plots for the BET surface area for the locally-produced activated carbon (impregnation ratio = 0.5)**

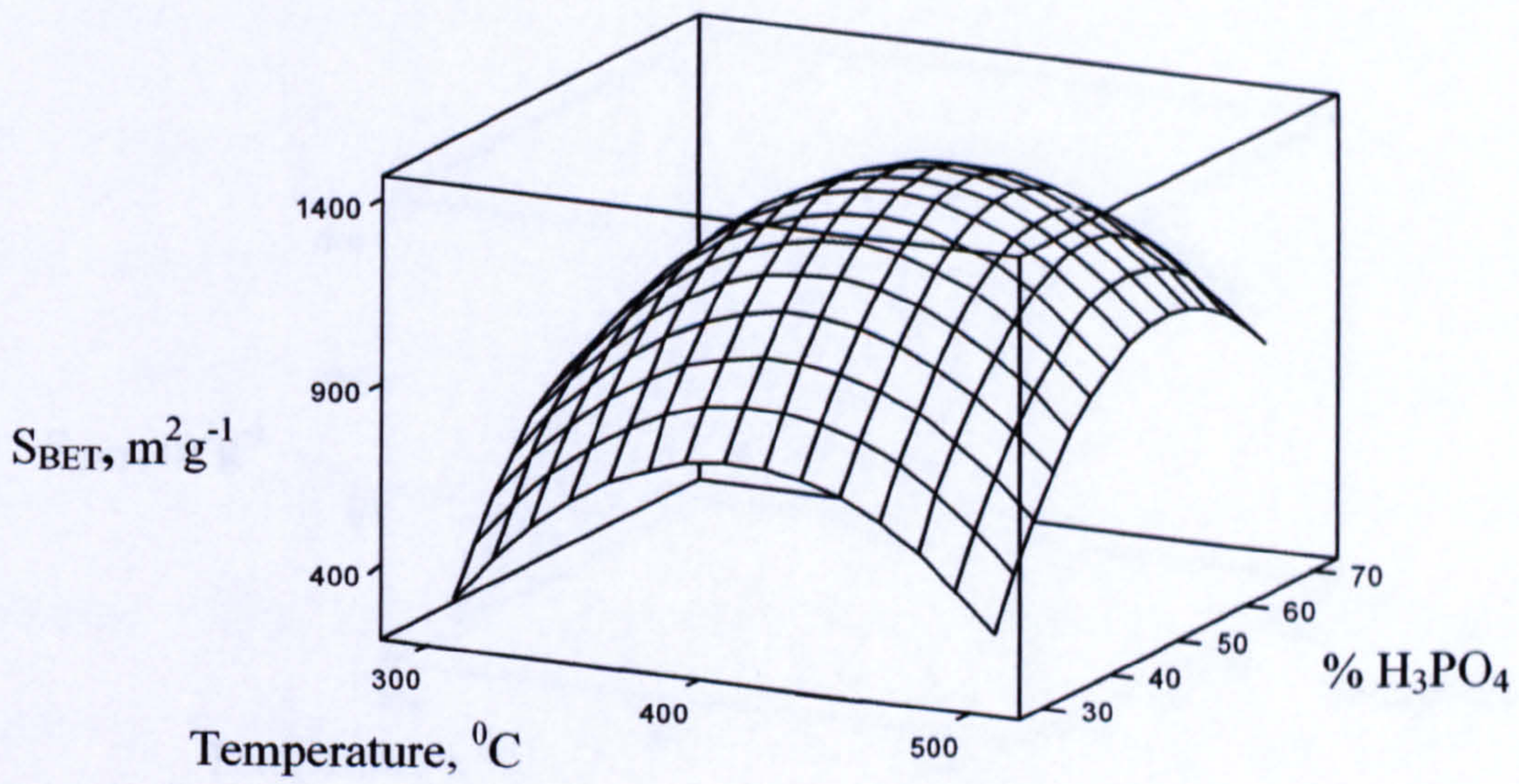


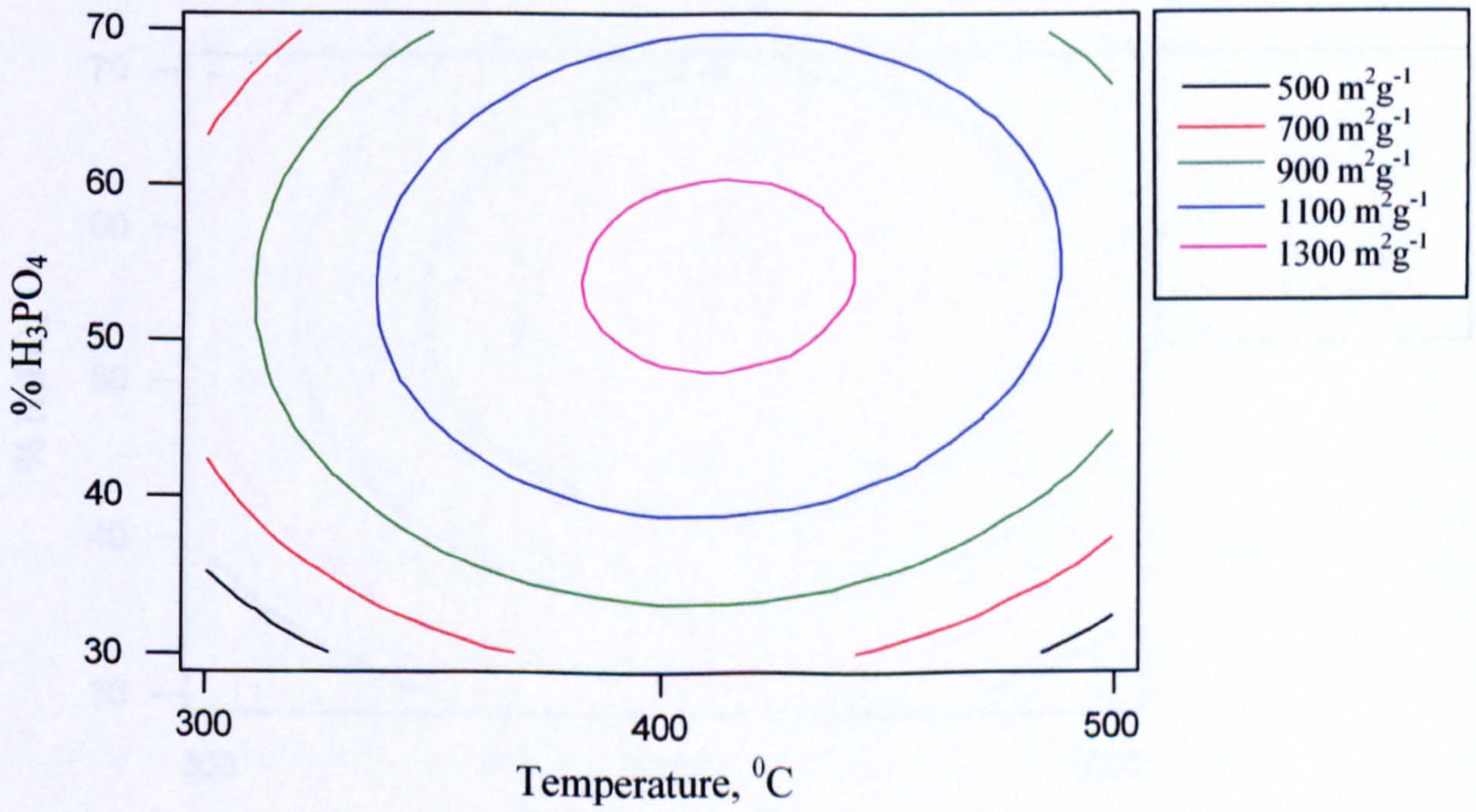


**Figure 5.8: Surface and contour response plots for the BET surface area for the locally-produced activated carbon (impregnation ratio = 1.45)**

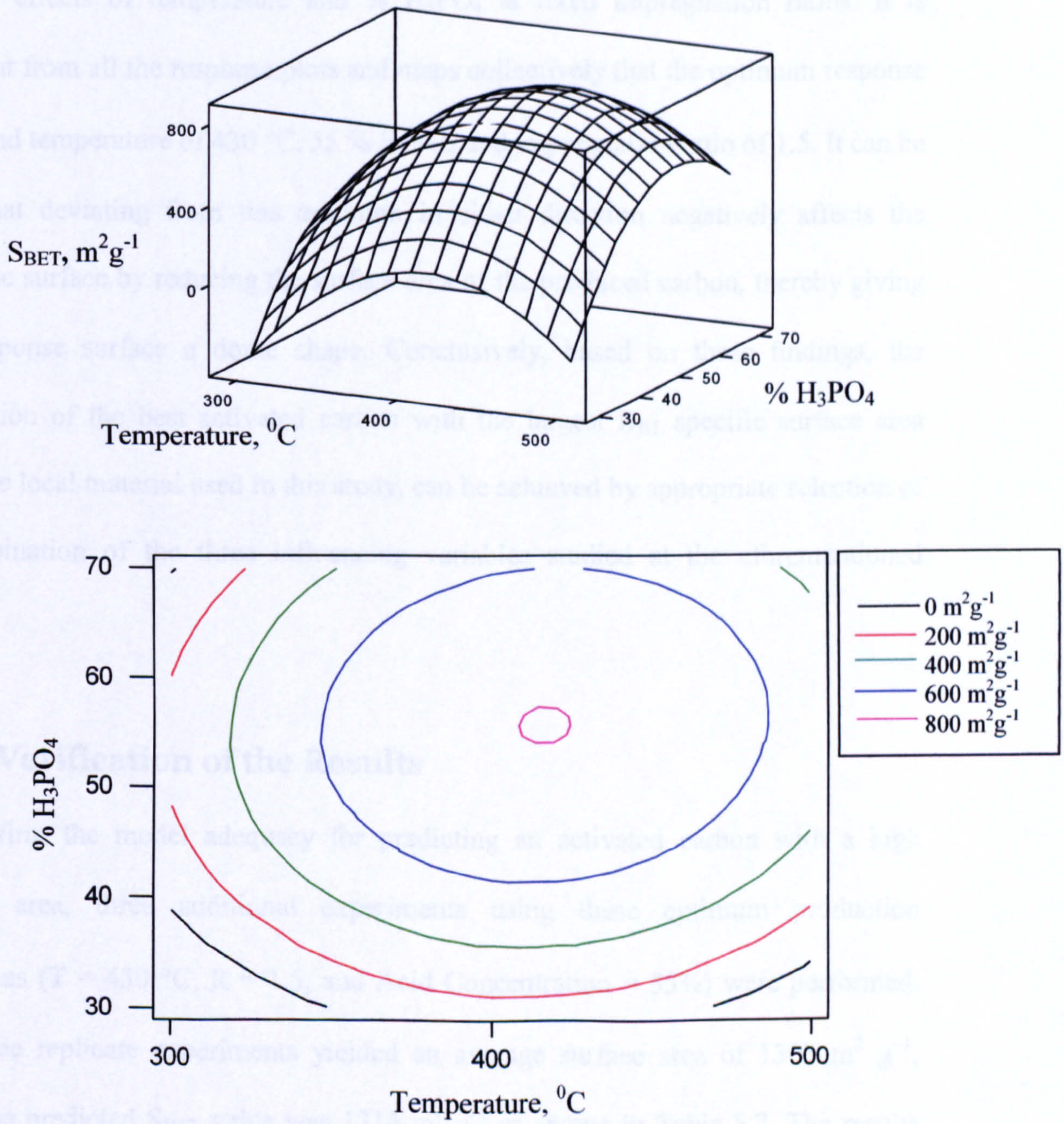


**Figure 5.9: Surface and contour response plots for the BET surface area for the locally-produced activated carbon (impregnation ratio = 2.4)**

fixed temperatures. Similarly, Figures 5.4, 5.5 and 5.6 show the effect of impregnation ratio and temperatures at fixed % $H_3PO_4$, and Figures 5.7, 5.8 and 5.9 display effects of temperature and % $H_3PO_4$ at fixed impregnation ratios. It is apparent from all the response plots and maps collectively that the optimum response is around temperature of 430 °C, 55 % $H_3PO_4$ and impregnation ratio of 1.5. It can be seen that deviating from this optimum in either direction negatively affects the response surface by reducing the surface area of the produced carbon, thereby giving the response surface a dome shape. Conclusively, based on these findings, the production of the best activated carbon with the largest $B_{ET}$ specific surface area from the local material used in this study, can be achieved by appropriate selection of a combination of the three influencing variables studied at the aforementioned values.

## 5.6 Verification of the Results

To confirm the model adequacy for predicting an activated carbon with a high surface area, three additional experiments using these optimum production conditions (T = 430 °C, R = 1.5, and Acid Concentration = 55%) were performed. The three replicate experiments yielded an average surface area of 1303 $m^2\ g^{-1}$, while the predicted $S_{BET}$ value was 1314 $m^2\ g^{-1}$ as shown in Table 5.7. The results derived from this study indicated that the response surface methodology is a powerful tool for optimising the individual factors.

**Table 5.7: Predicted and experimental values of $S_{BET}$ using optimum production conditions**

| # of Replicates | $S_{BET}$ value ($m^2 g^{-1}$) | |
|---|---|---|
| | Experimental | Predicted |
| Replicate # 1 | 1298 | 1314 |
| Replicate # 2 | 1312 | |
| Replicate # 3 | 1298 | |

# Chapter 6:

## CONCLUSIONS & RECOMMENDATIONS

Cheap and readily-available adsorbents such as activated carbon are widely-used for elimination of air and water pollution. The growing need for activated carbon in Saudi Arabia justifies the search for raw materials suitable for local production of this substance. Economic considerations require the use of inexpensive adsorbents which are either naturally available, or available as waste products from manufacturing processes.

At present, the Kingdom of Saudi Arabia imports a substantial amount of activated carbon each year. The research described in this thesis has shown that waste date pits could be used as raw materials for the production of activated carbon, with $H_3PO_4$ as the activation agent. This activated carbon can potentially meet the present needs in tertiary industrial wastewater treatment, and thus significantly reduce import costs. The present study has compared activated carbon produced from date pits with an imported activated carbon which is widely used in the Kingdom for the treatment of industrial wastewaters and promising results have been obtained. For example, the results for aqueous phenol removal show that the locally-produced activated carbon is more effective than the commercial activated carbon. However, both activated carbons were found to be comparable for methylene blue removal. Furthermore, the phenol removal exhaustion points for the commercial and local activated carbons were noted at 40 and 80 hours, respectively. Results from the present study indicate great potential for the production of high-quality activated carbon from date pits, a waste material.

## 6.1 Conclusions

The following conclusions can be drawn from this study:

1. Waste date pits can be used to produce an effective activated carbon with phosphoric acid as the activating agent.
2. The optimum phosphoric acid activant concentration, to achieve the best adsorbing carbons, corresponds to an acid to carbon mass ratio of 1.6:1.0.
3. For methylene blue, the best performing activated carbon was that produced under the following conditions: acid to pits ratio = 1.6:1.0; carbonization temperature = 500 °C; soaking time = 2 hours.
4. The column study showed that the locally-produced activated carbon performed better compared to a widely-used commercial activated carbon, for the case of phenol removal.
5. The activated carbon produced from date pits performed almost as well as the widely-used commercial activated carbon with respect to the adsorption of methylene blue.
6. Excess acid seems to form a protective solid layer on the date pits, and inhibits the activation of the raw material.
7. The adsorption process was found to conform to the Freundlich adsorption isotherm.
8. The values of adsorption capacity ($k$) and intensity of adsorption ($n$) indicate the greater affinity for phenol by the locally-produced activated carbon.
9. The low value of $k_2$ (desorption rate constant) indicates that the adsorbed phenol remains stable on the adsorbent. It can be recovered from the adsorbent by desorption with sodium hydroxide. The regenerated adsorbent can be reactivated and reused.

10. It is concluded that the activated carbon prepared from date palm pits could be exploited for commercial application in the tertiary treatment of industrial effluents.
11. It was found that the adsorption capacity of the locally-produced activated carbon was higher than that of the commercial activated carbon tested.
12. The utilisation of activated carbon from date pits for the removal of colour from water can provide an excellent use for the material.
13. The locally-produced activated carbon was tested with industrial effluent for the removal of total organic carbon and found to be effective.
14. It was found that the adsorption of phenol was influenced by flow rate. The breakthrough time decreased when the flow rate was increased, probably due to insufficient residence time of the phenol solution in the column. However, it should be noted that the use of low flow rates would result in long overall processing times that may not be desirable in practice when large volumes of phenol-contaminated wastewater have to be processed.
15. In all cases, greater adsorption took place under oxic conditions compared to anoxic conditions.
16. Electrochemical regeneration of the activated carbon was investigated and found not to be practical.
17. A response surface methodology (RSM) design was used to optimize the production of the activated carbon.
18. It was found from the RSM design that the optimum response is around a temperature of 430 °C, with $H_3PO_4$ concentration of 55% and an impregnation ratio of 1.5.

## 6.2 Recommendations for Further Work

1. Discharge of effluents containing heavy metals is a major concern in many parts of the world. It would be beneficial to study the removal of heavy metals from aqueous solutions using the produced carbon.
2. It might be worthy to study the effects of interaction between DO, pH, and temperature in batch and column studies.
3. The leachability and toxicity of polymers that are formed on the carbon surface could be another area of research
4. Study of the removal of other aromatic compounds apart from phenol, especially those of large molecular weight should be conducted.
5. The adsorption of chlorinated/halogenated organic compounds by the produced activated carbon is worthy of investigation, as this could lead to the use of the carbon in potable water treatment.
6. In the various possible uses of the produced carbon, a cost analysis should be undertaken to assess its economic viability.

# REFERENCES


1. Ahmad, A.L., Loh, M.M., and Aziz, J.A. (2007), Preparation and characterization of activated carbon from wood and its evaluation on methylene blue adsorption, *Dyes & Pigments*, **75** (2), pp. 263-272.

2. Ahmadpour, A., King, B., and Do, D. (1996), Preparation of active carbons from coal by chemical and physical activation, *Carbon*, **34** (4), pp. 471-479.

3. Ahmadpour, A., King, B., and Do, D. (1998), Comparison of equilibria and kinetics of high surface area activated carbon produced from different precursors and by different chemical treatments, *Ind. Eng. Chem. Res.*, **37**, No. 4, pp. 672-683.

4. Ahmadroup, A. and Do, D. (1997), The preparation of activated carbon from Macadamia nutshell by chemical activation, *Carbon*, **35**, pp. 1723-1732.

5. Ahmedna, M., Marshall, M.E., and Rao, R.M. (2000), Production of granular activated carbons from selected agricultural by-products and evaluation of their physical, chemical and adsorption properties, *Bioresource Technol.*, **71**, pp. 113-123.

6. Ahmedna, M., Marshall, M.E., Husseiny, A.A., Rao, R.M., and Goktepe, I. (2004), The use of nutshell carbons in drinking water filters for removal of trace metals, *Water Res.*, **38**, pp. 1062-1068.

7. Al-Mana, H.A. and Mahmoud, R.M. (1994), Date seed oil: Phenolic, tocopherol and sterol profiles, *J. of Lipids*, **111**, Issue 4, p. 251.

8. Al-Zahrani, M.A., Essa, M.H., and Al-Attas, O.G. (2005), Industrial pollutants removal using produced activated carbon amended sand, Final Report, Project # SABIC 2003/09, KFUPM/SABIC Research Committee, KFUPM, Dhahran.

9. American Public Health Association (APHA), American Water Works Association (AWWA), Water Environment Federation (WEF) (1998), Standard Methods for the Examination of Water and Wastewater, 20th edition, edited by Clesceri, L.S., Greenberg, A.E., and Eaton, A.D., APHA, AWWA, WEF, Washington, D.C.

10. Ariyadejwanich, A., Tanthapanichacoon, W., Nakagawa, K., Mukai, S.R., and Tamon, H. (2002), Preparation and characterization of mesoporous activated carbon from waste tyres, *Carbon*, **41**, pp. 157-164.

11. Aslan, S. and Turkman, A. (2005), Combined biological removal of nitrate and pesticides using wheat straw as substrates, *Process Biochem.*, **40**, pp. 935-943.

12. Aygun, A., Yenisoy-Karakas, S., and Duman, I. (2003), Production of granular activated carbon from fruit stones and nutshells and evaluation of their physical, chemical and adsorption properties, *Micropor Mesopor Mater.*, **66**, pp. 189-195.

13. Bansal, Donnet, J.B., and Stoeckli, F. (1988), *Active Carbon*, Marcel Dekker, New York.

14. Benefield, L.D., Judkin, J.F., and Weana, B.L. (1982), Process chemistry for water and wastewater treatment, 2nd edition, pp. 200-201.

15. Bestani, B., Benderdouche, B., Belhakem, M. and Addou, A. (2004), Methylene blue and iodine adsorption onto an activated desert plant, *Bioresources Technology*, **99** (17), pp. 8441-8444.

16. Caturla, F., Martin-Martinez, J.M., Molina-Sabio, M., Rodriguez-Reinoso, F., and Torregrosa, R. (1998), Adsorption of substituted phenols on activated carbon, *J. Coll. Interface Sci.*, **124**, pp. 528-534.

17. Cetin, E., Moghtaderi, B., Gupta, R., and Wall, T.F. (2004), Influence of pyrolysis conditions on the structure and gasification reactivity of biomass chars, *Fuel*, **83**, pp. 2139-2150.

18. Chamber of Commerce, Eastern Province, Kingdom of Saudi Arabia, Central Department of Statistics, Office Trade Statistics (2003).

19. Chern, J.M. and Chien, Y.W. (2002), Adsorption of nitrophenol onto activated carbon, *Water Research*, **36** (3), pp. 647-655.

20. Cooney, D.O. and Xi, Z. (1994), Activated carbon catalyzes reactions of phenolics during liquid phase adsorption, *AIChE J.*, **40**, pp. 361-364.

21. Coughlin, R.W. and Ezra, F.S. (1968), Role of surface acidity in the adsorption of organic pollutants on the surface of carbon, *Environ. Sci. Technol.*, **2**, pp. 291-297.

22. Cox, M., El-Shafeyey, E., Pichugin, A., and Appleton, Q. (1999), Preparation and characterization of a carbon adsorbent from flax shive by dehydration with sulphuric acid, *J. Chem. Technol. Biotechnol.*, **74**, pp. 1019-1029.

23. Crauford, H.B. and Cline, G. (1990), Water treatment plant design, American Society of Civil Engineers, *American Water Works Association*, McGraw Hill, New York, p. 457.

24. Cyr, P.J., Suri, R.P.S., and Helmig, E.D. (2002), A pilot scale evaluation of removal of mercury from pharmaceutical wastewater using granular activated carbon, *Water Research*, **36** (19), pp. 4725-4734.

25. Dabrowski, A., Podkoscielny, P., Hubicki, Z., and Barczak, M. (2005), Adsorption of phenolic compounds by activated carbon – a critical review, *Chemosphere*, **58**, pp. 1049-1070.

26. Dai, X. and Antal, M.J. (1999), Synthesis of a high yield activated carbon by air gasification of macadamia nut shell charcoal, *Ind. Eng. Chem. Res.*, **38**, pp. 3386-3395.

27. Daifullah, A.A.M., Girgis, B.S., and Gad, H.H.M. (2003), Utilization of agro-residues (rice husk) in small waste water treatment plants, *Mater. Lett.*, **57**, pp. 1723-1731.

28. Dastgheib, S.A. and Rockstraw, D.A. (2001), Pecan shell activated carbon synthesis, characterization, and application for the removal of copper from aqueous solution, *Carbon*, **39** (12), pp. 1849-1855.

29. Daud, W.M., Ali, W.S., and Sulaiman, M.Z. (2000), The effects of carbonization temperature on pore development in palm-shell-based activated carbon, *Carbon*, **38** (14), pp. 1925-1932.

30. Deo, N. and Ali, M.T. (1993), Dye adsorption by a new low cost material, *Indian Journal of Environmental Protection*, **13**, pp. 496-508.

31. Ding, J., Snoeyink, V.L., Larson, R.A., Recktenwalt, M.A., and Wedeking, C.A. (1987), Effect of temperature, time and biomass on wet air regeneration of carbon, *Journal of the Water Pollution Control Federation*, **59**, pp. 139-144.

32. El-Hendawy, A.N.A., Samra, S.E., and Girgis, B.S. (2001), Adsorption characteristics of activated carbons obtained from corncobs, *Colloid Surface A: Physicochem. Eng. Aspects*, **180**, pp. 209-221.

33. El-Sheikh, A.N., Newmana, A.P., Al-Daffaee, H.K., Phull, S., and Cresswell, N. (2004), Characterization of activated carbon prepared from a single cultivar of Jordanian olive stones by chemical and physicochemical techniques, *J. Anal. Appl. Pyrol.*, **71**, pp. 151-164.

34. Evans, M.J., Halliop, E., and MacDonald, J.A.F. (1999), Production of chemically-activated carbon, *Carbon*, **37** (2), pp. 269-274.

35. Ferro-Garcia, M.A., Utrera-Hidalgo, E., Rivera-Utrilla, J., and Moreno-Castilla, J.P. (1993), Regeneration of activated carbons exhausted with chlorophenols, *Carbon,* **31** (6), pp. 857-863.

36. Gergova, K., Galushko, A., Petrov, N., and Minkova, V. (1992), Investigation of the porous structure of activated carbons prepared by pyrolysis of agricultural by-products in a stream of water vapor, *Carbon*, **30** (15), pp. 721-727.

37. Gharaibeh, S.H., Moore, S.V., and Buck, A. (1998), Effluent treatment of industrial wastewater using processed solid residue of olive mill products and commercial activated carbon, *J. Chemical Technology & Biotechnology*, **71** (4), pp. 291-298.

38. Girgis, B.S., Yunis, S.S., and Soliman, A.M. (2002), Characteristics of activated carbon from peanut hulls in relation to conditions of preparation, *Mater. Lett.* **57**, pp. 164-172.

39. Grant, T.M. and King, C.J. (1990), Mechanism of irreversible adsorption of phenolic compounds by activated carbon, *Ind. Eng. Chem. Res.*, **29**, pp. 264-271.

40. Gullon, M.I. and Font, R. (2001), Dynamic pesticide removal with activated carbon fibers, *Water. Res.* **35**, pp. 516-520.

41. Guo, J. and Lua, A.C. (2000), Adsorption of sulphur dioxide onto activated carbon prepared from oil palm shells impregnated with potassium hydroxide, *J. Chem. Technol. Biotechnol.*, **75**, pp. 971-976.

42. Gupta, V.K., Saurabh, S., Yadav, I.S., and Dinesh, M. (1998), Utilisation of bagasse fly ash generated in the sugar industry for the removal and recovery of phenol and p-nitrophenol from wastewater, *J. Chem. Technol. Biotechnol.*, **71**, pp. 180-186.

43. Halhouli, K.A., Darwish, N.A., and Aldhoon, N.M. (1995), Effects of pH and inorganic salts on the adsorption of phenol from aqueous systems on activated decolourising charcoal, *Sep. Sci. Technol.*, **30**, pp. 3313-3324.

44. Hameed, B.H., Ahmad, A.L., and Latiff, K.N. (2007), Adsorption of methylene blue onto activated carbon prepared from sawdust, *Dyes & Pigments*, **75** (1), pp. 143-149

45. Hayashi, J., Kazehaya, A., Muroyama, K., and Watkinson, P. (2000), Preparation of activated carbon from lignin by chemical activation, *Carbon*, **38** (13), pp. 1873-1878.

46. Hsieh, C.T. and Teng, H. (2000), Liquid-phase adsorption of phenol onto activated carbons prepared with different activation levels, *J. Colloid. Interf. Sci.*, **230**, pp. 171-175.

47. Ikuo, A., Fukuhara, T., Maruyama, J., Tatsumoto, H., and Iwasaki, S. (2001), Preparation of carbonaceous adsorbents for removal of chloroform from drinking water, *Carbon*, **39** (7), pp. 1069-1073.

48. Jagtoyen, M., Thwaites, M., Stencel, J., McEnaney, B., and Derbyshire, F. (1992), Adsorbent carbon synthesis from coals by phosphoric acid activation, *Carbon*, **30** (7), pp. 1089-1096.

49. Jagtoyen, M., and Derbyshire, F. (1998), Activated carbons from yellow poplar and white oak by $H_3PO_4$ activation, *Carbon*, **36**, pp. 1085-1097.

50. Johns, M.M., Marshall, W.E., and Toles, C.A. (1997), Agricultural by-products as granular activated carbons for adsorbing dissolved metals and organics, *J. Chemical Technology & Biotechnology*, **71**, pp. 131-140.

51. Johns, M.M., Marshall, W.E., and Toles, C.A. (1999), The effect of activation method on the properties of pecan shell-activated carbon, *J. Chemical Technology & Biotechnology*, **74**, pp. 1037-1044.

52. Kadirvelu, V., Kavipiriya, M., Karthika, C., Radhika, M., Vennilamani, N., and Pablabhi, S. (2003), Utilization of various agricultural wastes for activated carbon production: preparation and application for the removal of dyes and metal ions from aqueous solutions, *Bioresource Technology*, **87**(1), pp. 129-132.

53. Lanzetta, M. and Di Blasi, C. (1998), Pyrolysis kinetics of wheat and corn straw, *J. Anal. Appl. Pyrol.*, **44**, pp. 181-192.

54. Low, K.S. and Lee, C.K. (1999), Column study on the sorption of Cr(VI) using quaternized rice hulls, *Bioresource Technol.*, **68**, Issue 2, May, pp. 205-208.

55. Lu, G.Q., Low, J.C.F., Liu, G.Y., and Lua, A.C. (1995), Surface area development of sewage sludge during pyrolysis, *Fuel*, **74**, pp. 344-348.

56. Lu, G.Q. (1996), Preparation and evaluation of adsorbents from waste carbonaceous materials for $SO_x$ and $NO_x$ removal, *Environmental Progress*, **151**, pp. 12-18.

57. Lua, A.C. and Guo, J. (1999), Chars pyrolyzed from oil palm wastes for activated carbon preparation, *ASCE Journal of Environmental Engineering*, **125** (1), pp. 72-76.

58. Malik, P.K. (2003), Use of activated carbon prepared from saw dust and rice husk for adsorption of acid dyes, *Dyes & Pigments*, **56**, pp. 239-249.

59. Mameri, N., Aioueche, F., Belhocine, D., Grib, H., Lounici, H., Piron, D., and Yahiat, Y. (2000), Preparation of activated carbon from olive mill solid residue, *J. Chem. Technol. Biotechnol.*, **75**, pp. 625-631.

60. Manju, G.N., Raji, C., and Anirudhan, T.S. (1998), Evaluation of coconut husk carbon for the removal of arsenic from water, *Water Res.*, **32**, pp. 3062-3070.

61. Marcilla, A., Garcia-Garcia, S., Asensio, M., and Conesa, J.A. (2000), Influence of thermal treatment regime on the density and reactivity of activated carbons from almond shells, *Carbon*, **38**, pp. 429-440.

62. Martin, R.J. and Ng, W.J. (1985), Chemical regeneration of exhausted activated carbon-II, *Water Research*, **19** (2), pp. 1527-1535.

63. Meshko, V., Markovska, L., Mincheva, M., and Rodriguez, A.E. (2001), Adsorption of basic dyes on granular activated carbon and natural zeolite, *Water Research*, **35** (14), pp. 3357-3366.

64. Ministry of Agriculture, Kingdom of Saudi Arabia, Agricultural Statistics for 1996-2000.

65. Minkova, V., Razvigorova, M., Bjornbom, E., Zanzi, R., Budinova, T., and Petrov, N. (2001), Effect of water vapour and biomass nature on the yield and quality of the pyrolysis products from biomass, *Fuel Proc. Technol.*, **70**, pp. 53-61.

66. Mirasol, J.R., Cordero, T., and Rodriguez, J.J. (1993), Preparation and characterization of activated carbons from eucalyptus kraft lignin, *Carbon*, **31** (1), pp. 87-95.

67. Montgometry, D.C. (1991), Design and analysis of experiments, 3rd edition, John Wiley & Sons, Incorporated, Hoboken, NJ, U.S.A., pp. 445-470.

68. Moreno-Castilla, C., Rivera-Utrilla, J., López-Ramón, M.V., and Carrasco-Marín, F. (1995a), Adsorption of some substituted phenols on activated carbons from a bituminous coal, *Carbon*, **33** (6), pp. 845-851.

69. Moreno-Castilla, C., Rivera-Utrilla, J., Joly, J.P., López-Ramón, M.V., Ferro-García, M.A., and Carrasco-Marín, F. (1995b), Thermal regeneration of an activated carbon exhausted with different substituted phenols, *Carbon*, **33** (10), pp. 1417-1423.

70. Mostafa, M.R., Sarma, S.E., and Yousef, A.M. (1989), Removal of organic pollutants from aqueous solution: Part 1. Adsorption of phenols by activated carbon, *Indian Journal of Chem.*, **28A**, pp. 946-948.

71. Namasivayam, C. and Kanchana, N. (1993), Waste banana pith as adsorbent for the removal of rhodamine-B from aqueous solutions, *Waste Management*, **13** (1), pp. 89-95.

72. Namasivayam, C. and Kadirvelu, K. (1994), Coirpith, an agricultural waste by-product, for the treatment of dyeing wastewater, *Bioresource Technol.*, **48** (1), pp. 79-81.

73. Namasivayam, C. and Yamuna, R.T. (1995), Adsorption of chromium (VI) by a low-cost adsorbent: Biogas residual slurry, *Chemosphere*, **30** (3), February, pp. 561-578.

74. Namasivayam, C., Muniasamy, N., Gayatri, K., Rani, M., and Ranganathan, K. (1996), Removal of dyes from aqueous solutions by cellulosic waste orange peel, *Bioresource Technol.*, **57** (1), July, pp. 37-43.

75. Namasivayam, C. and Arasi, D.J.S.E. (1997), Removal of congo red from wastewater by adsorption onto waste red mud, *Chemosphere*, **34** (2), January, pp. 401-417.

76. Namasivayam, C., Radhka, R., and Suba, S. (2001), Uptake of dyes by a promising locally available agricultural solid waste, *Waste Management*, **21**, pp. 381-387.

77. Negarathinam, Kannan., and Mariappam, Meenakshi Sundaram. (2001), Kinetics and mechanism of removal of methylene blue by adsorption on various carbons- a comparative study, *Dyes & Pigments*, **51** (1), pp. 25-40.

78. Oh, G.H. and Park, C.R. (2002), Preparation and characteristics of rice-straw-based porous carbons with high adsorption capacity, *Fuel*, **81**, pp. 327-336.

79. Patricia. L.L., Quinlivan, A., and Knappe, D.R. (2002), Effects of activated carbon surface chemistry and pore structure on the adsorption of organic contaminants from aqueous solution, *Carbon*, **40** (12), pp. 2085-2100.

80. Perez-Candela, M., Martin-Martinez, J., and Torregrosa-Macia, R. (1995), Chromium (VI) removal with activated carbon, *Water Research* , **29** (9), pp. 2174-2180.

81. Philip, C.A. and Girgis, B.S. (1996), Adsorption characteristics of microporous carbons from apricot stones activated by phosphoric acid, *J. Chem. Technol. Biotechnol.*, **67**, pp. 248-254.

82. Pollard, S.J.T., Thompson, F.E., and McConnachie, G.L. (1995), Microporous carbons from *Moringa oleifera* husks for water purification in less-developed countries, *Water Research*, **29** (1), January, pp. 337-347.

83. Presidency of Meteorology and Environment, KSA (2001), Environmental Protection Standards, 15 October.

84. Putun, A.E., Ozbay, N., Onal, E.P., and Putun, E. (2005), Fixed-bed pyrolysis of cotton stalk for liquid and solid products, *Fuel Process. Technol.*, **86**, pp. 1207-1219.

85. Puziy, A.M., Poddubnaya, O.I., Martinez-Alonso, A., Suarez-Garcia, F., and Tascon, J.M.D. (2001), Synthetic carbons activated with phosphoric acid: Surface chemistry and ion binding properties, *Carbon*, **40**, pp. 1493-1505.

86. Qiao, W., Ling, L., Zha, Q., and Liu, L., (1997), Preparation of a pitch-based activated carbon with a high specific surface area, *Journal of Material Science*, **32**, pp. 4447-4453.

87. Rahman, I.A. and Saad, B. (2003), Utilization of guava seeds as a source of activated carbon for removal of methylene blue from aqueous solution, *Malaysian Journal of Chemistry*, **5** (1), pp. 54-61.

88. Raygobal, S., Karthikeyan, T., Prakash Kumar, B.E., and Miranda, L.R. (2006), Utilization of fluidized bed reactor for the production of adsorbents in removal of malachite green, *Chemical Engineering Journal*, **116**(3), pp. 211-217.

89. Robinson, T., McMullan, G., Marchant, R., and Nigam, P. (2001), Remediation of dyes in textile effluents: a critical review of current treatment technologies, *Bioresource Technologies*, **77**, pp. 247-255.

90. Rodriguez-Reinoso (1997), Activated carbon: structure, characterization and applications. In: Marsh, H., Introduction to carbon technologies, Chapter 2, Publicaciones de la Universidad de Alicante, Apartado 99, E-03080 Alicante, Spain p. 35.

91. Ryoo, K.S., Kim, T.D., and Kim, Y.H. (1999), Regeneration of exhausted activated carbon by a countercurrent oxygen reaction, *Bull. Korean Chem. Soc.*, **20** (12), pp. 1447-1450.

92. Sai, P.M.S., Ahmed, J., and Krishnaiah, K. (1997), Production of activated carbon from coconut shell char in a fluidized bed reactor, *Ind. Eng. Chem. Res.*, **36**, pp. 3625-3630.

93. Salame, I.I. and Bandosz, T.J. (2000), Comparison of the surface features of two wood-based activated carbons, *Ind. Eng. Chem. Res.*, **39**, pp. 301-306.

94. Savova, D., Apak, E., Ekinci, E., Yardim, F., Petrova, N., and T. Budinova (2001), Biomass conversion to carbon adsorbents and gas, *Biomass Bioenergy*, **21**, pp. 133-142.

95. Singh, B.K., Mishra, N.M., and Rawat, N.S. (1994), Sorption characteristics of phenols on fly ash and impregnated fly ash, *Indian J. Environ. Hlth.*, **36**, pp. 1-7.

96. Sivaraj, R., Namasivayam, C., and Kadirvelu, K. (2001), Orange peel as an adsorbent in the removal of acid violet 17 (acid dye) from aqueous solutions, *Waste Management*, **21**, pp. 105-110.

97. Skoulou V. and Zabaniotou, A. (2005), Investigation of agricultural and animal wastes in Greece and their allocation to potential application for energy production. *Renew Sustain Energy Rev.*, **1**, pp. 24-32.

98. Srivastava, S.K., Gupta, V.K., Johri, N., and Dinesh, M. (1995), Removal of 2,4,6-trinitrophenol using bagasse fly ash – a sugar industry waste material, *Indian J. Chem. Technol.* **2**, pp. 333-336.

99. Streat, M., Patrick, J.W., and Camporro Perez, M.J. (1995), Sorption of phenol and parachlorophenol from water using conventional and novel activated carbons, *Water Research*, **29**, pp. 467-472.

100. Sudaryanto, Y., Hartono, S.B., Irawaty, W., Hindarso, H., and Ismadji, S. (2006), High surface area activated carbon prepared from cassava peel by chemical activation, *Bioresource Technol.*, **97**, pp. 734-739.

101. Tam, M. and Antal, M., (1999), Preparation of activated carbons from macadamia nut shell and coconut shell by air activation, *Ind. Eng. Chem. Res.*, **38**, pp. 4268-4276.

102. Teng, H. and Yeh, L. (1998), Preparation of activated carbon from bituminous coals with zinc chloride activation, *Ind. Eng. Chem. Res.*, **37**, pp. 58-65.

103. Teng, H. and Hsu, L. (1999), High porosity carbons prepared from bituminous coal with potassium hydroxide activation, *Ind. Eng. Chem. Res.*, **38**, pp. 2947-2953.

104. Urano, K., Yamamoto, E., Tonegawa, M., and Fujie, K. (1991), Adsorption of chlorinated organic compounds on activated carbon from water, *Water Research,* **25** (12), pp. 1459-1464.

105. Vidic, R.D., Suidan, M.T., Traegner, U.K., and Nakhla, G.F. (1990), Adsorption isotherm: illusive capacity and role of oxygen, *Water Research*, **4**, pp. 1187-1198.

106. Vidic, R.D., Suidan, M.T., and Brenner, R.C. (1993), Oxidative coupling of phenols on activated carbon: impact on adsorption equilibrium, *Environ. Sci. Technol.*, **27**, pp. 2079-2085.

107. Vidic, R.D., Tessmer, C. H., and Uranowski, L. J. (1998), Impact of surface properties of activated carbons on oxidative coupling of phenolic compounds, *Carbon.*, **35, (9)**, pp. 1349-1359.

108. Vinod, K. and Gupta, S.K., Srivastava, and Renu, T. (2000), Design parameters for the treatment of phenolic wastes by carbon columns (obtained from fertilizer waste material), *Water Research*, **34**, pp. 1543-1550.

109. Walker, G.M. and Weatherley, L.R. (1997), Adsorption of acid dyes onto granular activated carbon in fixed beds, *Water Research*, **31** (8), pp. 2093-2101.

110. Warhurst, A.M., McConnachie, G., and Pollard, S. (1996), The production of activated carbon for water treatment in Malawi from the waste seed husks of *Moringa oleifera*, *Water Science and Technology*, **34** (11), pp. 177-184.

111. Weber Jr., W.J. and Morris, J.C. (1963), Color removal from synthetic dye wastewater using a bioadsorbent, *J. Sanitary Eng. Div., ASCE*, **89** (SA2), p. 31.

112. Wu, Chi-Chin, Walawender, W.P., and Fan, L.T. (1997), Chemical agents for production of activated carbons from extrusion cooked grain products, In: Proceedings of Carbon'97, Extended Abstracts and Program, Vol. II, Carbonization/Industrial/Carbon Growth/Fibers. Carbon'97, 23rd Biennial Conference on Carbon, University Park, Pennsylvania, July 18-23.

113. www.cee.vt.edu / program_areas / environmental /teach / gwprimer / group23 /acraw_materials.html (2002) – date accessed: 18/12/03.

114. www.pme.gov.sa – date accessed: 22/10/04.

115. www.saudiembassy.net/publications/magazine-w (2002) - date accessed: 18/12/03.

116. Zhang, H., Ye, L., and Zhong, H. (2002), Regeneration of phenol-saturated activated carbon in an electrochemical reactor, *J. of chemical technology & biotechnology*, **77** (11), pp.1246-1250.

# APPENDICES

# Appendix A:

## Data for Activated Carbons Produced Using an Activation Time of 1 hour

**Table A.1: Texture characteristics of ACs obtained at T=300 °C (R=0.5)**

| Parameter | Texture Characteristics | | | | |
|---|---|---|---|---|---|
| % $H_3PO_4$ | 30% | 40% | 50% | 60% | 70% |
| $S_{BET}$ ($m^2/g$) | 104 | 152 | 206.4 | 204.2 | 208.5 |
| Total Pore Volume, $V_p$ ($cm^3\ g^{-1}$) | 0.19 | 0.20 | 0.28 | 0.36 | 0.22 |
| Average Pore Radius, nm | 3.65 | 2.63 | 2.71 | 3.52 | 2.11 |

**Table A.2: Texture characteristics of ACs obtained at T=400 °C (R=0.5)**

| Parameter | Texture Characteristics | | | | |
|---|---|---|---|---|---|
| % $H_3PO_4$ | 30% | 40% | 50% | 60% | 70% |
| $S_{BET}$ ($m^2/g$) | 146.3 | 157.4 | 216.8 | 204.5 | 214.7 |
| Total Pore Volume, $V_p$ ($cm^3\ g^{-1}$) | 0.22 | 0.16 | 0.28 | 0.30 | 0.18 |
| Average Pore Radius, nm | 3.01 | 2.03 | 2.58 | 2.93 | 1.68 |

**Table A.3: Texture characteristics of ACs obtained at T=500 °C (R=0.5)**

| Parameter | Texture Characteristics | | | | |
|---|---|---|---|---|---|
| % $H_3PO_4$ | 30% | 40% | 50% | 60% | 70% |
| $S_{BET}$ ($m^2/g$) | 165.8 | 178.6 | 172.6 | 178.6 | 187.8 |
| Total Pore Volume, $V_p$ ($cm^3\ g^{-1}$) | 0.18 | 0.17 | 0.20 | 0.22 | 0.20 |
| Average Pore Radius, nm | 2.17 | 1.91 | 2.31 | 2.46 | 2.13 |

**Table A.4: Texture characteristics of ACs obtained at T=600 °C (R=0.5)**

| Parameter | Texture Characteristics | | | | |
|---|---|---|---|---|---|
| % $H_3PO_4$ | 30% | 40% | 50% | 60% | 70% |
| $S_{BET}$ ($m^2/g$) | 157.6 | 169.2 | 170.6 | 184.6 | 179.8 |
| Total Pore Volume, $V_p$ ($cm^3\ g^{-1}$) | 0.14 | 0.17 | 0.18 | 0.14 | 0.22 |
| Average Pore Radius, nm | 1.78 | 2.01 | 2.11 | 1.51 | 2.45 |

**Table A.5: Texture characteristics of ACs obtained at T=700 °C (R=0.5)**

| Parameter | Texture Characteristics | | | | |
|---|---|---|---|---|---|
| % $H_3PO_4$ | 30% | 40% | 50% | 60% | 70% |
| $S_{BET}$ ($m^2/g$) | 154.7 | 163.8 | 164.6 | 179.4 | 169.5 |
| Total Pore Volume, $V_p$ ($cm^3\ g^{-1}$) | 0.14 | 0.16 | 0.17 | 0.18 | 0.17 |
| Average Pore Radius, nm | 1.81 | 1.95 | 2.06 | 2.01 | 2.01 |

**Table A.6: Texture characteristics of ACs obtained at T=300 °C (R = 0.8)**

| Parameter | Texture Characteristics | | | | |
|---|---|---|---|---|---|
| % $H_3PO_4$ | 30% | 40% | 50% | 60% | 70% |
| $S_{BET}$ ($m^2/g$) | 197.8 | 195.7 | 236.8 | 273.4 | 234.6 |
| Total Pore Volume, $V_p$ ($cm^3\ g^{-1}$) | 0.14 | 0.19 | 0.16 | 0.19 | 0.22 |
| Average Pore Radius, nm | 1.41 | 1.94 | 1.35 | 1.39 | 1.87 |

**Table A.7: Texture characteristics of ACs obtained at T=400 °C (R = 0.8)**

| Parameter | Texture Characteristics | | | | |
|---|---|---|---|---|---|
| % $H_3PO_4$ | 30% | 40% | 50% | 60% | 70% |
| $S_{BET}$ ($m^2/g$) | 180.6 | 196.5 | 208.7 | 212.3 | 219.6 |
| Total Pore Volume, $V_p$ ($cm^3\ g^{-1}$) | 0.20 | 0.22 | 0.19 | 0.18 | 0.17 |
| Average Pore Radius, nm | 2.21 | 2.24 | 1.82 | 1.69 | 1.55 |

**Table A.8: Texture characteristics of ACs obtained at T=500 °C (R = 0.8)**

| Parameter | Texture Characteristics | | | | |
|---|---|---|---|---|---|
| % $H_3PO_4$ | 30% | 40% | 50% | 60% | 70% |
| $S_{BET}$ ($m^2/g$) | 165.8 | 187.7 | 214.5 | 205.7 | 198.3 |
| Total Pore Volume, $V_p$ ($cm^3\ g^{-1}$) | 0.20 | 0.12 | 0.17 | 0.19 | 0.19 |
| Average Pore Radius, nm | 2.41 | 1.28 | 15.8 | 1.85 | 1.92 |

**Table A.9: Texture characteristics of ACs obtained at T=600 °C (R = 0.8)**

| Parameter | Texture Characteristics | | | | |
|---|---|---|---|---|---|
| % $H_3PO_4$ | 30% | 40% | 50% | 60% | 70% |
| $S_{BET}$ ($m^2/g$) | 177.4 | 182.5 | 176.6 | 189.5 | 191.1 |
| Total Pore Volume, $V_p$ ($cm^3\ g^{-1}$) | 0.18 | 0.10 | 0.22 | 0.18 | 0.23 |
| Average Pore Radius, nm | 2.03 | 1.09 | 2.49 | 1.90 | 2.41 |

**Table A.10: Texture characteristics of ACs obtained at T=700 °C (R = 0.8)**

| Parameter | Texture Characteristics | | | | |
|---|---|---|---|---|---|
| % $H_3PO_4$ | 30% | 40% | 50% | 60% | 70% |
| $S_{BET}$ ($m^2/g$) | 176.4 | 182.3 | 180.8 | 189.9 | 193.4 |
| Total Pore Volume, $V_p$ ($cm^3\ g^{-1}$) | 0.19 | 0.22 | 0.24 | 0.11 | 0.22 |
| Average Pore Radius, nm | 2.15 | 2.41 | 2.65 | 1.16 | 2.27 |

**Table A.11: Texture characteristics of ACs obtained at 300 °C (R=1.0)**

| Parameter | Texture Characteristics | | | | |
|---|---|---|---|---|---|
| % $H_3PO_4$ | 30% | 40% | 50% | 60% | 70% |
| $S_{BET}$ ($m^2/g$) | 165.6 | 198.4 | 276.8 | 280.4 | 279.8 |
| Total Pore Volume, $V_p$ ($cm^3\ g^{-1}$) | 0.23 | 0.18 | 0.12 | 0.22 | 0.24 |
| Average Pore Radius, nm | 2.78 | 1.81 | 0.86 | 1.57 | 1.71 |

**Table A.12: Texture characteristics of ACs obtained at 400 °C (R=1.0)**

| Parameter | Texture Characteristics | | | | |
|---|---|---|---|---|---|
| % $H_3PO_4$ | 30% | 40% | 50% | 60% | 70% |
| $S_{BET}$ ($m^2/g$) | 184.4 | 193.5 | 266.7 | 295.8 | 284.7 |
| Total Pore Volume, $V_p$ ($cm^3\ g^{-1}$) | 0.17 | 0.18 | 0.32 | 0.40 | 0.26 |
| Average Pore Radius, nm | 1.84 | 1.86 | 2.40 | 2.70 | 1.83 |

**Table A.13: Texture characteristics of ACs obtained at 500 °C (R=1.0)**

| Parameter | Texture Characteristics | | | | |
|---|---|---|---|---|---|
| % $H_3PO_4$ | 30% | 40% | 50% | 60% | 70% |
| $S_{BET}$ ($m^2/g$) | 392.6 | 658.3 | 1008.7 | 824.5 | 704.3 |
| Total Pore Volume, $V_p$ ($cm^3\ g^{-1}$) | 0.22 | 0.19 | 0.26 | 0.14 | 0.22 |
| Average Pore Radius, nm | 1.12 | 0.58 | 0.51 | 0.34 | 0.62 |

**Table A.14: Texture characteristics of ACs obtained at 600 °C (R=1.0)**

| Parameter | Texture Characteristics | | | | |
|---|---|---|---|---|---|
| % $H_3PO_4$ | 30% | 40% | 50% | 60% | 70% |
| $S_{BET}$ ($m^2/g$) | 476.3 | 488.3 | 588.7 | 685.7 | 704.8 |
| Total Pore Volume, $V_p$ ($cm^3\ g^{-1}$) | 0.24 | 0.19 | 0.31 | 0.23 | 0.27 |
| Average Pore Radius, nm | 1.01 | 0.78 | 1.05 | 0.67 | 0.77 |

**Table A.15: Texture characteristics of ACs obtained at 700 °C (R=1.0)**

| Parameter | Texture Characteristics | | | | |
|---|---|---|---|---|---|
| % $H_3PO_4$ | 30% | 40% | 50% | 60% | 70% |
| $S_{BET}$ ($m^2/g$) | 395.6 | 508.8 | 646.3 | 608.7 | 601.5 |
| Total Pore Volume, $V_p$ ($cm^3\ g^{-1}$) | 0.20 | 0.33 | 0.36 | 0.40 | 0.26 |
| Average Pore Radius, nm | 1.01 | 1.30 | 1.11 | 1.31 | 0.86 |

**Table A.16: Texture characteristics of ACs obtained at 300 °C (R=1.2)**

| Parameter | Texture Characteristics | | | | |
|---|---|---|---|---|---|
| % $H_3PO_4$ | 30% | 40% | 50% | 60% | 70% |
| $S_{BET}$ ($m^2/g$) | 386.8 | 681.7 | 887.5 | 973.4 | 969.3 |
| Total Pore Volume, $V_p$ ($cm^3\ g^{-1}$) | 0.32 | 0.36 | 0.39 | 0.46 | 0.52 |
| Average Pore Radius, nm | 1.65 | 1.06 | 0.88 | 0.94 | 1.07 |

**Table A.17: Texture characteristics of ACs obtained at 400 °C (R=1.2)**

| Parameter | Texture Characteristics | | | | |
|---|---|---|---|---|---|
| % $H_3PO_4$ | 30% | 40% | 50% | 60% | 70% |
| $S_{BET}$ ($m^2/g$) | 320.8 | 404.6 | 903.4 | 904.6 | 967.3 |
| Total Pore Volume, $V_p$ ($cm^3\ g^{-1}$) | 0.33 | 0.35 | 0.48 | 0.53 | 0.42 |
| Average Pore Radius, nm | 2.05 | 1.73 | 1.06 | 1.17 | 0.87 |

**Table A.18: Texture characteristics of ACs obtained at 500 °C (R=1.2)**

| Parameter | Texture Characteristics | | | | |
|---|---|---|---|---|---|
| % $H_3PO_4$ | 30% | 40% | 50% | 60% | 70% |
| $S_{BET}$ ($m^2/g$) | 698.1 | 881.6 | 1001.6 | 967.3 | 985.8 |
| Total Pore Volume, $V_p$ ($cm^3\ g^{-1}$) | 0.32 | 0.52 | 0.36 | 0.49 | 0.33 |
| Average Pore Radius, nm | 0.92 | 1.18 | 0.72 | 1.01 | 0.67 |

**Table A.19: Texture characteristics of ACs obtained at 600 °C (R=1.2)**

| Parameter | Texture Characteristics | | | | |
|---|---|---|---|---|---|
| % $H_3PO_4$ | 30% | 40% | 50% | 60% | 70% |
| $S_{BET}$ ($m^2/g$) | 648.5 | 621.3 | 848.3 | 906.5 | 913.8 |
| Total Pore Volume, $V_p$ ($cm^3\ g^{-1}$) | 0.33 | 0.26 | 0.40 | 0.42 | 0.37 |
| Average Pore Radius, nm | 1.02 | 0.84 | 0.99 | 0.93 | 0.81 |

**Table A.20: Texture characteristics of ACs obtained at 700 °C (R=1.2)**

| Parameter | Texture Characteristics | | | | |
|---|---|---|---|---|---|
| % $H_3PO_4$ | 30% | 40% | 50% | 60% | 70% |
| $S_{BET}$ ($m^2/g$) | 584.3 | 724.8 | 914.6 | 877.8 | 906.5 |
| Total Pore Volume, $V_p$ ($cm^3\ g^{-1}$) | 0.34 | 0.24 | 0.42 | 0.43 | 0.41 |
| Average Pore Radius, nm | 1.16 | 0.66 | 0.92 | 0.98 | 0.90 |

**Table A.21: Texture characteristics of ACs obtained at 300 °C (R=1.4)**

| Parameter | Texture Characteristics | | | | |
|---|---|---|---|---|---|
| % $H_3PO_4$ | 30% | 40% | 50% | 60% | 70% |
| $S_{BET}$ ($m^2/g$) | 267.7 | 389.7 | 607.8 | 681.5 | 634.6 |
| Total Pore Volume, $V_p$ ($cm^3\ g^{-1}$) | 0.33 | 0.32 | 0.36 | 0.31 | 0.37 |
| Average Pore Radius, nm | 2.46 | 1.64 | 1.18 | 0.91 | 1.17 |

**Table A.22: Texture characteristics of ACs obtained at 400 °C (R=1.4)**

| Parameter | Texture Characteristics | | | | |
|---|---|---|---|---|---|
| % $H_3PO_4$ | 30% | 40% | 50% | 60% | 70% |
| $S_{BET}$ ($m^2/g$) | 364.8 | 414.6 | 626.8 | 766.4 | 816.7 |
| Total Pore Volume, $V_p$ ($cm^3\ g^{-1}$) | 0.30 | 0.41 | 0.36 | 0.42 | 0.27 |
| Average Pore Radius, nm | 1.64 | 1.97 | 1.15 | 1.09 | 0.66 |

**Table A.23: Texture characteristics of ACs obtained at 500 °C (R=1.4)**

| Parameter | Texture Characteristics | | | | |
|---|---|---|---|---|---|
| % $H_3PO_4$ | 30% | 40% | 50% | 60% | 70% |
| $S_{BET}$ ($m^2/g$) | 398.7 | 496.3 | 634.6 | 801.5 | 894.3 |
| Total Pore Volume, $V_p$ ($cm^3\ g^{-1}$) | 0.27 | 0.42 | 0.20 | 0.35 | 0.27 |
| Average Pore Radius, nm | 1.35 | 1.69 | 0.63 | 0.87 | 0.60 |

**Table A.24: Texture characteristics of ACs obtained at 600 °C (R=1.4)**

| Parameter | Texture Characteristics | | | | |
|---|---|---|---|---|---|
| % $H_3PO_4$ | 30% | 40% | 50% | 60% | 70% |
| $S_{BET}$ ($m^2/g$) | 426.5 | 514.3 | 691.3 | 874.3 | 903.4 |
| Total Pore Volume, $V_p$ ($cm^3\ g^{-1}$) | 0.31 | 0.36 | 0.45 | 0.57 | 0.43 |
| Average Pore Radius, nm | 1.45 | 1.40 | 1.30 | 1.18 | 0.95 |

**Table A.25: Texture characteristics of ACs obtained at 700 °C (R=1.4)**

| Parameter | Texture Characteristics | | | | |
|---|---|---|---|---|---|
| % $H_3PO_4$ | 30% | 40% | 50% | 60% | 70% |
| $S_{BET}$ ($m^2/g$) | 392.4 | 416.5 | 606.7 | 848.3 | 923.5 |
| Total Pore Volume, $V_p$ ($cm^3\ g^{-1}$) | 0.33 | 0.29 | 0.49 | 0.42 | 0.39 |
| Average Pore Radius, nm | 1.68 | 1.40 | 1.61 | 0.99 | 0.84 |

**Table A.26: Texture characteristics of ACs obtained at 300 °C (R=1.6)**

| Parameter | Texture Characteristics | | | | |
|---|---|---|---|---|---|
| % $H_3PO_4$ | 30% | 40% | 50% | 60% | 70% |
| $S_{BET}$ ($m^2/g$) | 211.4 | 285.3 | 297.5 | 308.3 | 315.3 |
| Total Pore Volume, $V_p$ ($cm^3\ g^{-1}$) | 0.29 | 0.22 | 0.19 | 0.35 | 0.33 |
| Average Pore Radius, nm | 2.74 | 1.66 | 1.27 | 2.28 | 2.09 |

**Table A.27: Texture characteristics of ACs obtained at 400 °C (R=1.6)**

| Parameter | Texture Characteristics | | | | |
|---|---|---|---|---|---|
| % $H_3PO_4$ | 30% | 40% | 50% | 60% | 70% |
| $S_{BET}$ ($m^2/g$) | 298.7 | 353.5 | 436.7 | 611.3 | 588.9 |
| Total Pore Volume, $V_p$ ($cm^3\ g^{-1}$) | 0.41 | 0.45 | 0.42 | 0.61 | 0.57 |
| Average Pore Radius, nm | 2.74 | 2.54 | 1.92 | 1.99 | 1.77 |

**Table A.28: Texture characteristics of ACs obtained at 500 °C (R=1.6)**

| Parameter | Texture Characteristics | | | | |
|---|---|---|---|---|---|
| % $H_3PO_4$ | 30% | 40% | 50% | 60% | 70% |
| $S_{BET}$ ($m^2/g$) | 276.4 | 808.4 | 954.6 | 928.3 | 1007.8 |
| Total Pore Volume, $V_p$ ($cm^3\ g^{-1}$) | 0.48 | 0.38 | 0.33 | 0.48 | 0.67 |
| Average Pore Radius, nm | 1.24 | 0.94 | 0.69 | 1.03 | 1.23 |

**Table A.29: Texture characteristics of ACs obtained at 600 °C (R=1.6)**

| Parameter | Texture Characteristics | | | | |
|---|---|---|---|---|---|
| % $H_3PO_4$ | 30% | 40% | 50% | 60% | 70% |
| $S_{BET}$ ($m^2/g$) | 509.6 | 584.4 | 604.5 | 628.3 | 624.8 |
| Total Pore Volume, $V_p$ ($cm^3\ g^{-1}$) | 0.23 | 0.38 | 0.48 | 0.33 | 0.38 |
| Average Pore Radius, nm | 0.90 | 1.30 | 1.59 | 1.05 | 1.22 |

**Table A.30: Texture characteristics of ACs obtained at 700 °C (R=1.6)**

| Parameter | Texture Characteristics | | | | |
|---|---|---|---|---|---|
| % $H_3PO_4$ | 30% | 40% | 50% | 60% | 70% |
| $S_{BET}$ ($m^2/g$) | 496.3 | 585.6 | 628.1 | 606.9 | 748.5 |
| Total Pore Volume, $V_p$ ($cm^3\ g^{-1}$) | 0.23 | 0.25 | 0.27 | 0.23 | 0.34 |
| Average Pore Radius, nm | 0.93 | 0.85 | 0.86 | 0.76 | 0.91 |

**Table A.31: Texture characteristics of ACs obtained at 300 °C (R=1.8)**

| Parameter | Texture Characteristics | | | | |
|---|---|---|---|---|---|
| % $H_3PO_4$ | 30% | 40% | 50% | 60% | 70% |
| $S_{BET}$ ($m^2/g$) | 408.5 | 488.1 | 525.4 | 593.7 | 680.6 |
| Total Pore Volume, $V_p$ ($cm^3\ g^{-1}$) | 0.23 | 0.27 | 0.26 | 0.25 | 0.29 |
| Average Pore Radius, nm | 1.13 | 1.11 | 0.99 | 0.84 | 0.85 |

**Table A.32: Texture characteristics of ACs obtained at 400 °C (R=1.8)**

| Parameter | Texture Characteristics | | | | |
|---|---|---|---|---|---|
| % $H_3PO_4$ | 30% | 40% | 50% | 60% | 70% |
| $S_{BET}$ ($m^2/g$) | 396.4 | 427.5 | 511.8 | 576.4 | 625.3 |
| Total Pore Volume, $V_p$ ($cm^3\ g^{-1}$) | 0.24 | 0.31 | 0.23 | 0.27 | 0.26 |
| Average Pore Radius, Å | 12.1 | 14.5 | 9.0 | 9.4 | 8.3 |

**Table A.33: Texture characteristics of ACs obtained at 500 °C (R=1.8)**

| Parameter | Texture Characteristics | | | | |
|---|---|---|---|---|---|
| % $H_3PO_4$ | 30% | 40% | 50% | 60% | 70% |
| $S_{BET}$ ($m^2/g$) | 387.6 | 425.8 | 520.7 | 583.9 | 620.7 |
| Total Pore Volume, $V_p$ ($cm^3\ g^{-1}$) | 0.23 | 0.36 | 0.23 | 0.29 | 0.34 |
| Average Pore Radius, nm | 1.18 | 1.69 | 0.88 | 0.99 | 1.09 |

**Table A.34: Texture characteristics of ACs obtained at 600 °C (R=1.8)**

| Parameter | Texture Characteristics | | | | |
|---|---|---|---|---|---|
| % $H_3PO_4$ | 30% | 40% | 50% | 60% | 70% |
| $S_{BET}$ ($m^2/g$) | 387.6 | 380.4 | 506.7 | 618.3 | 630.5 |
| Total Pore Volume, $V_p$ ($cm^3\ g^{-1}$) | 0.27 | 0.35 | 0.22 | 0.33 | 0.45 |
| Average Pore Radius, nm | 1.39 | 1.84 | 0.87 | 1.07 | 1.43 |

**Table A.35: Texture characteristics of ACs obtained at 700 °C (R=1.8)**

| Parameter | Texture Characteristics | | | | |
|---|---|---|---|---|---|
| % $H_3PO_4$ | 30% | 40% | 50% | 60% | 70% |
| $S_{BET}$ ($m^2/g$) | 411.3 | 408.3 | 513.4 | 524.1 | 617.3 |
| Total Pore Volume, $V_p$ ($cm^3\ g^{-1}$) | 0.19 | 0.22 | 0.36 | 0.25 | 0.33 |
| Average Pore Radius, nm | 0.92 | 1.08 | 1.40 | 0.95 | 1.07 |

**Table A.36: Texture characteristics of ACs obtained at 300 °C (R=2.0)**

| Parameter | Texture Characteristics | | | | |
|---|---|---|---|---|---|
| % $H_3PO_4$ | 30% | 40% | 50% | 60% | 70% |
| $S_{BET}$ ($m^2/g$) | 715.8 | 718.1 | 723.5 | 793.4 | 721.6 |
| Total Pore Volume, $V_p$ ($cm^3\ g^{-1}$) | 0.39 | 0.31 | 0.33 | 0.53 | 0.39 |
| Average Pore Radius, nm | 1.09 | 0.86 | 0.91 | 1.34 | 1.08 |

**Table A.37: Texture characteristics of ACs obtained at 400 °C (R=2.0)**

| Parameter | Texture Characteristics | | | | |
|---|---|---|---|---|---|
| % $H_3PO_4$ | 30% | 40% | 50% | 60% | 70% |
| $S_{BET}$ ($m^2/g$) | 937.5 | 1008.4 | 984.3 | 1019.8 | 1238.4 |
| Total Pore Volume, $V_p$ ($cm^3\ g^{-1}$) | 0.39 | 0.44 | 0.45 | 0.46 | 0.53 |
| Average Pore Radius, nm | 0.83 | 0.87 | 0.91 | 0.90 | 0.86 |

**Table A.38: Texture characteristics of ACs obtained at 500 °C (R=2.0)**

| Parameter | Texture Characteristics | | | | |
|---|---|---|---|---|---|
| % $H_3PO_4$ | 30% | 40% | 50% | 60% | 70% |
| $S_{BET}$ ($m^2/g$) | 818.7 | 933.5 | 1204.6 | 1019.3 | 1276.3 |
| Total Pore Volume, $V_p$ ($cm^3\ g^{-1}$) | 0.39 | 0.57 | 0.55 | 0.43 | 0.66 |
| Average Pore Radius, nm | 0.95 | 1.11 | 0.91 | 0.84 | 1.03 |

**Table A.39: Texture characteristics of ACs obtained at 600 °C (R=2.0)**

| Parameter | Texture Characteristics | | | | |
|---|---|---|---|---|---|
| % $H_3PO_4$ | 30% | 40% | 50% | 60% | 70% |
| $S_{BET}$ ($m^2/g$) | 626.5 | 798.1 | 913.6 | 947.3 | 997.6 |
| Total Pore Volume, $V_p$ ($cm^3\ g^{-1}$) | 0.40 | 0.41 | 0.49 | 0.53 | 0.57 |
| Average Pore Radius, nm | 12.7 | 10.3 | 10.7 | 11.2 | 11.4 |

**Table A.40: Texture characteristics of ACs obtained at 700 °C (R=2.0)**

| Parameter | Texture Characteristics | | | | |
|---|---|---|---|---|---|
| % $H_3PO_4$ | 30% | 40% | 50% | 60% | 70% |
| $S_{BET}$ ($m^2/g$) | 534.9 | 696.4 | 934.1 | 955.8 | 927.3 |
| Total Pore Volume, $V_p$ ($cm^3\ g^{-1}$) | 0.44 | 0.32 | 0.43 | 0.41 | 0.44 |
| Average Pore Radius, nm | 1.64 | 0.92 | 0.92 | 0.86 | 0.95 |

**Table A.41: Texture characteristics of ACs obtained at 300 °C (R=2.2)**

| Parameter | Texture Characteristics | | | | |
|---|---|---|---|---|---|
| % $H_3PO_4$ | 30% | 40% | 50% | 60% | 70% |
| $S_{BET}$ ($m^2/g$) | 644.3 | 724.5 | 949.5 | 924.3 | 896.3 |
| Total Pore Volume, $V_p$ ($cm^3\ g^{-1}$) | 0.36 | 0.39 | 0.40 | 0.51 | 0.49 |
| Average Pore Radius, nm | 1.12 | 1.08 | 0.84 | 1.10 | 1.09 |

**Table A.42: Texture characteristics of ACs obtained at 400 °C (R=2.2)**

| Parameter | Texture Characteristics | | | | |
|---|---|---|---|---|---|
| % $H_3PO_4$ | 30% | 40% | 50% | 60% | 70% |
| $S_{BET}$ ($m^2/g$) | 743.8 | 824.5 | 913.3 | 923.4 | 904.7 |
| Total Pore Volume, $V_p$ ($cm^3\ g^{-1}$) | 0.39 | 0.56 | 0.48 | 0.47 | 0.43 |
| Average Pore Radius, nm | 1.05 | 1.24 | 1.05 | 1.02 | 0.95 |

**Table A.43: Texture characteristics of ACs obtained at 500 °C (R=2.2)**

| Parameter | Texture Characteristics | | | | |
|---|---|---|---|---|---|
| % $H_3PO_4$ | 30% | 40% | 50% | 60% | 70% |
| $S_{BET}$ ($m^2/g$) | 617.3 | 928.4 | 1276.3 | 1245.8 | 948.1 |
| Total Pore Volume, $V_p$ ($cm^3\ g^{-1}$) | 0.27 | 0.51 | 0.54 | 0.49 | 0.43 |
| Average Pore Radius, nm | 0.87 | 1.10 | 0.846 | 0.79 | 0.91 |

**Table A.44: Texture characteristics of ACs obtained at 600 °C (R=2.2)**

| Parameter | Texture Characteristics | | | | |
|---|---|---|---|---|---|
| % $H_3PO_4$ | 30% | 40% | 50% | 60% | 70% |
| $S_{BET}$ ($m^2/g$) | 623.8 | 883.5 | 1156.7 | 991.7 | 956.3 |
| Total Pore Volume, $V_p$ ($cm^3\ g^{-1}$) | 0.41 | 0.35 | 0.41 | 0.44 | 0.46 |
| Average Pore Radius, nm | 1.31 | 0.79 | 0.71 | 0.88 | 0.96 |

**Table A.45: Texture characteristics of ACs obtained at 700 °C (R=2.2)**

| Parameter | Texture Characteristics | | | | |
|---|---|---|---|---|---|
| % $H_3PO_4$ | 30% | 40% | 50% | 60% | 70% |
| $S_{BET}$ ($m^2/g$) | 698.3 | 857.4 | 984.8 | 891.7 | 885.8 |
| Total Pore Volume, $V_p$ ($cm^3\ g^{-1}$) | 0.32 | 0.37 | 0.41 | 0.41 | 0.37 |
| Average Pore Radius, nm | 0.92 | 0.86 | 0.83 | 0.92 | 0.84 |

**Table A.46: Texture characteristics of ACs obtained at 300 °C (R=2.4)**

| Parameter | Texture Characteristics | | | | |
|---|---|---|---|---|---|
| % $H_3PO_4$ | 30% | 40% | 50% | 60% | 70% |
| $S_{BET}$ ($m^2/g$) | 287.8 | 317.8 | 320.7 | 408.7 | 428.9 |
| Total Pore Volume, $V_p$ ($cm^3\ g^{-1}$) | 0.19 | 0.34 | 0.27 | 0.42 | 0.35 |
| Average Pore Radius, nm | 1.32 | 2.14 | 1.68 | 2.05 | 1.63 |

**Table A.47: Texture characteristics of ACs obtained at 400 °C (R=2.4)**

| Parameter | Texture Characteristics | | | | |
|---|---|---|---|---|---|
| % $H_3PO_4$ | 30% | 40% | 50% | 60% | 70% |
| $S_{BET}$ ($m^2/g$) | 277.3 | 328.1 | 376.8 | 411.7 | 498.1 |
| Total Pore Volume, $V_p$ ($cm^3\ g^{-1}$) | 0.21 | 0.23 | 0.31 | 0.38 | 0.46 |
| Average Pore Radius, nm | 1.51 | 1.40 | 1.64 | 1.85 | 1.85 |

**Table A.48: Texture characteristics of ACs obtained at 500 °C (R=2.4)**

| Parameter | Texture Characteristics | | | | |
|---|---|---|---|---|---|
| % $H_3PO_4$ | 30% | 40% | 50% | 60% | 70% |
| $S_{BET}$ ($m^2/g$) | 327.1 | 391.4 | 441.5 | 508.9 | 522.7 |
| Total Pore Volume, $V_p$ ($cm^3\ g^{-1}$) | 0.27 | 0.29 | 0.22 | 0.49 | 0.53 |
| Average Pore Radius, nm | 1.65 | 1.48 | 0.99 | 1.93 | 2.03 |

**Table A.49: Texture characteristics of ACs obtained at 600 °C (R=2.4)**

| Parameter | Texture Characteristics | | | | |
|---|---|---|---|---|---|
| % $H_3PO_4$ | 30% | 40% | 50% | 60% | 70% |
| $S_{BET}$ ($m^2/g$) | 328.1 | 402.7 | 411.9 | 521.7 | 533.8 |
| Total Pore Volume, $V_p$ ($cm^3\ g^{-1}$) | 0.25 | 0.42 | 0.49 | 0.31 | 0.34 |
| Average Pore Radius, nm | 1.52 | 2.08 | 2.38 | 1.19 | 1.27 |

**Table A.50: Texture characteristics of ACs obtained at 700 °C (R=2.4)**

| Parameter | Texture Characteristics | | | | |
|---|---|---|---|---|---|
| % $H_3PO_4$ | 30% | 40% | 50% | 60% | 70% |
| $S_{BET}$ ($m^2/g$) | 302.1 | 322.6 | 413.7 | 428.3 | 499.7 |
| Total Pore Volume, $V_p$ ($cm^3\ g^{-1}$) | 0.31 | 0.35 | 0.41 | 0.46 | 0.53 |
| Average Pore Radius, nm | 2.05 | 2.17 | 1.98 | 2.15 | 2.12 |

# Appendix B:

## Data for Activated Carbons Produced Using an Activation Time of 2 hours

**Table B.1: Texture characteristics of ACs obtained at T=300 °C (R=0.5)**

| Parameter | Texture Characteristics | | | | |
|---|---|---|---|---|---|
| % $H_3PO_4$ | 30% | 40% | 50% | 60% | 70% |
| $S_{BET}$ ($m^2/g$) | 192.5 | 201.2 | 223.4 | 254.6 | 196.9 |
| Total Pore Volume, $V_p$ ($cm^3\ g^{-1}$) | 0.17 | 0.24 | 0.26 | 0.30 | 0.18 |
| Average Pore Radius, nm | 1.77 | 2.38 | 2.33 | 2.35 | 1.83 |

**Table B.2: Texture characteristics of ACs obtained at T=400 °C (R=0.5)**

| Parameter | Texture Characteristics | | | | |
|---|---|---|---|---|---|
| % $H_3PO_4$ | 30% | 40% | 50% | 60% | 70% |
| $S_{BET}$ ($m^2/g$) | 184.5 | 199.3 | 219.2 | 227.1 | 218.9 |
| Total Pore Volume, $V_p$ ($cm^3\ g^{-1}$) | 0.14 | 0.21 | 0.22 | 0.25 | 0.23 |
| Average Pore Radius, nm | 1.52 | 2.11 | 2.01 | 2.20 | 2.10 |

**Table B.3: Texture characteristics of ACs obtained at T=500 °C (R=0.5)**

| Parameter | Texture Characteristics | | | | |
|---|---|---|---|---|---|
| % $H_3PO_4$ | 30% | 40% | 50% | 60% | 70% |
| $S_{BET}$ ($m^2/g$) | 176.5 | 181.3 | 197.6 | 203.4 | 199.5 |
| Total Pore Volume, $V_p$ ($cm^3\ g^{-1}$) | 0.11 | 0.13 | 0.16 | 0.19 | 0.17 |
| Average Pore Radius, nm | 1.25 | 1.43 | 1.62 | 1.87 | 1.70 |

**Table B.4: Texture characteristics of ACs obtained at T=600 °C (R=0.5)**

| Parameter | Texture Characteristics | | | | |
|---|---|---|---|---|---|
| % $H_3PO_4$ | 30% | 40% | 50% | 60% | 70% |
| $S_{BET}$ ($m^2/g$) | 164.7 | 170.5 | 182.4 | 193.2 | 188.1 |
| Total Pore Volume, $V_p$ ($cm^3\ g^{-1}$) | 0.10 | 0.12 | 0.15 | 0.17 | 0.16 |
| Average Pore Radius, nm | 1.21 | 1.41 | 1.64 | 1.76 | 1.70 |

**Table B.5: Texture characteristics of ACs obtained at T=700 °C (R=0.5)**

| Parameter | Texture Characteristics | | | | |
|---|---|---|---|---|---|
| % $H_3PO_4$ | 30% | 40% | 50% | 60% | 70% |
| $S_{BET}$ ($m^2/g$) | 158.9 | 162.8 | 177.9 | 185.6 | 181.5 |
| Total Pore Volume, $V_p$ ($cm^3\ g^{-1}$) | 0.10 | 0.11 | 0.13 | 0.15 | 0.14 |
| Average Pore Radius, nm | 1.26 | 1.35 | 1.46 | 1.62 | 1.54 |

**Table B.6: Texture characteristics of ACs obtained at T=300 °C (R = 0.8)**

| Parameter | Texture Characteristics | | | | |
|---|---|---|---|---|---|
| % $H_3PO_4$ | 30% | 40% | 50% | 60% | 70% |
| $S_{BET}$ ($m^2/g$) | 201.3 | 224.6 | 245.8 | 266.2 | 261.9 |
| Total Pore Volume, $V_p$ ($cm^3\ g^{-1}$) | 0.18 | 0.21 | 0.24 | 0.27 | 0.26 |
| Average Pore Radius, nm | 1.79 | 1.87 | 1.95 | 2.03 | 1.98 |

**Table B.7: Texture characteristics of ACs obtained at T=400 °C (R = 0.8)**

| Parameter | Texture Characteristics | | | | |
|---|---|---|---|---|---|
| % $H_3PO_4$ | 30% | 40% | 50% | 60% | 70% |
| $S_{BET}$ ($m^2/g$) | 196.8 | 211.8 | 227.2 | 242.4 | 238.9 |
| Total Pore Volume, $V_p$ ($cm^3\ g^{-1}$) | 0.17 | 0.19 | 0.22 | 0.24 | 0.23 |
| Average Pore Radius, nm | 1.73 | 1.79 | 1.94 | 1.98 | 1.92 |

**Table B.8: Texture characteristics of ACs obtained at T=500 °C (R = 0.8)**

| Parameter | Texture Characteristics | | | | |
|---|---|---|---|---|---|
| % $H_3PO_4$ | 30% | 40% | 50% | 60% | 70% |
| $S_{BET}$ ($m^2/g$) | 194.3 | 205.5 | 216.8 | 224.3 | 219.7 |
| Total Pore Volume, $V_p$ ($cm^3\ g^{-1}$) | 0.16 | 0.18 | 0.20 | 0.23 | 0.21 |
| Average Pore Radius, nm | 1.65 | 1.75 | 1.84 | 2.05 | 1.91 |

**Table B.9: Texture characteristics of ACs obtained at T=600 °C (R = 0.8)**

| Parameter | Texture Characteristics | | | | |
|---|---|---|---|---|---|
| % $H_3PO_4$ | 30% | 40% | 50% | 60% | 70% |
| $S_{BET}$ ($m^2/g$) | 192.7 | 198.4 | 206.3 | 213.8 | 211.8 |
| Total Pore Volume, $V_p$ ($cm^3\ g^{-1}$) | 0.15 | 0.16 | 0.18 | 0.20 | 0.19 |
| Average Pore Radius, nm | 1.55 | 1.61 | 1.74 | 18.7 | 1.79 |

**Table B.10: Texture characteristics of ACs obtained at T=700 °C (R = 0.8)**

| Parameter | Texture Characteristics | | | | |
|---|---|---|---|---|---|
| % $H_3PO_4$ | 30% | 40% | 50% | 60% | 70% |
| $S_{BET}$ ($m^2/g$) | 191.3 | 195.6 | 199.2 | 204.1 | 202.6 |
| Total Pore Volume, $V_p$ ($cm^3\ g^{-1}$) | 0.14 | 0.15 | 0.16 | 0.18 | 0.17 |
| Average Pore Radius, nm | 1.46 | 1.53 | 1.61 | 1.76 | 1.68 |

**Table B.11: Texture characteristics of ACs obtained at 300 °C (R=1.0)**

| Parameter | Texture Characteristics | | | | |
|---|---|---|---|---|---|
| % $H_3PO_4$ | 30% | 40% | 50% | 60% | 70% |
| $S_{BET}$ ($m^2/g$) | 187.2 | 226.3 | 304.8 | 316.4 | 298.7 |
| Total Pore Volume, $V_p$ ($cm^3\ g^{-1}$) | 0.19 | 0.23 | 0.26 | 0.26 | 0.30 |
| Average Pore Radius, nm | 2.030 | 2.033 | 1.706 | 1.643 | 2.008 |

**Table B.12: Texture characteristics of ACs obtained at 400 °C (R=1.0)**

| Parameter | Texture Characteristics | | | | |
|---|---|---|---|---|---|
| % $H_3PO_4$ | 30% | 40% | 50% | 60% | 70% |
| $S_{BET}$ ($m^2/g$) | 203.6 | 246.5 | 302.8 | 342.7 | 326.8 |
| Total Pore Volume, $V_p$ ($cm^3\ g^{-1}$) | 0.21 | 0.25 | 0.36 | 0.28 | 0.32 |
| Average Pore Radius, nm | 2.063 | 2.028 | 2.378 | 1.634 | 1.958 |

**Table B.13: Texture characteristics of ACs obtained at 500 °C (R=1.0)**

| Parameter | Texture Characteristics | | | | |
|---|---|---|---|---|---|
| % $H_3PO_4$ | 30% | 40% | 50% | 60% | 70% |
| $S_{BET}$ ($m^2/g$) | 428.3 | 798.6 | 1312.1 | 934.1 | 797.4 |
| Total Pore Volume, $V_p$ ($cm^3\ g^{-1}$) | 0.18 | 0.26 | 0.24 | 0.32 | 0.28 |
| Average Pore Radius, nm | 0.840 | 0.651 | 0.366 | 0.685 | 0.702 |

**Table B.14: Texture characteristics of ACs obtained at 600 °C (R=1.0)**

| Parameter | Texture Characteristics | | | | |
|---|---|---|---|---|---|
| % $H_3PO_4$ | 30% | 40% | 50% | 60% | 70% |
| $S_{BET}$ ($m^2/g$) | 540.3 | 578.3 | 674.9 | 745.6 | 769.3 |
| Total Pore Volume, $V_p$ ($cm^3\ g^{-1}$) | 0.20 | 0.16 | 0.22 | 0.19 | 0.23 |
| Average Pore Radius, nm | 0.740 | 0.553 | 0.652 | 0.510 | 0.598 |

**Table B.15: Texture characteristics of ACs obtained at 700 °C (R=1.0)**

| Parameter | Texture Characteristics | | | | |
|---|---|---|---|---|---|
| % $H_3PO_4$ | 30% | 40% | 50% | 60% | 70% |
| $S_{BET}$ ($m^2/g$) | 427.3 | 566.8 | 728.4 | 696.4 | 694.5 |
| Total Pore Volume, $V_p$ ($cm^3\ g^{-1}$) | 0.24 | 0.28 | 0.55 | 0.34 | 0.32 |
| Average Pore Radius, nm | 1.123 | 0.988 | 1.510 | 0.976 | 0.922 |

**Table B.16: Texture characteristics of ACs obtained at 300 °C (R=1.2)**

| Parameter | Texture Characteristics | | | | |
|---|---|---|---|---|---|
| % $H_3PO_4$ | 30% | 40% | 50% | 60% | 70% |
| $S_{BET}$ ($m^2/g$) | 482.6 | 726.5 | 976.8 | 1033.7 | 1028.5 |
| Total Pore Volume, $V_p$ ($cm^3\ g^{-1}$) | 0.28 | 0.52 | 0.45 | 0.53 | 0.48 |
| Average Pore Radius, nm | 1.160 | 1.431 | 0.921 | 1.025 | 0.933 |

**Table B.17: Texture characteristics of ACs obtained at 400 °C (R=1.2)**

| Parameter | Texture Characteristics | | | | |
|---|---|---|---|---|---|
| % $H_3PO_4$ | 30% | 40% | 50% | 60% | 70% |
| $S_{BET}$ ($m^2/g$) | 396.4 | 487.4 | 974.2 | 1048.7 | 1076.8 |
| Total Pore Volume, $V_p$ ($cm^3\ g^{-1}$) | 0.26 | 0.32 | 0.42 | 0.49 | 0.53 |
| Average Pore Radius, nm | 1.311 | 1.313 | 0.862 | 0.934 | 0.984 |

**Table B.18: Texture characteristics of ACs obtained at 500 °C (R=1.2)**

| Parameter | Texture Characteristics | | | | |
|---|---|---|---|---|---|
| % $H_3PO_4$ | 30% | 40% | 50% | 60% | 70% |
| $S_{BET}$ ($m^2/g$) | 784.7 | 967.2 | 1214.1 | 1089 | 1096 |
| Total Pore Volume, $V_p$ ($cm^3\ g^{-1}$) | 0.38 | 0.49 | 0.58 | 0.52 | 0.56 |
| Average Pore Radius, nm | 0.968 | 1.013 | 0.955 | 0.955 | 1.022 |

**Table B.19: Texture characteristics of ACs obtained at 600 °C (R=1.2)**

| Parameter | Texture Characteristics | | | | |
|---|---|---|---|---|---|
| % $H_3PO_4$ | 30% | 40% | 50% | 60% | 70% |
| $S_{BET}$ ($m^2/g$) | 697.2 | 726.4 | 983.2 | 1011.3 | 996.7 |
| Total Pore Volume, $V_p$ ($cm^3\ g^{-1}$) | 0.30 | 0.34 | 0.38 | 0.53 | 0.49 |
| Average Pore Radius, nm | 0.860 | 0.936 | 0.773 | 1.048 | 0.983 |

**Table B.20: Texture characteristics of ACs obtained at 700 °C (R=1.2)**

| Parameter | Texture Characteristics | | | | |
|---|---|---|---|---|---|
| % $H_3PO_4$ | 30% | 40% | 50% | 60% | 70% |
| $S_{BET}$ ($m^2/g$) | 667.3 | 762.5 | 972.3 | 958.6 | 960.2 |
| Total Pore Volume, $V_p$ ($cm^3\ g^{-1}$) | 0.26 | 0.29 | 0.38 | 0.32 | 0.36 |
| Average Pore Radius, nm | 0.779 | 0.761 | 0.782 | 0.668 | 0.750 |

**Table B.21: Texture characteristics of ACs obtained at 300 °C (R=1.4)**

| Parameter | Texture Characteristics | | | | |
|---|---|---|---|---|---|
| % $H_3PO_4$ | 30% | 40% | 50% | 60% | 70% |
| $S_{BET}$ ($m^2/g$) | 324.1 | 445.8 | 672.2 | 724.7 | 702.9 |
| Total Pore Volume, $V_p$ ($cm^3\ g^{-1}$) | 0.19 | 0.22 | 0.18 | 0.23 | 0.29 |
| Average Pore Radius, nm | 1.172 | 0.987 | 0.935 | 0.635 | 0.825 |

**Table B.22: Texture characteristics of ACs obtained at 400 °C (R=1.4)**

| Parameter | Texture Characteristics | | | | |
|---|---|---|---|---|---|
| % $H_3PO_4$ | 30% | 40% | 50% | 60% | 70% |
| $S_{BET}$ ($m^2/g$) | 426.8 | 498.5 | 693.8 | 824.7 | 844.6 |
| Total Pore Volume, $V_p$ ($cm^3\ g^{-1}$) | 0.22 | 0.26 | 0.28 | 0.30 | 0.32 |
| Average Pore Radius, nm | 1.031 | 1.043 | 0.807 | 0.727 | 0.758 |

**Table B.23: Texture characteristics of ACs obtained at 500 °C (R=1.4)**

| Parameter | Texture Characteristics | | | | |
|---|---|---|---|---|---|
| % $H_3PO_4$ | 30% | 40% | 50% | 60% | 70% |
| $S_{BET}$ ($m^2/g$) | 466.2 | 523.8 | 729.6 | 866.4 | 926.8 |
| Total Pore Volume, $V_p$ ($cm^3\ g^{-1}$) | 0.22 | 0.25 | 0.26 | 0.29 | 0.34 |
| Average Pore Radius, nm | 0.944 | 0.954 | 0.713 | 0.669 | 0.734 |

**Table B.24: Texture characteristics of ACs obtained at 600 °C (R=1.4)**

| Parameter | Texture Characteristics | | | | |
|---|---|---|---|---|---|
| % $H_3PO_4$ | 30% | 40% | 50% | 60% | 70% |
| $S_{BET}$ ($m^2/g$) | 473.2 | 548.5 | 774.3 | 956.4 | 1011.4 |
| Total Pore Volume, $V_p$ ($cm^3\ g^{-1}$) | 0.26 | 0.28 | 0.37 | 0.49 | 0.52 |
| Average Pore Radius, nm | 1.098 | 1.021 | 0.956 | 1.025 | 1.028 |

**Table B.25: Texture characteristics of ACs obtained at 700 °C (R=1.4)**

| Parameter | Texture Characteristics | | | | |
|---|---|---|---|---|---|
| % $H_3PO_4$ | 30% | 40% | 50% | 60% | 70% |
| $S_{BET}$ ($m^2/g$) | 468.1 | 517.3 | 699.8 | 924.6 | 978.5 |
| Total Pore Volume, $V_p$ ($cm^3\ g^{-1}$) | 0.28 | 0.34 | 0.30 | 0.36 | 0.42 |
| Average Pore Radius, nm | 1.196 | 1.314 | 0.857 | 0.779 | 0.858 |

**Table B.26: Texture characteristics of ACs obtained at 300 °C (R=1.6)**

| Parameter | Texture Characteristics | | | | |
|---|---|---|---|---|---|
| % $H_3PO_4$ | 30% | 40% | 50% | 60% | 70% |
| $S_{BET}$ ($m^2/g$) | 286 | 322 | 354 | 378 | 358 |
| Total Pore Volume, $V_p$ ($cm^3\ g^{-1}$) | 0.12 | 0.16 | 0.14 | 0.19 | 0.16 |
| Average Pore Radius, nm | 0.839 | 0.993 | 0.791 | 1.005 | 0.894 |

**Table B.27: Texture characteristics of ACs obtained at 400 °C (R=1.6)**

| Parameter | Texture Characteristics | | | | |
|---|---|---|---|---|---|
| % $H_3PO_4$ | 30% | 40% | 50% | 60% | 70% |
| $S_{BET}$ ($m^2/g$) | 368.7 | 416 | 522 | 685 | 645.8 |
| Total Pore Volume, $V_p$ ($cm^3\ g^{-1}$) | 0.372 | 0.392 | 0.395 | 0.522 | 0.482 |
| Average Pore Radius, nm | 2.018 | 1.884 | 1.513 | 1.524 | 1.493 |

**Table B.28: Texture characteristics of ACs obtained at 500 °C (R=1.6)**

| Parameter | Texture Characteristics | | | | |
|---|---|---|---|---|---|
| % $H_3PO_4$ | 30% | 40% | 50% | 60% | 70% |
| $S_{BET}$ ($m^2/g$) | 898.6 | 937.5 | 1314 | 1022 | 1319 |
| Total Pore Volume, $V_p$ ($cm^3\ g^{-1}$) | 0.492 | 0.498 | 0.572 | 0.536 | 0.785 |
| Average Pore Radius, nm | 1.095 | 1.062 | 0.871 | 1.049 | 1.19 |

**Table B.29: Texture characteristics of ACs obtained at 600 °C (R=1.6)**

| Parameter | Texture Characteristics | | | | |
|---|---|---|---|---|---|
| % $H_3PO_4$ | 30% | 40% | 50% | 60% | 70% |
| $S_{BET}$ ($m^2/g$) | 561.3 | 639.4 | 679 | 682 | 661.4 |
| Total Pore Volume, $V_p$ ($cm^3\ g^{-1}$) | 0.166 | 0.279 | 0.32 | 0.26 | 0.30 |
| Average Pore Radius, nm | 0.59 | 0.872 | 0.942 | 0.762 | 0.907 |

**Table B.30: Texture characteristics of ACs obtained at 700 °C (R=1.6)**

| Parameter | Texture Characteristics | | | | |
|---|---|---|---|---|---|
| % $H_3PO_4$ | 30% | 40% | 50% | 60% | 70% |
| $S_{BET}$ ($m^2/g$) | 545 | 685.5 | 722.8 | 698.7 | 822.7 |
| Total Pore Volume, $V_p$ ($cm^3\ g^{-1}$) | 0.24 | 0.27 | 0.21 | 0.24 | 0.28 |
| Average Pore Radius, nm | 0.880 | 0.787 | 0.581 | 0.687 | 0.681 |

**Table B.31: Texture characteristics of ACs obtained at 300 °C (R=1.8)**

| Parameter | Texture Characteristics | | | | |
|---|---|---|---|---|---|
| % $H_3PO_4$ | 30% | 40% | 50% | 60% | 70% |
| $S_{BET}$ ($m^2/g$) | 487.8 | 533.4 | 624.9 | 688.4 | 734.5 |
| Total Pore Volume, $V_p$ ($cm^3\ g^{-1}$) | 0.24 | 0.18 | 0.22 | 0.29 | 0.33 |
| Average Pore Radius, nm | 0.984 | 0.675 | 0.704 | 0.842 | 0.898 |

**Table B.32: Texture characteristics of ACs obtained at 400 °C (R=1.8)**

| Parameter | Texture Characteristics | | | | |
|---|---|---|---|---|---|
| % $H_3PO_4$ | 30% | 40% | 50% | 60% | 70% |
| $S_{BET}$ ($m^2/g$) | 467.2 | 505.7 | 599.4 | 648.4 | 709.6 |
| Total Pore Volume, $V_p$ ($cm^3\ g^{-1}$) | 0.28 | 0.24 | 0.16 | 0.34 | 0.32 |
| Average Pore Radius, nm | 1.198 | 0.949 | 0.534 | 1.048 | 0.902 |

**Table B.33: Texture characteristics of ACs obtained at 500 °C (R=1.8)**

| Parameter | Texture Characteristics | | | | |
|---|---|---|---|---|---|
| % $H_3PO_4$ | 30% | 40% | 50% | 60% | 70% |
| $S_{BET}$ ($m^2/g$) | 458.9 | 532.2 | 601.5 | 674.2 | 714.8 |
| Total Pore Volume, $V_p$ ($cm^3\ g^{-1}$) | 0.27 | 0.33 | 0.26 | 0.36 | 0.30 |
| Average Pore Radius, nm | 1.177 | 1.240 | 0.864 | 1.068 | 0.839 |

**Table B.34: Texture characteristics of ACs obtained at 600 °C (R=1.8)**

| Parameter | Texture Characteristics | | | | |
|---|---|---|---|---|---|
| % $H_3PO_4$ | 30% | 40% | 50% | 60% | 70% |
| $S_{BET}$ ($m^2/g$) | 442.7 | 494.2 | 588.4 | 624.2 | 676.9 |
| Total Pore Volume, $V_p$ ($cm^3\ g^{-1}$) | 0.24 | 0.29 | 0.34 | 0.38 | 0.42 |
| Average Pore Radius, nm | 1.084 | 1.174 | 1.156 | 1.217 | 1.241 |

**Table B.35: Texture characteristics of ACs obtained at 700 °C (R=1.8)**

| Parameter | Texture Characteristics | | | | |
|---|---|---|---|---|---|
| % $H_3PO_4$ | 30% | 40% | 50% | 60% | 70% |
| $S_{BET}$ ($m^2/g$) | 432.5 | 469.3 | 549.8 | 572.3 | 622.4 |
| Total Pore Volume, $V_p$ ($cm^3\ g^{-1}$) | 0.28 | 0.34 | 0.32 | 0.36 | 0.39 |
| Average Pore Radius, nm | 1.295 | 1.449 | 1.164 | 1.258 | 1.253 |

**Table B.36: Texture characteristics of ACs obtained at 300 °C (R=2.0)**

| Parameter | Texture Characteristics | | | | |
|---|---|---|---|---|---|
| % $H_3PO_4$ | 30% | 40% | 50% | 60% | 70% |
| $S_{BET}$ ($m^2/g$) | 723.4 | 762.8 | 811.3 | 826.5 | 803.4 |
| Total Pore Volume, $V_p$ ($cm^3\ g^{-1}$) | 0.33 | 0.37 | 0.42 | 0.45 | 0.44 |
| Average Pore Radius, nm | 0.912 | 0.970 | 1.035 | 1.089 | 1.095 |

**Table B.37: Texture characteristics of ACs obtained at 400 °C (R=2.0)**

| Parameter | Texture Characteristics | | | | |
|---|---|---|---|---|---|
| % $H_3PO_4$ | 30% | 40% | 50% | 60% | 70% |
| $S_{BET}$ ($m^2/g$) | 983.6 | 1087.1 | 1278.3 | 1232 | 1206 |
| Total Pore Volume, $V_p$ ($cm^3\ g^{-1}$) | 0.46 | 0.52 | 0.57 | 0.54 | 0.55 |
| Average Pore Radius, nm | 0.935 | 0.957 | 0.892 | 0.877 | 0.912 |

**Table B.38: Texture characteristics of ACs obtained at 500 °C (R=2.0)**

| Parameter | Texture Characteristics | | | | |
|---|---|---|---|---|---|
| % $H_3PO_4$ | 30% | 40% | 50% | 60% | 70% |
| $S_{BET}$ ($m^2/g$) | 876.2 | 996.3 | 1309 | 1026 | 1313 |
| Total Pore Volume, $V_p$ ($cm^3\ g^{-1}$) | 0.46 | 0.51 | 0.64 | 0.55 | 0.76 |
| Average Pore Radius, nm | 1.050 | 1.024 | 0.978 | 1.072 | 1.158 |

**Table B.39: Texture characteristics of ACs obtained at 600 °C (R=2.0)**

| Parameter | Texture Characteristics | | | | |
|---|---|---|---|---|---|
| % $H_3PO_4$ | 30% | 40% | 50% | 60% | 70% |
| $S_{BET}$ ($m^2/g$) | 699.3 | 876.2 | 1026.3 | 983.2 | 1017.3 |
| Total Pore Volume, $V_p$ ($cm^3\ g^{-1}$) | 0.45 | 0.49 | 0.54 | 0.50 | 0.63 |
| Average Pore Radius, nm | 1.287 | 1.118 | 1.052 | 1.017 | 1.238 |

**Table B.40: Texture characteristics of ACs obtained at 700 °C (R=2.0)**

| Parameter | Texture Characteristics | | | | |
|---|---|---|---|---|---|
| % $H_3PO_4$ | 30% | 40% | 50% | 60% | 70% |
| $S_{BET}$ ($m^2/g$) | 583.4 | 796.8 | 982.1 | 1011.4 | 995.8 |
| Total Pore Volume, $V_p$ ($cm^3\ g^{-1}$) | 0.38 | 0.42 | 0.47 | 0.56 | 0.52 |
| Average Pore Radius, nm | 1.303 | 1.054 | 0.957 | 1.107 | 1.044 |

**Table B.41: Texture characteristics of ACs obtained at 300 °C (R=2.2)**

| Parameter | Texture Characteristics | | | | |
|---|---|---|---|---|---|
| % $H_3PO_4$ | 30% | 40% | 50% | 60% | 70% |
| $S_{BET}$ ($m^2/g$) | 736.4 | 816.5 | 977.3 | 948.3 | 903.6 |
| Total Pore Volume, $V_p$ ($cm^3\ g^{-1}$) | 0.44 | 0.48 | 0.51 | 0.49 | 0.50 |
| Average Pore Radius, nm | 1.195 | 1.176 | 1.044 | 1.033 | 1.107 |

**Table B.42: Texture characteristics of ACs obtained at 400 °C (R=2.2)**

| Parameter | Texture Characteristics | | | | |
|---|---|---|---|---|---|
| % $H_3PO_4$ | 30% | 40% | 50% | 60% | 70% |
| $S_{BET}$ ($m^2/g$) | 826.5 | 876.4 | 1046.2 | 981.5 | 962.3 |
| Total Pore Volume, $V_p$ ($cm^3\ g^{-1}$) | 0.44 | 0.48 | 0.54 | 0.50 | 0.487 |
| Average Pore Radius, nm | 1.065 | 1.095 | 1.032 | 1.019 | 1.012 |

**Table B.43: Texture characteristics of ACs obtained at 500 °C (R=2.2)**

| Parameter | Texture Characteristics | | | | |
|---|---|---|---|---|---|
| % $H_3PO_4$ | 30% | 40% | 50% | 60% | 70% |
| $S_{BET}$ ($m^2/g$) | 676.3 | 948.3 | 1318.0 | 1300.5 | 992.1 |
| Total Pore Volume, $V_p$ ($cm^3\ g^{-1}$) | 0.36 | 0.48 | 0.56 | 0.54 | 0.51 |
| Average Pore Radius, nm | 1.065 | 1.012 | 0.850 | 0.830 | 1.028 |

**Table B.44: Texture characteristics of ACs obtained at 600 °C (R=2.2)**

| Parameter | Texture Characteristics | | | | |
|---|---|---|---|---|---|
| % $H_3PO_4$ | 30% | 40% | 50% | 60% | 70% |
| $S_{BET}$ ($m^2/g$) | 726.4 | 936.4 | 1248.3 | 1025.1 | 983.4 |
| Total Pore Volume, $V_p$ ($cm^3\ g^{-1}$) | 0.38 | 0.46 | 0.53 | 0.52 | 0.50 |
| Average Pore Radius, nm | 1.046 | 9.82 | 8.49 | 10.14 | 10.17 |

**Table B.45: Texture characteristics of ACs obtained at 700 °C (R=2.2)**

| Parameter | Texture Characteristics | | | | |
|---|---|---|---|---|---|
| % $H_3PO_4$ | 30% | 40% | 50% | 60% | 70% |
| $S_{BET}$ ($m^2/g$) | 743.8 | 928.7 | 1046.3 | 948.3 | 901.8 |
| Total Pore Volume, $V_p$ ($cm^3\ g^{-1}$) | 0.40 | 0.45 | 0.51 | 0.48 | 0.42 |
| Average Pore Radius, nm | 1.075 | 0.969 | 0.975 | 1.012 | 0.931 |

**Table B.46: Texture characteristics of ACs obtained at 300 °C (R=2.4)**

| Parameter | Texture Characteristics | | | | |
|---|---|---|---|---|---|
| % $H_3PO_4$ | 30% | 40% | 50% | 60% | 70% |
| $S_{BET}$ ($m^2/g$) | 296.4 | 322.5 | 376.4 | 411.7 | 486.4 |
| Total Pore Volume, $V_p$ ($cm^3\ g^{-1}$) | 0.24 | 0.30 | 0.36 | 0.38 | 0.39 |
| Average Pore Radius, nm | 1.619 | 1.860 | 1.913 | 1.846 | 1.604 |

**Table B.47: Texture characteristics of ACs obtained at 400 °C (R=2.4)**

| Parameter | Texture Characteristics | | | | |
|---|---|---|---|---|---|
| % $H_3PO_4$ | 30% | 40% | 50% | 60% | 70% |
| $S_{BET}$ ($m^2/g$) | 316.4 | 353.2 | 403.1 | 488.2 | 518.5 |
| Total Pore Volume, $V_p$ ($cm^3\ g^{-1}$) | 0.26 | 0.33 | 0.37 | 0.41 | 0.43 |
| Average Pore Radius, nm | 1.643 | 1.869 | 1.836 | 1.680 | 1.659 |

**Table B.48: Texture characteristics of ACs obtained at 500 °C (R=2.4)**

| Parameter | Texture Characteristics | | | | |
|---|---|---|---|---|---|
| % $H_3PO_4$ | 30% | 40% | 50% | 60% | 70% |
| $S_{BET}$ ($m^2/g$) | 349.2 | 426.1 | 496.3 | 541.8 | 593.8 |
| Total Pore Volume, $V_p$ ($cm^3\ g^{-1}$) | 0.32 | 0.35 | 0.38 | 0.42 | 0.44 |
| Average Pore Radius, nm | 1.833 | 1.643 | 1.531 | 1.550 | 1.482 |

**Table B.49: Texture characteristics of ACs obtained at 600 °C (R=2.4)**

| Parameter | Texture Characteristics | | | | |
|---|---|---|---|---|---|
| % $H_3PO_4$ | 30% | 40% | 50% | 60% | 70% |
| $S_{BET}$ ($m^2/g$) | 339.7 | 417.9 | 482.4 | 538.0 | 546.9 |
| Total Pore Volume, $V_p$ ($cm^3\ g^{-1}$) | 0.33 | 0.38 | 0.41 | 0.43 | 0.46 |
| Average Pore Radius, nm | 1.943 | 1.819 | 1.699 | 1.598 | 1.682 |

**Table B.50: Texture characteristics of ACs obtained at 700 °C (R=2.4)**

| Parameter | Texture Characteristics | | | | |
|---|---|---|---|---|---|
| % $H_3PO_4$ | 30% | 40% | 50% | 60% | 70% |
| $S_{BET}$ ($m^2/g$) | 318.5 | 394.9 | 449.6 | 491.8 | 505.7 |
| Total Pore Volume, $V_p$ ($cm^3\ g^{-1}$) | 0.28 | 0.32 | 0.37 | 0.42 | 0.45 |
| Average Pore Radius, nm | 1.758 | 1.621 | 1.646 | 1.708 | 1.780 |

# Appendix C:

## Data for Activated Carbons Produced Using an Activation Time of 3 hours

**Table C.1: Texture characteristics of ACs obtained at T=300 °C (R=0.5)**

| Parameter | Texture Characteristics | | | | |
|---|---|---|---|---|---|
| % $H_3PO_4$ | 30% | 40% | 50% | 60% | 70% |
| $S_{BET}$ ($m^2/g$) | 176.2 | 184.6 | 220.5 | 236.8 | 216.7 |
| Total Pore Volume, $V_p$ ($cm^3\ g^{-1}$) | 0.22 | 0.26 | 0.24 | 0.33 | 0.16 |
| Average Pore Radius, nm | 2.49 | 2.82 | 2.18 | 2.79 | 1.48 |

**Table C.2: Texture characteristics of ACs obtained at T=400 °C (R=0.5)**

| Parameter | Texture Characteristics | | | | |
|---|---|---|---|---|---|
| % $H_3PO_4$ | 30% | 40% | 50% | 60% | 70% |
| $S_{BET}$ ($m^2/g$) | 172.8 | 191.6 | 224.8 | 218.6 | 220.6 |
| Total Pore Volume, $V_p$ ($cm^3\ g^{-1}$) | 0.19 | 0.24 | 0.14 | 0.28 | 0.25 |
| Average Pore Radius, nm | 2.19 | 2.51 | 1.24 | 2.56 | 2.27 |

**Table C.3: Texture characteristics of ACs obtained at T=500 °C (R=0.5)**

| Parameter | Texture Characteristics | | | | |
|---|---|---|---|---|---|
| % $H_3PO_4$ | 30% | 40% | 50% | 60% | 70% |
| $S_{BET}$ ($m^2/g$) | 172.4 | 184.6 | 188.5 | 199.7 | 192.6 |
| Total Pore Volume, $V_p$ ($cm^3\ g^{-1}$) | 0.14 | 0.21 | 0.17 | 0.17 | 0.19 |
| Average Pore Radius, nm | 2.28 | 2.27 | 1.80 | 1.71 | 1.97 |

**Table C.4: Texture characteristics of ACs obtained at T=600 °C (R=0.5)**

| Parameter | Texture Characteristics | | | | |
|---|---|---|---|---|---|
| % $H_3PO_4$ | 30% | 40% | 50% | 60% | 70% |
| $S_{BET}$ ($m^2/g$) | 173.2 | 166.4 | 178.6 | 182.3 | 192.6 |
| Total Pore Volume, $V_p$ ($cm^3\ g^{-1}$) | 0.19 | 0.16 | 0.22 | 0.19 | 0.18 |
| Average Pore Radius, nm | 2.19 | 1.92 | 2.46 | 2.08 | 1.87 |

**Table C.5: Texture characteristics of ACs obtained at T=700 °C (R=0.5)**

| Parameter | Texture Characteristics | | | | |
|---|---|---|---|---|---|
| % $H_3PO_4$ | 30% | 40% | 50% | 60% | 70% |
| $S_{BET}$ ($m^2/g$) | 162.3 | 154.7 | 171.6 | 186.3 | 178.7 |
| Total Pore Volume, $V_p$ ($cm^3\ g^{-1}$) | 0.17 | 0.21 | 0.23 | 0.21 | 0.22 |
| Average Pore Radius, nm | 2.09 | 2.71 | 2.68 | 2.25 | 2.46 |

**Table C.6: Texture characteristics of ACs obtained at T=300 °C (R = 0.8)**

| Parameter | Texture Characteristics | | | | |
|---|---|---|---|---|---|
| % $H_3PO_4$ | 30% | 40% | 50% | 60% | 70% |
| $S_{BET}$ ($m^2/g$) | 211.6 | 218.7 | 240.6 | 258.3 | 248.6 |
| Total Pore Volume, $V_p$ ($cm^3\ g^{-1}$) | 0.20 | 0.23 | 0.21 | 0.24 | 0.19 |
| Average Pore Radius, nm | 1.89 | 2.11 | 1.74 | 1.86 | 1.53 |

**Table C.7: Texture characteristics of ACs obtained at T=400 °C (R = 0.8)**

| Parameter | Texture Characteristics | | | | |
|---|---|---|---|---|---|
| % $H_3PO_4$ | 30% | 40% | 50% | 60% | 70% |
| $S_{BET}$ ($m^2/g$) | 188.7 | 214.6 | 214.3 | 248.6 | 215.7 |
| Total Pore Volume, $V_p$ ($cm^3\ g^{-1}$) | 0.14 | 0.26 | 0.23 | 0.26 | 0.22 |
| Average Pore Radius, nm | 1.48 | 2.42 | 2.15 | 2.09 | 2.04 |

**Table C.8: Texture characteristics of ACs obtained at T=500 °C (R = 0.8)**

| Parameter | Texture Characteristics | | | | |
|---|---|---|---|---|---|
| % $H_3PO_4$ | 30% | 40% | 50% | 60% | 70% |
| $S_{BET}$ ($m^2/g$) | 187.6 | 211.8 | 207.4 | 218.6 | 201.4 |
| Total Pore Volume, $V_p$ ($cm^3\ g^{-1}$) | 0.24 | 0.14 | 0.22 | 0.27 | 0.24 |
| Average Pore Radius, nm | 2.56 | 1.32 | 2.12 | 2.47 | 2.38 |

**Table C.9: Texture characteristics of ACs obtained at T=600 °C (R = 0.8)**

| Parameter | Texture Characteristics | | | | |
|---|---|---|---|---|---|
| % $H_3PO_4$ | 30% | 40% | 50% | 60% | 70% |
| $S_{BET}$ ($m^2/g$) | 203.8 | 207.8 | 215.6 | 209.8 | 204.7 |
| Total Pore Volume, $V_p$ ($cm^3\ g^{-1}$) | 0.22 | 0.19 | 0.24 | 0.25 | 0.28 |
| Average Pore Radius, nm | 2.16 | 1.83 | 2.23 | 2.38 | 2.73 |

**Table C.10: Texture characteristics of ACs obtained at T=700 °C (R = 0.8)**

| Parameter | Texture Characteristics | | | | |
|---|---|---|---|---|---|
| % $H_3PO_4$ | 30% | 40% | 50% | 60% | 70% |
| $S_{BET}$ ($m^2/g$) | 182.7 | 184.6 | 189.9 | 201.8 | 205.7 |
| Total Pore Volume, $V_p$ ($cm^3\ g^{-1}$) | 0.27 | 0.18 | 0.19 | 0.15 | 0.19 |
| Average Pore Radius, nm | 2.95 | 1.95 | 2.00 | 1.49 | 1.85 |

**Table C.11: Texture characteristics of ACs obtained at 300 °C (R=1.0)**

| Parameter | Texture Characteristics | | | | |
|---|---|---|---|---|---|
| % $H_3PO_4$ | 30% | 40% | 50% | 60% | 70% |
| $S_{BET}$ ($m^2/g$) | 178.8 | 210.9 | 287.5 | 296.6 | 277.4 |
| Total Pore Volume, $V_p$ ($cm^3\ g^{-1}$) | 0.14 | 0.13 | 0.17 | 0.19 | 0.26 |
| Average Pore Radius, nm | 1.57 | 1.23 | 1.18 | 1.28 | 1.87 |

**Table C.12: Texture characteristics of ACs obtained at 400 °C (R=1.0)**

| Parameter | Texture Characteristics | | | | |
|---|---|---|---|---|---|
| % $H_3PO_4$ | 30% | 40% | 50% | 60% | 70% |
| $S_{BET}$ ($m^2/g$) | 194.6 | 224.5 | 288.7 | 206.7 | 311.5 |
| Total Pore Volume, $V_p$ ($cm^3\ g^{-1}$) | 0.24 | 0.26 | 0.40 | 0.24 | 0.38 |
| Average Pore Radius, nm | 2.47 | 2.32 | 2.77 | 1.56 | 2.44 |

**Table C.13: Texture characteristics of ACs obtained at 500 °C (R=1.0)**

| Parameter | Texture Characteristics | | | | |
|---|---|---|---|---|---|
| % $H_3PO_4$ | 30% | 40% | 50% | 60% | 70% |
| $S_{BET}$ ($m^2/g$) | 416.7 | 724.5 | 1276.3 | 876.3 | 776.3 |
| Total Pore Volume, $V_p$ ($cm^3\ g^{-1}$) | 0.34 | 0.22 | 0.34 | 0.21 | 0.33 |
| Average Pore Radius, nm | 1.63 | 0.61 | 0.53 | 0.48 | 0.85 |

**Table C.14: Texture characteristics of ACs obtained at 600 °C (R=1.0)**

| Parameter | Texture Characteristics | | | | |
|---|---|---|---|---|---|
| % $H_3PO_4$ | 30% | 40% | 50% | 60% | 70% |
| $S_{BET}$ ($m^2/g$) | 498.6 | 524.3 | 624.3 | 701.8 | 716.5 |
| Total Pore Volume, $V_p$ ($cm^3\ g^{-1}$) | 0.26 | 0.23 | 0.27 | 0.33 | 0.31 |
| Average Pore Radius, nm | 1.04 | 0.88 | 0.86 | 0.94 | 0.87 |

**Table C.15: Texture characteristics of ACs obtained at 700 °C (R=1.0)**

| Parameter | Texture Characteristics | | | | |
|---|---|---|---|---|---|
| % $H_3PO_4$ | 30% | 40% | 50% | 60% | 70% |
| $S_{BET}$ ($m^2/g$) | 408.9 | 524.3 | 687.8 | 628.3 | 636.8 |
| Total Pore Volume, $V_p$ ($cm^3\ g^{-1}$) | 0.31 | 0.45 | 0.42 | 0.39 | 0.41 |
| Average Pore Radius, nm | 1.52 | 1.72 | 1.21 | 1.24 | 1.29 |

**Table C.16: Texture characteristics of ACs obtained at 300 °C (R=1.2)**

| Parameter | Texture Characteristics | | | | |
|---|---|---|---|---|---|
| % $H_3PO_4$ | 30% | 40% | 50% | 60% | 70% |
| $S_{BET}$ ($m^2/g$) | 403.9 | 699.5 | 916.4 | 995.8 | 987.3 |
| Total Pore Volume, $V_p$ ($cm^3\ g^{-1}$) | 0.44 | 0.41 | 0.33 | 0.42 | 0.43 |
| Average Pore Radius, nm | 2.15 | 1.17 | 0.72 | 0.84 | 0.87 |

**Table C.17: Texture characteristics of ACs obtained at 400 °C (R=1.2)**

| Parameter | Texture Characteristics | | | | |
|---|---|---|---|---|---|
| % $H_3PO_4$ | 30% | 40% | 50% | 60% | 70% |
| $S_{BET}$ ($m^2/g$) | 365.4 | 421.3 | 846.8 | 891.3 | 992.4 |
| Total Pore Volume, $V_p$ ($cm^3\ g^{-1}$) | 0.42 | 0.46 | 0.38 | 0.44 | 0.37 |
| Average Pore Radius, nm | 2.30 | 2.18 | 0.90 | 0.99 | 0.75 |

**Table C.18: Texture characteristics of ACs obtained at 500 °C (R=1.2)**

| Parameter | Texture Characteristics | | | | |
|---|---|---|---|---|---|
| % $H_3PO_4$ | 30% | 40% | 50% | 60% | 70% |
| $S_{BET}$ ($m^2/g$) | 714.5 | 924.8 | 1114.3 | 983.8 | 1003.8 |
| Total Pore Volume, $V_p$ ($cm^3\ g^{-1}$) | 0.44 | 0.42 | 0.44 | 0.50 | 0.42 |
| Average Pore Radius, nm | 1.23 | 0.91 | 0.79 | 1.02 | 0.84 |

**Table C.19: Texture characteristics of ACs obtained at 600 °C (R=1.2)**

| Parameter | Texture Characteristics | | | | |
|---|---|---|---|---|---|
| % $H_3PO_4$ | 30% | 40% | 50% | 60% | 70% |
| $S_{BET}$ ($m^2/g$) | 655.3 | 684.3 | 924.6 | 985.5 | 936.3 |
| Total Pore Volume, $V_p$ ($cm^3\ g^{-1}$) | 0.42 | 0.34 | 0.31 | 0.56 | 0.43 |
| Average Pore Radius, nm | 1.28 | 0.99 | 0.67 | 1.03 | 0.92 |

**Table C.20: Texture characteristics of ACs obtained at 700 °C (R=1.2)**

| Parameter | Texture Characteristics | | | | |
|---|---|---|---|---|---|
| % $H_3PO_4$ | 30% | 40% | 50% | 60% | 70% |
| $S_{BET}$ ($m^2/g$) | 618.5 | 714.4 | 950.3 | 923.7 | 933.8 |
| Total Pore Volume, $V_p$ ($cm^3\ g^{-1}$) | 0.45 | 0.36 | 0.51 | 0.49 | 0.32 |
| Average Pore Radius, nm | 1.45 | 1.01 | 1.07 | 1.06 | 0.68 |

**Table C.21: Texture characteristics of ACs obtained at 300 °C (R=1.4)**

| Parameter | Texture Characteristics | | | | |
|---|---|---|---|---|---|
| % $H_3PO_4$ | 30% | 40% | 50% | 60% | 70% |
| $S_{BET}$ ($m^2/g$) | 287.6 | 404.7 | 633.8 | 711.7 | 685.7 |
| Total Pore Volume, $V_p$ ($cm^3\ g^{-1}$) | 0.54 | 0.44 | 0.24 | 0.28 | 0.41 |
| Average Pore Radius, nm | 3.75 | 2.17 | 0.76 | 0.79 | 1.19 |

**Table C.22: Texture characteristics of ACs obtained at 400 °C (R=1.4)**

| Parameter | Texture Characteristics | | | | |
|---|---|---|---|---|---|
| % $H_3PO_4$ | 30% | 40% | 50% | 60% | 70% |
| $S_{BET}$ ($m^2/g$) | 387.5 | 446.4 | 613.5 | 748.6 | 853.6 |
| Total Pore Volume, $V_p$ ($cm^3\ g^{-1}$) | 0.39 | 0.37 | 0.45 | 0.49 | 0.39 |
| Average Pore Radius, nm | 2.01 | 1.66 | 1.47 | 1.31 | 0.91 |

**Table C.23: Texture characteristics of ACs obtained at 500 °C (R=1.4)**

| Parameter | Texture Characteristics | | | | |
|---|---|---|---|---|---|
| % $H_3PO_4$ | 30% | 40% | 50% | 60% | 70% |
| $S_{BET}$ ($m^2/g$) | 408.7 | 516.7 | 696.8 | 832.6 | 887.6 |
| Total Pore Volume, $V_p$ ($cm^3\ g^{-1}$) | 0.35 | 0.36 | 0.29 | 0.43 | 0.39 |
| Average Pore Radius, nm | 1.71 | 1.39 | 0.80 | 1.03 | 0.88 |

**Table C.24: Texture characteristics of ACs obtained at 600 °C (R=1.4)**

| Parameter | Texture Characteristics | | | | |
|---|---|---|---|---|---|
| % $H_3PO_4$ | 30% | 40% | 50% | 60% | 70% |
| $S_{BET}$ ($m^2/g$) | 416.8 | 507.8 | 727.3 | 908.4 | 985.7 |
| Total Pore Volume, $V_p$ ($cm^3\ g^{-1}$) | 0.42 | 0.48 | 0.41 | 0.43 | 0.56 |
| Average Pore Radius, nm | 2.01 | 1.89 | 1.12 | 0.95 | 1.03 |

**Table C.25: Texture characteristics of *ACs* obtained at 700 °C (R=1.4)**

| Parameter | Texture Characteristics | | | | |
|---|---|---|---|---|---|
| % $H_3PO_4$ | 30% | 40% | 50% | 60% | 70% |
| $S_{BET}$ ($m^2/g$) | 406.5 | 487.3 | 628.5 | 885.3 | 916.3 |
| Total Pore Volume, $V_p$ ($cm^3\ g^{-1}$) | 0.41 | 0.44 | 0.57 | 0.55 | 0.47 |
| Average Pore Radius, nm | 2.01 | 1.80 | 1.65 | 1.24 | 1.02 |

**Table C.26: Texture characteristics of ACs obtained at 300 °C (R=1.6)**

| Parameter | Texture Characteristics | | | | |
|---|---|---|---|---|---|
| % $H_3PO_4$ | 30% | 40% | 50% | 60% | 70% |
| $S_{BET}$ ($m^2/g$) | 211.4 | 285.3 | 297.5 | 308.2 | 315.3 |
| Total Pore Volume, $V_p$ ($cm^3\ g^{-1}$) | 0.34 | 0.31 | 0.23 | 0.47 | 0.41 |
| Average Pore Radius, nm | 3.27 | 2.09 | 1.49 | 2.91 | 2.69 |

**Table C.27: Texture characteristics of ACs obtained at 400 °C (R=1.6)**

| Parameter | Texture Characteristics | | | | |
|---|---|---|---|---|---|
| % $H_3PO_4$ | 30% | 40% | 50% | 60% | 70% |
| $S_{BET}$ ($m^2/g$) | 322.4 | 397.3 | 498.3 | 626.3 | 608.1 |
| Total Pore Volume, $V_p$ ($cm^3\ g^{-1}$) | 0.33 | 0.57 | 0.48 | 0.39 | 0.44 |
| Average Pore Radius, nm | 2.05 | 2.62 | 1.93 | 1.24 | 1.45 |

**Table C.28: Texture characteristics of ACs obtained at 500 °C (R=1.6)**

| Parameter | Texture Characteristics | | | | |
|---|---|---|---|---|---|
| % $H_3PO_4$ | 30% | 40% | 50% | 60% | 70% |
| $S_{BET}$ ($m^2/g$) | 814.5 | 876.6 | 1008.3 | 967.6 | 1287.3 |
| Total Pore Volume, $V_p$ ($cm^3\ g^{-1}$) | 0.55 | 0.62 | 0.19 | 0.36 | 0.61 |
| Average Pore Radius, nm | 1.35 | 1.41 | 0.38 | 0.74 | 0.95 |

**Table C.29: Texture characteristics of ACs obtained at 600 °C (R=1.6)**

| Parameter | Texture Characteristics | | | | |
|---|---|---|---|---|---|
| % $H_3PO_4$ | 30% | 40% | 50% | 60% | 70% |
| $S_{BET}$ ($m^2/g$) | 526.7 | 608.8 | 626.3 | 616.7 | 601.5 |
| Total Pore Volume, $V_p$ ($cm^3\ g^{-1}$) | 0.36 | 0.41 | 0.53 | 0.22 | 0.26 |
| Average Pore Radius, nm | 13.7 | 13.5 | 16.9 | 7.1 | 8.6 |

**Table C.30: Texture characteristics of ACs obtained at 700 °C (R=1.6)**

| Parameter | Texture Characteristics | | | | |
|---|---|---|---|---|---|
| % $H_3PO_4$ | 30% | 40% | 50% | 60% | 70% |
| $S_{BET}$ ($m^2/g$) | 518.3 | 616.3 | 681.4 | 638.8 | 781.8 |
| Total Pore Volume, $V_p$ ($cm^3\ g^{-1}$) | 0.31 | 0.32 | 0.18 | 0.16 | 0.23 |
| Average Pore Radius, nm | 1.19 | 1.01 | 0.53 | 0.50 | 0.60 |

**Table C.31: Texture characteristics of ACs obtained at 300 °C (R=1.8)**

| Parameter | Texture Characteristics | | | | |
|---|---|---|---|---|---|
| % $H_3PO_4$ | 30% | 40% | 50% | 60% | 70% |
| $S_{BET}$ ($m^2/g$) | 424.6 | 506.7 | 586.4 | 627.3 | 701.9 |
| Total Pore Volume, $V_p$ ($cm^3\ g^{-1}$) | 0.30 | 0.15 | 0.18 | 0.21 | 0.24 |
| Average Pore Radius, nm | 1.41 | 0.59 | 0.6.1 | 0.67 | 0.68 |

**Table C.32: Texture characteristics of ACs obtained at 400 °C (R=1.8)**

| Parameter | Texture Characteristics | | | | |
|---|---|---|---|---|---|
| % $H_3PO_4$ | 30% | 40% | 50% | 60% | 70% |
| $S_{BET}$ ($m^2/g$) | 414.3 | 496.3 | 537.3 | 616.5 | 684.3 |
| Total Pore Volume, $V_p$ ($cm^3\ g^{-1}$) | 0.20 | 0.27 | 0.19 | 0.25 | 0.23 |
| Average Pore Radius, nm | 0.96 | 1.08 | 0.71 | 0.81 | 0.67 |

**Table C.33: Texture characteristics of ACs obtained at 500 °C (R=1.8)**

| Parameter | Texture Characteristics | | | | |
|---|---|---|---|---|---|
| % $H_3PO_4$ | 30% | 40% | 50% | 60% | 70% |
| $S_{BET}$ ($m^2/g$) | 414.6 | 485.3 | 581.3 | 638.9 | 696.4 |
| Total Pore Volume, $V_p$ ($cm^3\ g^{-1}$) | 0.35 | 0.41 | 0.19 | 0.23 | 0.26 |
| Average Pore Radius, nm | 1.68 | 1.63 | 0.65 | 0.72 | 0.75 |

**Table C.34: Texture characteristics of ACs obtained at 600 °C (R=1.8)**

| Parameter | Texture Characteristics | | | | |
|---|---|---|---|---|---|
| % $H_3PO_4$ | 30% | 40% | 50% | 60% | 70% |
| $S_{BET}$ ($m^2/g$) | 408 | 507.3 | 544.6 | 638.6 | 624.4 |
| Total Pore Volume, $V_p$ ($cm^3\ g^{-1}$) | 0.18 | 0.23 | 0.31 | 0.42 | 0.53 |
| Average Pore Radius, nm | 0.88 | 0.91 | 1.14 | 1.31 | 1.70 |

**Table C.35: Texture characteristics of ACs obtained at 700 °C (R=1.8)**

| Parameter | Texture Characteristics | | | | |
|---|---|---|---|---|---|
| % $H_3PO_4$ | 30% | 40% | 50% | 60% | 70% |
| $S_{BET}$ ($m^2/g$) | 400.9 | 423.5 | 563.4 | 598.3 | 602.8 |
| Total Pore Volume, $V_p$ ($cm^3\ g^{-1}$) | 0.24 | 0.27 | 0.28 | 0.31 | 0.37 |
| Average Pore Radius, nm | 1.20 | 1.27 | 0.99 | 1.04 | 1.23 |

**Table C.36: Texture characteristics of ACs obtained at 300 °C (R=2.0)**

| Parameter | Texture Characteristics | | | | |
|---|---|---|---|---|---|
| % $H_3PO_4$ | 30% | 40% | 50% | 60% | 70% |
| $S_{BET}$ ($m^2/g$) | 736.1 | 709.3 | 794.5 | 835.3 | 789.6 |
| Total Pore Volume, $V_p$ ($cm^3\ g^{-1}$) | 0.48 | 0.45 | 0.30 | 0.36 | 0.32 |
| Average Pore Radius, nm | 1.30 | 1.27 | 0.75 | 0.86 | 0.81 |

**Table C.37: Texture characteristics of ACs obtained at 400 °C (R=2.0)**

| Parameter | Texture Characteristics | | | | |
|---|---|---|---|---|---|
| % $H_3PO_4$ | 30% | 40% | 50% | 60% | 70% |
| $S_{BET}$ ($m^2/g$) | 924.7 | 997.7 | 1081.1 | 1181.7 | 1195.8 |
| Total Pore Volume, $V_p$ ($cm^3\ g^{-1}$) | 0.40 | 0.49 | 0.51 | 0.40 | 0.47 |
| Average Pore Radius, nm | 0.86 | 0.98 | 0.94 | 0.68 | 0.79 |

**Table C.38: Texture characteristics of ACs obtained at 500 °C (R=2.0)**

| Parameter | Texture Characteristics | | | | |
|---|---|---|---|---|---|
| % $H_3PO_4$ | 30% | 40% | 50% | 60% | 70% |
| $S_{BET}$ ($m^2/g$) | 866.5 | 973.6 | 1277.3 | 1038.5 | 1296.1 |
| Total Pore Volume, $V_p$ ($cm^3\ g^{-1}$) | 0.53 | 0.48 | 0.42 | 0.57 | 0.73 |
| Average Pore Radius, nm | 1.22 | 0.99 | 0.66 | 1.00 | 1.13 |

**Table C.39: Texture characteristics of ACs obtained at 600 °C (R=2.0)**

| Parameter | Texture Characteristics | | | | |
|---|---|---|---|---|---|
| % $H_3PO_4$ | 30% | 40% | 50% | 60% | 70% |
| $S_{BET}$ ($m^2/g$) | 616.3 | 814.4 | 985.9 | 936.3 | 1026.8 |
| Total Pore Volume, $V_p$ ($cm^3\ g^{-1}$) | 0.45 | 0.38 | 0.44 | 0.42 | 0.51 |
| Average Pore Radius, nm | 1.46 | 0.93 | 0.89 | 0.90 | 0.99 |

**Table C.40: Texture characteristics of ACs obtained at 700 °C (R=2.0)**

| Parameter | Texture Characteristics | | | | |
|---|---|---|---|---|---|
| % $H_3PO_4$ | 30% | 40% | 50% | 60% | 70% |
| $S_{BET}$ ($m^2/g$) | 526.8 | 718.4 | 926.5 | 988.9 | 913.6 |
| Total Pore Volume, $V_p$ ($cm^3\ g^{-1}$) | 0.33 | 0.37 | 0.41 | 0.45 | 0.47 |
| Average Pore Radius, nm | 1.25 | 1.03 | 0.89 | 0.91 | 1.03 |

**Table C.41: Texture characteristics of ACs obtained at 300 °C (R=2.2)**

| Parameter | Texture Characteristics | | | | |
|---|---|---|---|---|---|
| % $H_3PO_4$ | 30% | 40% | 50% | 60% | 70% |
| $S_{BET}$ ($m^2/g$) | 698.1 | 787.4 | 938.5 | 908.7 | 874.5 |
| Total Pore Volume, $V_p$ ($cm^3\ g^{-1}$) | 0.47 | 0.41 | 0.45 | 0.37 | 0.44 |
| Average Pore Radius, nm | 1.35 | 1.04 | 0.96 | 0.81 | 1.01 |

**Table C.42: Texture characteristics of ACs obtained at 400 °C (R=2.2)**

| Parameter | Texture Characteristics | | | | |
|---|---|---|---|---|---|
| % $H_3PO_4$ | 30% | 40% | 50% | 60% | 70% |
| $S_{BET}$ ($m^2/g$) | 796.8 | 811.4 | 948.3 | 918.5 | 926.1 |
| Total Pore Volume, $V_p$ ($cm^3\ g^{-1}$) | 0.57 | 0.43 | 0.32 | 0.39 | 0.37 |
| Average Pore Radius, nm | 1.31 | 1.06 | 0.67 | 0.85 | 0.80 |

**Table C.43: Texture characteristics of ACs obtained at 500 °C (R=2.2)**

| Parameter | Texture Characteristics | | | | |
|---|---|---|---|---|---|
| % $H_3PO_4$ | 30% | 40% | 50% | 60% | 70% |
| $S_{BET}$ ($m^2/g$) | 638.4 | 911.9 | 1298.4 | 1288.3 | 964.8 |
| Total Pore Volume, $V_p$ ($cm^3\ g^{-1}$) | 0.31 | 0.42 | 0.47 | 0.42 | 0.48 |
| Average Pore Radius, nm | 0.97 | 0.92 | 0.72 | 0.65 | 0.96 |

**Table C.44: Texture characteristics of ACs obtained at 600 °C (R=2.2)**

| Parameter | Texture Characteristics | | | | |
|---|---|---|---|---|---|
| % $H_3PO_4$ | 30% | 40% | 50% | 60% | 70% |
| $S_{BET}$ ($m^2/g$) | 681.7 | 894.8 | 1178.4 | 1036.4 | 1005.7 |
| Total Pore Volume, $V_p$ ($cm^3\ g^{-1}$) | 0.33 | 0.39 | 0.47 | 0.45 | 0.42 |
| Average Pore Radius, nm | 0.97 | 0.87 | 0.80 | 0.87 | 0.84 |

**Table C.45: Texture characteristics of ACs obtained at 700 °C (R=2.2)**

| Parameter | Texture Characteristics | | | | |
|---|---|---|---|---|---|
| % $H_3PO_4$ | 30% | 40% | 50% | 60% | 70% |
| $S_{BET}$ ($m^2/g$) | 717.3 | 883.7 | 1005.8 | 913.7 | 917.5 |
| Total Pore Volume, $V_p$ ($cm^3\ g^{-1}$) | 0.39 | 0.32 | 0.31 | 0.34 | 0.31 |
| Average Pore Radius, nm | 1.09 | 0.72 | 0.62 | 0.74 | 0.68 |

**Table C.46: Texture characteristics of ACs obtained at 300 °C (R=2.4)**

| Parameter | Texture Characteristics | | | | |
|---|---|---|---|---|---|
| % $H_3PO_4$ | 30% | 40% | 50% | 60% | 70% |
| $S_{BET}$ ($m^2/g$) | 308.4 | 306.3 | 348.5 | 423.4 | 456.8 |
| Total Pore Volume, $V_p$ ($cm^3\ g^{-1}$) | 0.13 | 0.22 | 0.21 | 0.29 | 0.25 |
| Average Pore Radius, nm | 0.84 | 1.44 | 1.21 | 1.37 | 1.09 |

**Table C.47: Texture characteristics of ACs obtained at 400 °C (R=2.4)**

| Parameter | Texture Characteristics | | | | |
|---|---|---|---|---|---|
| % $H_3PO_4$ | 30% | 40% | 50% | 60% | 70% |
| $S_{BET}$ ($m^2/g$) | 294.8 | 317.8 | 394.4 | 433.6 | 529.8 |
| Total Pore Volume, $V_p$ ($cm^3\ g^{-1}$) | 0.19 | 0.27 | 0.28 | 0.33 | 0.35 |
| Average Pore Radius, nm | 12.9 | 17.0 | 14.2 | 15.2 | 13.2 |

**Table C.48: Texture characteristics of ACs obtained at 500 °C (R=2.4)**

| Parameter | Texture Characteristics | | | | |
|---|---|---|---|---|---|
| % $H_3PO_4$ | 30% | 40% | 50% | 60% | 70% |
| $S_{BET}$ ($m^2/g$) | 318.7 | 408.1 | 427.3 | 557.3 | 580.7 |
| Total Pore Volume, $V_p$ ($cm^3\ g^{-1}$) | 0.39 | 0.21 | 0.31 | 0.35 | 0.36 |
| Average Pore Radius, nm | 2.44 | 1.03 | 14.5 | 12.6 | 12.4 |

**Table C.49: Texture characteristics of ACs obtained at 600 °C (R=2.4)**

| Parameter | Texture Characteristics | | | | |
|---|---|---|---|---|---|
| % $H_3PO_4$ | 30% | 40% | 50% | 60% | 70% |
| $S_{BET}$ ($m^2/g$) | 317.6 | 424.4 | 438.7 | 505.8 | 561.3 |
| Total Pore Volume, $V_p$ ($cm^3\ g^{-1}$) | 0.28 | 0.31 | 0.33 | 0.46 | 0.35 |
| Average Pore Radius, nm | 1.76 | 1.46 | 1.50 | 1.82 | 1.25 |

**Table C.50: Texture characteristics of ACs obtained at 700 °C (R=2.4)**

| Parameter | Texture Characteristics | | | | |
|---|---|---|---|---|---|
| % $H_3PO_4$ | 30% | 40% | 50% | 60% | 70% |
| $S_{BET}$ ($m^2/g$) | 289.4 | 376.4 | 408.5 | 463.4 | 518.1 |
| Total Pore Volume, $V_p$ ($cm^3\ g^{-1}$) | 0.22 | 0.27 | 0.24 | 0.33 | 0.39 |
| Average Pore Radius, nm | 1.52 | 1.43 | 1.17 | 1.42 | 1.50 |